

# **A Localization System for Optimizing the Deployment of Small Cells in 2-Tier Heterogeneous Wireless Networks**



**Dorathy Obianuju Abonyi**

Department of Electronic and Electrical Engineering  
The University of Sheffield

This dissertation is submitted for the degree of  
*Doctor of Philosophy*

February 2019



*To God Almighty, my strength  
and  
To my Family for their patience and prayers.*



## **Declaration**

I hereby declare that except for where specific references are made to the works of others and duly acknowledged, the contents of this dissertation are original and the results of my own work. Nothing in it is an outcome of any collaboration except where specifically indicated in the text and the contents of this dissertation have not been submitted either in whole or part for consideration for any other degree or qualification except to this University.

Dorathy Obianuju Abonyi

February 2019



## **Acknowledgements**

First and foremost I thank the Almighty God who made it possible for me to make it to this final stage of my PhD research. For keeping me alive and taking care of my health through all the challenging periods of emotional, psychological and academic traumas. For being my hope in all hopelessness. God, am grateful!

I most sincerely thank my supervisor Dr Jonathan Rigelsford for his guidance, patience, contributions and support throughout this research. You are the best supervisor any researcher would wish to have, I am grateful Sir. My thanks also go to my second supervisor, Dr Lee Ford.

I deeply appreciate the patience, support and understanding from my husband, Hon. Dr. Godwin Ejikeme Abonyi and also thank him in a special way for proof reading my work not minding the professional diversity. Thanks for holding on and carrying the burden of bringing up the children all alone while I was away for study, you are awesome! An unquantifiable thanks goes to my lovely children, Onyedikachukwu, Chiamaka, Chibuokem, Nzubechukwu and Obianuju for four years of having a struggling mother in far away Europe not being available nor in a good state of mind to care and attend to your needs. At my worst moments, my thoughts of you all, kept me going. So thankful for your little voices of encouragement, "mummy, we are fine and we are praying for you to come back tomorrow", the tomorrow that kept reoccurring, most times we all ended in tears. You all have been wonderful and am happy to tell you that the 'tomorrow' is here! God bless you all as I look forward to beholding you all soon.

Thanks to my other family members especially my mother, Mrs Susanna Mamah (Mama Uju) whose determination to train all her seven children through the university all alone having lost our daddy when I was only three built me up for hard work and determination. Mummy, I appreciate all your hard work and prayers, may God bless you and keep you in good health. To my sister Sochima for all the love, sacrifices and support, thanks so much. To all the people that kept my home running and showing love and care to my children; Blessing, Cecilia, Oge, Chidi and Celestina, God bless you all.

To my colleagues at C34, Portobello Center, University of Sheffield, friends at home and in United Kingdom and everyone I met in one way or the other on this PhD journey, I say thanks and God bless you all.



## Abstract

Due to the ever growing population of mobile device users and expansion on the number of devices and applications requiring data usage, there is an increasing demand for improved capacity in wireless cellular networks. Cell densification and 2-tier heterogeneous networks (HetNets) are two solutions which will assist 5G systems in meeting these growing capacity demands. Small-cell deployment over existing heterogeneous networks have been considered by researchers. Different strategies for deploying these small-cells within the existing network among which are random, cell-edge and high user concentration (HUC) have also been explored. Small cells deployed on locations of HUC offloads traffic from existing network infrastructure, ensure good Quality of Service (QoS) and balanced load in the network but there is a challenge of identifying HUC locations.

There has been considerable research performed into techniques for determining user location and cell deployment. Currently localization can be achieved using time dependent methods such as Time of Arrival (ToA), Time Difference of Arrival (TDoA), or Global Positioning Systems (GPS). GPS based solutions provide high accuracy user positioning but suffer from concerns over user privacy, and other time dependent approaches require regular synchronization which can be difficult to achieve in practice. Alternatively, Received Signal Strength (RSS) based solutions can provide simple anonymous user data, requiring no extra hardware within the mobile handset but often rely on triangulation from adjacent Base Stations (BS). In mobile cellular networks such solutions are therefore often only applicable near the cell edge, as installing additional BS would increase the complexity and cost of a network deployment.

The work presented in this thesis overcomes these limitations by providing an observer system for wireless networks that can be used to periodically monitor the cell coverage area and identify regions of high concentrations of users for possible small cell deployment in 2-tier heterogeneous networks. The observer system comprises of two collinear antennas separated by  $\lambda/2$ . The relative phase of each antenna was varied using a phase shifter so that the combined output of the two antennas were used to create sum and difference radiation patterns, and to steer the antenna radiation pattern creating different azimuth positions for AoA estimation. Statistical regression analysis was used to develop range estimation models based on four different environment empirical pathloss models for user range estimation. Users were located into clusters by classifying them into azimuth-range classes and counting the number of users in each class. Locations for small cell deployment were identified

based on class population. *BPEM*, *ADEM*, *BUEM*, *EARM* and *NLOS<sub>Mit</sub>* models were developed for more accurate range estimation. A prototype system was implemented and tested both outdoor and indoor using a network of WiFi nodes. Experimental results show close relationship with simulation and an average PER in range estimation error of 80% by applying developed error models. Based on both simulation and experiment, system showed good performance.

By deploying micro-, pico-, or femto-cells in areas of higher user concentration, high data rates and good quality of service in the network can be maintained. The observer system provides the network manager with relative angle of arrival (AoA), distance estimation and relative location of user clusters within the cell. The observer system divides the cell into a series of azimuthal and range sectors, and determines which sector the users are located in. Simulation and a prototype design of the system is presented and results have shown system robustness and high accuracy for its purpose.

# Table of contents

<b>List of figures</b>	<b>xvii</b>
<b>List of tables</b>	<b>xxiii</b>
<b>List Symbols and Acronyms</b>	<b>xxiv</b>
<b>1 Introduction</b>	<b>1</b>
1.1 Research Background . . . . .	1
1.2 Motivation . . . . .	5
1.3 Research Problem Statement . . . . .	6
1.4 Proposed Approach . . . . .	7
1.5 Main Contribution Of Research . . . . .	8
1.5.1 List Of Publications . . . . .	10
1.6 Thesis Outline . . . . .	11
<b>2 Literature Review</b>	<b>13</b>
2.1 Introduction . . . . .	13
2.2 Overview of Wireless Networks . . . . .	13
2.2.1 Types of Wireless Network . . . . .	14
2.2.2 Cellular Networks . . . . .	14
2.2.3 Wireless Network Deployment . . . . .	15
2.2.4 Heterogeneous Networks . . . . .	16
2.2.5 WiFi Networks . . . . .	18
2.2.6 Internet of Things Technology . . . . .	19
2.2.7 Capacity and Coverage in Wireless Networks . . . . .	20
2.2.8 Capacity Enhancing Techniques . . . . .	20
2.2.9 Small Cell Deployment . . . . .	22
2.3 Brief History of Tracking Systems . . . . .	24

2.3.1	Radar . . . . .	24
2.3.2	Global Positioning System (GPS) . . . . .	26
2.3.3	Other Location Based Services (LBS) . . . . .	26
2.3.4	Localization In Wireless Networks . . . . .	27
2.3.5	Localization Classification . . . . .	28
2.4	Antenna Systems . . . . .	32
2.4.1	Antenna Array . . . . .	33
2.4.2	Broadside and Endfire Array . . . . .	34
2.4.3	Adaptive Antenna Systems . . . . .	35
2.4.4	Antenna Array Feed Network . . . . .	36
2.4.5	Two-Element Array System . . . . .	38
2.5	Delay and Sum Beam Steering . . . . .	39
2.5.1	Phase Delay Calculation . . . . .	40
2.5.2	Beam Scanning By Phase Weighting . . . . .	41
2.6	Phase Shifter . . . . .	41
2.6.1	Switched Line Phase Shifter (SLPS) . . . . .	42
2.6.2	Switched Line Phase Shifter Design . . . . .	43
2.6.3	RF Transmission Lines For SLPS Design . . . . .	43
2.7	Localization Algorithm in Mobile Networks . . . . .	44
2.8	Angle of Arrival Localization Algorithm . . . . .	44
2.8.1	Maximum Likelihood Estimation (MLE) . . . . .	46
2.8.2	Approximate Maximum Likelihood (AML) Estimation . . . . .	47
2.8.3	Hybrid Approximate Maximum Likelihood (HAML) Estimation . . . . .	48
2.9	Range Estimation . . . . .	49
2.9.1	Time Of Arrival (TOA) Based Range Estimation . . . . .	49
2.9.2	Time Difference Of Arrival (TDOA) Based Range Estimation . . . . .	49
2.10	RSS Based Localization . . . . .	50
2.10.1	Radio Wave Propagation . . . . .	50
2.10.2	RSS Based Localization Algorithm . . . . .	52
2.10.3	RSS Fingerprinting . . . . .	53
2.10.4	Localization Systems Based on RSS . . . . .	53
2.11	Radio Location Errors . . . . .	54
2.12	Localization Performance Metrics . . . . .	54
2.13	Localization Applications . . . . .	55
2.14	Summary . . . . .	56

---

<b>3</b>	<b>System Modelling and Simulation</b>	<b>57</b>
3.1	Introduction . . . . .	57
3.2	Simplified Hybrid Approximate Maximum Likelihood (SHAML) . . . . .	58
3.2.1	Error Mitigation in SHAML . . . . .	59
3.3	Proposed System Block Diagram . . . . .	59
3.4	Antenna Model . . . . .	61
3.4.1	A Half Wave Dipole Antenna Model . . . . .	61
3.4.2	High Gain Antenna Model . . . . .	61
3.4.3	Array System Modeling . . . . .	62
3.5	Grounded Coplanar Waveguide (GCPW) SLPS Design . . . . .	63
3.6	Radio Coverage and Channel Model . . . . .	65
3.6.1	Propagation Channel Link Model . . . . .	66
3.6.2	Received Signal Strength (RSS) Model . . . . .	67
3.7	Adaptive Array Smart Antenna Model . . . . .	69
3.7.1	Beam-forming and Beam-steering Simulation . . . . .	70
3.8	Environment Model . . . . .	70
3.8.1	Environment Pathloss Model Analysis . . . . .	72
3.8.2	Effect Of Environment On Measured RSS . . . . .	72
3.8.3	Effect Of Directional Beam On Measured RSS . . . . .	73
3.9	Localization algorithm . . . . .	74
3.9.1	Azimuth Location Position Model . . . . .	75
3.9.2	Angle Of Arrival Estimation Model . . . . .	77
3.9.3	Angle Of Arrival Estimation Of Sample Users . . . . .	77
3.10	Range Estimation . . . . .	79
3.10.1	Range Estimation Of Users In Known Environment . . . . .	83
3.11	Errors in Range Estimation . . . . .	84
3.11.1	Effect of Beam Position on Range Estimation . . . . .	85
3.11.2	Effect of User Azimuth Direction on Range Estimation . . . . .	86
3.11.3	Effect of Unknown Environment on Range Estimation . . . . .	87
3.11.4	Range Estimation Of Random Users In Unknown Environment . . . . .	88
3.12	Range Estimation Error Prediction . . . . .	90
3.12.1	Error Due To Beam Position . . . . .	90
3.12.2	Beam Position Error Model (BPEM) . . . . .	90
3.12.3	Error Due To Angular Deviation . . . . .	92
3.12.4	Improved Angular Deviation Error Model (IADEM) . . . . .	94

3.12.5	Range Estimation Of Random Sample Users With BPEM and ADEM	95
3.12.6	Boundary User Error Model (BUEM)	97
3.12.7	Performance Analysis of System Error Models	98
3.12.8	Environment Adaptive Range Model (EARM)	100
3.12.9	Noise Model	103
3.13	System Application in 2-tier HetNet	106
3.14	Effect Of Non Line Of Sight On Range Estimation	107
3.15	Summary of Simulation Study	109
<b>4</b>	<b>System Implementation</b>	<b>113</b>
4.1	Introduction	113
4.2	Implementing Network	113
4.3	Array System Implementation	115
4.3.1	System Array Elements	115
4.3.2	Antenna Array Testing	115
4.3.3	Antenna Array Result and Analysis	117
4.3.4	Antenna Array Measurement Error Investigation	119
4.3.5	Antenna Array Radiation Pattern Of Interest	120
4.4	Phase Shifter implementation	121
4.4.1	SLPS Implementation with Coaxial Cables	121
4.5	Phase shifter Testing	123
4.5.1	Phase Measurement	123
4.5.2	Phase Measurement Result Analysis	124
4.5.3	Return Loss Result and Analysis	125
4.6	Summing Array Output Implementation	125
4.7	Small Cell Localization Algorithm Implementation	127
4.7.1	Hardware Implementation	127
4.7.2	Software Implementation of Network	129
4.7.3	Data filtering and analysis	134
4.7.4	User localization and small cell deployment Implementation	134
4.8	Conclusion	135
<b>5</b>	<b>Experimental Validation</b>	<b>137</b>
5.1	Introduction	137
5.2	Methodology	137
5.2.1	Outdoor Experimental Setup	138

---

5.2.2	Indoor Experimental Setup . . . . .	139
5.3	Outdoor Round-Trip RSS Measurement . . . . .	140
5.4	Outdoor RSS-Distance Relationship Test . . . . .	141
5.4.1	Outdoor Measured RSS Distribution . . . . .	142
5.4.2	Effect Of Noise on Measured RSS . . . . .	142
5.4.3	Attenuation Rate (Ar) . . . . .	144
5.4.4	Difference In Measured RSS Per Distance Test . . . . .	144
5.4.5	Measured RSS At Same Distance But Different Scans . . . . .	145
5.4.6	Experimental Range Estimation Model . . . . .	145
5.5	Outdoor Network Trial Experiment . . . . .	146
5.5.1	AoA Estimation . . . . .	147
5.5.2	Range Estimation and Environment Prediction . . . . .	148
5.5.3	User Cluster Localization And Small Cell Deployment . . . . .	150
5.6	Outdoor Final Experiment . . . . .	151
5.6.1	AoA Estimation . . . . .	152
5.6.2	Range Estimation and Environment Prediction . . . . .	152
5.6.3	User Cluster Localization And Small Cell Deployment . . . . .	155
5.7	Indoor Wireless Local Area Network Application . . . . .	156
5.7.1	Indoor Experimental AoA Estimation . . . . .	156
5.7.2	Indoor Experimental Range Estimation . . . . .	156
5.7.3	Indoor Experimental Range Estimation with NLOS Mitigation . . . . .	157
5.7.4	Indoor User Cluster Localization and Small Cell Deployment . . . . .	158
5.8	Conclusions . . . . .	159
<b>6</b>	<b>Conclusions and Future Work</b>	<b>161</b>
6.1	Conclusions . . . . .	161
6.2	Research Contribution To Science, Engineering and Technology . . . . .	163
6.3	Future Work . . . . .	165
	<b>References</b>	<b>167</b>
	<b>Appendix A Experimental Validation</b>	<b>193</b>



# List of figures

1.1	Predicted global mobile data traffic from 2015 to 2021 [3]	2
1.2	Problem background and proposed approach	4
1.3	Problem background and proposed approach	7
2.1	Traditional homogeneous network	16
2.2	Heterogeneous Network: A mixture of high power macrocell and low power small cells	17
2.3	Some small cell deployment strategies (a) Cell edge (b) Uniform small cell deployment strategies	24
2.4	Some milestone in the history of tracking technology	25
2.5	Layers of a localization system	27
2.6	Radiating Regions	33
2.7	Standard array system [144] used in adaptive smart antennas	34
2.8	Radiation pattern for a 2 element array showing main beam on (a) broadside (b) end-fire	35
2.9	Possible antenna array feed networks for 2 element array system (a) parallel (b) series approaches	37
2.10	Two Dipole antenna array system showing plane wave arriving from broadside direction of interest	38
2.11	Required delay to steer main beam to positions (a) $135^\circ$ (b) $45^\circ$ (c) $180^\circ$ (d) $0^\circ$	40
2.12	Switched Line phase shifter schematic with (a) SP2T (b) SP4T switches	42
2.13	Switched line phase shifter schematic	43
2.14	Three major approaches to PCB transmission line design (a) microstrip (b) grounded coplanar waveguide (c) stripline	44
2.15	Mobile device localization algorithm trend of research	45
3.1	Approach to system simulation	58

3.2	Localization system block diagram used in this work . . . . .	60
3.3	A single half-wave dipole antenna model showing Omni-directional radiation pattern on azimuth . . . . .	62
3.4	High gain collinear antenna model on CST . . . . .	63
3.5	Array radiation pattern simulation on CST . . . . .	63
3.6	PCB based phase shifter schematic design using diptrace software . . . . .	65
3.7	Designed phase shifter using diptrace software (a) top (b) Bottom layers . . . . .	66
3.8	Modeled relative (a) range and (b) angle from the observer system position . . . . .	66
3.9	Illustration of wireless communication channel for link budget calculation . . . . .	67
3.10	Effect of antenna gain on RSS and coverage range . . . . .	68
3.11	Beam-forming and beam-steering for (a) [0,0] (b) [120,0] (c) [0,120] phase (d) [180,0] phases (degrees) . . . . .	71
3.12	Four environment path loss characteristics based on empirical models of Table 3.7 in a log-log scale . . . . .	73
3.13	Calculated RSS with dipole omni-directional receiver antenna showing coverage in four different environments . . . . .	74
3.14	Calculated RSS with 2-element array receiver antenna showing greater directional coverage in four different environments . . . . .	75
3.15	Illustration of (a) azimuthal sectors for AoA classification (b) range ring for cluster identification . . . . .	75
3.16	AoA Estimation of 20 random users (a) actual location (b) AoA classification of users . . . . .	79
3.17	Range estimation models based on beam position in four environments . . . . .	80
3.18	FSPL range estimation model showing RSS-Range data and the 6 <sup>th</sup> order polynomial curve fitting as an optimum fit for the data . . . . .	82
3.19	Range estimation of users in four different known ideal environments showing greater range error with users 1, 2, 3, 4, 5, 8, 12, 13, 17, 18 located in azimuth positions +I and -I but lesser error with other users because they were located in other azimuth positions . . . . .	84
3.20	Range estimation in all known environments for both broadside and off broadside users showing over-estimation error as users are deviated from peak . . . . .	85
3.21	Estimated range of azimuth peak users for four different environments showing correct estimation for broadside and difference users but under-estimation for left and right of broadside users . . . . .	86

3.22	Range estimation of FSPL beam edge users showing that there is difference in range estimation for users at +I position left and right edges . . . . .	87
3.23	Range estimation in unknown four environments using (a) FSPL, (b) HATA (c) ITU-R (d) WINNER-11 range estimation models for users located at the center of azimuth position 0 showing that in ideal case, accurate estimation is only achieved with correct environment model . . . . .	88
3.24	Range estimation of randomly distributed users in unknown ideal (a) FSPL (b) HATA (c) ITU-R (d) WINNER-11 environments showing that randomly distributed users encounter different kinds of errors based user azimuth location but best estimate is achieved if environment is known . . . . .	89
3.25	Improved range estimate with BPEM (a) BPEV for development of BPEM Equation (b) estimated range in FSPL environment for users in azimuth position +I centre before and after BPEM . . . . .	91
3.26	Angular deviation error model (ADEM) (a) angular deviation error model (ADEM) for FSPL environment based on half the residual (b) range estimation error reduced by half for +I azimuth position edge users . . . . .	93
3.27	Dividing factor used in developing ADEM to achieve optimum error reduction in range estimation . . . . .	96
3.28	Range estimation of randomly distributed users (a) before (after BPEM) (b) after ADEM showing better range estimation accuracy for users located at azimuth positions +I and -I and users deviated from the azimuth center . . .	97
3.29	Boundary user error model (BUEM) (a) calculated BUEV used to develop the BUEM in all four environments (b) range estimation error of +B1 boundary users reduced by half . . . . .	98
3.30	Performance evaluation of BPEM, IADEM and BUEM using random sample users . . . . .	101
3.31	Range prediction using estimated range in four different environments with four range models in each environment for EARM development . . . . .	101
3.32	Boundary user error model using +B1 boundary users (a) error spread with distance for $\pm 0.5$ error in measured RSS (b) +B1 expected error for multiples of random error in measured RSS . . . . .	104
3.33	Measured RSS of twenty sample users at four main azimuth positions (a) 0 (b) +I (c) -I (d) +II with mean, median and mode to determine the best statistical tool for more accurate result . . . . .	105

3.34	Fifty distributed users in a macro-pico HetNet for user cluster localization and small cell deployment location identification . . . . .	107
3.35	User cluster localization (a) optimum location for small cell deployment (b) coordinates of small cell deployment positions with opportunity for cell type deployment decision . . . . .	107
3.36	User cluster localization in a noisy environment (a) optimum location for Small cell deployment in a noisy environment (b) coordinates of positions for Small cell deployment in a noisy environment . . . . .	108
3.37	Effect of NLOS on range estimation (a) line of sight and Non line of sight ITU and WINNER channel models (b) estimated range before and after NLOS mitigation in WINNER environment . . . . .	110
4.1	Structural illustration of the observer system . . . . .	114
4.2	Input reflection coefficient ( $S_{11}$ ) test of the antennas used for the observer system implementation . . . . .	116
4.3	Array measurement in GBSAR anechoic chamber (a) schematic setup (b) experimental setup inside the chamber . . . . .	117
4.4	Array measurement in GBSAR anechoic chamber . . . . .	118
4.5	Measured RSS from the horn antenna transmitter by the array system receiver at all phase states . . . . .	118
4.6	Angles of highest RSS for each antenna phase combinations showing unique beam maximum radiation at all angles . . . . .	119
4.7	Phase offset error investigation showing that error is as a result of chamber features and not the array system under test . . . . .	120
4.8	Measured and simulated array radiation patterns at each beam steered positions	121
4.9	Implemented switched line phase shifter using two HMC241ALP3E SP4T switches . . . . .	122
4.10	Phase Switching between PS1 and PS2 with (a) PS1 line 1 as reference (b) PS2 line 1 as reference showing phase switching at $-179^\circ$ . . . . .	124
4.11	Phase shift $S_{11}$ measurement of PS1 . . . . .	126
4.12	Input reflection coefficient measurement ( $S_{11}$ ) of the 2 Way SMA power combiner to ensure proper impedance matching and good radio wave radiation	127
4.13	Hardware implementation of network users (a) ESP8266 Thing used for adaptive algorithm implementation (b) programmed micro-controller as users	128

---

4.14	Implemented hardware of the observer system showing both internal and external circuitries . . . . .	129
5.1	Outdoor experimental setup showing some of the distributed users on red and deployed observer system on yellow . . . . .	139
5.2	Indoor experimental setup . . . . .	139
5.3	On-the-fly to and fro movement from 1 to 100m to check RSS-distance relationship . . . . .	140
5.4	Ten measured RSS using omni-directional antenna to test RSS-distance hypothesis . . . . .	141
5.5	Histogram plot of average measured RSS to check the distribution of measured RSS data . . . . .	143
5.6	Deviation of measured RSS at each distance for ten scans (a) deviation from mean RSS (b) amount of deviation . . . . .	143
5.7	Comparison of simulated and experimental (a) RSS (dBm) in relation to distance (b) attenuation rate . . . . .	146
5.8	User deployment for trial experiment showing (a) actual user position before localization (b) measured RSS from user devices at all azimuth positions . .	147
5.9	AoA estimation results (a) experiment (b) simulation showing accurate AoA estimation for both simulation and experiment . . . . .	148
5.10	Experimental range estimation showing actual, simulated and experimental estimate . . . . .	150
5.11	User cluster localization and optimum small cell deployment position identification using (a) experimental (b) simulation data . . . . .	151
5.12	User deployment for final experiment showing (a) actual user position before localization (b) measured RSS from user devices at all azimuth positions . .	152
5.13	AoA Estimation Results (a) experiment (b) simulation showing accurate AoA estimation for both simulation and experiment . . . . .	153
5.14	Estimated range of users using all four range models with experimental measured RSS as input . . . . .	153
5.15	Experimental validation of developed error models showing mean absolute error in range estimation after AARM, BPEM, ADEM and BUEM . . . . .	154
5.16	Experimental small cell deployment strategy showing (a) user cluster localization (b) small cell deployment position coordinates relative to BS . . . .	155

---

5.17	User deployment for Indoor experiment showing (a) actual user position before localization (b) measured RSS from user devices at all azimuth positions	156
5.18	AoA Estimation Results (a) Experiment (b) Simulation showing accurate AoA estimation for both simulation and experiment in indoor environment .	157
5.19	Actual, simulated and experimental range estimated in indoor environment using all four range estimation models before NLOS mitigation . . . . .	157
5.20	Indoor Experimental range estimation with all four range estimation models after NLOS mitigation using (a) ITU (b) WINNER based NLOS mitigation models . . . . .	158
5.21	Indoor cluster localization and small cell deployment positions (a) before (b) after NLOS error mitigation . . . . .	159

# List of tables

2.1	Common Types of Wireless Network . . . . .	14
2.2	Wifi protocols and data rate . . . . .	19
3.1	Simulation parameters . . . . .	61
3.2	Collinear antenna CST modeling parameters . . . . .	62
3.3	Antenna array radiation pattern simulation on CST . . . . .	64
3.4	CST calculated phase shifts for frequency span of 2.4 to 2.5GHz . . . . .	64
3.5	CST calculated phase shifts for frequency span of 2.4 to 2.5GHz . . . . .	65
3.6	Simulated result of RSS by two different antennas . . . . .	68
3.7	Propagation Models Applied for Line of Sight (LOS) Channel Modeling . .	72
3.8	Range estimation model equations for four azimuth positions in different environments . . . . .	82
3.9	Mean absolute error in range estimation of users for all environments using all range models . . . . .	89
3.10	ADEM equations for four main azimuth positions in different environments	93
3.11	IADEM equations for four main azimuth positions in different environments	96
3.12	BUEM equations for four main azimuth positions in different environments	98
3.13	Performance evaluation of BPDM, IADEM and BUEM using systematic users	100
3.14	Environment adaptive range estimation models . . . . .	102
3.15	Mean absolute error after EARM for four different environments . . . . .	103
3.16	Statistical Evaluation of Measured RSS with Random Noise . . . . .	105
3.17	LTE-A Parameters For Simulation . . . . .	106
3.18	Range Estimation Model Equations For Four azimuth Positions in Different Environments . . . . .	108
4.1	Control Truth Table Of SLPS design . . . . .	123
4.2	Measured Phase Result of PS1 and PS2 . . . . .	124

4.3	Phase Plot Over Frequency Span of 2.4 to 2.5GHz . . . . .	125
4.4	System Control Truth Table . . . . .	129
5.1	Correlation between different scans for the same distance range . . . . .	145

# Chapter 1

## Introduction

### 1.1 Research Background

Mobile devices have been a driving force to wireless technological growth since the inception of mobile phones in 1973. Mobile phone technology constantly grew from a device for wireless voice calls to a hand-held machine that is capable of doing everything that can be imagined of a computer system and even more. Smartphones and tablets are hand-held data hungry computers that have the capability of making a voice call, browsing the internet, sending media data etc. Mobile devices became very popular and unavoidable because of the convenience of doing things on the go and with their friendly mobile applications that make life easy and interesting. There has therefore, been a constant growth in mobile device usage as compared to a desktop computer. According to Comscore's mobile data 2017, mobile devices have become the leading digital platform, with majority of activities on smartphones and tablets [1].

The availability and affordability of smartphones with expansion in mobile app usage led to an exponential growth [2] in number of mobile device users generating traffic concern on existing network infrastructure. Due to insecurity in the world and development in the mode of teaching and assessment in education system, age groups of people that use mobile phones have also expanded from fully grown adults to youths and children as well. Data by Cisco's Global Visual Networking Index (VNI) of Figure 1.1 shows that by 2021, there will be 11.6 billion mobile-connected devices generating mobile data traffic of 49 billion gigabytes per month as against 7 billion gigabytes for 2016 [3]. This growth is mostly caused by tremendous increase in the number of smart phones and machine to machine (M2M) modules like wearable devices and IoT devices — most of which have embedded cellular

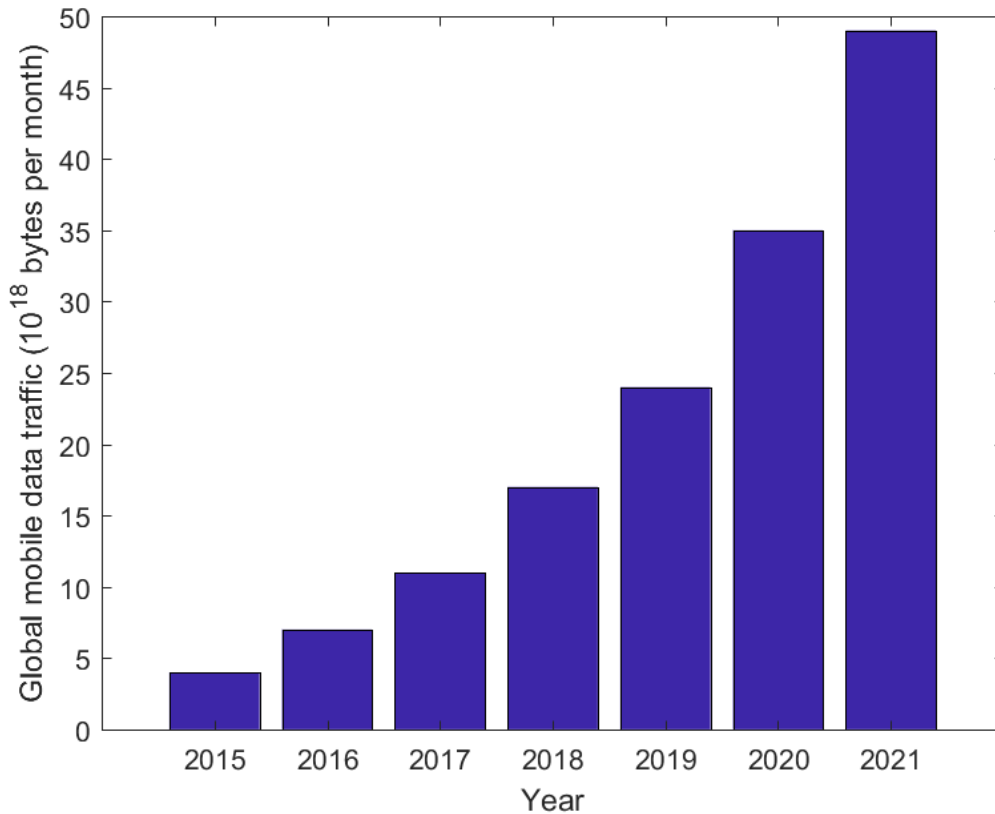


**Fig. 1.1** *Predicted global mobile data traffic from 2015 to 2021 [3]*

connections. By Cisco's prediction, there will be more mobile-connected devices than the human population by 2021.

In other to cope with traffic requirements of future wireless networks [4] driven by increasing number of mobile broadband data subscribers and bandwidth-intensive services competing for limited radio resources, there is need for increased capacity to keep up with these challenges. Network Operators have tried meeting this challenge by increasing capacity with new radio spectrum, adding multi-antenna techniques and implementing more efficient modulation and coding schemes. Unfortunately spectrum is very expensive and rarely available, there are limit to the number of antennas that can be used in a single mast and more efficient modulation scheme results in increased complexity of the system.

Network densification which means adding more cell sites and bringing the network closer to users is another option the operators are exploring. This can be achieved by adding more sectors or by reducing the macro-cell site area and maintaining a homogeneous network. This is not economical and such cell sites are not always available especially in city centers.

---

Another way is to underlay low power small cells within the existing macro-cell and integrate them to work together forming a heterogeneous network (HetNet) [5, 6]. Small cells can be a microcell, picocell, femtocell or a relay depending on the size of its coverage area and its transmission power. Site acquisition is easier and cheaper with small cell base transceiver station (BTS) equipment as they are correspondingly smaller.

Appropriately deployed small cell will offload traffic from macrocell, ensure good Quality Of Service (QoS) and balanced load in the network. Small cells can be deployed randomly within the macrocell[7], at the cell edge[8, 9], around high traffic user [10] or within high user concentration (HUC) location [11]. Though there is fear over random small cell deployment, [12] proposed an analytical framework to test probability of outage in heterogeneous cellular network and reports that random deployment does not affect quality of service. It was reported in [5] that small cells are under-loaded unless they are deployed in dense traffic locations. This implies that even though a randomly deployed small cell does not reduce the quality of service, it can be under-loaded causing waste of network resources and can be a potential source of interference in the network. On the other hand, it may not necessarily offload the traffic from macrocell especially when it falls in no or less user locations. Cell edge deployment strategy will provide better quality signal to users at the cell edge but will not offload the traffic from macrocell since there may be only but few users at the cell edge to use the network. Heavy user location may by some percentage offload traffic from the macrocell but need traffic data recording for years to be able to identify location of heavy users. Deployment of small cells in HUC location will offload considerable amount of traffic from the macrocell and balance the load on the network by removing a chunk of users from the big cell but then, the operators need to be able to identify locations of HUC.

In traditional network planning, sites are selected and base station (BS) environment modeled using RF tools. Optimal balance between capacity and coverage was achieved in homogeneous network using this traditional network-centric design. This traditional homogeneous network deployment strategy solved the capacity problem of early network but it is not a good solution for the traffic requirement of present and future network where hotspots are inevitable. Hotspots are persistent cluster of users in an existing network which were not considered in the original network planning. Heterogeneous network is a solution that will help operators meet up with capacity requirement of 5G. Network operators primarily deploy small cells to increase capacity in hotspots like airports, hotels, coffee shops, stadium and other places where business people tend to congregate. These areas are hotspots expected location and traffic solution can be provided by deploying small cells. Researchers are also exploring using WiFi in hotspots to offload traffic from cellular networks [13]. Due

to development, migration and unemployment in developing countries like Nigeria and India, unexpected hotspots are very common. In some dynamic expected hot spots like sports stadium, traffic and small cell requirement may not be the same at all times. A mobile small cell deployment strategy for unexpected hotspots was proposed in [14] with the assumption that the operators are able to identify locations of hotspots. If operators are able to identify hotspots, small cells will be promptly and optimally deployed to offload traffic from existing network infrastructure and ensure good service quality in the network. There is therefore need to periodically monitor the macro-cell coverage area to be able to identify areas of traffic hot and dead zones for prompt and optimal deployment of a small cell to ensure maintained QoS and traffic load balance within the network.

A precise location is not a necessity in this case since anywhere within the highly populated area will still serve as an optimum position for small cell deployment. For instance, Figure 1.2 is a recruitment scene at Abuja national stadium, Nigeria where applicants gathered for Nigerian immigration service recruitment test on March 15th, 2014. This is a typical

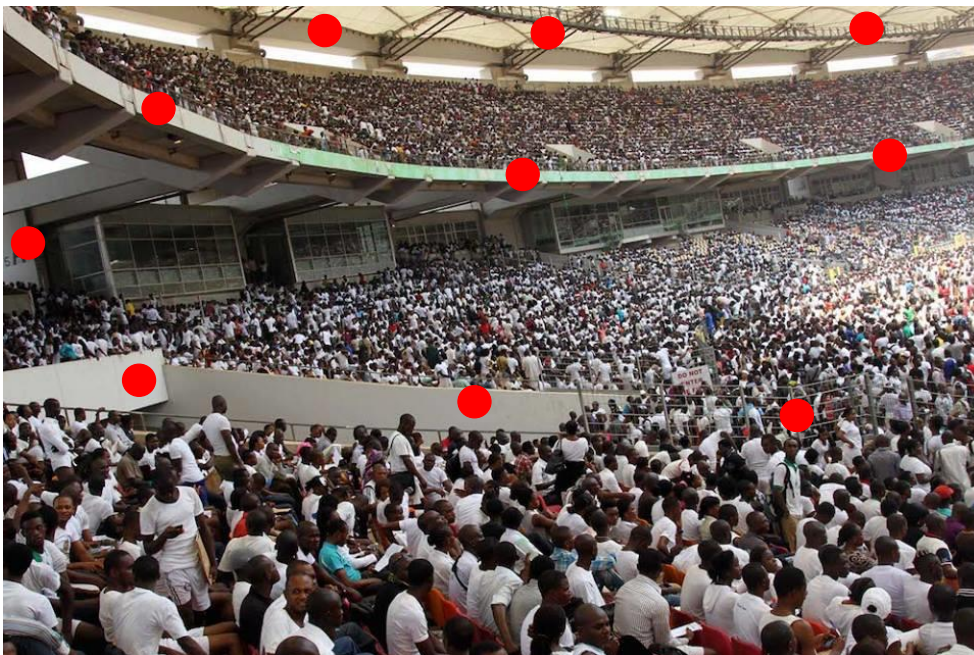


**Fig. 1.2 Problem background and proposed approach**

hotspot scenario and deploying a small cell anywhere within this area, examples shown with red circles will still offer the solution expected of the small cell. In this research therefore, an area location within which a small cell can be deployed is of interest and not a precise location. Currently localization can be achieved using time dependent methods such as time of arrival (TOA) [15], time difference of arrival (TDOA) [16] or global positioning systems

(GPS). GPS based solutions provide high accuracy user positioning but suffer from concerns over user privacy [17] and indoor usage. Other time dependent approaches require regular synchronization which can be difficult to achieve in practice. Alternatively, received signal strength (RSS) based solutions can provide simple anonymous user data, requiring no extra hardware within the mobile handset but often rely on triangulation [18, 19] from adjacent BTS. In mobile cellular networks such solutions are therefore often only applicable near the cell edge as installing additional base station (BS) would increase the complexity and cost of a network deployment.

The work presented in this thesis aims to overcome these limitations by providing an observer system that can be easily incorporated in a wireless network BTS with low complexity. This system can be used to periodically monitor the cell coverage area and identify regions of high concentrations of mobile users for possible small cell deployment in 2-tier heterogeneous networks.

## 1.2 Motivation

Due to continuous growth in wireless network and the traffic demand that accompany it, there is a need to balance the ever growing demand with network facilities to ensure good quality of service within the network. Led by poor, expensive and unreliable internet services in my home country, Nigeria due to unavailability of fixed access and total dependence on limited mobile broadband (3G and 4G), numerous amount of people connect to the network at the same time from Universities, businesses, job centers etc. making the services frustrating and unusable. Cell densification and 2-tier heterogeneous networks (HetNets) are two solutions which will assist future wireless networks like 5G systems in meeting these growing capacity demands. Due to developmental, political and social nature of man, users tend to cluster in certain locations causing hotspots. In developing countries like Nigeria where unemployment is an issue, any job interview centre is a potential unexpected hotspot. In some other countries, unexpected hotspots are created for different reasons like sales in shops, sporting events, shows and promotions etc. In busy places like airports, stadia and universities, hotspots are inevitable. Appropriately deployed small-cells offload traffic from a macro-cell and ensure balanced load as well as good quality of service (QoS) in the network. HetNet planning was usually based on expected user distribution and long-term collection of mobile traffic data which creates latency in small cell deployment and would not solve the problem of promptly offloading traffic from the umbrella cell to effect a balance in the network for an unexpected hotspots. If the network coverage area is periodically monitored and relative locations for small cell deployment displayed on a laptop or phone screen, the operator is able to identify locations of hotspots as they occur and be able to deploy say

mobile small cell with little or no delay. Deployment time will only be based on efficiency of network operator and other factors like road traffic as the small cell is being conveyed to the identified deployment location.

Small cell deployment strategies in literature focused more on positions to deploy small cells and mathematical algorithms that optimizes the positions for better throughput, in most cases with the assumption that the operators can identify those locations. Different strategies for small cell deployment in high user concentration location have been proposed in [14, 20] but with the assumption that locations of hotspots are known by the operators. According to the report by Real Wireless for OfCom [21] on Techniques for increasing the capacity of wireless broadband networks: UK, 2012-2030, it was reported that if the operators would be able to identify locations of hotspots, effective use of outdoor small cells would provide a low cost solution to capacity problems in wireless networks. To the best of our knowledge, there is no system in place or in any research paper that proposes a practical approach that will help operators to promptly identify locations of hotspots. The aim is for the location algorithm to have a level of accuracy which is within the reasonable constraints of the urban built environment i.e  $\pm 5$  to 15m.

Our research question is: *"Is it possible to develop a system that can easily be integrated into the existing network infrastructure to help wireless network operators promptly identify locations for small cell deployment in a two tier heterogeneous network?"*

### **1.3 Research Problem Statement**

Consider a tri-sector network base transceiver station (BTS) with hexagonal homogeneous macrocells as illustrated in Figure 1.3 and considering only 180 degrees coverage of this network. A cell or multiple cells within the network have obvious clusters of users within the cell causing an overload on the macrocell bts servicing those cells resulting in low quality service and customer dissatisfaction. Deploying a small cell BTS randomly [22] have no certainty of offloading traffic from the big cell. On the other hand, deploying small cell uniformly among the three cell will result to a waste of resources as the three cells do not equally need the same amount of small cells. If small cells are deployed round the cell edge [23], loads of resources will be wasted and most of the small cells will be under utilized such that instead of being an advantage, they will become a disadvantage causing interference in the network. This indicates that the aim of HetNet will not be achieved by blind or random placement of small cells in this network. Only by deploying small cells to areas of HUC will the full potential of multi-tier HetNets be achieved.

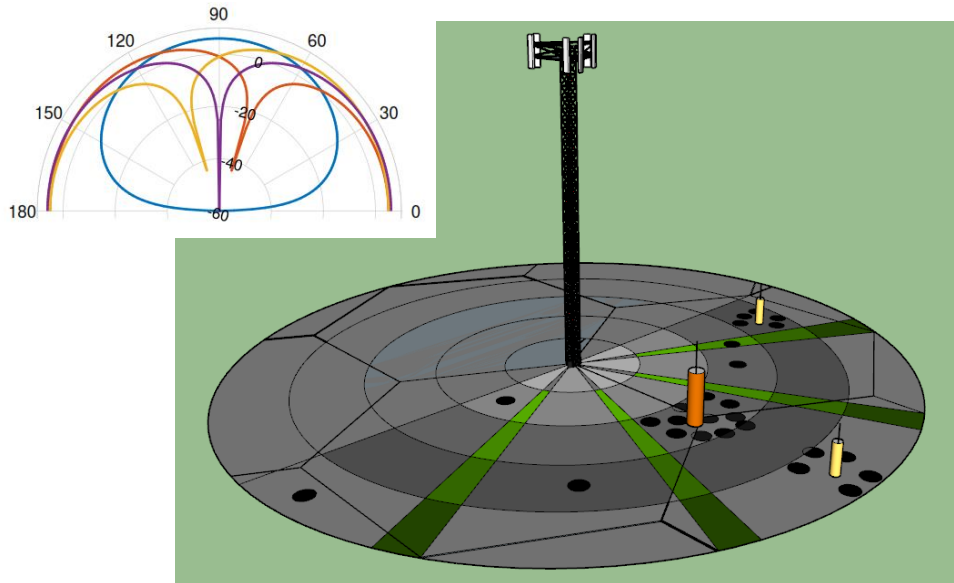


**Fig. 1.3** *Problem background and proposed approach*

## 1.4 Proposed Approach

The approach in this research is to share the network space into azimuth sectors and range from a reference point. With an observer system to monitor the entire space, users sector angle as well as range are calculated to group users into clusters in each angle-range sector. By calculating the number of users in each section of the space, locations for small cell deployment is identified based on the area with high user concentration.

Considering a tri-sector wireless network of Figure 1.3 for example, using a directional beam and beam steering the coverage space is shared into azimuth locations defined by beam positions as shown in Figure 1.3 meaning that AoA estimation model can be developed based on how RSS measured from each azimuth position compares with RSS measured from other azimuth positions. By further sharing the coverage area into range sections of defined intervals, the entire space is divided into angle-range sections creating different azimuth-range classes for user cluster localization and small cell deployment. Depending on the operator agreed threshold of number of users for small cell deployment and the types of small cell, locations for small cell deployment can be identified. This research focuses only on a  $180^\circ$  coverage but can be expanded to  $360^\circ$  coverage in future work.

## 1.5 Main Contribution Of Research

In this research, a novel and practical small cell deployment strategy for a 2-tier HetNet has been proposed and also a prototype system was designed to demonstrate the proposed strategy. The main contributions in this research include:

- A practical approach that will help operators identify optimum locations for small cell deployment with minimal adjustment to the existing network infrastructure is presented in this research.
- Secondly, a strategy that will help mobile operators make good decisions on the type of small cell to be deployed based on the number of users in each cluster is also presented.
- Third, a simple yet effective RSS based angle of arrival estimation algorithm that can be applied in any localization system both indoor and outdoor has been simulated and experimented.
- Forth, a simple range estimation model that is both environment and angle adaptive (angle adaptive range model (AARM)) for the purpose of reduced error in estimation has been simulated and experimented. On the range estimation, three error models which include beam position error model (BPEM), angular deviation error model (ADEM), boundary user error model (BUEM) and also a model for environment adaptive range estimation (environment adaptive range model (EARM)) were developed for application in RSS based range estimation systems.
- Fifth, a novel but simple switched line phase shifter on a printed circuit board for phase switching of  $60^\circ$  step that can be applied in a phased array antenna system for array scanning has been designed and implemented.
- Finally, simulation and experimentation of a simple but accurate localization system for user and user-cluster localization in a wireless network has been carried out. This can also be applied to identify a particular room where a user is located like in the case of elderly in an emergency cases.

Large-scale path loss and small-scale fading statistics are parameters obtained prior to deployment of a new network BS. These are calculated by determining the appropriate propagation characteristics (pathloss and multipath) of the deployment environment. With the pathloss information, the network coverage as well as BS placement and optimization is determined. The statistics of small-scale fading provides information on local field variation which is used for calculation of parameters used in improving the design of radio receiver and to mitigate against multipath fading. Among the approaches for Pathloss prediction are empirical models. These are a set of equations obtained from extensive field measurement

---

that qualitatively describe different environment scenarios like open, urban, suburban and rural areas. Though not as accurate as theoretical or site-specific models, it is known for its simplicity [24]. This research applied four different empirical pathloss models to characterize radio propagation and develop range estimation models so that in unknown open environment each model is used to estimate rate and most likely environment predicted. This means that instead of generalizing the open space environment, the most likely open space for better accuracy can be obtained. The novelty of this research can be summarized in three places as follows;

- ⇒ **Novelty Of Application:** In the literature, there is no practical solution to network operators identifying locations for small cell deployment. This is an entirely new strategy for optimal small cell deployment with optimum position detection. Adopting the application of a localization system in this area of wireless network is novel because to the best of our knowledge, there is no place in literature where localization system is applied to identify locations for small cell deployment. The deploying network environment is assumed to be one of the four implemented radio propagation environments. The network coverage area is segmented into a series of azimuth classes defined by beam position and also relative range from the BS. Each of the implemented propagation models are applied to classify users as clusters into each of the azimuth-range classes. Based on the environment model that returns average least error in range estimation of all deployed users, most likely model is predicted. Estimations by the predicted environment is displayed giving operators the ability to identify locations of user cluster for small cell deployment.
- ⇒ **Novelty Of System:** The existing theory of beam-forming and beam-steering was adopted to develop an AoA and range based system with minimal possible number of antennas. Phased array antenna systems were characterized with multiple antennas but this system was developed with only two antennas. A new idea of sharing the network coverage area into azimuthal positions defined by the beam positions was also developed. By adopting the statistical regression analysis, range estimation model was developed for four different environments which resolves user range in real time and based on all users estimated range in an unknown environment, predicts the closest environment among all four range models. This is the first practical localization system with only 2 antenna elements that resolve AoA, range, user cluster as well as predict most likely environment using only measured RSS. The simplicity of approach makes it attractive.

⇒ **Novelty Of Algorithm:** A novel centralized hybrid AoA/RSS localization algorithm with only one BS and one phase has been developed. The existing AoA/RSS algorithms are based on fingerprinting which involves two phases or based on using at least two base stations but the approach in this research has bypassed multiple BS and phases by using only RSS data measured from only one BS to estimate both AoA and range in real time without the need for off-line phase. Normally the offline phase is to obtain accurate propagation of the deployment environment but this algorithm uses four closely related empirical models (open space) that estimates range and predicts the most likely model out of all implemented models for more accurate localization. In case of non line of sight application (NLOS), the algorithm incorporates NLOS mitigation factor to compensate for NLOS effect. The algorithm in this research promotes customer privacy as it works with new assigned IDs of users with only measured RSS which makes it anonymous.

Based on the listed contributions of the research, the following publications have been achieved and three journal papers in the pipeline.

### 1.5.1 List Of Publications

1. Dorathy Abonyi, Jonathan Michael Rigelsford, "Localisation system for network planning in 2-tier heterogeneous networks", Progress In Electromagnetics Research Symposium (PIERS), Shanghai, China, Aug. 2016.
2. Dorathy O Abonyi, Jonathan M Rigelsford, "A hardware localisation system for ZigBee wireless sensor networks", Progress In Electromagnetics Research Symposium (PIERS), Shanghai, China, Aug. 2016.
3. Dorathy O Abonyi, Jonathan M Rigelsford, "Cellular Network Load Balancing Strategy For Unexpected Hotspots in Developing Countries", International Conference of Women Engineers and Scientists (ICWES), New Dehli, India, Oct. 2017.
4. Dorathy O Abonyi, Jonathan M Rigelsford, "A System for Optimizing Small-Cell Deployment in 2-Tier HetNets", International Workshop on Computer Aided Modeling and Design of Communication Links and Networks (CAMAD), Barcelona, Spain, Sep. 2018.

Based on the key novelty areas mentioned above, the following journal papers are on the pipeline to be sent out for publication;

- (a) Dorathy Abonyi, Jonathan Michael Rigelsford, "A Novel Strategy For Prompt Small-Cell Deployment in 2-Tier HetNets".

- (b) Dorathy O Abonyi, Jonathan M Rigelsford, "An Observer System for Optimizing Small-Cell Deployment in 2-Tier HetNets".
- (c) Dorathy O Abonyi, Jonathan M Rigelsford, "Localization Algorithm For Optimizing Small-Cell Deployment in 2-Tier HetNets".

## **1.6 Thesis Outline**

Chapter 1 is an introduction to the research which includes motivation, problem statement and the objective to meet up with in this research. Chapter 2 is a review of the literature within the research area, Chapter 3 presents the system block diagram and the models of the individual components as well as the system simulation which shows the possibility of this system working in real sense. Chapter 4 is the system hardware implementation and Chapter 5 is the experimental validation in both indoor and outdoor scenarios. Chapter 6 concludes the thesis and draws attention to future work.



# Chapter 2

## Literature Review

### 2.1 Introduction

Right from the beginning of mankind, man has always been inquisitive of finding where things are in the universe. The birth of wireless technology and the onset of world war II promoted the technology of finding objects popularly known as localization. The very popular and foremost technology was applied in radar systems for military tracking of enemy ships and aeroplanes. From this, other localization technologies using mobile phones and other radio devices emerged. This chapter looks at the technology of wireless networks, capacity requirements/improvement and then localization itself. It also reviews literature on phased array antennas, beam steering and phase shifters.

### 2.2 Overview of Wireless Networks

Wireless networks are one of the most transforming technology of the past decade enabling unprecedented connectivity, user convenience and mobility [25]. Users are able to access all on-line services (email, web browsing etc) regardless of location, time or circumstances. Users at present are proactive about finding wireless network connectivity like looking for a wifi hotspot to connect to but the future wireless network looks forward to an omnipresent connectivity. Due to different multiple use cases and applications of wireless networks, many wireless technology exist. These include; WiFi, Bluetooth, ZigBee, Near Field Communication (NFC), earlier 3G standards, Worldwide Interoperability for Microwave Access (WiMAX), Long-Term Evolution (LTE), High Speed Packet Access (HSPA), Long-Term Evolution Advance (LTE-A), 5G, Evolution-Data Optimized (EV-DO), satellite services etc. Notwithstanding the diversity, most wireless technologies operate on common principles, have common trade-offs, and are subject to common performance criteria and constraints. Although the mechanics of data delivery through radio communication are

fundamentally different, all applications perform well creating the same user experience. This section explores some wireless technologies and their standards with more interest on using small cell to improve capacity.

### 2.2.1 Types of Wireless Network

Communication between devices in wireless network is achieved using electromagnetic waves like radio frequencies (RF), infra-red etc. Within the radio communication platform, there are different technologies designed for use at different scales, topologies, and for different applications as summarized in Table 2.1. Global technological specifications and standards are made by Institute of Electrical and Electronics Engineers (IEEE) and wireless work group is IEEE 802, they develop and maintain networking standards and recommend practices for local, metropolitan, and other area networks.

**Table 2.1 Common Types of Wireless Network**

Type	Range	Applications	Standards
Personal area network (PAN)	Within reach of a person	Cable replacement for peripherals	Bluetooth (IEEE 802.15.1), ZigBee (IEEE 802.15.4) , Near Field Communication (NFC)
Local area network (LAN)	Within a building or campus	Wireless extension of wired network	IEEE 802.11 (WiFi)
Metropolitan area network (MAN)	Within a city	Wireless inter-network connectivity	IEEE 802.15 (WiMAX)
Wide area network (WAN)	Worldwide	Wireless network access	Cellular (UMTS, LTE, etc.)

### 2.2.2 Cellular Networks

A Cellular network is a type of wireless area network which achieve long range wireless connectivity using cells, each served by at least one fixed-location transceiver called the base station (BS). Cellular communication technology has many technical standards, which are named according to their generation, such as 1G, 2G, 3G, 4G and 5G with increasing data rates.

Improving capacity using small cells in cellular networks started with 1G when analog Advanced Mobile Phone Service (AMPS) operators deployed micro-cells of 100 meter radius and inter-cell distance of 200 meters at the corners of nearby cities in North America. This provided a good solution to traffic and customer satisfaction was assured but it was quite expensive [26]. GSM (2G) provided a lower cost solution with better performance using extra spectrum, high spectrum efficiency and frequency reuse capability thereby reducing the

---

need for small cells [27, 28]. A laptop size 2G pico-cell BTS existed. Technological advances for efficient spectrum usage such as MIMO and high order modulation were alternatives that delayed the expansion of small cells during this time. On the other hand, small cell required excessively high operational expenditure requiring leased line for backhaul. Moreover at this time there was limited traffic pressure for mobile broadband to necessitate the need for small cells. Small cells in 3G needed an entire carrier to operate but operator had only limited carriers. At this time, small cells were seen as an offload technique but in 4G, the principle of heterogeneous network (HetNet) was introduced where the mobile network is constructed with layers of small and large cells from where small cells became popular [29].

LTE and LTE-A are the driving force for small cells. A major requirement in 3GPP Release 12 was the need to support rapid increase in mobile data usage [30] of which small cells for LTE was one of the resolutions. Three main purposes for small cell deployment in LTE and LTE-A are first to increase capacity density in areas with high user densities mostly in (indoor) public places, dense urban areas and inside buildings with a high subscriber density [31]. Second, to improve coverage and thus available data rates and service quality in user-dense, marginal-coverage areas that cannot be adequately reached by macro cells such as at cell edges or in “black spots,” both outdoors and indoors [32]. Third, to extend handset battery life raised up by higher-order modulations, broader bandwidth, MIMO, and enhanced processor power. The energy efficiency of small cell deployment was analysed in [33].

### **2.2.3 Wireless Network Deployment**

To deploy a wireless network, first operators decide the type of wireless network to be deployed by considering expected number of users to serve, type of traffic, the amount of throughput to provide and the number of access points or cells needed and placement positions to achieve optimal coverage. This is done by interviewing stakeholders or by using network monitoring tool. This enables the operator to gather information about the goals and expected uses of the wireless network. Secondly, the operator carries out a predictive site survey using a planning tool to estimate how many APs or cells are needed, where to place them and the required power levels to set so as to meet the coverage and capacity requirements. Lastly a manual real-time site survey is carried out to verify the accuracy of predictive survey to the real environment of application. Necessary adjustments are then made to realize the network design goals and deliver a wireless solution that meets the level of service required. This traditional network deployment strategy results in a well organized uniform cell/AP of Figure 2.1 known as a homogeneous network [34] which is not a sufficient solution for capacity in present day wireless networks. A homogeneous network is therefore a network with the same access technology like a cellular network of

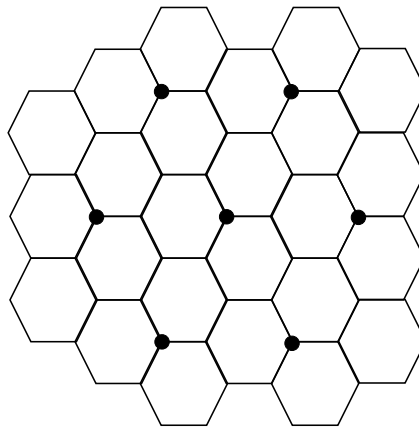


**Fig. 2.1** *Traditional homogeneous network*

only macrocells or a network of only WiFi. An improved performance in homogeneous network using reconfigurable antennas that switches between narrow beam and wide beam was explored in [35].

#### **2.2.4 Heterogeneous Networks**

A heterogeneous network (HetNet) is a network with different formats of base stations, access technologies and power levels. For example, a Wide Area Network that uses macrocells, picocells, and/or femtocells in order to offer wireless coverage in an environment with a wide variety of wireless coverage zones, ranging from an open outdoor environment to office buildings, homes, and underground areas as shown in Figure 2.2 is referred to as a HetNet. These low power nodes are overlaid on existing cells of homogeneous network to achieve higher coverage and capacity as well as proximity between transmitter and receiver ensuring a better QoS [36]. Different tiers of HetNet exist, while macro cells are used to provide coverage, pico cells and micro cells are used to enhance capacity in busy and hotspot areas. Femto cells and Wi-Fi are used at the offices and at homes. Deployment of these low power cells are key feature of the HetNet approach as they are flexible with their placement positions. Wi-Fi plays a significant role in HetNets, both in terms of data offload and in terms of roaming, especially between an outdoor and indoor environments. Proper cell planning is required to ensure optimal performance in a HetNet.

Cell planning optimization is driven by three main factors which include, interference, radio propagation and user locations [37]. A considerable amount of work has focused on resource management and interference mitigation in heterogeneous networks [38, 39]. Modeling techniques that are used for optimized cellular network include:

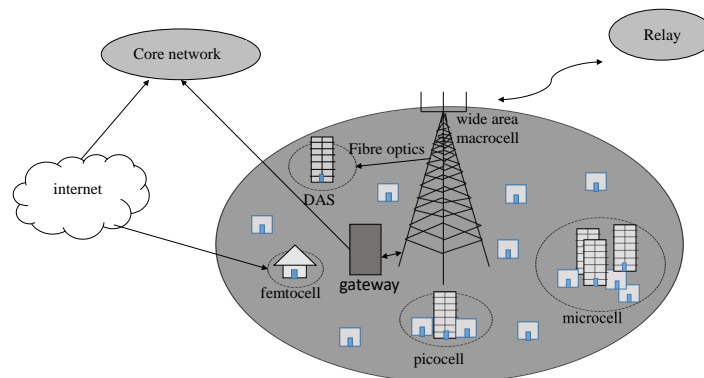


**Fig. 2.2 Heterogeneous Network: A mixture of high power macrocell and low power small cells**

1. Monte-Carlo multi-cell model which is a simulation based approach involving multi-effect which cannot be easily described using mathematical functions like pathloss models, antenna patterns, ray tracing, terrain, cluster and specific cell configuration data. A large volume of data is required to model a specific site. The Monte-Carlo simulation model is used with detailed terrain maps and ray-tracing pathloss model so that given a set of possible small cell deployment locations, the optimal positions are determined using any of the optimization techniques like integer programming, genetic programming or simulated annealing. Monte-Carlo simulation approach was described in [40].
2. Stochastic geometry model which is a statistical approach used to capture network performance in a non-uniform network deployment scenario. In this approach, only stochastic effects which are mathematically resolvable are included. A tutorial description of this approach is presented in [41].
3. Single cell linear model which is a deterministic model that captures the performance of a single cell in a multi-cell network [42]. In this approach only a dominating interfering BS is considered which gives it a limitation.
4. Automated small cell deployment position approach which uses knowledge of existing cell, user locations and the propagation environment to develop an algorithm that determines the optimal location for new small cell deployment in HetNets. This is the state-of-art approach. The work in [43] presented a theoretical solution where a closed-form mathematical expression that maximizes the throughput given some key statistical parameters of the network was derived. Another theoretical solution was

presented in [42] where a theoretical framework that considers the effect of interference and capacity saturation to determine the optimal small cell deployment positions was presented. The work presented in [37] focused on optimizing the cell deployment location based on the interference pattern for a given user distribution and propagation model. By simulation with real network data, this researcher found out that network degradation occurs when optimal small cell deployment is not determined but an intelligent HetNet with low complexity results when optimum positions are known prior to deployment.

These and other recent works [44–46] have presented theoretical optimization solution for automated small cell deployment in HetNet. Non of these approaches have given a practical solution that will help network operators to be able to determine optimum positions for small cell deployment with less latency in deployment decision taking.

### **2.2.5 WiFi Networks**

WiFi is a WLAN protocol based on the 802.11 IEEE network standard, operating in the 2.4 and 5 GHz Industrial, Scientific and Medical (ISM) radio bands. It is the most popular means of wireless data communication. To keep up with capacity requirement driven by more users and traffic requirement, there has been a constant improvement on the technology resulting in different existing protocols as summarized in Table 2.2. WiFi has a range of approximately 70 meters. With continuous increase in deployment of WiFi hotspots in both home and public indoor environments, indoor localization using WiFi infrastructures is being intensively studied [47–50]. Wifi networks are deployed in hotspots, where there are multiple users like in hotels, airports, coffee shops etc. Hotspots are generally owned by Wireless service providers (WSP) and technically they consist of one or several wireless access points (APs) installed inside buildings and/or adjoining outdoor areas.

Access points are small physical devices consisting of radio transceivers, antennas and device firmware closely resembling home broadband routers. Wireless routers used for home networking have these access points built into the hardware, and can work together with standalone AP units. These APs are typically networked to printers and/or a shared high-speed Internet connections. While most homes only require one wireless router (AP) to cover the physical space, businesses need many APs. Determining the optimal locations for where to install an AP can be a challenging task even for network professionals due to the need to cover spaces with a reliable signal. A WiFi AP deployment model was proposed in [51] where using generic algorithm multiple objective decision-making problem were solved addressing AP types, cost and instances of multiple APs. With the proposed system in this research, WiFi operators will be able to identify locations of high user concentration

for optimum deployment of APs. On the other hand this system can also be used for room location of users indoors for elderly tracking if implemented on WiFi AP.

Table 2.2 shows the different wifi protocols with their different data rates [52]. 802.11n is the most widely available of the standards and is backward compatible with a, b and g. The shown data rates are theoretical and gets a lot lower in practice. For instance, even though 802.11g can theoretically handle up to 54 megabits of data per second, it only achieves real-world speeds of about 24 megabits of data per second because of network congestion. Also 802.11n can transmit up to four streams of data, each at a maximum of 150 megabits per second, but most routers only allow for two or three streams.

**Table 2.2 Wifi protocols and data rate**

Protocol	Frequency	Maximum data rate
802.11ac wave2	5 GHz	1.73 Gbps
802.11ac wave1	5 GHz	866.7 Mbps
802.11n	2.4 , 5 GHz	450 Mbps
802.11g	2.4 GHz	54 Mbps
802.11a	5 GHz	54 Mbps
802.11b	2.4 GHz	11 Mbps

Several devices with wifi adapter can connect to the Internet via one router. This connection is convenient, virtually invisible and fairly reliable; however, if the router fails or if too many people try to use high-bandwidth applications at the same time, users can experience interference or lose their connections. To avoid this, there is need to offload traffic from congested APs by deploying more APs in the appropriate locations and to ensure balanced loading of the network. This is important as cellular network Operators are exploring WiFi as a complementary technology and an extension of their network to help offload traffic from existing network infrastructure [53].

### **2.2.6 Internet of Things Technology**

Internet of Things (IoT) is a new approach to wireless communication where numerous devices are interconnected using different wireless communication technologies like WiFi, bluetooth, ZigBee and cellular network all together to make the world a smart and small place, closing the gap of distance. LoRaWAN is a low power WAN technology that appears promising for Internet of Things. In a LoRaWAN, thousands to millions of smart devices are connected to the gateway through only one hop of connectivity [54]. A good architecture for IoT technology is shown and explained in [55] and an overview of bluetooth technology was explored in [56]. The IoT concept is very popular these days because of the availability of low power, low cost sensor nodes and their numerous applications like different system man-

agement like street light, building, parking, energy efficiency, fire fighting, home automation, personal assistant system, smart lighting solution, weather monitoring, agriculture, smart city, sports etc [57, 58]. In all these applications, numerous sensors are distributed around the coverage space and then linked in chunks of mesh network with APs to communicate with the sensors and extend data to the coordinator/gateway or to another AP. The target is that all sensors in the network transmit their data through to the gateway which takes the data over to the Internet. If an AP is overloaded, data is lost, therefore, monitoring the network to identify locations where more APs are needed would reduce the risk of data loss.

### 2.2.7 Capacity and Coverage in Wireless Networks

In wireless networks, capacity also known as throughput is the maximum amount of data that can be transferred between network locations over a link or network path. Capacity is dependent on the network engineering, services rendered to subscriber and the rate of network usage. Shannon's information theory states the amount of information a channel can carry as:

$$C = B \log_2(1 + S/N) \quad (2.1)$$

where C is the maximum capacity of the channel in bits/second, B is the bandwidth of the channel in Hertz, S is the signal power and N is the noise power, both in Watts. Equation (2.1) shows that the maximum rate at which information can be transmitted without any error is limited by the bandwidth, the signal level, and the noise level. It was shown in [59] that the communication distance to maximize network capacity depended on user density.

Coverage is the physical geographical area where the radio signal is usable. Coverage is dependent on the power settings which are Country dependent, antenna gain, and the physical environment. In any wireless network deployment, one major task is setting coverage and capacity goals. This is done by creating a predictive model that calculates how many access points (APs) that is needed and where to place them to satisfy those goals within the physical environment of the site. The accuracy of predictions is also verified by performing a manual site survey, and then making any adjustments as necessary. This of course equates to the traditional network strategy.

### 2.2.8 Capacity Enhancing Techniques

Capacity and hence coverage in any wireless network can be improved by buying more radio spectrum, making a more efficient use of available spectrum by applying more sophisticated technology that will increase the throughput capacity of each spectrum band within a given geographic area or by using a more effective topology in the form of cell densification that will allow for more and better intensive geographic reuse of spectrum. Network densifi-

cation is the current option and basically means adding more cell sites to increase the amount of available capacity. Cell sites, strategically placed in capacity-strained areas, add more capacity where it is most needed and also help offload traffic from surrounding sites. Urban areas and large public venues are primary candidates for network densification because of the high concentration of mobile users.

### **Radio Spectrum For Capacity Improvement**

Equation (2.1) show a linear relationship between the bandwidth and the channel capacity, therefore increasing radio bandwidth will increase the capacity. Radio Spectrum (3Hz - 3THz) used for wireless communication is managed by Government and it is assigned through licensing. There are some licensed-exempt spectrum like Industrial, Scientific and Medical radio band (ISM) which are free to use. Spectrum are not readily available and when available it is auctioned by government agency at a very expensive rate [59]. The use of cognitive radio for spectrum expansion was discussed in [60]. The ISM spectrum is getting congested due to expanded usage and so it is prone to interferences.

### **Technologies for Capacity Improvement**

Another approach to capacity enhancement is on the technology like use of additional antennas in the form of cell sectorisation or multiple antennas like Multiple Input Multiple Output (MIMO) [61]. As a general rule network capacity is proportional to the number of transmitters. Multiple antennas are used to create multiple cells or sectors, or to create multiple 'MIMO layers' thereby re-using the spectral resource multiple times from the same cell site. Provided these are orthogonal and do not interfere with each other, capacity increases linearly. Significant spectrum efficiency gains can be achieved with MIMO but multiple antennas are required on both the base station as well as mobile device which is a very big challenge. Enhanced modulation and coding efficiency [62] is another technology approach to expanding spectrum. Coordinated Multipoint and Cloud radio access network (RAN) which involves joint signal processing at different sites to transform interference into useful signal [63] is another approach. A fast and low latency interconnection (like optic-fibre) between sites is required. Carrier Aggregation [64] allows devices to access multiple increments of spectrum, potentially in multiple bands, facilitates re-farming of existing spectrum and increases effective device bandwidth which can extend coverage. This approach does not directly increase available supply of capacity but just access to the available spectrum. Also device support is limited to specific band combinations and RF performance is less than a single band solution. Even though the use of more antennas give higher spectral efficiency, it incurs higher site costs and doubling the number of antennas does not necessarily double the spectral efficiency.

### **Improved Cell Topology For Capacity Improvement**

The third main approach to capacity enhancement is by cell densification [65] which can be by adding more macrocells or by offloading of traffic from existing macrocell using small cells like microcell, picocell or femtocells or by using WiFi networks. The difficulty in finding a suitable site and the cost of implementing more macrocells is a challenge and so small cells are better option. Small cells are of two types, customer or enterprise managed small cell (indoor femtocell) and network operator managed small cells (micro, pico, femto cells) [21]. Deploying femtocells and using WiFi are suitable for offloading indoor traffic which constitutes a large proportion of current and expected total demand. Femtocells have the advantage of being targeted and deployed in specific areas of need and uses licensed spectrum giving operators sole management of the network. Micro and pico cells are deployed outdoors to offload traffic from the existing macrocell. Extensive use of outdoors is a cost effective means of supplying capacity to hotspots but also have a major challenge of operators being unable to establish the locations of hotspots having in mind that they may significantly change location with time. Small cell can also be used to extend coverage to small settlements in rural areas. Networks densification is the hope for future network capacity requirement [66] and it has good energy saving capability [67]. This approach is supported by all mobile devices and it improves both capacity, coverage and user experience. The challenges are interference between small cells (co-tier) and interference between small cells and macro cell (cross-tier) [68], mobility coordination with the umbrella macrocell and other small cells [69], the availability of suitable back-haul and maintaining or increasing the proportion of offload with time. Interference mitigation was discussed in [70, 71]. The simplest approach to interference management in a HetNet is by carrier partitioning in which case cells of different tiers occupy different carriers. For instance a macro-pico HetNet where the macrocell is deployed on a frequency band of say 800MHz and picocells are deployed at 3.5GHz. In this case, the carrier allocation difference takes care of the interference between the HetNet tiers. Another major challenge is the difficulty in targeting these cells in the most needed locations so as to reduce the cost effectiveness. Network densification has an upper limit beyond which densification becomes destructive or cost-ineffective. This limit is dependent on properties of the channel power distribution, noise level, and pathloss [72]. Well targeted small cell will ensure a good management of this limit.

#### **2.2.9 Small Cell Deployment**

Small cell is a general term that refers to the network operator-controlled, low powered radio communication base stations that provide both voice and Internet data services within

---

a localized area. Small cells encompass different technologies and are deployed to solve network capacity issues in a relatively small area like hotspots or an important zone that is a subset of the umbrella macro site coverage. It also serves to offload traffic from the macrocell and save mobile device energy by bringing the network closer to the user. They occupy small space and operators use them to support more users per square kilometer ensuring fewer blocked calls and more consistent data speeds in highly user concentrated areas. Initially small cells were deployed as a Passive Distributed Antenna System (DAS) which works by taking a donor feed from the macrocell and distributing it over fibre throughout a building or outside space [73]. A dedicated radio base station connected to a DAS ensures both coverage and capacity, enhancing the quality of both voice and data services. It is also a highly effective and efficient way to distribute wireless connections inside a large building and eliminate dead zones. In large campus areas, malls and airports where passive DAS has practical limitations in terms of scalability, active DAS are considered. Active DAS is an optical repeater that converts electrical signals into optical signals for wider reach. At the receiving end, it translates optical signals back into electromagnetic waves in a selective manner.

Recent small cells refer to the low-power radio technologies like integrated micro, pico or femto base stations that operators deploy for localized capacity and coverage solutions. These small cells are overlaid within the macrocells to form a HetNet. Strategies proposed in literature for small cell deployment can be broadly classified as Random Small-cell Deployment Strategy (RSDS) and Deterministic Small-cell Deployment Strategy (DSDS). In RSDS, small cells are randomly deployed within the macrocell while in DSDS, the position for small cell deployment is determined based on some standing factors. In most cases, RSDS is used as a benchmark to test the performance of other strategies. The network performance for DSDS and RSDS were compared in [74] and their result indicates that DSDS is a better option. DSDS can further be classified into uniform distributed small cell strategy (UDC), Cell on edge strategy (COE) and user aware deployment strategy (UAD). Uniformly distributed small cell deployment strategy follows a pre-determined pattern for all macrocells [75] as shown in Figure 2.3b. Small cells are arranged around the macrocell edge in COE as shown in Figure 2.3a and presented in [23].

User aware deployment strategy is presently based on long term traffic information as reported in [76]. This approach does not provide prompt solution to capacity and coverage in hotspots rather it depends on years of data collection and analysis. This approach does not solve the problem of unexpected hotspots. A mobile small cell deployment strategy for unexpected but reoccurring hotspot was proposed in [14] but with the assumption that

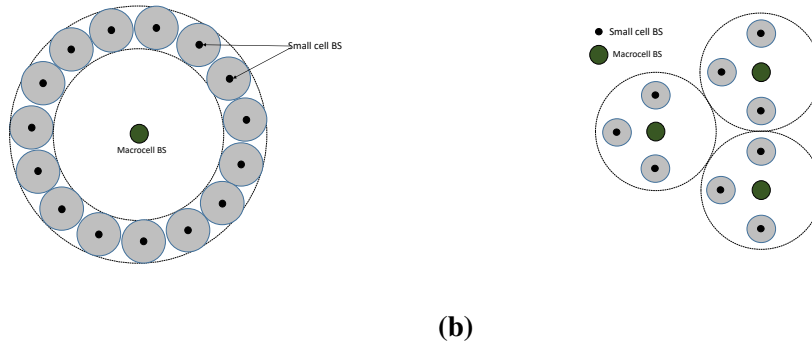


**Fig. 2.3** Some small cell deployment strategies (a) Cell edge (b) Uniform small cell deployment strategies

location of hotspot is known by network operator. It was shown in [77] that deploying small cell in hotspot locations optimizes network performance. Hotspots are locations of high demand and are characterized by high user concentration. Appropriately deployed small cell have been reported in [78] as the most efficient and cost-effective solution to capacity and coverage to localized hotspots but presented the challenge of mobile operators being able to identify the location of hotspot.

This research work fills the gap of identifying the locations of hotspots by proposing a simple localization system that can help the mobile operators to identify locations of hotspots for possible deployment of small cells.

## 2.3 Brief History of Tracking Systems

Our approach is based on locating users in space which is a technology that is anchored on the technology of tracking system. This area of technology has tremendously grown over the years and has progressively expanded in applications. We therefore in this section, explore the history of where this tracking technology started and how it grew to the popular indoor and outdoor localization systems, a summary of which is shown in Figure 2.4.

### 2.3.1 Radar

The idea of tracking was based on the theory proposed by Maxwell in 1864 [79] which state that radio wave can be reflected by a metallic surface and refracted by a dielectric medium. The first demonstration to prove this theory was performed by Heinrich Hertz's between 1885 and 1889 [80]. Based on this, early bi-static radar which consists of a transmitter located at a considerable distance from the receiver emerged [81]. Detection of target was achieved when transmitted radio wave is reflected by a target and received by the

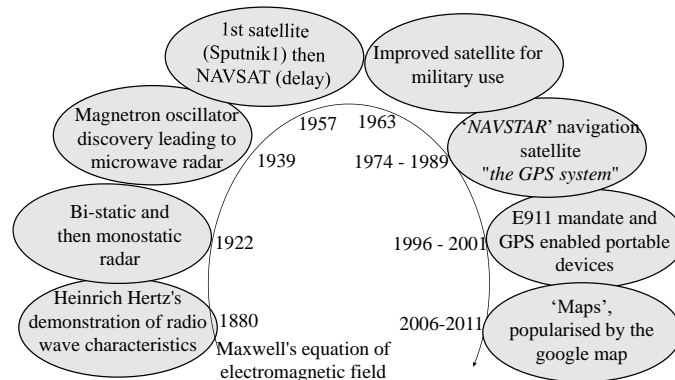


**Fig. 2.4 Some milestone in the history of tracking technology**

receiver. Discovery of the capability of a single antenna to work on both transmit and receive mode gave birth to mono-static radar which uses the same antenna for both [82, 83].

Prior to World War II, all successful radar systems were in the VHF band and was associated with problems of broad beam width causing low accuracy, less resolution, presence of unwanted echoes on received signal. Secondly, the VHF portion of the electromagnetic spectrum does not permit the wide bandwidths required for the short pulses that allow for greater accuracy in range determination and also VHF is subject to atmospheric noise, which limits receiver sensitivity. Radar developers desired the operation of radar at higher frequencies with the knowledge that narrow beam can be achieved without an excessively large antenna.

High frequency radar emerged with the invention of microwave radar. The technology of this radar was based on the invention of cavity magnetron oscillator at the University of Birmingham in 1939. The magnetron is a high-powered vacuum tube, that works as self-excited microwave oscillator producing the high-power output that is used in radar transmitters as either pulsed or continuous waveform (CW) oscillators at frequencies ranging from approximately 600 to 30,000 MHz. The disadvantage was that Magnetron usually can work only on a constructively fixed frequency. Review on progress in this area is well explained in [84]. Some important publications that lead to significant progress in radar development was made in 1950's on some theories like statistical theory for detection of signals in noise [85], matched filter theory which showed how to configure a radar receiver to maximize detection of weak signals [86], Woodward ambiguity theory [87] which made clear the trade-offs in waveform design for good range and radial velocity measurement and resolution. With the emergence of digital technology which made signal and data processing applicable, radar systems like highly accurate monopulse tracking radar [88] emerged. Most

recent work in this area are on radar millimeter-wave (30GHz to 300GHz) such as [89] which operates at a frequency between 78GHz and 92GHz with a resolution of 6mm.

### **2.3.2 Global Positioning System (GPS)**

A new era of technological development was ushered in with the launch of world's first ever artificial satellite, Sputnik 1 in October 4, 1957 which gave birth to space technology. In 1959, the first operational satellite navigation system, 'TRANSIT' a.k.a NAVSAT or NNSS (Navy Navigation Satellite System) was built by the navy for location of submarines. There was delays in signal reception from this system which was a major problem. Therefore, there was need for a satellite system that would continuously send signal to receivers on earth surface. This was achieved in 1963 by Aerospace Corporation in their study for the military [90]. With a functional space satellite continuously sending signal to earth, they came up with the concept of having GPS receivers on phone, vehicles and other devices to derive a precise set of location coordinates by measuring the transmission times of radio signals from satellites.

Another major breakthrough in tracking and localization was achieved by the birth of space technology. The launch of 27 operational GPS satellites in space (completed in 1995), 24 active and 3 spares in different orbits around the Earth gave room for global positioning system. The satellites, circled the globe twice a day and were situated such that at least four of them were visible from any place on earth at any time of day. GPS receiver is able to determine its location if it receives GPS signals from at least four satellites [91]. GPS was initially used by military only until year 2000 when GPS was extended to civilian use. By 2001, private companies began rolling out personal GPS products as GPS receiver technology got much smaller and cheaper. In 2004, a telecommunication equipment company, Qualcomm developed and tested "assisted GPS" technology allowing phones to use cellular signal in combination with GPS signal to locate user with high accuracy. This technique was applied in [92] for human and animal tracking. A GPS based taxi tracking system was proposed in 1993 [93] and today it has been implemented and efficiently working. GPS was also applied for soccer tracking in [94]. A technique for energy saving in GPS tracking systems was presented in [95]. A Russian version of GPS called Global Navigation Satellite System (GLONASS) with a network of 24 satellites also exist [96].

### **2.3.3 Other Location Based Services (LBS)**

In June 1996, United States government passed a mandate that emergency calls emanating from a mobile phone should deliver the caller location up to an accuracy of 125 m in 67 percent of all calls by October 31, 2001 [97]. This was termed the Enhanced 911 (E911). In effort to meet up with this mandate, mobile network operators came up with series of

location based services like delivering to users on request nearby restaurants or gas stations. In May, 2005, the Federal Communication Commission (FCC) required that Internet service providers who provide services for VoIP calls must provide E911 service for their customers [98]. The emergence of GPS-capable mobile devices, the advent of Web 2.0 paradigm, and the introduction of 3G broadband wireless services provided enabling environment for this application.

The technology of Location Based Services (LBS) were initially based on cell-ID using triangulation techniques, which suffered from low accuracy and only worked for users at cell edge. Soon they were replaced by GPS and then a combination of GPS and Cell-ID [99]. An overlay of geolocation technologies consisting of cellular and WiFi triangulations, in addition to low-power GPS receivers (assisted GPS), made it possible for location information to be available most of the time and with variable accuracies. The emergence of maps for mobile platforms [100, 101] further accelerated the widespread of LBS's with hundreds of powerful applications available today that are location/map based.

### 2.3.4 Localization In Wireless Networks

Localization in wireless network is the process of estimating the spatial coordinates of radio devices scattered at unknown positions in space from at least one anchor (beacon) node or a BS (coordinator node) of known location. Using the location stacks presented in [102], the main layers of any localization system can be summarized as shown in Figure 2.5. First

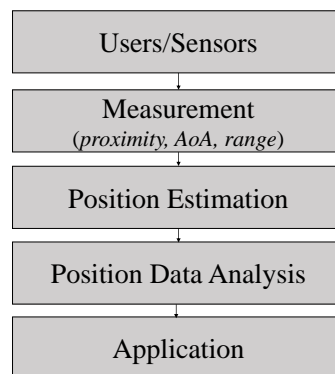


**Fig. 2.5** *Layers of a localization system*

layer in the case of cellular network is the users which is the user device having the ability to communicate (switched on) so that required RSS can be measured. In the case of RFID, IoT and other sensor based applications, sensors occur in this layer and should be capable of sensing the required physical or logical quantity. The output of this layer is a raw data that is used in the measurement layer (second layer) to estimate user proximity, AoA or range

with some level of uncertainty which is subject to measuring equipment and environment condition. Third layer is the position estimation stage where data from layer 2 is applied to estimate the position coordinates of users or sensors as the case may be. This stage applies different localization techniques like proximity sensing, triangulation, fingerprinting or a hybrid approach to determine user positions. The robustness, accuracy and reliability of any localization system is determined by layers 2 and 3 and so are considered as very important stages in any localization system [103]. On the fourth layer, the estimated user position is then resolved in accordance to a relative coordinate system to obtain an absolute or relative user position. The final layer is the application layer which applies the user absolute or relative position to achieve the purpose of its design. This stage involves three main actions, first the system relates gathered information with a threshold for instance to room temperature in the case of temperature sensing or to required number of users for small cell deployment. Second is the analysis of the comparison and then finally the system takes action if automated or sends a form of alert for action to be taken.

### **2.3.5 Localization Classification**

The emergence of GPS, E911 and sensor technology attracted many research interest to the area of localization resulting in different classifications of localization as presented;

#### **GPS based and GPS free Localization**

A GPS Based localization system involves a GPS receiver that receives the signal from the space satellites to locate its position in space. The space satellites transmit repeating signals indicating their current location and time and because the satellites have synchronized operations, these signals are transmitted at the same time. These signals traveling with the speed of light arrive at the GPS receiver at different times depending on the location of the satellites in orbit. Knowing the time the signal was transmitted and the time of arrival at the receiver, the receiver can estimate its distance from the satellite. When the receiver estimates its distance to at least four satellites, the receiver can then determine its own position in three dimensions using multilateration. With the GPS receiver attached to any object, that object can be located. This approach was applied in [104] for vehicle tracking, [105] for animal tracking and in [106] for delivery order system. In all these, they worked fine because they are all outdoor localization but unfortunately, GPS fails in indoor scenario [107] because it requires a line of sight communication between the transmitter and the receiver to work. In a fully GPS based localization system, all devices or users within the network have a GPS receiver and are able to locate their own position. This potentially makes the entire network very expensive. In order to reduce the cost of having a GPS receiver in all nodes, a few anchors are equipped with GPS receivers and are used to locally determine the locations of

---

other nodes [108]. In [109], mobile anchor nodes equipped with GPS receiver move around the coverage area broadcasting their location periodically, nodes with unknown locations on receiving the signal, calculate their position using the RSS received from the mobile anchor. In GPS based localization systems, cost increases with the number of anchor nodes needed to be equipped with a GPS receiver and on the other hand, if the anchor nodes are located indoors, accurate localization cannot be achieved. For cellular networks there are concerns about user privacy for GPS based localization systems. A GPS-free system does not require a GPS receiver rather user location is locally resolved using the cellular network or PAN. A GPS-free localization which is dependent on hop distance between neighbouring nodes was presented in [110]. In [111], distance vector hop (DV-hop) based algorithm was applied and with 2% better accuracy in [112]. A hybrid approach with neighbouring information as well as distance estimation was presented in [113].

#### **Anchor-based or Anchor-free Localization Technique**

Anchor-based localization techniques involve the use of one single anchor or multiple anchors of known positions to estimate the location of unknown nodes relative to anchor node position. In multiple anchor based localization, one approach involves placement of anchors in different corners of the coverage area to locate all sensor nodes using trilateration or fingerprinting [114]. Each anchor can be static or mobile [115]. Located nodes may be upgraded to anchor nodes and can locate the position of other sensor nodes in the network [116]. In a multiple anchor based scheme, accuracy highly depends on the number of anchor nodes. Both hardware and software complexity increase as the number of anchor nodes increases. The single anchor approach uses only one anchor node of known location, which can also be stationary [117] or mobile [118] to achieve localization. One approach is that the anchor broadcasts its position and the sensor nodes use the RSS of the signal received from the anchor node to estimate their positions relative to the position of the anchor node. Another is that the anchor nodes receive signals from sensor nodes and estimate their distances relative to its position. Anchor-free algorithms apply hop distance and can only estimate relative positions of nodes instead of computing absolute node positions [119]. In this approach, a network of distances between the reference anchor and users along the path to the unknown user position is determined and added up to obtain the location of unknown user [120]. Using this approach in most cases does not calculate the shortest path distance rather depends on the hop path which is subject to user that is ready to receive a packet at the time of transmission. This results to inaccuracy of range estimation when the path between anchor and user are not co-linear. Anchor free localization is mainly applied in sensor node localization where the

operator has deployed and is in control of all users. In cellular networks this approach is not practical.

### **Centralized or Distributed Localization**

Localization can also be classified based on where the localization computation algorithm is hosted. Centralized system utilize a central node or a base station that collects all the measurement data and performs the system localization estimation of all other sensor nodes. In distributed system, the sensor nodes estimate their positions individually and then communicate with the anchor node [121].

### **Area based and Point based Localization**

Localization algorithm can also be classified as area based or point based. In area based localization algorithm, a possible area location of a sensor node is returned as the location while in point based, a particular coordinate point of location of the node is returned as the possible location estimate of the node [122]. Area based algorithm has an advantage of being robust in describing localization uncertainty. This method can systematically describe trade-off of accuracy for precision. Accuracy in this case refers to the likelihood that the node is within a particular area location and precision describes the size of the returned area. With accuracy and precision, the limits of different localization approaches can be compared by observing the precision (less area) on localization accuracy. Point based accuracy in localization is not necessary for some applications like safety and information systems because switching between accessed area and un-accessed area is needed for a trigger to occur. Also for the purpose of small cell deployment, no exact point location is required. A point based algorithm is used when high precision is paramount like in health sector where the exact location of a cancerous or tumor cell [123] is required. It is a more complex approach because there is need to reduce error to almost zero value to be able to achieve desired result.

### **Range Free and Range Based Localization**

The range-based localization approach involves the knowledge of location of a base station node, a coordinator node or an anchor node from where the location of the target nodes are estimated. The signal received from the target node during this communication can be characterized by the time of arrival (TOA) [124] or time-difference-of arrival, (TDOA) [125] or its reduction in power as it propagates over distance (attenuation) in the form of received signal strength (RSS) [126]. This information can then be used to calculate the angle of arrival (AOA) [127] or the position [128]. Time dependent localization method require accurate clock synchronization which makes the system complex and difficult to implement. RSS-based localization system is simple and cheap requiring no extra hardware

---

or synchronization thereby making it popular in wireless sensor networks [129]. Range free is a proximity based localization method that determines the location of nodes using hop-counts or connectivity between nodes. The hop-count values between anchors and unknown nodes are transformed to distance information based on the computed average size of a hop (hop-distance). Complexity of range free method increases as the network coverage area increases so it is not ideal for large networks. On the other hand, if the hop path between start and end are not co-linear, the estimated distance is not the correct straight path distance. The advantage of RSS-based localization method is that the existing wireless infrastructure is being reused requiring no additional hardware.

### **Time Dependent and Non-time Dependent Localization**

This class defines the metric that is measured and used in localization algorithm to resolve node location. Time dependent approach involves measuring the time of arrival (TOA) [130] or time difference of arrival [131] of signal flight from transmitter to receiver. Non-time dependent approach involve measuring the received signal strength (RSS) of the signal that have been transmitted from transmitter to receiver. Time dependent approach requires high clock synchronization at all time because precision is highly dependent on the clock accuracy. On the other hand, because environment characteristics is not considered in time dependent approach, it is highly affected by multipath causing inaccuracy in range estimation. To improve localization performance, papers like [132] explored a hybrid approach of both TOA and RSS.

### **Indoor and Outdoor Localization**

The major reason for localization category into the indoor and outdoor localization is because the two cases have very different propagation requirements. The outdoor environment suffers from less signal propagation obstructions than the indoor environment. Localization in indoor scenario suffer from more obstructions that cause reflection, diffraction, multipath and scattering of the signal than in outdoor. Propagation modelling is more difficult indoor because of all these effects but there are some path loss models that have been developed to take care of walls and floor losses for approximate modelling of signal propagation in indoor environment. Due to the unpredictable nature of the losses in signal within the indoor environment, researchers tried to investigate if RSS is a good metric for localization indoors. It was presented that indoor localization can be achieved within a certain regional space using RSS [133]. In other to reduce the effect of these interfering signals in indoor, [134] proposed an expanded RSS approach to localization where RSS was expanded to  $\pm 5\text{dB}$  to achieve a more accurate localization result. The most popular localization technique for outdoor scenario is the GPS based localization. This is because it is an existing technology

and have been certified to provide accurate localization in outdoor environment. GPS free localization using RSS has also been used for outdoor. [135] proposed a model that describe the relationship between mean value and the RSS data error for possible application in outdoor WSN localization. Investigation of the applicability of RSS based localization in outdoor scenario was investigated in [136] showing that RSS can be used in outdoor localization when well defined topology constraints is applied. RSS have also been extensively used for indoor localization but in most cases using fingerprinting approach [137, 138].

## 2.4 Antenna Systems

In wireless communication, antennas are a means of coupling the transmitter to a receiver using free space as a medium of propagation. Antennas can be omni-directional or directional. The radiated energy of an antenna is characterized by its radiation pattern which is the graphical representation of the radiation properties of the antenna as a function of spherical coordinates  $(\theta, \phi)$ . There are three radiating regions of an antenna; the reactive Near Field, radiating Near Field (Fresnel) and the far-field (Fraunhofer) regions. Figure 2.6 shows these regions and their extent, where  $r$  is the radius,  $D$  is the largest dimension of the antenna and  $\lambda$  is the wavelength. The near field region is predominantly reactive (non-radiating), has all three components in spherical coordinates  $(r, \theta, \phi)$  and decays as  $1/r^3$ .

The radiating field begins to dominate just beyond the reactive field. The radiating near-field region, is divided into two sub-regions as shown in Figure 2.6. In this region, fields decay more rapidly than  $1/r$  and the radiation pattern is dependent on  $r$ . Beyond the radiating near-field region, the field becomes only radiating and has only two components in spherical coordinates  $(\theta, \phi)$ . The fields decay as  $1/r$  and the radiation pattern is independent of  $r$ . In wireless communication, the far field region is where the antenna is operational and the radiation pattern does not change shape with distance. The direction of propagation in this region is that of a plane wave i.e. wave with constant frequency and amplitude with an infinite wavefront. The far field conditions are  $r > 2D^2/\lambda$ ,  $r \gg D$  and  $r \gg \lambda$ , therefore for a half-wave dipole, a radius,  $r \geq 10\lambda$  which is approximately 1m for 2.45GHz frequency is considered as far-field.

An antenna can be omni-directional or directional. Omni-directional antenna is an antenna that radiates its energy equally in all directions. The simplest though not practical type is the isotropic antenna which is used as a reference antenna to quantify other antennas. The simplest and most popular practical omni-directional antenna is a half-wave dipole which has a gain of approximately 2.14dB above isotropic in all angular directions on azimuth plane. When a dipole antenna is mounted so that it is vertically oriented with respect to

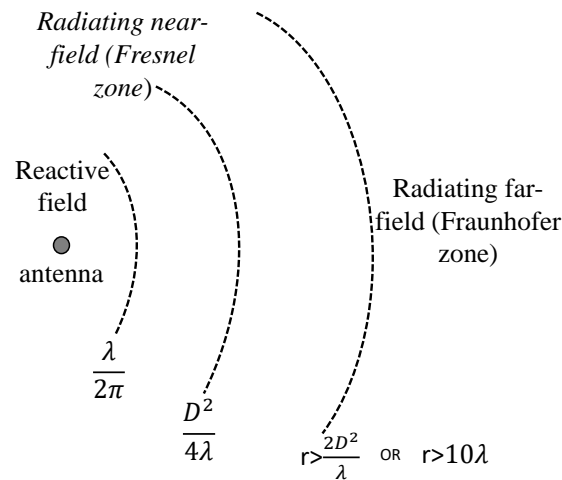


**Fig. 2.6 Radiating field regions**

ground, maximum energy is radiated toward the intended coverage area and nulls pointing up and down producing a toroidal pattern.

A directional antenna or beam antenna is an antenna which radiates or receives greater power in specific directions allowing for increased performance and reduced interference from unwanted sources. For satellite and space applications, antenna directionality matters in both azimuth and elevation plane, but in most terrestrial wireless communications applications, directionality only matters in azimuth or horizontal plane. The dish is the most common directional antenna for consumer applications normally used for satellite communications. Yagi-uda [139], quad [140] and helical [141] antennas are other types of directional antennas. Multiple omni-directional antennas can be combined in an array to obtain a directional beam [142]. A common application of antenna array is in a smart antenna system that focuses its main beam in direction of interest. This is the method adopted for the proposed system.

### 2.4.1 Antenna Array

An antenna array is two to thousands of antenna elements that are so spaced and phased such that the individual element's contributions add constructively in one direction and destructively in another direction. These element clusters are used in applications where a single antenna element does not meet the required gain and radiation pattern. Common geometries for antenna arrays are linear, planar, circular or conformal. The arrangement can be in one or two dimension [143]. Common elements used in an antenna array systems are dipoles, monopoles, printed patch design or Yagi-uda. Every antenna exhibits a particular radiation pattern but when they are combined in an array, the overall radiation pattern changes due to the array factor (AF) which quantifies the effect of combining radiating elements without an account of the individual patterns. The overall array radiation pattern is

a combination of the array factor and the element radiation pattern. The array factor depends on the number of elements, the element spacing, amplitude and phase difference between the elements. The number of elements and the element spacing determine the aperture of the overall radiating structure. A typical antenna array system is characterized by multiple elements as shown in Figure 2.7 because array directivity increases with the number of elements. Unfortunately, the number of side lobes and the side lobe level increase as well. On

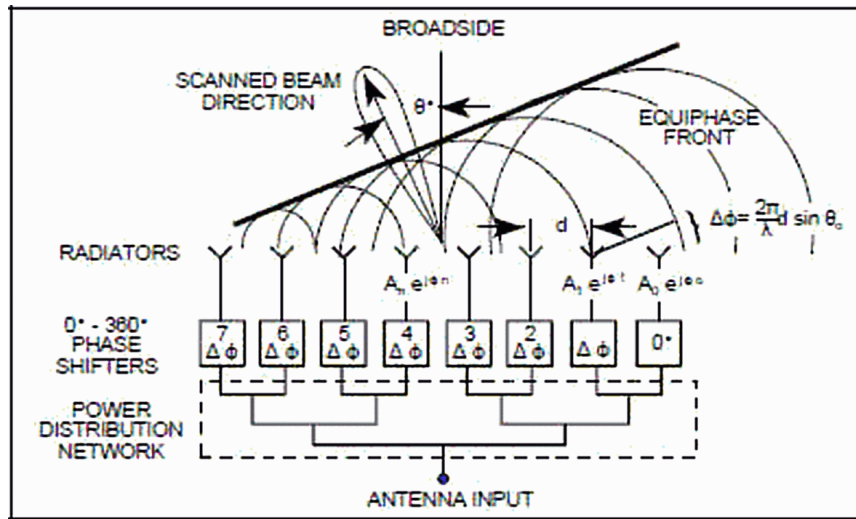


Fig. 2.7 Standard array system [144] used in adaptive smart antennas

the other hand, cost, size, and complexity also increase. The larger the element spacing the higher the directivity but then grating lobes which is an undesirable peak occurs. A grating lobe that is the same amplitude as the beam peak occur at element spacing that is equal to the wavelength beyond which the array becomes unusable due to multiple high grating lobes. For our system design, a precise location is not necessary for its application only a sector location is required. We will therefore choose only two antenna elements spaced by  $\lambda/2$  for reduced cost and complexity.

### 2.4.2 Broadside and Endfire Array

Two design approaches to antenna array are broadside and endfire array. A broadside array is the simplest form of array design and it is characterized by elements with uniform spacing, no phase difference and elements are fed with same power. Endfire array, are characterized with progressive phase difference between element in an array which makes the feeding network more complex. Considering two antenna elements in an array design, the normalized electric field at a point in far field is given by Equation (2.2) and 2.3 for

broadside and endfire designs respectively.

$$E = \cos((\pi/2) \cos \theta) \quad (2.2)$$

$$E = \sin((\pi/2) \cos \theta) \quad (2.3)$$

This gives a maximum radiation pattern at  $90^\circ$  and  $270^\circ$  nulls at  $0^\circ$  and  $180^\circ$  for broadside but a maximum radiation at  $0^\circ$  and  $180^\circ$  nulls at  $90^\circ$  and  $270^\circ$  for endfire. Figures 2.8a and 2.8b show the bi-directional radiation pattern of broadside and endfire design with main beam perpendicular to array orientation and in the same direction as the array orientation respectively. Just as expected from analytical calculations, two symmetric peaks are obtained

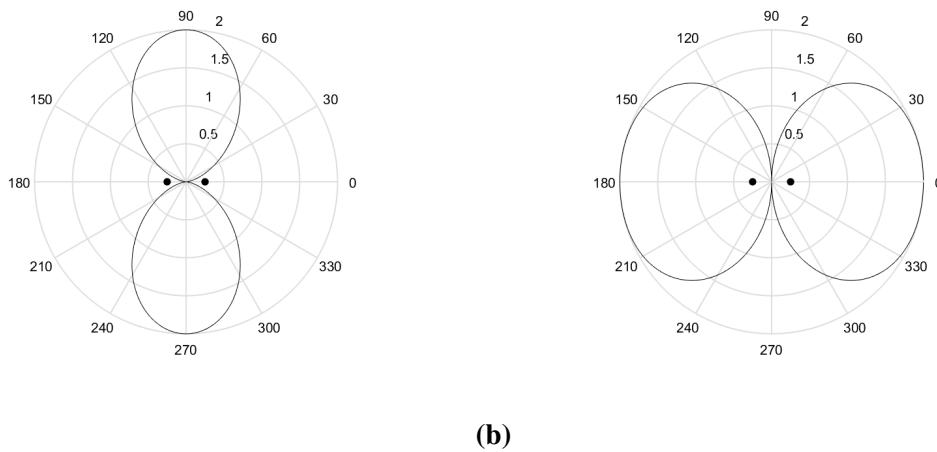


**Fig. 2.8** Radiation pattern for a 2 element array showing main beam on (a) broadside (b) end-fire

in each case. Broadside beam has a half power beamwidth of  $60^\circ$  as against the endfire design that has a beam width of  $120^\circ$ . For our design, broadside design is adopted and beam steering will be used to create azimuth positions at endfire and also between broadside and endfire.

### 2.4.3 Adaptive Antenna Systems

Adaptive antenna system are capable of steering the antenna main beam in the direction of signal of interest (SOI). Some can steer nulls in the direction of interference. These use multiple antennas in either a phased array, a mechanically steerable antenna or reconfigurable antenna system [114]. Mechanically steerable antenna systems involve the use of electromechanical devices such as stepper motor [145] to rotate the antenna main beam over coverage area. The additional hardware increases the overall cost and power consumption. Reconfigurable antennas are capable of dynamically modifying its frequency and bandwidth,

polarization or radiation pattern in a controlled and reversible manner. It works like a phased antenna system but often comprises of only a single antenna element [146]. In multiple antenna system, two or more antennas are used in an array to produce a beam that is electronically steered to multiple directions to receive signals and estimate the AOA and distance for localization [119]. Using multiple antennas is straight forward and adaptiveness can be achieved. One advantage of an adaptive antenna is that it improves signal-to-noise ratios (SNRs) by means of beam-forming techniques. Beam-forming operates by manipulating the amplitude and phase vector of two or more input signals to create modified output signals. In this case, instead of physically moving the antennas, the beam is steered electronically to ensure reception in a desired direction and a null in undesired direction.

Adaptive antenna can be switched beam or fully adaptive. Switched beam is a fixed beam approach where the beams are generated and fixed in different directions [147]. Switched beam require large implementation area and they are not capable of separating signal of interest from interfering signals. Therefore they are prone to be affected by noise and co-channel interference. In fully adaptive approaches, a main beam is produced and manipulated to the desired direction and nulls can be steered to undesired direction at any time. This can be achieved by using a phased array antenna system that manipulates the amplitude and phase of two or more signals arriving at the antenna system to form a vector of complex weight. Performance is characterized by the number of antenna elements, array geometry, antenna type and element spacing. Different antenna array structures have been proposed for localization estimations but the most common is the linear arrays geometry from where most other configurations emanate [148]. Normally multiple antenna elements are used to achieve localization. The more the antenna elements, the more complex the system and the more the cost of implementation. Adaptive localization is achieved with adaptive antenna system accompanied by an adaptive algorithm [118] or only an adaptive localization algorithm [149]. In general, the performance of an antenna array (for whatever application it is being used) increases with the number of elements in the array but unfortunately with increased cost, size, and complexity. Therefore, in this research, two antenna elements (only) will be studied.

#### **2.4.4 Antenna Array Feed Network**

Depending on the desired array characteristics, elements in an array are excited using amplitude/phase shift devices, or the feed network, or a combination of both. Three common feed networks are parallel, series and hybrid approach. In a parallel approach a.k.a corporate feed network, elements are feed from one source using parallel connections. This is achieved using RF power splitters or combiners. In a series fed network, elements are fed from one source using series connection so that as the signal travels from one antenna point to the other

from source, antennas tap the power resulting in an uneven power distribution among the antennas. At one wavelength transmission line length, the elements are fed with same phase at that frequency. By changing the frequency, electrical length of transmission line changes thereby changing the phase between elements. In this way frequency scanning method is applied to steer the broadside beam to other directions. Hybrid approach is a combination of both parallel and series approaches in one feed network for instance a series-fed groups of elements, fed by a common signal from a parallel feed structure.

Since the design in this research considers only two antenna elements, parallel or series feed networks are considered as two possible feed network configuration as shown in Figures 2.9a and 2.9b respectively. Series approach has an advantage of reduced losses because no phase shift devices are required but power fed to each antenna are unequal. For the design in this research, a broadside beam is adopted which requires that same power is fed to each element of the array. One advantage of a parallel feed network is that equal power is fed to all elements, therefore a parallel configuration is adopted.

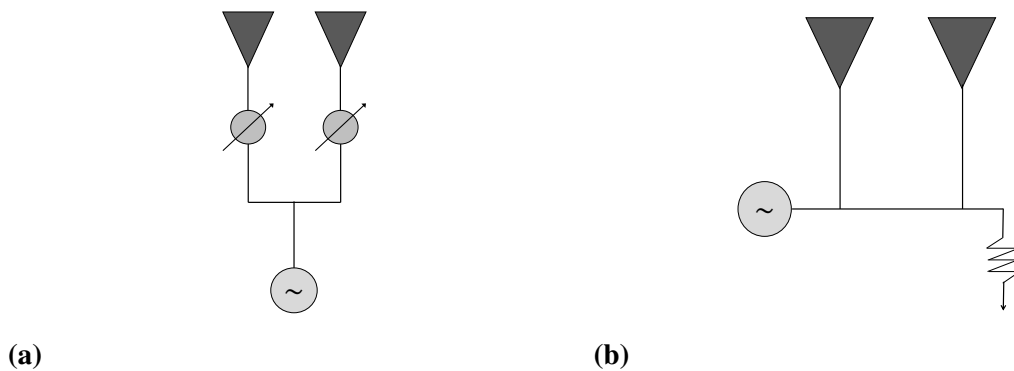


**Fig. 2.9 Possible antenna array feed networks for 2 element array system (a) parallel (b) series approaches**

Complexity of an array system is highly dependent on the feed network. Three main factors that contribute to the complexity of any feed network are; number of elements, the amplitude and/or phase distribution and the beam steering ability. Though an array with unequal power and phase distribution to the individual elements is used to modify the side lobe level, directivity and direction of the main lobe, arrays with equal power and phase distribution are simpler and easier to implement. Also a deep null is achieved when the amplitude ratio between the antenna elements is unity and this is only achieved when the signals arriving at both elements have equal amplitude. When power distribution is optimized to reduce side lobe levels [150], efficiency is reduced and when phase distribution is optimized [151] for beam steering, side lobe may occur. To keep our system simple and

less complex, we opted for minimum possible number of antenna elements, equal power and phase distribution and a simple electronic only-phase steering control with equal amplitude to ensure total cancellation at directions of no interest.

### 2.4.5 Two-Element Array System

Considering two dipole antennas separated by  $\lambda/2$  and vertically orientated along z-axis as shown in Figure 2.10. The aim is to focus the main beam on the direction of plane wave

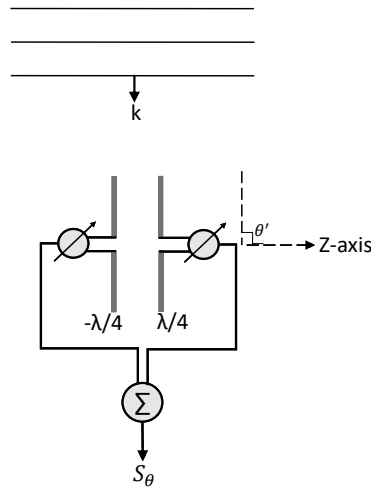


**Fig. 2.10** Two Dipole antenna array system showing plane wave arriving from broadside direction of interest

shown (broadside) which is at  $\theta' = 90^\circ$  from array axis. The field due to antennas 1 and 2 are proportional to their currents and has equal amplitude but different phases at far field so that the excitation current for antennas 1 and 2 is given by  $E_1/\beta_1^\circ$  and  $E_2/\beta_2^\circ$  respectively. Since both antennas are identical, current is supplied with equal amplitude and so the electric field generated by both elements are assumed to be equal,  $E_1 = E_2$ . The phase of each antenna comprises of two components, the current phase and the wave propagation phase so that the phase of the fields due to antennas 1 is given by and 2 is given  $\varphi_1 = kz_1 \cos 90 + \beta_1$  and that of antenna 2 is given by  $\varphi_2 = kz_2 \cos 90 + \beta_1$  where  $kz_i \cos \theta'$  is the propagation phase and  $\beta_i$  is the current phase of  $i^{th}$  antenna.  $z_i = (i - 1)d - ((n - 1)d/2)$  is the antenna position.  $k = (2\pi/\lambda)$  is the wave constant,  $\theta'$  is the angle of arrival of plane wave which is  $90^\circ$  for broadside.

The weight vector for this array is therefore given by (2.4).

$$w = \begin{bmatrix} e^{-j(\pi/2)\cos(90)+\beta_1} \\ e^{j(\pi/2)\cos(90)+\beta_2} \end{bmatrix} \quad (2.4)$$

The array factor,  $AF = w^T V(k)$  where  $V(k)$  is the steering vector given by Equation (2.5) for antennas 1 and 2.

$$V(k) = \begin{bmatrix} e^{j(\pi/2)\cos\theta} \\ e^{-j(\pi/2)\cos\theta} \end{bmatrix} \quad (2.5)$$

where  $\theta$  goes from  $0^\circ$  to  $180^\circ$ . The array output,  $S_\theta$  is the sum of the signal from each antenna and it is given by Equation (2.6).

$$S_\theta = \sum_{i=1}^n e^{j(kz_i \cos(90) + \beta_i)} \times e^{-jkz_i \cos\theta} \quad (2.6)$$

Using Equation (2.6), a broadside main beam is achieved at  $\beta_1 = \beta_2 = 0$ . At far field, the phase of signal incident on the antenna array is a function of the angle of arrival of the plane wave so that if the signals are added together, they may either add constructively or destructively depending on the phases. To receive a signal from any other desired direction,  $\theta'$ , the phases of antennas 1 and 2 are adjusted as pre-calculated in Section 2.5 to form a complex weight that multiplies the signal to cancel out the phase change due to propagation of the wave so that summation of the signal from both antennas will place the main beam in the new desired direction.

## 2.5 Delay and Sum Beam Steering

At same phase, the array produces a maximum radiation pattern perpendicular to the array axis i.e. broadside design. To steer the beam to other directions, left and right of broadside, antenna 1 is taken as the reference antenna and the amount of delay required for the wave to travel between the reference antenna and antenna 2 is calculated using the difference in distance,  $\Delta d$  as illustrated in Figure 2.11. The angle of arrival of the plane wave,  $\theta$  is the angle the wave makes with the reference antenna. For a focusing angle of  $135^\circ$  as shown in Figure 2.11a, a plane wave incident from angle  $135^\circ$  will arrive antenna 1 earlier than antenna 2, giving a difference in distance,  $\Delta d = d \sin\theta$ , where  $\theta$  is the angle of plane wave and  $d$  is the separation distance between both antennas. To make both antennas look like they are operating at the same phase, antenna 1 need to be delayed by  $\Delta d$  amount. Reverse is the case for a focusing angle of  $45^\circ$  where wave arrives antenna 2,  $d \sin\theta$  distance earlier than antenna 1 as in Figure 2.11b. Figures 2.11c and 2.11d show the focusing angles of  $180^\circ$  and  $0^\circ$  with antenna 1 leading and lagging respectively. To ensure a constructive interference at any focusing angle, the leading signal is delayed by calculated amount so that both signals arrive at same time giving the same effect as if they have equal phase.

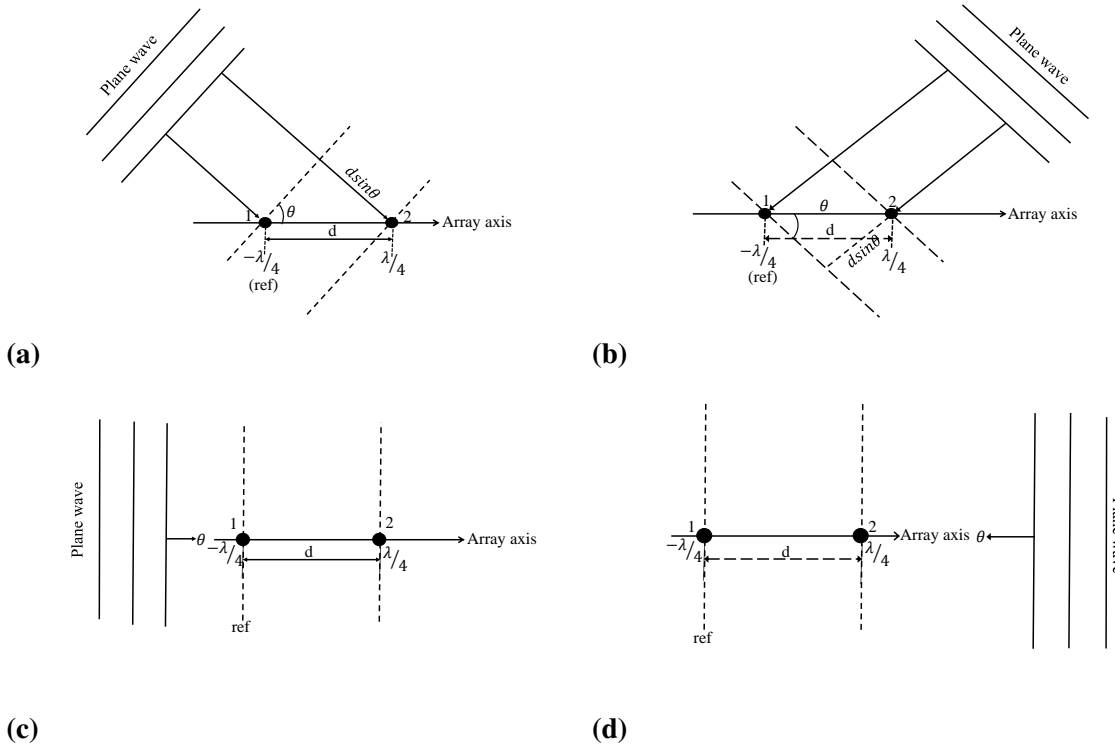


**Fig. 2.11** Required delay to steer main beam to positions (a)  $135^\circ$  (b)  $45^\circ$  (c)  $180^\circ$  (d)  $0^\circ$

### 2.5.1 Phase Delay Calculation

Phase delay,  $\Delta\phi$  between any two successive elements in an array system is the product of path difference and the wave constant as given by Equation (2.7). The Required phase delay of antenna 2 with respect to antenna 1 to achieve the desired look-in angles of  $-45^\circ$ ,  $45^\circ$ ,  $-90^\circ$  and  $90^\circ$  off broadside were calculated to obtain  $-127^\circ$ ,  $127^\circ$ ,  $-180^\circ$ ,  $180^\circ$  respectively. Based on this calculation, all antenna phase states for beam-forming and beam-steering were selected with the syntax  $(\beta_1, \beta_2)$  to represent the phase state of Antennas 1 and 2 as  $(0, 0)$ ,  $(127, 0)$ ,  $(0, 127)$ ,  $(180, 0)$ .

$$\Delta\phi = \frac{2\pi \times d \times \sin \theta'}{\lambda} \quad (2.7)$$

where  $\Delta\phi$  is phase shift between two successive elements,  $d$  is distance between the radiating elements,  $\theta'$  is the beam steering angle and  $\lambda$  is the wavelength of radio wave. Substituting for  $d = \lambda/2$ , Equation (2.7) is reduced to 2.8.

$$\Delta\phi = \pi \sin \theta' \quad (2.8)$$

### 2.5.2 Beam Scanning By Phase Weighting

Phase weighting is a process of selecting the appropriate phase delay for the individual element to focus the main beam in the direction of interest and nulls in the direction not of interest. Substituting for the calculated values of  $\beta_1$  and  $\beta_2$ , the array output, S of Figure 2.10 is obtained placing the main beam on the desired broadside direction when both antennas are on the same phase. By changing the phase of the signal arriving each element to a pre-calculated value as presented in Subsection 2.5.1, the main beam is steered to other desired angular positions, left and right of broadside. This is called the delay and sum approach and it is the simplest method to beam steering. The idea here is to add a delay stage to each antenna array element such that the signal from direction of interest are aligned before they are summed to ensure maximum gain in that direction of interest. At the interference direction, the delayed signal is further delayed to ensure the signals are uncorrelated and cancel each other to form a null in that direction.

## 2.6 Phase Shifter

To delay signals that arrive each element by certain amount, a phase shifter is required. A phase shifter is a device that shifts the phase of an electromagnetic wave of a given frequency as it propagates along a transmission line. There are four important characteristics of a phase shifter which include; low insertion loss, equal amplitude in all phase states, reciprocity and flat phase shift over frequency. In phased array system, flat phase shift over frequency is the most sort after and can be used on its own to judge a phase shifter because when a beam is steered to a desired focusing angle, the desire is that the pointing angle does not change even when there is a shift in frequency. Phase shifters can be electrically [152], magnetically [153] or mechanically [154] controlled.

Phase shifters can be analog or digital. Analog Phase Shifters are devices whose phase shift changes continuously with a voltage level controlled input. Varactor [155] and Schottky diodes [156] are examples of switching element in analog phase shifters. When a varactor diode operates in a reverse-biased mode, it provides a junction capacitance that vary with applied voltage. It therefore acts as an electrically variable capacitor in tuned circuits [157]. Digital phase shifters provide a discrete set of phase delays and its control is usually achieved using switches. An n-bit phase shifter provides phase shifts between 0 and 360 of phase in steps of  $360/2^n$  where n is the number of control bits. They are programmable and can be controlled using a computer system. The switch technology in digital phase shifter can be based on Micro Electro Mechanical System (MEM), Field Effect Transistor (FET), or PIN diode. Switching in PIN diodes is obtained by changing bias point from forward to reverse

direction and vice versa [158]. Phase shifters designed using MEMS was shown to have compact size and wide frequency band [159].

### 2.6.1 Switched Line Phase Shifter (SLPS)

Phase shifters can be implemented using switched line [160], loaded line [161], or reflection theories [162]. The Switched Line approach is the most straight-forward approach. This involves the use of a simple time delay difference between two direct paths to provide desired phase shift. The simplest switched line Phase Shifter is dependent only on the lengths of line used. One of the two transmission lines is a reference line, and the other a delay line. An important advantage of this approach is that the phase shift is approximately a linear function of frequency getting a wide-band frequency range of the circuit. Secondly, the phase shift is only dependent on the length of transmission lines, and so the Phase Shifter is very stable over time and temperature. Basically, a switched-line Phase Shifter with two Single Pole Double Throw (SPDT) mechanical switches consists of one reference line and a delay line. By switching the signal between reference line and the delay line, a specific shift in phase ( $\Delta\phi$ ) at a given frequency is achieved as in Equation (2.9).

$$\Delta\phi = 2\pi \times \frac{\Delta L}{\lambda} \quad (2.9)$$

where  $\Delta\phi$  is the phase shift,  $\Delta L$  is the difference between the physical lengths of the delay line ( $L_2$ ) and the reference line ( $L_{ref}$ ), and  $\lambda$  is the wavelength. A standard switched line phase shifter with SP2T shown in Figure 2.12a require 4 switches [163]. The more the number of switching elements in a phase shifter, the more losses in the system. With SP4T of Figure 2.12b the number of switches are reduced to two, meaning less losses. On the other

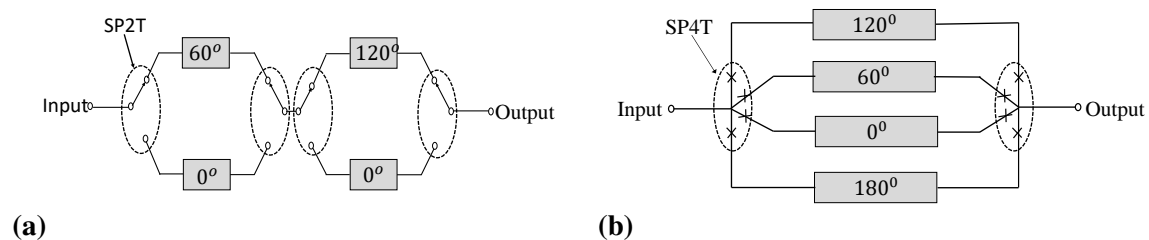


**Fig. 2.12 Switched Line phase shifter schematic with (a) SP2T (b) SP4T switches**

hand if a bit is not used, the energy does not pass through a "dead" section of transmission line. Comparing SP4T to reflect-line design approach, there is no required 3dB coupler and so no round-trip loss [164]. Based on calculated line lengths and with only two SP4T switches, a simple and straight forward phase shifter with reduced losses can be designed.

## 2.6.2 Switched Line Phase Shifter Design

Following the reviewed approaches to a simple SLPS design, schematic of a 180° switched line phase shifter (SLPS) to be implemented for this project is shown in Figure 2.13. This is a 2-bit Phase Shifter at a phase step of 60° resulting to four differential phase

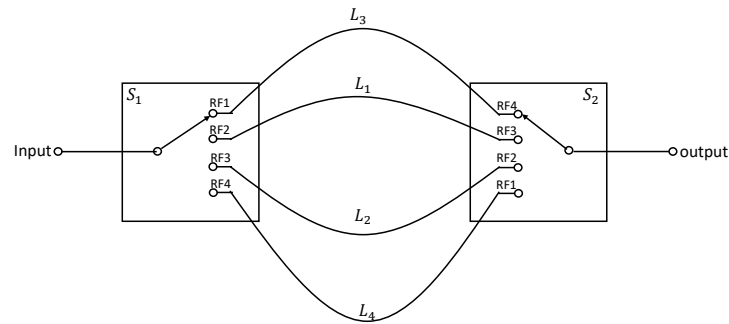


**Fig. 2.13 Switched line phase shifter schematic**

states, 0 (reference), 60, 120, and 180 degrees. S1 and S2 are single pole four throw (SP4T) switches 1 and 2 respectively. L1, L2, L3 and L4 are RF transmission lines of different lengths where  $L1 < L2 < L3 < L4$ . L1 is the shortest length representing the reference path while L2 to L4 are delay lines. L1 was located at the center for convenience of the design layout. Phase shift between any line length is calculated with reference to L1 and it is given by  $\Delta\phi = \phi_L - \phi_{ref}$  where  $\phi_L$  is the phase of any given transmission line length, L and  $\phi_{ref}$  is the phase of reference line length, L1.

## 2.6.3 RF Transmission Lines For SLPS Design

Transmission lines for SLPS design can be a simple two-wire line, a coaxial cable, or a printed circuit board (PCB) trace. Using wires or coaxial cables are simpler but a controlled impedance RF transmission line is always desirable for any RF design. RF transmission lines can be implemented on an exterior layer (top or bottom), or buried in an internal layer. Common RF transmission line designs include microstrip, suspended stripline and grounded coplanar waveguide (GCPW). A microstrip transmission line consists of fixed width conductor routing along with a solid unbroken ground plane located directly underneath on the adjacent layer. Stripline consists of a fixed-width routing on an inner layer, with solid ground planes above and below the center conductor. GCPW consists of a center conductor with ground planes on either side and below. All three types are labeled and shown in Figure 2.14. A coplanar waveguide provides for better isolation between nearby RF lines. In PCB transmission line design, width of the routing, thickness of the dielectric layer, and the type of dielectric determine the characteristic impedance which is typically 50 or 75 ohms. In

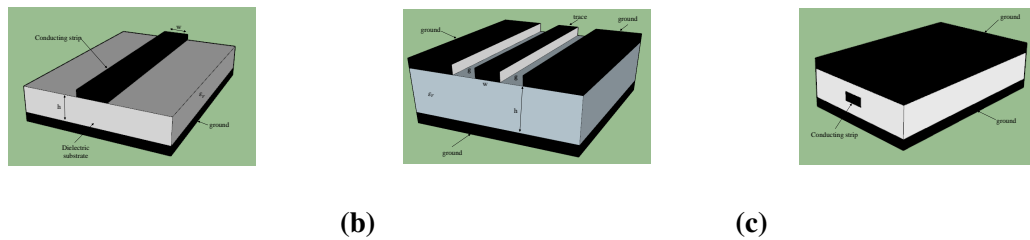


**Fig. 2.14** Three major approaches to PCB transmission line design (a) microstrip (b) grounded coplanar waveguide (c) stripline

a delay line stripline phase shifter, the delay per distance is the same for every trace while in microstrip design the delay is dependent on the trace width and height above the ground plane.

## 2.7 Localization Algorithm in Mobile Networks

In mobile network, localization algorithm can be either mobile-based, network-based or a combination of the two as shown in the flow chart of Figure 2.15. In a Mobile-based algorithm, the mobile device determines its own location using GPS. In network-based approach, the location of mobile device is determined by the network operator using network infrastructure. In this case, no hardware or software upgrading is required on the mobile device. Another approach that apply 'pinging' exist. In this case, the mobile network sends a message to mobile device who responds with data that include its location that was determined using GPS receiver on the mobile device. This is where users question their privacy. On purely network based approach, two major categories exist; angle-based and range-based. In the former, the direction of arrival of transmission from a mobile device is resolved as the intersection point of line of bearing from two or more base stations [165]. On the later, TOA, TDOA or RSS from two or more base stations are used to determine the location of mobile device. A hybrid approach where two or more scheme is combined for instance TOA/AoA [166], TOA/RSS [132], TDOA/AoA [167] and ToA/TDOA for more accurate localization is the state of art.

## 2.8 Angle of Arrival Localization Algorithm

Adaptive Array based AoA Estimation can be achieved using one of the two available techniques, first, conventional technique which is based on Bartlett method or delay and sum and capon method a.k.a Minimum Variance Distortionless Response (MVDR). Second is subspace technique which is based on orthogonality of signal to noise subspace. Multiple Signal Classification (MUSIC) and Estimation of Signal Parameter through Rotational

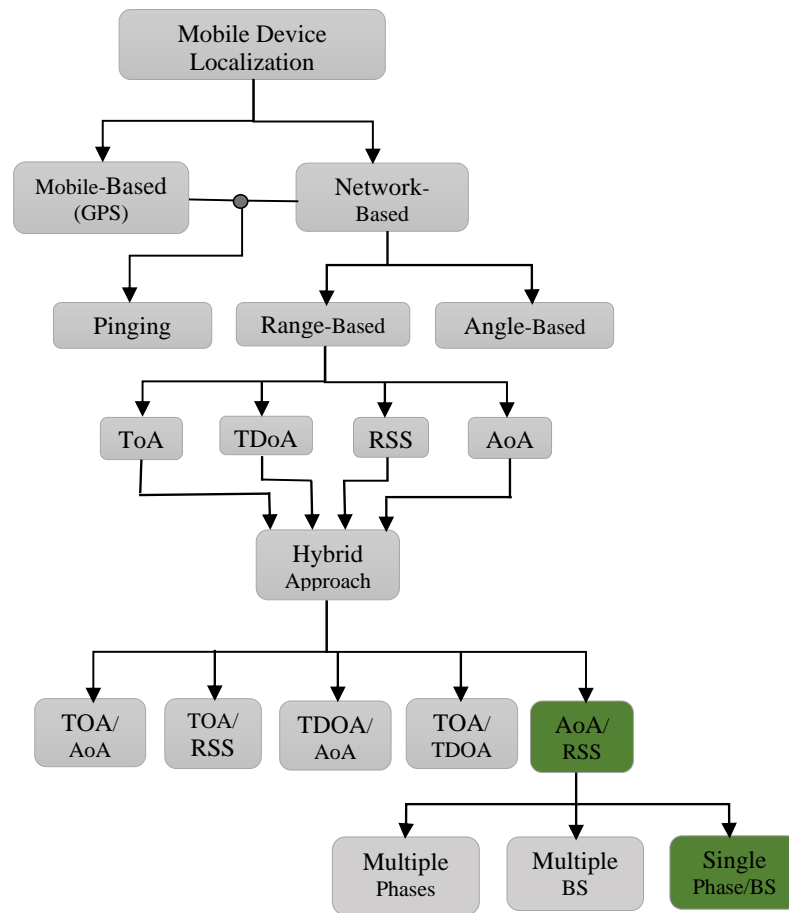


**Fig. 2.15** Mobile device localization algorithm trend of research

Invariance Technique (ESPRIT) are the two widely used subspace based estimation methods [168]. Conventional approach is shown to be simple but of lesser resolution compared to subspace approach which is complex but with high resolution [169]. Conventional approach can also achieve accurate result but with massive antenna elements [170]. Techniques such as MUSIC, ESPRIT [171], Matrix Pencil [172] method or one of their derivatives [173] involves findings of a spatial spectrum of the antenna array and calculating the DOA from the peaks of this spectrum. These calculations are computationally intensive. Matrix Pencil is very efficient in case of real time systems and under the correlated sources. With the conventional approach, DOA estimation is treated as spatial estimation because there is a relationship between the beam pattern and the array excitation as already discussed. For several  $m$  signals impinge on a linear, equally spaced array with  $n$  elements each with direction,  $\theta_i$ , the goal of DOA estimation is to use the data received at the array to estimate,  $\theta_i$  where  $i = 1$  to  $m$ . It is

generally assumed that  $m < n$ , but approaches such as maximum likelihood estimation [174] do not place this constraint. For our system, since position accuracy is not a requirement and complexity must be avoided, conventional approach is the most suitable. In this case, the array excitation is used to define different beam positions for AoA estimation.

### 2.8.1 Maximum Likelihood Estimation (MLE)

This is a popular method for AoA estimation. It is based on maximizing the likelihood that the signal received came from a particular angle. To determine the DOA of a single user and generalizing the vector  $n$  to be the interference vector which includes the signal from every other user, the interfering vector can generally be given as:

$$E[nn^H] = R_n \quad (2.10)$$

The MLE is given by:

$$\hat{\alpha}, \hat{\theta} = \max [f_{x/\alpha,\theta}(x)] \quad (2.11)$$

where,  $f_{x/\alpha,\theta}(x)$  is the Probability density function of  $x$  given the parameters  $\alpha$  and  $\theta$ . The maximization in the above equation is equivalent to:

$$\hat{\alpha}, \hat{\theta} = \min_{\alpha,\theta} [(x - \alpha S)^H R_n^{-1} (x - \alpha S)] \quad (2.12)$$

Expanding will give;

$$\hat{\alpha}, \hat{\theta} = \min_{\alpha,\theta} [x^H R_n^{-1} x - \alpha x^H R_n^{-1} S - \alpha^* S^H R_n^{-1} x + \alpha^* \alpha S^H R_n^{-1} S] \quad (2.13)$$

Minimizing this function over both  $\alpha$  and  $\theta$ , first minimizing  $\alpha$ ; Treating  $\alpha$  as an independent variable and differentiating with respect to  $\alpha^*$ :

$$\frac{\partial}{\partial \alpha} = S^H R_n^{-1} (x - \alpha S) \quad (2.14)$$

This implies that:

$$\hat{\alpha} = \frac{S^H R_n^{-1} x}{S^H R_n^{-1} S} \quad (2.15)$$

Using this value of  $\alpha$ , we get:

$$\hat{\theta} = \max_{\theta} [P_{MLE}(\theta)] \quad (2.16)$$

$$\hat{\theta} = \max_{\theta} \left[ \frac{|S^H R_n^{-1} x|^2}{S^H R_n^{-1} S} \right] \quad (2.17)$$

where,  $P_{MLE}(\theta)$  is the maximum likelihood estimate of the spectrum or the beam position of the incoming signal.

The DOA estimate is the point where  $P_{MLE}(\theta)$  takes its maximum. This method have high resolution when number of snap shots is large even with small number of sensors [175]. It can efficiently resolve very closely spaced signal sources but it is known for its complex computational demand which is a major issue that affects its performance. For this reason, researchers have tried to reduce its complexity in many ways like using spatial aliasing to reduce the range and number of candidate values to be searched [176]. For our system, only five beam positions are involved and so computational complexity is reduced as compared to using pencil beam to resolve many angular positions for each user.

### 2.8.2 Approximate Maximum Likelihood (AML) Estimation

In other to reduce the complexity of MLE, AML was proposed in [177] as follows, assuming number of BSs  $n \geq 3$ , vector of measured distances is:

$$\Delta = [d_1 \dots d_n]^T \quad (2.18)$$

where  $d_i$  is the measured distance at  $i^{th}$  BS. Considering measured distance with independent additive white gaussian noise (AWGN) with noise covariance of:

$$Q = \text{diag}\{Var_{data_1} \dots Var_{data_n}\} \quad (2.19)$$

where ' $data_i$ ' means measured data used for range estimation (TOA, TDOA, RSS) at  $i^{th}$  base station.  $Var_{data_i}$  at all base stations are not necessarily the same. Vector of calculated distances obtained from the estimated vector  $\theta = [xy]^T$  where (x,y) are mobile device coordinates is given by:

$$R(\theta) = [r_1 \dots r_n]^T \quad (2.20)$$

where,  $(r_i)^2 = S + K_i - 2xx_i - 2yy_i$ ,  $S = x^2 + y^2$  and  $K_i = (x_i)^2 + (y_i)^2$  where  $(x_i, y_i)$  is coordinates of  $i^{th}$  BS. The probability distribution function (pdf) is given by

$$f(\Delta|\theta) = (2\pi)^{-n/2} \det(Q)^{-1/2} \exp\{-J/2\} \quad (2.21)$$

where  $J$  is a Bessel function given by:

$$J = (\Delta - R(\theta))^T Q^{-1} (\Delta - R(\theta)) \quad (2.22)$$

Maximization of  $f(\Delta|\theta)$  is what ML approach seek to achieve. Therefore the maximum likelihood estimate is the vector  $\theta$  that minimizes J. This approach achieved close to optimum performance with reduced complexity when compared to ML approach. The drawbacks with AML is that at least three BSs are required and only one set of data which is TOA was used to resolve user location. This means that if there is hearability problem between mobile device and BS, data is lost. On the other hand, network overload occur due to complex messaging and synchronization among BSs..

### 2.8.3 Hybrid Approximate Maximum Likelihood (HAML) Estimation

To mitigate against the drawbacks of AML, [178] proposed a hybrid AML where only two BSs were used with two data sets of TOA and AOA to reduce the problem of hearability and system overload. One of the two BSs was used as the serving BS that provides both AoA and TOA data while the second BS provides only the TOA data. In this way, instead of two wrong measurements to one good one due to hearability, it will be one good to one wrong measurement for a more accurate result. On the other hand, synchronization issue are also reduced by the reduces number of BSs. The vector of measured data is then given as:

$$\Delta_h = [d_1 \ d_2 \ \beta_1]^T \quad (2.23)$$

where  $d_1$  and  $d_2$  are measured distances at 1st and 2nd BSs respectively.  $\beta_1$  is the AoA at 1st BS which is assumed to be the serving BS with noise variance ( $Var_{AoA}$ ) which is independent of ( $Var_{data_1}$ ). Assuming additive white Gaussian noise (AWGN), the noise covariance matrix is:

$$Q_h = \text{diag}\{Var_{data_1} \ Var_{data_2} \ Var_{AoA}\} \quad (2.24)$$

where ' $data_1$ ' and ' $data_2$ ' are measured data at 1<sup>st</sup> and 2<sup>nd</sup> BSs respectively. Vector of calculated distances is obtained from the estimated vector  $\theta = [xy]^T$  where (x,y) are mobile device coordinates is given by:

$$R_h(\theta) = [r_1 \ r_2 \ \alpha]^T \quad (2.25)$$

where  $\alpha = \arctan(y/x)$

Assuming 1<sup>st</sup> BS to be located at (0,0) coordinate. The pdf of  $\Delta_h$  given  $\theta$  is expressed as:

$$f(\Delta_h|\theta) = (2\pi)^{-3/2} \det(Q)^{-1/2} \exp\{-J_h/2\} \quad (2.26)$$

where,  $J_h$  is a Bessel function given by:

$$J_h = \sum_{i=1}^2 \frac{(d_i - r_i)^2}{Var_{data_i}} + \frac{(\beta - \alpha)^2}{Var_{AoA}} \quad (2.27)$$

The ML estimate is therefore the vector  $\theta$  that minimizes  $J_h$ . This approach achieves better performance than AML but with more complexity. On the other hand, two BSs are still used and non-line of sight (NLOS) effect was not considered. The author in [178] incorporated the effect of NLOS using scattering model approach. A weighting approach to NLOS effect presented in [179] finds a true range by multiplying the measured range by a restricted factor to compensate for the error due to NLOS.

## 2.9 Range Estimation

Range estimation resolves how far from a known position a user is. Considering the application in this research, the observer system position is considered the reference position from where relative range of users scattered all over the network coverage is measured. Range can be estimated using time dependent approach (Time of Arrival (TOA) or Time Difference Of Arrival (TDOA)) or received signal strength (RSS).

### 2.9.1 Time Of Arrival (TOA) Based Range Estimation

Time of arrival (TOA) a.k.a Time Of Flight (ToF), is the travel time of a radio wave from a single transmitter (Tx) to a remote receiver (Rx). For this one-way radio wave propagation time to be correctly measured, both transmitter and all the receivers must be accurately synchronized at all time [180]. The distance between transmitter and receiver is the product of measured TOA and the speed of light which is a constant as expressed using Equation (2.28). Assuming a transmitter, Tx radiates radio signal at time  $t_1$  and a user device, s receives it at a time  $t_2$ . The distance,  $d_s$  between Tx and s is calculated as follows;

$$d_s = (t_2 - t_1) \times c \quad (2.28)$$

where  $c$  is the speed of radio wave in free space.  $t_1$  is time of take off while  $t_2$  is time of arrival at the receiver.

### 2.9.2 Time Difference Of Arrival (TDOA) Based Range Estimation

In this case, the signal take off time is not required rather only time of arrival of the signal and speed of propagation is required as expressed in Equation (2.29). Difference in the received time at two different known positions are used to calculate the difference in

distances between the target and the two known points.

$$\Delta d = \Delta t \times c \quad (2.29)$$

where  $c$  is the speed of light and  $\Delta t$  is the difference in arrival times at each known point.

TDOA approach has advantage over TOA because there is no need for user device synchronization rather only beacon node are required to be synchronized. Synchronization among beacons becomes a burden for hardware implementation especially when the beacons are sparsely spaced. Generally, time dependent approaches like TOA and TDOA require regular synchronization which can be difficult to achieve in practice. Received Time of Flight (RTOF) is another time dependent approach that tries to solve the problem with beacon node synchronization. In this approach, time and distance of signal received is not measured, rather the beacons sends back the signal or an acknowledgment signal back to the sender who now calculates the round trip time of the signal, divide it by two and then used it to calculate how far away it is from the beacon that means self localization. In real life application, the latency in response maybe unpredictable and uncontrollable since it is subject to many factors such as how busy the receiver was when the message arrived and so the accuracy of RTOF approach is not assured.

## 2.10 RSS Based Localization

RSS is a measure of the signal power received from a distant transmitter. RSS based range estimation algorithm uses the radio wave propagation models to classify RSS to distance. Based on this and using a statistical model like regression analysis, a range estimation model is developed that is used for future prediction of distance for any measured RSS.

### 2.10.1 Radio Wave Propagation

As a radio signal propagates through a channel, the power of the signal is spread over a wave front, the area of which increases as the distance from the transmitter increases, this makes the power density diminish. The effect of this was captured in free space path loss model. Any obstruction on the path of the radio signal will further reduce its power. These obstructions can be due to building, vegetation, landscaping etc, causing reflection, scattering, absorption or diffraction. For this reason many other path loss models has been developed considering different geographical locations and losses peculiar to those areas. For urban areas, the effect of buildings and other man-made obstacles are taken care of while if rural areas, shadowing, scattering and absorptions by trees and other vegetation are considered. In indoor environment, additional losses known as the penetration losses are considered. These losses are dependent on the type of material, architecture (numbers of windows), floor within

building, etc. Models developed for indoor propagation take care of this additional losses. Radio planners use propagation models by either creating their own models for different sites or apply the existing models which are generic in nature and can be used for every area. There are three kinds of propagation models, deterministic models, semi-deterministic models and empirical models.

### **Deterministic models**

Deterministic models are site-specific models, they require large number of geometry information about the site, therefore it is immensely time-consuming to construct because it requires considerable computational efforts. One advantage about this type of model is that it gives accurate results when used for range estimation. This is the best model but the required site information is always not readily available, therefore the most convenient option with researchers is to apply an empirical path loss model for a wireless sensor network scenario being considered and ascertain the level of achievable accuracy for its application.

### **Semi-empirical models**

Semi-Empirical models are based on a combination of empirical and deterministic models. A semi-empirical path loss model comprising of an empirical log-distance model and a deterministic antenna gain model that takes care of possible non-uniform base station antenna radiation was proposed in [181]. It is applied to macro cellular environment in [182].

### **Empirical models**

Empirical models are measurement and observation based path loss model, requiring only few parameters like path loss decay exponents, effective antenna heights or average clutter loss factors characterizing the average propagation environment [183] to predict the path loss in a channel [184, 185]. Empirical models are statistical representations of the environmental scenarios. They are not very accurate compared to site specific models but it is popular because it is economical, computationally friendly and does not require site specific information and can be applied to different applications for channel modeling and path loss prediction. It was used in [186] to check the impact of near ground path loss model on the life time of a WSN. Other popular models of this type that define different environment are the ITU-R [187], Okumura-Hata-Model and Lee's model [188] and Winner-II models. A general approach found in literature is the use of log-normal shadowing equation (2.30) to model any environment with approximate parameters that best describe such environment which is defined by the pathloss exponent [189].

$$P_L = P_L(d_0) + 10\alpha \log_{10} \frac{d}{d_0} + X_\sigma \quad (2.30)$$

where  $X_\sigma \approx N(0, \sigma^2)$  describes the random shadowing effect with normal distribution, zero mean and  $\sigma^2$  variance.  $P_L$  is the path-loss in dB,  $P_L(d_0)$  is the path loss at reference distance  $d_0$  often used as 1m distance in free space.  $\alpha$  is the path-loss exponent.

Usage of the standard models is economical from the time and money perspective, but these models have limited accuracy. The empirical models uses Existing equations obtained from results of several measurement efforts to calculate the path-loss for different environment scenarios. Using the normal link budget equation of Equation (2.31), the connectivity of radios within a wireless network can be calculated.

$$P_{Rx} = P_{Tx}(dBm) + G_{Tx}(dB) + G_{Rx}(dB) - L(dB) \quad (2.31)$$

where  $P_{Rx}$  is the received power,  $P_{Tx}$  is the transmitted power,  $G_{Tx}$  and  $G_{Rx}$  are the transmitter and receiver gains respectively.  $L$  is a combination of all losses which may include; transmitter and receiver feeder/connector losses, signal propagation losses like fading margin, polarization mismatch, path-loss and other losses associated with environment of propagation etc.

Comparing RSS range estimation and time dependent range estimation, the later has high accuracy, highly complex, needs time synchronization at all time and it is power consuming. The former has an advantage of low complexity and less cost, no time synchronization is required and low power consumption but it has poor accuracy. Considering the specified design criteria for our system, we trade off accuracy in RSS based range estimation for complexity and cost and as much as possible we will try to improve accuracy by developing algorithm implemented error models that will help reduce error in range estimation.

### 2.10.2 RSS Based Localization Algorithm

RSS based localization algorithm are normally based on fingerprinting, in which case a set of measured RSS from different locations within the coverage area are acquired prior to deployment and stored in the database as a radio map of that area. During operation, measured RSS is matched to the existing RSS-distance values in the database and the closest match forms the location of the sensor node. This approach involves extensive measurement and needs to be updated as the environment changes due to new construction etc. Another approach to building RSS based localization algorithms are by using mathematical models like the path loss models that relate the losses in the environment to the RSS expected at different distances between transmitter and receiver. This is mostly applied in a centralized localization requiring only a single anchor node [190] which determine the location of every other node in that network. Alternative approaches are by triangulation [191], trilateration

or multilateration [192] These approach involve the use of multiple anchor nodes of known positions each of which estimates the distance or angle or both from a sensor node. The intersection of these distances or angle form the location of the sensor node.

### 2.10.3 RSS Fingerprinting

RSS fingerprinting localization approach applies offline and online phase for user localization. During offline phase a radio map of the proposed implementation environment is built. This results to a database of different measured RSS from locations of interest within the network coverage area relative to different reference points (AP) with their corresponding measured range. During the online phase, for any measured RSS, the system uses appropriate search algorithm to search the database to find the most likely range for the measured RSS. Some of the popular search algorithms include;

1. The use of wireless fading channel models which is described by pathloss and multipath. In this case, instead of using real location fingerprint, wireless fading channel models is simulated to calculate range at every location in the environment [193]. In this work, the relationship between RSS and distance from three base stations are determined and Apollonius circle is then applied for user localization.
2. Use of linear interpolation. In this approach, the linear interpolation technique is used to calculate RSS of a specific location from a set of nearby feedback locations based on the spacial correlation of adjacent locations [194].
3. The k-nearest neighbor (KNN) algorithm. This is a deterministic approach that finds the Euclidean distance of the current measured fingerprint to the pre-stored fingerprint in the database. This is done by calculating the residual between current measured fingerprint and fingerprint for  $i^{th}$  location stored in the database [195]. The first K-locations of  $i$  in the database that returns the smallest residual value are chosen to estimate the user position.

### 2.10.4 Localization Systems Based on RSS

The most popular localization system that is based on RSS algorithm is RADAR [196]. This system was based on IEEE 802.11 and introduced by Microsoft Research Group in year 2000 to track users indoors. The design was based on fingerprinting with off-line and on-line phases. During the off-line phase, radio map of the indoor coverage is collected and stored in database so that during the on-line phase, measured data is matched with the stored data. Best match is returned as the location estimate. A similar system like RADAR called Horus was introduced in year 2005 [197]. This system used RSS from AP for location estimation.

Horus integrated easily with existing network infrastructure because network cards measure RSS of received frame as part of normal operation. SpotOn is system introduced in 2001 by University of Washington and Intel Research. This is an RSS based 3D localization system for RFID application. It applied distributed rather than centralized approach.

## 2.11 Radio Location Errors

Common errors that affect the accuracy of radio location are; first, error emanating from measuring instrument, second is error due to condition of the channel of propagation which includes channel noise and third is error due to non-line of sight (NLOS) effect causing obstructions, delays and multipath. This error is common with AoA where reflected signal affect the AoA estimate and also with ToA where obstructed signal travel longer distance than normal and so are miscalculated.

Solutions to NLOS effect on radio locations that have shown good results include, weighting using geometrical equations. One approach to weighting is by applying calculated weights to measured values to compensate for error due to NLOS effect as discussed in [198, 199]. In this approach, known data relating to range and BS layout in relation to the cell geometry are used to adjust the measured range close to LOS values. A scaling factor obtained from a constrained nonlinear optimization problem is used for the range adjustment. Another approach is applying a residual fitting in a scaling factor as discussed in [200]. In this approach, the residual between calculated and estimated range is used to form a scaling factor for adjusting future estimates. Another approach to mitigating NLOS error is by using pre-processing stage to identify NLOS base stations (BSs) and then using data from LOS BSs only for location evaluation [177]. This approach is only feasible when there is a LOS BS. In [201], radio propagation channel is modelled by a scattering model and measured statistics is matched with result of assumed model to get the best estimate.

## 2.12 Localization Performance Metrics

Performance of a localization system is a measure of how well the system works. Metrics for measuring the performance of a location system include, accuracy and precision, complexity, robustness, cost and scalability. Accuracy is a measure of the difference between the estimated location and the actual location while precision is a measure of degree of similarity of results of repeated trials under the same condition. Measuring indicator for accuracy is mean distance error or Root Mean Squared Error (RMSE) to show the deviation of the localization system from ideal. Precision show the stability of a localization system to its performance. High precision indicate that large number of location estimate are close to actual location. Cumulative Distribution function (CDF) is normally used to show the error

distribution between the estimated and actual locations [202]. The more the accuracy of the system the higher the cost.

Complexity of a localization system is driven by the technological make up of both the hardware and software. The popularity and availability of a particular technology reduces the complexity of a system needing the technology to operate. For instance, a localization system requiring a cellular network or a WiFi infrastructure is classified as less complex because it can easily be deployed and used. On the same way, RSS based localization algorithm would make for a less complex system since there will be no need for extra hardware on the mobile device.

Scalability means that the localization system should be flexible to upgrading with less adjustment. A localization system is said to be robust if it can still function well under some say environmental changes like rain, cloud, vegetation etc.

Cost as a matrix for performance in a localization system refers to the money, time, and effort applied to the development and implementation of such system. A localization system based on existing infrastructure is said to substantially save cost. If the system is robust, scalable, easy to install and maintain then we can say it is time saving. Space saving also saves cost. If the system is compact, it saves space. Power saving is also another way of saving cost, for instance if the location estimation is carried out only by the server, then power consumption of mobile devices are reduced.

## **2.13 Localization Applications**

There are different purposes for which the location of RF signal source is being sought after. These purpose can be categorized into Localization for public safety, navigation, social network and others. To safeguard the masses, enemy aircraft, ship or even robots are being tracked by military for the purpose of attacking them before they strike. For this reason, surveillance in the form of localization systems are kept in strategic places to keep watch. This is one of the earliest location based services in the form of radar system. It was discussed in [203] how localization, tracking and targeting is applied in military and [204] studied security in localization systems to avoid incorrect military plans and decision making. With the mandate required of cellular network operators, emergency phone callers for ambulance, fire, police or alarms are located to ensure prompt response as described in [205]. In [206], localization for environmental disasters emergency monitoring and rescue was also reported. On the other hand, cellular operators track users for the purpose of successful handover as they move around the globe or for emergency services. This is achieved using GPS or triangulation for phones without GPS receiver. Everything is going 'smart' with the technology of Internet Of Thing (IoT), ranging from smart house, farming, animal rearing,

health system and also smart parenting and child care. Numerous sensor nodes are deployed randomly in different location both outdoor and indoor [207], localization of the position of a reporting sensor node gives meaning to the data being delivered by the sensor [208].

## 2.14 Summary

From the reviewed literature, automated small cell deployment position is the state-of-art in HetNet. In this approach, knowledge of locations of existing cells, users and propagation environment is used to develop an algorithm that resolves optimum small cell deployment positions with minimal delay. A great deal of work have been performed where different network parameters were considered to develop an optimization problem which resulted in a mathematical framework for small cell deployment giving a theoretical solution. There is no practical solution found in literature that would help operators in this matter. This research work will explore a practical solution by adopting a localization system technology for this application. Localization took its history from tracking systems and has recently attracted research interest leading to different classifications and vast technological expansion and applications as presented in this chapter. An option would be for the mobile operator to use pinging which involves the operator sending broadcast message and mobile devices responding with their ID and location. Most recent mobile devices have an inbuilt GPS receiver but since there is still others that are not, accurate result will not be obtained with pinging. Most importantly, GPS localization approach is not user privacy friendly which customers frown at in recent times. For these reasons, this approach is not an option for further exploration. Distributed system is not an option too because the mobile users cannot be used as anchors in the network, therefore centralized system will be explored. This chapter has also presented a basic expected design layout for any localization system which will guide the decisions in the modeling and implementation in this research. Next chapter will present the localization system block diagram suitable for the proposed application and the modeling and simulation to check the applicability of the system before going into implementation.

# Chapter 3

## System Modelling and Simulation

### 3.1 Introduction

This chapter presents the system block diagram and the modeling of individual components as well as the system simulation. The process was approached in three stages which include, broadside beam-forming with 2 antennas, delay and sum beam-steering with phase shifters and localization algorithm which include channel propagation and error investigation and solution. Broadside is assumed to be the  $\theta = 0^\circ$  reference angle and array axis is at  $\theta = 90^\circ$  off broadside. A broadside beam and beam-steering will be simulated as shown in the sketch of Figure 3.1. This figure shows that looking at a network coverage as a semi-circular grid, our desire is to generate broadside beam at  $0^\circ$  i.e.  $90^\circ$  from array axis and then steer the beam to  $45^\circ$ ,  $-45^\circ$ ,  $90^\circ$  and  $-90^\circ$  off broadside as shown. The values in bracket represent the radial angle and the angle outside the bracket is in relation to the broadside beam. First the two antenna elements were simulated to generate main beam on broadside, then the required phase delays were calculated to place main beam on the specified angles and implemented on the simulation to steer the beam to other directions. AoA and Range estimation using calculated RSS were then implemented to resolve the position of users and identify optimum small cell deployment positions.

Four different radio channel propagation models for open space has been used throughout the simulation to represent different but theoretically the same environment scenarios. These models were chosen because they all represent an open space environment and were developed covering the required frequency range. This means that in network propagation prediction at the frequency of 2.45GHz in open space, any of these models would be a good model to characterize the environment. Our desire therefore is to know how well these models represent the same open space environment and find out what errors are encountered

when they are approximated for the same application. All simulation were performed using MATLAB.

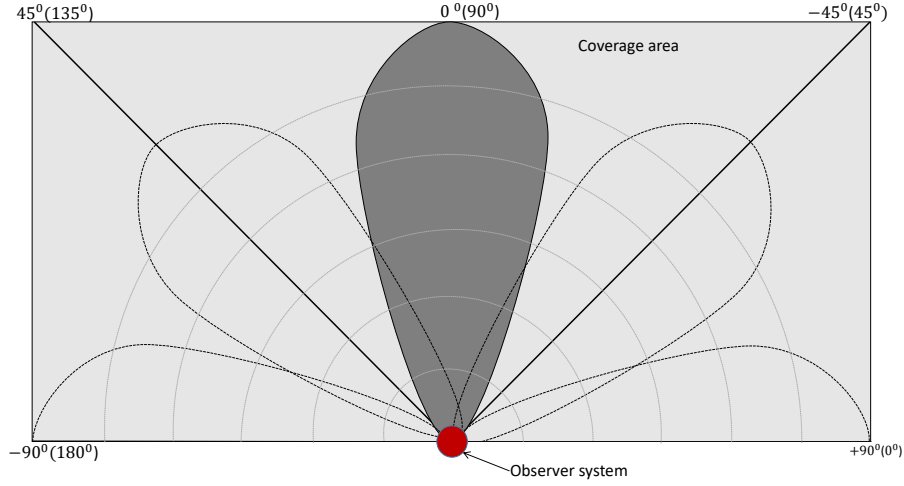


**Fig. 3.1 Approach to system simulation**

### 3.2 Simplified Hybrid Approximate Maximum Likelihood (SHAML)

A SHAML based on [178] is developed using only one BS and two data sets (AoA and distance). In this algorithm, the BS resolves both AoA and range using only measured RSS by one BS to keep the algorithm simple. The red spot on the simulation schematics of Figure 3.1 represent the single BS that houses the observer system that monitors the network coverage area for user cluster. By using only one BS, the problem of hearability, network overload and BS linear layout are prevented. Assuming the vector of measured data to be given by:

$$\Delta_s = [d \ \beta]^T \quad (3.1)$$

where  $d$  is measured users distances and  $\beta$  is users AoA at BS.

Even though two data sets are measured at the BS, both data were determined using the same measured RSS. Assuming additive white Gaussian noise (AWGN) in measured RSS with zero mean and variance:

$$Q_s = (\text{Var}_{RSS}) \quad (3.2)$$

Vector of measured data is given by::

$$R_s(\theta) = [D \ \alpha]^T \quad (3.3)$$

where  $\alpha = \arctan(y/x)$

Assuming BS to be located at (0,0) coordinate. The pdf of  $\Delta_s$  given  $\theta$  is expressed as:

$$f(\Delta_s|\theta) = (2\pi)^{-1/2} \det(Q)^{-1/2} \exp\{-J_s/2\} \quad (3.4)$$

where,  $J_s$  is a Bessel function given by:

$$J_s = (d - D)^2 \quad (3.5)$$

The maximum likelihood estimate,  $\delta_s$  is therefore the vector  $\theta$  that minimizes the squared difference between the measured and calculated distances. From [178], the mobile position estimate, A for a single BS is given by:

$$A : \begin{cases} x = d_m \cos \varphi_m \\ y = d_m \sin \varphi_m \end{cases} \quad (3.6)$$

where  $m = \arg \min_i(d_i)$ .  $d_i$  is the distance between  $i^{th}$  mobile device and BS while  $\varphi_i$  is it's AoA which in this case is a sector angle and not a precise angle.

### 3.2.1 Error Mitigation in SHAML

Two main errors common with range estimation are measuring error and error due to NLOS. To take care of these errors, Residual Weighting Algorithm presented in [200] was combined with the weighting algorithm presented in [198, 199]. The former applied least square estimate that minimizes the residual while the later applied geometric equations to compensate for error. By applying a known characteristics of four different environments, residuals were worked out for any identified system error. By applying a least square polynomial fitting, an equation is formed to compensate for system and NLOS errors.

## 3.3 Proposed System Block Diagram

The proposed system is presented in Figure 3.2. It is a two element adaptive antenna array system separated by  $\lambda/2$ , where  $\lambda$  is wavelength of the radio signal. Phase weights of each element is controlled by the adaptive algorithm using pre-selected phases,  $[\beta_1, \beta_2]$  of  $[0, 0]$ ,  $[127, 0]$ ,  $[0, 120]$ ,  $[180, 0]$ , for Antennas [1, 2] respectively. At first phase selection which is  $\beta_1 = \beta_2 = 0$ , the weights of antennas 1 and 2 are calculated using Equation (2.4) to obtain  $w_1$  and  $w_2$  respectively. The steering vector for each antenna is also calculated for all radial angles using Equation 2.5. The array output is then calculated using Equation (2.6) to place the main beam in direction  $90^\circ$  from array axis as indicated in Figure 3.2. By changing

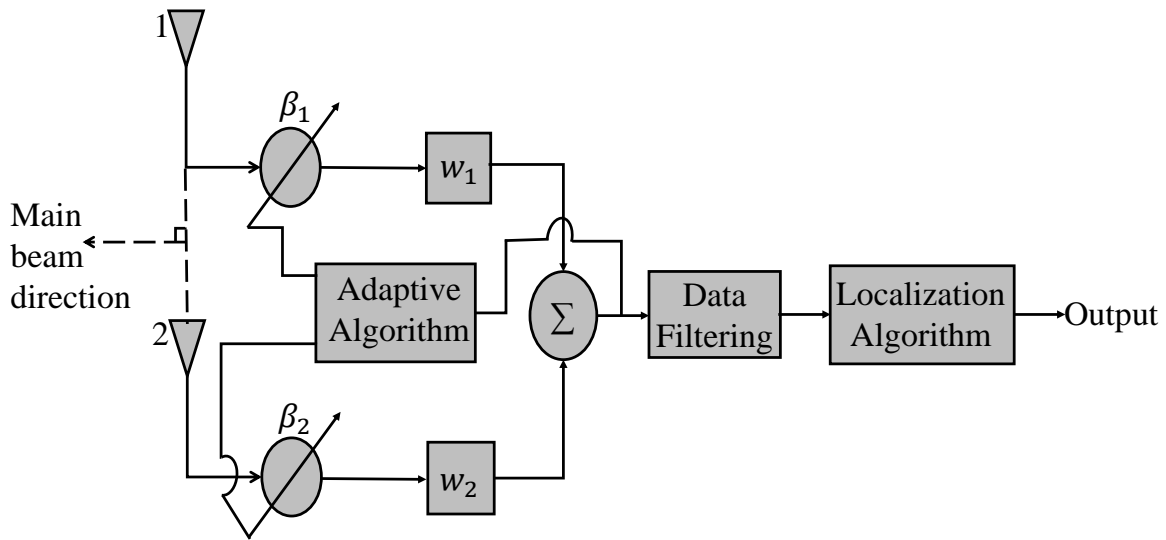


**Fig. 3.2** Localization system block diagram used in this work

the values of  $\beta_1$  and  $\beta_2$  to the second phase state of  $[127, 0]$  and then  $[127, 0]$ , the main beam is steered to left and right of broadside respectively. Finally the main beam is steered to left and right endfire direction at the selection of  $[180, 0]$  and  $[0, 180]$  for  $[\beta_1, \beta_2]$  respectively.

At each main beam position, the adaptive algorithm measures Received Signal Strength Indicator (RSSI) from radio devices in the network of operation to acquire data for localization. Data collected is then filtered to remove data from devices that do not belong to the chosen network. The filtered data are used in localization algorithm to compute AoA, range and user clusters. Optimum position for small cell deployment based on high user concentration areas are then identified.

Throughout the simulation in this chapter, radiation is assumed to be within the far field. The observer system of Figure 3.2 is assumed to be located at the red spot position as shown in Figure 3.1. Unless where otherwise stated, both transmit and receive antenna elements are assumed to be half wave dipole and parameters on Table 3.1 are used. A 0dBm transmitter power is assumed. Two 0.5m, RG8 type coaxial cable of 7dB per 100ft (30.5m) [209] is assumed to be connected to the receiving antennas via sma connectors (typical insertion loss of 0.17dB) [210] at both ends. The losses at the transmitter is assumed to be negligible. Receiver loss  $L_{RX} = (C1_{RX} \times 2) + (C2_{RX} \times 4)$ . Based on the typical value for receiver sensitivity which lies between  $-90$  and  $-120$  in dBm [211], a receiver sensitivity of

–110 is assumed giving room for fade margin. All simulation parameters are summarized in Table 3.1.

**Table 3.1 Simulation parameters**

Parameters	Value
Nominal range, $R_{max}$ (m)	100
range step, $s$ (m)	1
Frequency, $f$ (MHz)	2450
Number of elements, $n$	2
Element separation distance, $d$ ( $\lambda$ )	0.5
Looking in angle ( $^\circ$ )	90
Transmitter power, $P_{TX}$ (dBm)	0
Transmitter antenna gain, $G_{TX}$ (dBi)	2.14
Receiver antenna gain (dBi), $G_{RX}$	2.14
Receiver loss, $L_{TX}$ (dB)	0
Transmitter loss $L_{RX}$ (dB)	0.88
Receiver sensitivity, $RX_{in}$ (dBm)	–110
Radial angle ( $^\circ$ )	$0 \leq \theta \leq 180$
Current amplitude	1

### 3.4 Antenna Model

This section presents single and array antenna models, modeled and simulated using CST microwave studio with particular interest on the gain and radiation pattern for the purpose of confirming antenna suitability for the designed system.

#### 3.4.1 A Half Wave Dipole Antenna Model

First a single vertically oriented half-wave dipole was modeled on CST at a frequency band of 2.4GHz to 2.5GHz. Dipole radius,  $r = \lambda/1000$ , length of dipole,  $l = 0.5\lambda$ , optimization factor of 0.956 and a perfect electric conductor (PEC) material were parameters used for the dipole model. Figure 3.3 shows result of CST simulation of the dipole model. This result shows a toroidal shaped pattern with maximum radiation on the horizontal and nulls pointing up and down. The pattern is omni-directional on azimuth with a gain of 2.14dB as expected.

#### 3.4.2 High Gain Antenna Model

To obtain a high gain and omni-directional radiation pattern antenna, a collinear antenna was modeled in CST using dipole elements. The relationship between gain and number of elements in a collinear array is given as;  $Gain(dBi) = 10\log(n) + 2.14dBi$  where  $n$  is the number of elements and 2.14dBi is the gain of a single dipole element. Analytically, with six dipole elements collinear design a gain of 9.93dBi gain is expected. A six element collinear

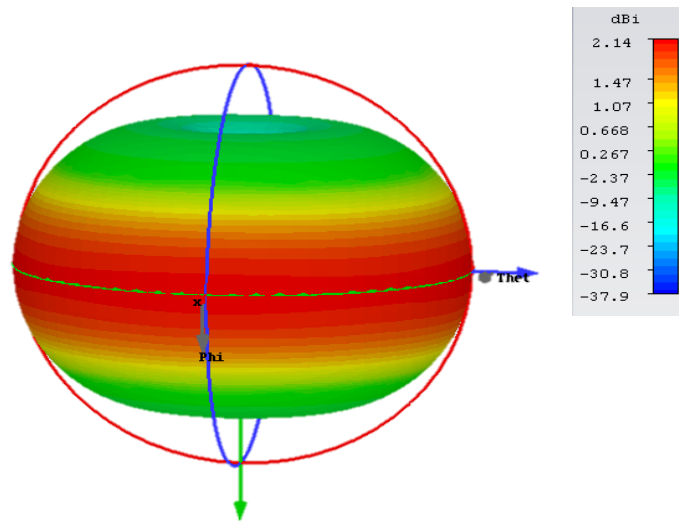


**Fig. 3.3** A single half-wave dipole antenna model showing Omni-directional radiation pattern on azimuth

antenna was modeled in CST using parameters of Table 3.2 to obtain a gain of 9.45dBi and an omni directional pattern as shown in Figure 3.4. An optimization factor of 0.956 was used to optimize the antenna design to resonate at center frequency.

**Table 3.2** Collinear antenna CST modeling parameters

Parameter	Value
frequency, $f$ (GHz)	2.45
radio wave speed, $c$ (m)	$3 \times 10^8$
wavelength (mm)	$u \times 1000 \times (c/f)$
dipole radius, $r$ (mm)	$\lambda/1000$
dipole length, $l$ (mm)	$0.475 \times \lambda$
optimization factor, $u$ (mm)	$0.965 \times \lambda$

### 3.4.3 Array System Modeling

Analytically, phase combinations for the two antennas as calculated in the design of Chapter 3 were  $(0^\circ, 0^\circ)$ ,  $(127^\circ, 0^\circ)$ ,  $(0^\circ, 127^\circ)$ ,  $(180^\circ, 0^\circ)$  but considering possible phase steps of the phase shifter,  $(0^\circ, 0^\circ)$ ,  $(120^\circ, 0^\circ)$ ,  $(0^\circ, 120^\circ)$ ,  $(180^\circ, 0^\circ)$  were simulated. The modeled collinear antenna was simulated in far-field as an array of two elements oriented on z-axis and separated by  $\lambda/2$ . The elements were simulated for these four selected phase states for the two antennas. The radiation pattern for each phase state was obtained as shown in Figure 3.5 and the result summarized in Table 3.3.

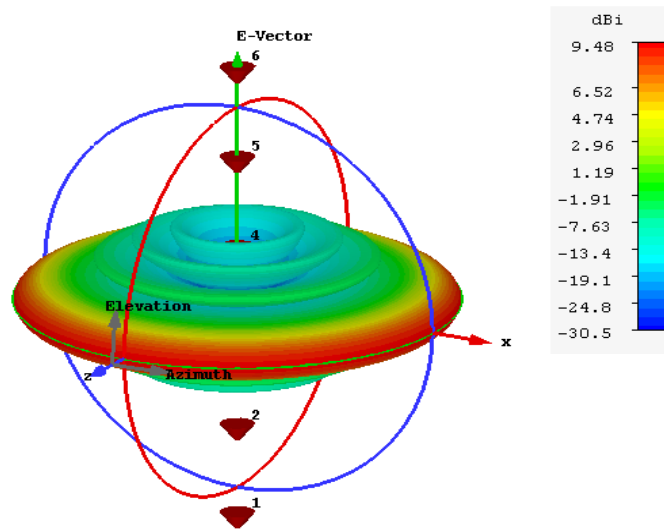


Fig. 3.4 High gain collinear antenna model on CST

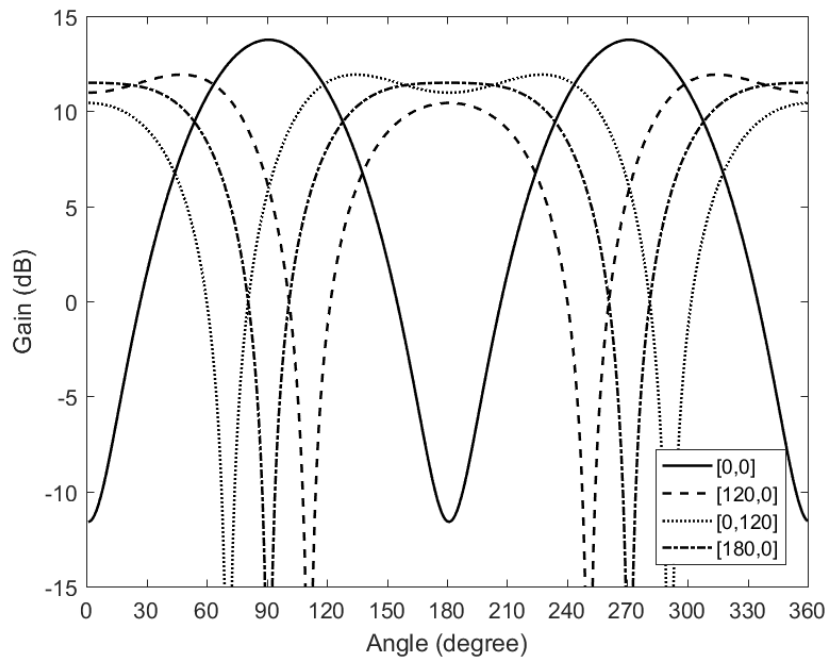


Fig. 3.5 Array radiation pattern simulation on CST

### 3.5 Grounded Coplanar Waveguide (GCPW) SLPS Design

To achieve the phase switching as modeled on the previous section, phase shifters are required. Two state of art PCB phase shifters have been described in [212, 213]. The SLPS shown in Figure 2.13 was designed and modeled on a single printed circuit board using

**Table 3.3 Antenna array radiation pattern simulation on CST**

Items	(0°, 0°)	(120°, 0°)	(0°, 120°)	(180°, 0°) left	(180°, 0°) right
Min beam Angle (degrees)	-117	-158	-62	-159	-21
Max beam Angle (degrees)	-63	-118	-22	159	21
Beamwidth (degrees)	54	40	40	41	42
Beam peak gain (dBi)	13.8	11.9	11.9	11.5	11.5
Beam peak angle (degrees)	-90	-134	-46	-180	0

diptrace software [214]. Considering a Rogers TMM 4 material with Relative permittivity  $\epsilon_r$  of 4.5 and using a trace gap of 0.3mm and a substrate height of 0.8mm, an impedance calculation for a frequency span of 2.4GHz to 2.5GHz was carried out on CST microwave environment to obtain a line width of 1.103mm for a 50 ohms impedance at a reference transmission line length of zero. Using these parameters, line lengths for the required change in phase were also calculated. Rogers was shown to have a better performance among other substrate materials for microstrip designs like FR4, bakelite, GaAs [215]. For a phase step of 60° required in this design, a line length increment of  $\Delta L = 11.8mm$  was determined from calculation. For three frequencies of 2.4GHz, 2.45GHz and 2.5GHz the phase shift for line lengths of  $L_1 = 11.8mm$ ,  $L_2 = 23.5mm$ , and  $L_3 = 35.3mm$  are shown in Table 3.4. Following the requirements for connecting HMC241ALP3E switch from the data sheet [216],

**Table 3.4 CST calculated phase shifts for frequency span of 2.4 to 2.5GHz**

Frequency	2.4GHz	2.45GHz	2.5GHz
L1	0°	0°	0°
L2	59°	60°	61°
L3	118°	120°	122°
L4	176°	180°	184°

RF coupling capacitors were used for dc blocking and to couple the RF energy from one point to another on the phase shifter. The HMC241ALP3E switch manufactured by analog devices is a general purpose non-reflective SP4T switch in a low cost leadless surface mount package. Covering DC 100 MHz to 4 GHz, this switch offers high isolation of 43dB and has a low insertion loss of 0.7 dB at 2 GHz. The switch operates at a single, positive supply voltage range of 3 to 5 Volts. A 2:4 line decoder is integrated on the switch providing logic control from two logic input lines to select one of the four radio frequency (RF) lines as shown in Figure 3.6. By these features, this switch was considered suitable as the switching element in this design. The schematic diagram of the designed phase shifter is shown in Figure 3.6.

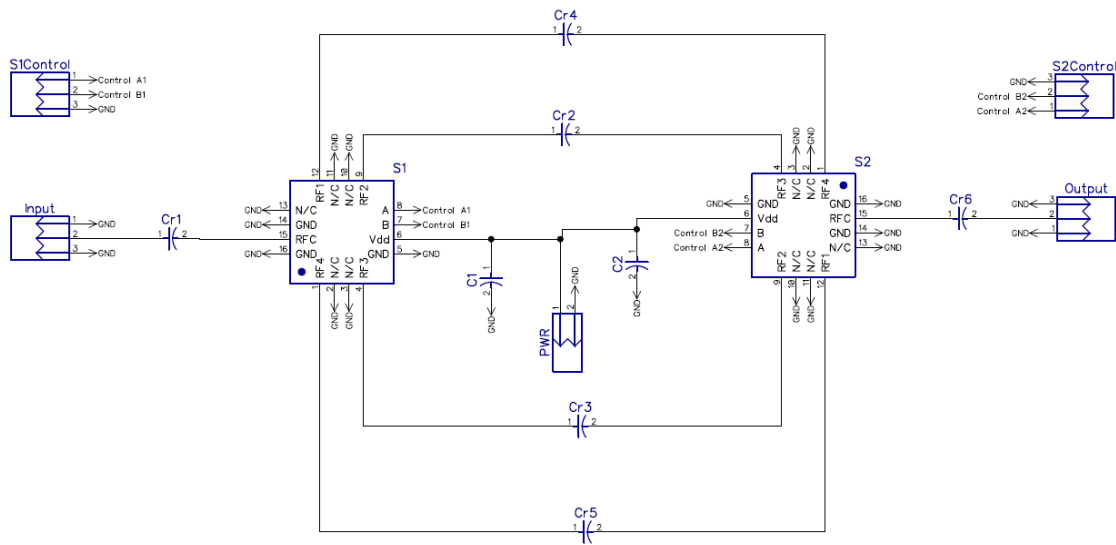


**Fig. 3.6 PCB based phase shifter schematic design using diptrace software**

Considering component placement, size and other logistics, a reference transmission line length of 11.768mm and delay line lengths of 23.535mm, 35.295mm and 47.058mm were used on this model. Table 3.5 shows a summary of CST calculated transmission line lengths for required phases and also the PCB modeled line lengths with their corresponding phases as recalculated on CST.

**Table 3.5 CST calculated phase shifts for frequency span of 2.4 to 2.5GHz**

Lines	Phases (CST)	Line length (CST)	Line length (diptrace)	Phases (diptrace)
L1	0°	0mm	11.768mm	60.02°
L2	60°	11.8mm	23.535mm	120.04°
L3	120°	23.5mm	35.295mm	180.02°
L4	180°	35.3mm	47.058mm	240.01°

Converting the designed schematic on diptrace to PCB and doing some placement modifications and routing, the PCB model of the design was obtained. The top and bottom layers of designed GCPW switched line phase shifter are shown in Figures 3.7a and 3.7b respectively with board size of 39.8 × 39.8mm.

### 3.6 Radio Coverage and Channel Model

The aim here is to build a 2 dimensional model of a wireless network with the observer system deployed at one point and users at other points in the network to form an operational test bed for the observer system model. Assuming the radio coverage schematic of Figure 3.1 to be a semi-circular grid of pixel points separated by 1m distance from each other.

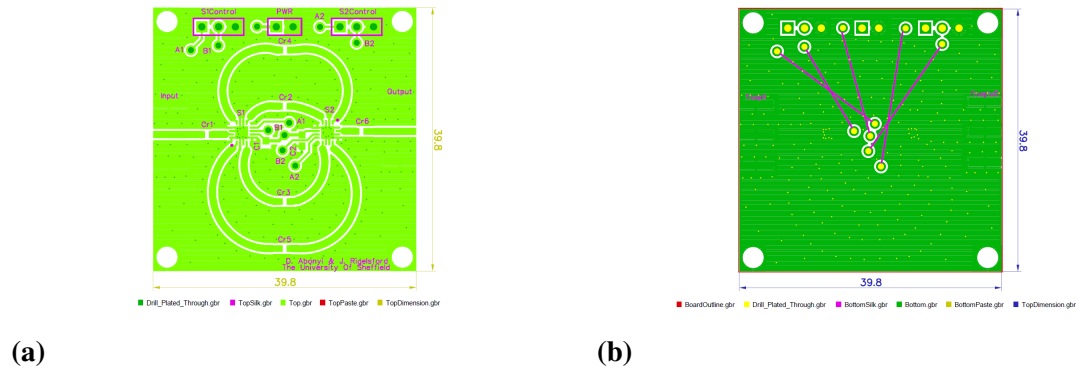


**Fig. 3.7** Designed phase shifter using diptrace software (a) top (b) Bottom layers

Each pixel point has a known coordinate  $(x_i, y_i)$  which was formed as a meshgrid of  $x$  and  $y$  data points where  $-100 \leq x \leq 100$  and  $0 \leq y \leq 100$ . The observer system is located at  $(0,0)$ . Pixel range and angle from the observer point position (red dot) were calculated using  $\theta_i = \arctan(y_i/x_i)$  and  $d_i = \sqrt{(x_i - x_{ref})^2 + (y_i - y_{ref})^2}$  respectively. Where  $(x_i, y_i)$  and  $(x_{ref}, y_{ref})$  are coordinates of  $i^{th}$  point and the observer system respectively.  $\theta_i$  and  $d_i$  are angle and distance of  $i^{th}$  pixel point respectively. A model of some calculated distance and angle are shown in Figures 3.8a and 3.8a respectively.

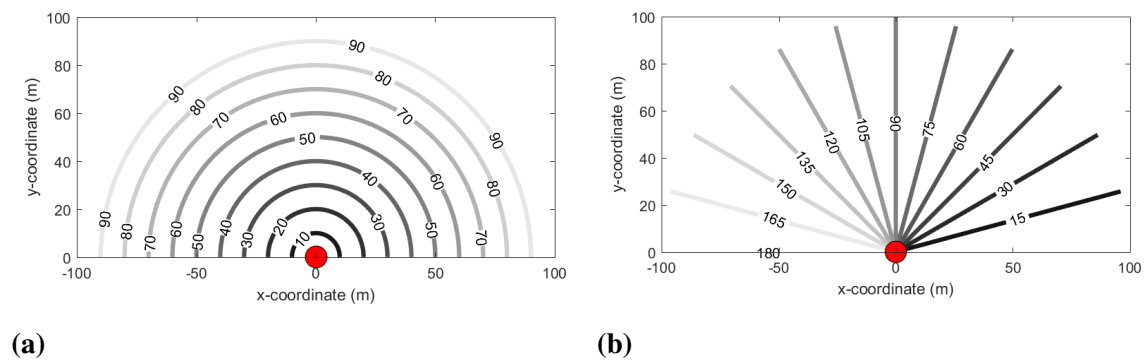


**Fig. 3.8** Modeled relative (a) range and (b) angle from the observer system position

### 3.6.1 Propagation Channel Link Model

The aim here is to model the wireless connectivity between the observer system and the users in the network and to do this, a link budget is needed. A link budget calculates the signal level through the link and predicts the received signal strength (RSS) at the other end of the communication channel as illustrated in Figure 3.9.

There are three stages in the link budget schematic shown. The transmitting end (Access point (AP), TX antenna cable and TX antenna) transmits  $P_{TX}$  power with an assumption

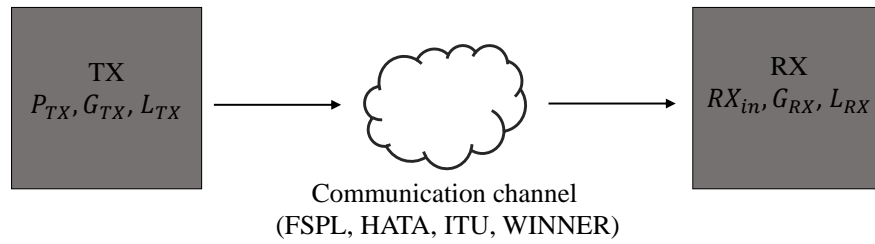


**Fig. 3.9** Illustration of wireless communication channel for link budget calculation

that both cable and connector losses are negligible ( $L_{TX} = 0$ ). The channel is the air interface characterized by pathloss and other influential factors like humidity and terrain roughness. For the link budget modeling in this simulation, the only environmental factor to be considered is the pathloss with the assumption that other factors contribute a negligible loss to the environment. The receiving end (AP, RX antenna cable and RX antenna) has some losses due to connector and cables which were not neglected. It also has sensitivity,  $RX_{in}$  which defines the minimum useful RSS that the receiver can handle. The length of a communication link has a major influence on the link budget. The link budget equation is given by:

$$P_{Rx} = P_{Tx} + G_{Tx}(dB) + G_{Rx} - (L_{TX} + L_{RX} + PL) \quad (3.7)$$

where  $L_{RX} = C1_{RX} + C2_{RX}$  and  $L_{TX} = 0$ .  $C1$  and  $C2$  are cable and connector losses in dB respectively.  $P_{Rx}$  is the received power (RSS) and  $P_{Tx}$  is the transmitted power both in dBm.  $G_{Tx}$  and  $G_{Rx}$  are the transmitting and receiving antenna gains in dBi respectively.  $Rin$  is the receiver sensitivity in dBm and  $PL$  is the channel pathloss. Assuming a free space environment, the link budget equation above then becomes:

$$P_{Rx} = P_{Tx} + G_{Tx}(dB) + G_{Rx} - (L_{TX} + L_{RX} + FSPL) \quad (3.8)$$

where

$$FSPL = -27.5 + 20\log(f) + 20\log(d) \quad (3.9)$$

where  $f$  is radio wave carrier frequency in MHz,  $d$  is distance between transmitter and receiver in meters.

### 3.6.2 Received Signal Strength (RSS) Model

At this point, the desire is to apply the link budget model equation to calculate what the received signal strength will be at the observer system position from all possible user positions. The effect of antenna gain on measured RSS were also investigated by modeling a dipole as well as a collinear antenna radiating in free space. Using Equations 3.8 and

3.9 and considering parameters of Table 3.1, the RSS from users at the observer system position were calculated following the steps of Algorithm 1. since there is flexibility of choice for receiver antenna, RSS model using 5 dipole element collinear antenna with gain of 9.13dBi was also implemented at the receiver. Where gain of a collinear antenna  $G_c(dBi) = 10\log(n) + G_e(dBi)$ ,  $n$  is the number of elements and  $G_e$  is the element gain in dBi. Both results were plotted in Figure 3.10 and summarized in Table 3.6.

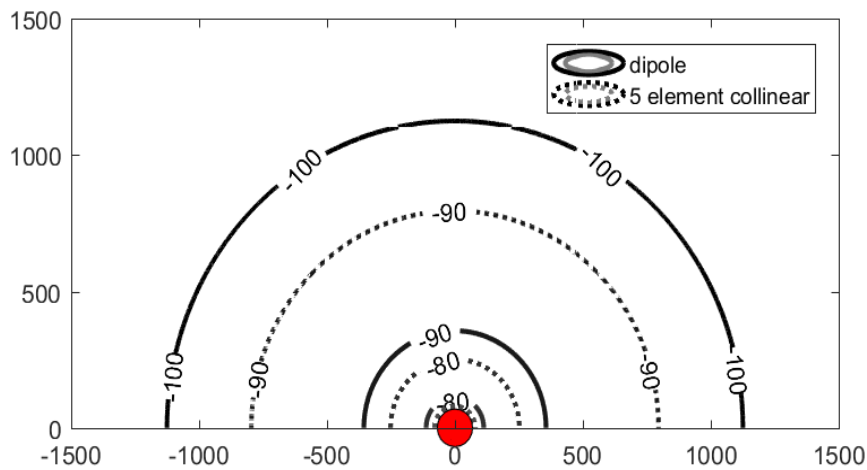


**Fig. 3.10** Effect of antenna gain on RSS and coverage range

**Table 3.6** Simulated result of RSS by two different antennas

Antenna	RSS (dBm)	Distance (km)
Dipole	-100	1.1
Collinear	-98	2

This result has shown that with dipole at the transmitter and receiver, an RSS value of  $-100\text{dBm}$  is obtained at 1.1km and upgrading receiver antenna to a collinear antenna would measure RSS value of  $-98\text{dB}$  at a distance of 2km. This is an indication that with a high gain antenna, better RSS will be received from a longer distance and so more coverage area can be achieved. Based on this result, a high gain antenna will be used at the receiver end during implementation but in other to see the worst practical case in the simulation, both transmitter and receiver will be modeled as dipole elements for a nominal coverage range of 100m as given in Table 3.1. Algorithm 1 shows a step by step approach to modeling the radio wave coverage area to obtain calculated RSS from different points on the grid.

---

**Algorithm 1** RF Coverage and RSS calculation Algorithm
 

---

**Input:**

$$R_{max} = 100$$

$$s = 1$$

$$L_{TX} = 0$$

$$L_{RX} = 0.88$$

**Output:**x-coordinates  $X$ y-coordinates  $Y$ Angle  $\theta'$ distance  $d$ RSS,  $RSS$ **Step1: Generate vectors x and y**

$$1: x \leftarrow -R_{max} \leq s \leq R_{max}$$

$$2: y = x$$

**Step2: Transform x and y vectors to matrix**

$$3: [X, Y] \leftarrow \text{meshgrid}(x, y)$$

**Step3: Calculate Angle and range**

$$4: \text{for } i \leftarrow 1 : m \text{ do}$$

▷  $m$  is the number of users

$$5: \theta'_i \leftarrow \arctan(y_i/x_i)$$

$$6: d_i \leftarrow \sqrt{(x_i - x_{ref})^2 + (y_i - y_{ref})^2}$$

7: Consider only pixels with  $d_i \leq r$  to get required semi circle grid**Step4: Calculate path-loss at each pixel point relative to system position**

$$8: PL \leftarrow (-27.5 + 20 \log(f) + 20 \log(d))$$

$$9: RSS_i \leftarrow (P_{Tx} + G_{Tx}(dB) + G_{Rx} - (L_{TX} + L_{RX} + PL))$$

$$10: RSS \leftarrow RSS_1 : RSS_m$$


---

### 3.7 Adaptive Array Smart Antenna Model

The aim in this section is to simulate the two element array system that adapts to required azimuth positions. It is expected that a broadside main beam is generated and steered to other required positions. Since the approach in this research does not want any hardware implementation on the mobile device and a typical portable phone antenna has a gain of 0dB ie unity gain, user devices were modeled as being equipped with a half-wave dipole element throughout this simulation. The adaptive array is only implemented on the observer system which will also be used for AoA classification. To this end, beam-forming and beam-steering simulations are presented in this section.

### 3.7.1 Beam-forming and Beam-steering Simulation

Beam-forming and beam-steering simulations were carried out by applying the calculated phase weights of the individual antenna elements (Chapter 3) to form a beam perpendicular to array axis (broadside design) and to steer the simulated broadside beam to other selected positions. The selected phase combinations are [0,0], [120,0], [0,120], and [180,0] for antennas 1 and 2 respectively. Figure 3.11 is simulation result of the two elements at the selected phases showing maximum radiation at desired directions of  $\theta = 90^\circ$ ,  $\theta = 135^\circ$ ,  $\theta = 45^\circ$ ,  $\theta = 0^\circ$  ( $180^\circ$ ) and nulls at  $\theta = 0^\circ$ ,  $\theta = 73^\circ$ ,  $\theta = 107^\circ$ ,  $\theta = 90^\circ$  respectively. From this simulation result, the (lower, upper) boundary positions are (70, 110), (111, 148), (32, 69) and (149, 180) respectively. These boundary positions are the azimuth edge between beam positions. Therefore at each radial angle, there is only one unique beam with a maximum gain compared with other beam positions forming a boundary of  $1^\circ$  between beams since a 1m grid was modeled. This figure have shown that using only phase difference, beam steering as well as null steering can be achieved with only two antenna elements in an array. Algorithm 2 is the beam-forming and beam-steering algorithm as applied in the simulation.

---

#### Algorithm 2 Beam-forming and Beam-steering Algorithm

---

##### Input:

Frequency  $f$   
 Antenna phase states  $\beta = [(\beta_1, \beta_2)_1 : (\beta_1, \beta_2)_j]$  for all  $j$  phase combinations  
 Maximum radial angle  $\theta_{max}$   
 Angle  $\theta'$   
 Number of elements  $n$   
 Element separation distance  $d$

##### Output:

Array Gain,  $G_j|_{j \leftarrow 1:4}$

```

1: for  $\beta_j = 1$  to 4 do ▷  $\beta_j = [\beta_1, \beta_2]$ 
2:   for  $\theta = 0$  to  $\theta_{max}$  do ▷ path angle  $0^\circ$  to  $180^\circ$ 
3:     for  $i = 1$  to  $n$  do
4:        $z_1 = -\lambda/4$  and  $z_2 = \lambda/4$  ▷ section 2.4.5
5:        $w_1 = e^{-j(\pi/2)\cos(90)+\beta_1}$  and  $w_2 = e^{j(\pi/2)\cos(90)+\beta_2}$ 
6:       Compute  $S_\theta$  using Equation 2.6 ▷ array output
7:      $G = [G_{j \leftarrow 1} : G_{j \leftarrow 4}]$  ▷ array gain per angle for all phase states

```

---

## 3.8 Environment Model

This section presents a model of the wireless network existence environment with the aim of mimicking the propagation of radio wave in the modeled environments. The target

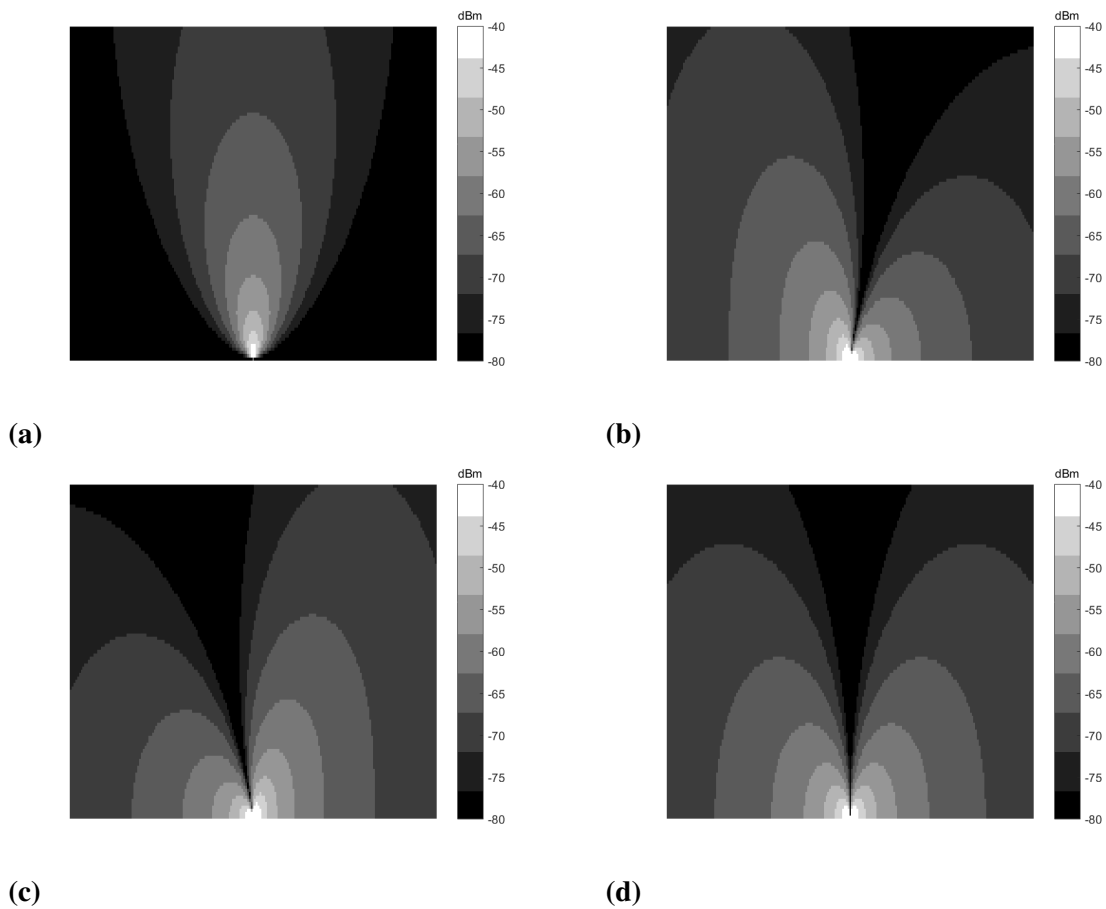


**Fig. 3.11** *Beam-forming and beam-steering for (a) [0,0] (b) [120,0] (c) [0,120] phase (d) [180,0] phases (degrees)*

is to understand how a radio signal transmitted from a certain distance is affected by the channel and in turn how all these affect the received signal strength and the localization accuracy. RSS based localization is environment dependent so to ensure system robustness, four different environmental scenarios for radio wave propagation from transmitter to receiver were modeled using four popular empirical pathloss models given in Table 3.7. These models include Free Space Pathloss (FSPL), Cost 231 Walfish-Ikegami LOS (HATA), International Telecommunication Union Radio communication (ITU-R) and Wireless World Initiative New Radio (WINNER-11) models. These four radio propagation models were used to represent different environmental scenarios for this study. In each case, line of sight version of the model was used for a closely related scenario for fairer comparison. Practically, any of these environments can be chosen for propagation prediction in open space at the frequency of 2.45GHz, it is our desire to also find out how well these models represent the same open space environment and what the effect of choosing one over another would be. First we assumed

that path-loss was the only loss in the environment and later random errors were added in measured RSS to represent other losses in the environment. Path-loss model equations for these models are shown in Table 3.7 with their standard deviations as seen in literature. This was applied on the link budget of Equation 2.31 to determine the received signal strength map.

**Table 3.7 Propagation Models Applied for Line of Sight (LOS) Channel Modeling**

Propagation Model	Equation	$\sigma$ (dB)	Ref.
Free space pathloss (FSPL)	$-27.5 + 20\log(f[\text{MHz}]) + 20\log(d[m])$	3.5	[217]
HATA (Cost 231 Walfish-Ikegami LOS)	$-35.4 + 20\log(f[\text{MHz}]) + 26\log(d[m])$	5.10	[218, 219]
ITU-R	$-28 + 20\log(f[\text{MHz}]) + 20\log(d[m])$	3.62	[219, 220]
WINNER-11 (D1)	$-29.8 + 20\log(f[\text{MHz}]) + 21.5\log(d[m])$	4	[221]

Where,  $d$  is the distance between transmitter and receiver in  $m$  and  $f$  is the carrier frequency in MHz.

### 3.8.1 Environment Pathloss Model Analysis

For a given frequency,  $20\log(f)$  is a constant, therefore the pathloss model equations of Table 3.7 can be expressed as given in Equation 3.10.

$$PL(\text{dB}) = L_0(\text{dB}) + \gamma 10\log d \quad (3.10)$$

This makes the equations similar to the equation of a straight line of the form,  $y = c + mx$  so that  $y = PL$  is the pathloss in dB,  $c = L_0$  is a constant,  $m = \gamma$  is the slope (pathloss exponent) and  $10\log d$  is the distance in logarithmic scale.

Figure 3.12 shows the pathloss characteristics for a frequency of 2450MHz for the four environments. Results from this plot show that FSPL, HATA, ITU and WINNER as slopes of 2, 2.6, 2, and 2.15, and intercepts at 40.2dB, 32.3dB, 39.7dB, and 37.9dB. This means that signal strength will diminish by  $d^2$ ,  $d^{2.6}$ ,  $d^2$  and  $d^{2.15}$  in FSPL, HATA, ITU and WINNER environments respectively.

### 3.8.2 Effect Of Environment On Measured RSS

To compare the four environment scenarios, both the transmitter and receiver were modeled as omni-directional dipole elements in all four environments. This is to find out how RSS is characterized in each individual environment and be able to identify the extent at which useful signal can be received in each environment. Calculated RSS at the observer

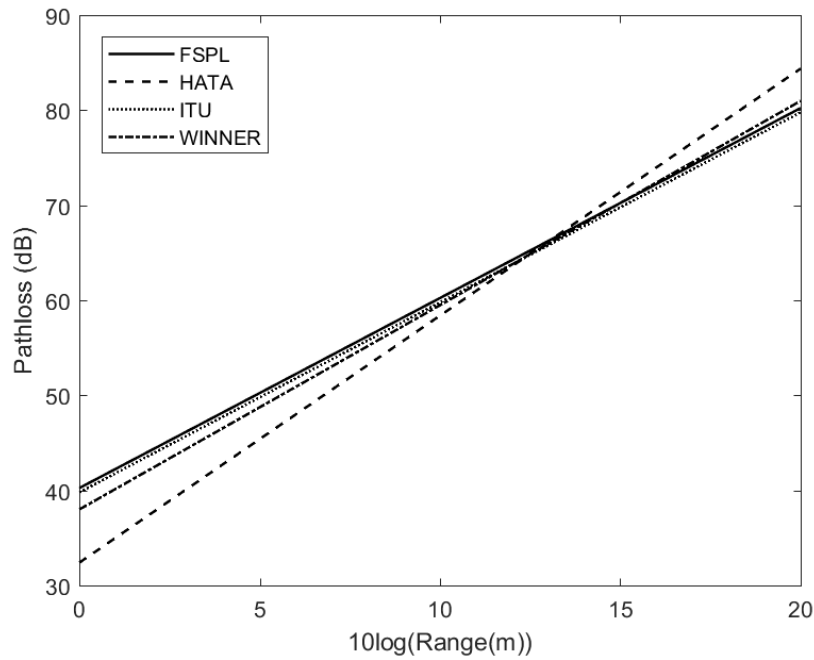


**Fig. 3.12** Four environment path loss characteristics based on empirical models of Table 3.7 in a log-log scale

point are shown in Figure 3.13. An RSS measurement of  $-80\text{dBm}$  which is well above the receiver sensitivity value was obtained at 91m in HATA but  $> 100\text{m}$  in FSPL, ITU and WINNER environments. This is an indication that even though these environments are meant to represent the same environment scenario, they have shown to be different and can be differently classified using RSS. This result has shown that for the same system, a greater coverage area is obtainable using the ITU pathloss model and the HATA environment provides the smallest coverage area. In all four environments, a good signal reception is expected at up to 100m in worst practical case.

### 3.8.3 Effect Of Directional Beam On Measured RSS

To check the effect of using a directional beam on the measured RSS and coverage, two dipole element array separated by  $\lambda/2$  was considered as the receiving antenna while the transmitting antenna remained a single dipole. RSS measured at broadside when both elements are on the same phase for all different environments is shown in Figure 3.14. This result shows a directional main beam with  $-80\text{dBm}$  RSS value in all environment measured at a distance  $> 100\text{m}$  in main beam direction. This indicates that radiation was focused on one direction achieving better coverage only in that focusing direction and cancellation in other directions which shows that with only two elements, RSS will be strong enough in

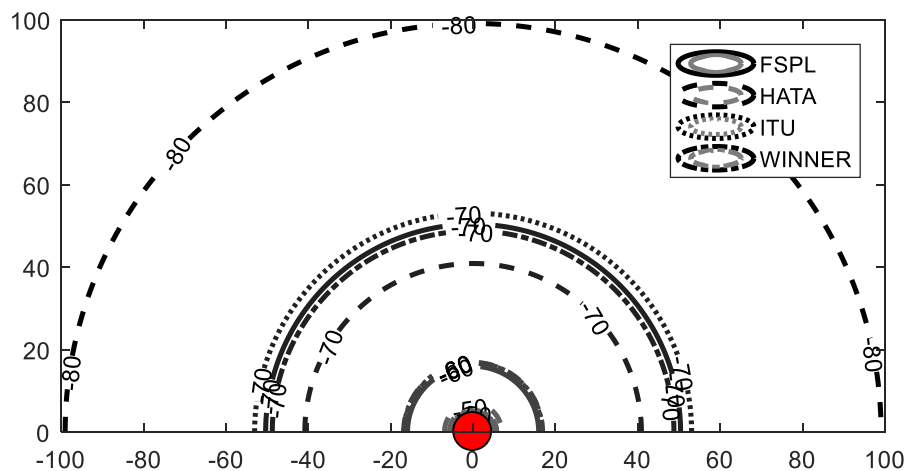


**Fig. 3.13** Calculated RSS with dipole omni-directional receiver antenna showing coverage in four different environments

the focusing direction and weak in direction not of interest for accurate localization. This is because signals perpendicular to the array axis are received by both elements at the same time (same phase) and so add constructively while signal from array axis, are received at  $180^\circ$  out of phase and so add destructively by canceling each other to form a null in that direction. It can also be observed that  $-70\text{dB}$  was measured in FSPL, HATA, ITU and WINNER at distances of 91m, 64m, 95m and 84m respectively. This confirms that greater coverage is obtained in ITU environment than others. Comparing with the omni-directional case above, where  $-70\text{dB}$  is calculated at distance  $< 50\text{m}$  in all environments, it is obvious that more coverage in a localized direction is achieved with two element array. From this plot, it is also obvious that FSPL, ITU and WINNER are more closely related than HATA. This result has shown that at the worst parameter case, 100m distance is a suitable network coverage to model all environments used in this research.

### 3.9 Localization algorithm

In this section, the AoA and range estimation models were developed using the simulated network coverage as the radio network, UDs as transmitters, simulated antenna array system as the receiver positioned as shown with red dot in Figure 3.8a. For each model, performance on sample users for both ideal and noisy environments were tested. The environment adaptive localization algorithm was also developed and tested. Results were analyzed in each case.

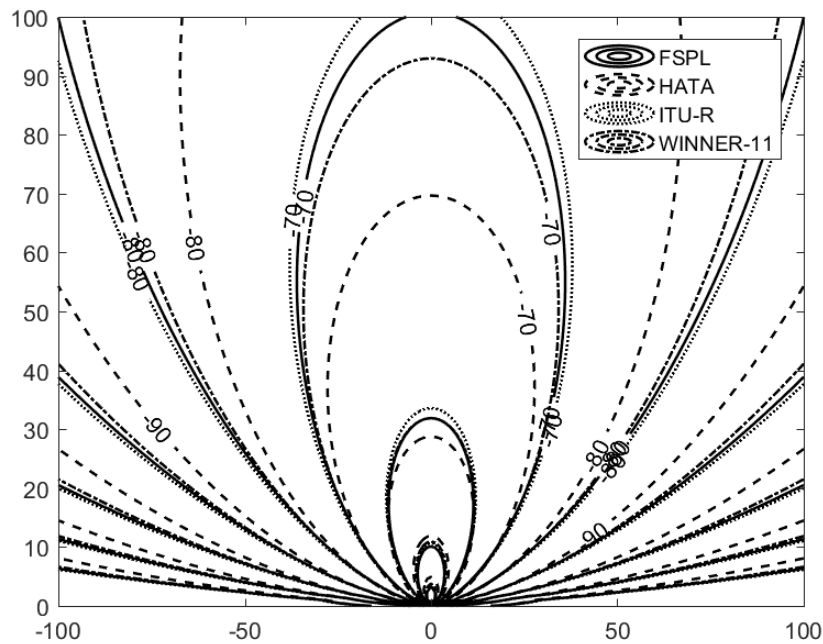


**Fig. 3.14** Calculated RSS with 2-element array receiver antenna showing greater directional coverage in four different environments

### 3.9.1 Azimuth Location Position Model

Azimuth positions for AoA classification of users was created using the angle of array beam with maximum gain at each steered azimuth position when compared with gain at other beam positions. Figure 3.15a is the resulting AoA localization positions.

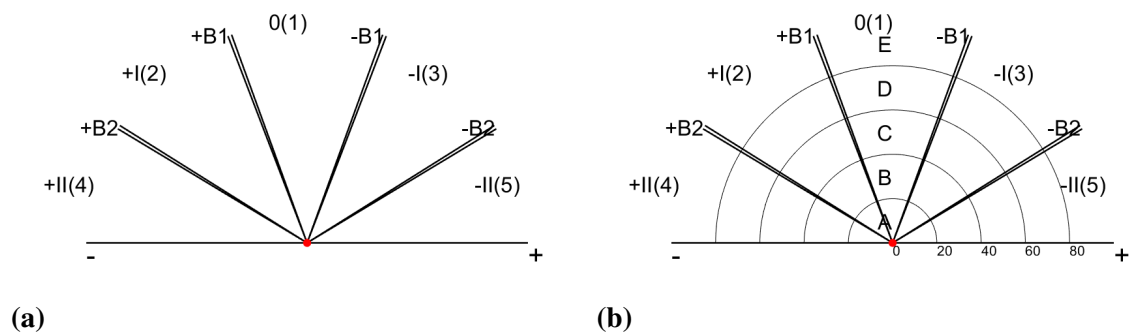


**Fig. 3.15** Illustration of (a) azimuthal sectors for AoA classification (b) range ring for cluster identification

From this figure, 0(1) position represent the broadside beam position, +I(2), +II(4) and -I(3), +II(5) are two positions right and left of broadside respectively. Two names have been assigned to each azimuth position, first is name due to their position off broadside (outside bracket) and second is their numerical numbering (enclosed in a bracket) for easy referencing. A fifth position was created from the bidirectional property of the radiation pattern for (0,180) to form position -II(5), thereby saving time on phase switching. The peak gain angle in each steered beam position is the center of each azimuth AoA localization positions sector. Boundary positions were also created using the difference between the antenna array gains at beam boundary positions of two beams sharing a boundary. Four boundary positions (+B1(102), +B2(103), -B1(204), -B2(305)) were established where +B1 is the boundary between positions 0 and +I, +B2 is the boundary between positions +I and +II, -B1 is the boundary between positions 0 and -I and -B2 is the boundary between positions -I and -II. The boundary conditions to govern the classification of users into these position were also defined based on the value of this difference in beam position gain in dB which is calculated in real time by the system depending on the antenna system beam characteristics. If beam of smaller or higher beam-width is generated, the system recalculates the boundary condition to classify users into appropriate positions. This ensures the robustness of the system. By sharing all coverage area into five rings of equal radius, more positions for range estimation was created as shown in Figure 3.15b. This figures gives the created positions for user classification and small cell deployment. Algorithms 3 is a step by step approach to developing the AoA localization positions and creating positions for user location classification.

---

### Algorithm 3 Azimuth Positions For Localization

---

**Input:**

Array Gain for four main beam positions,  $G_j|_{j \leftarrow 1:4}$

**Output:**

Boundary Conditions,  $Bc = [Bc_1, Bc_2, Bc_3, Bc_4]$

- 1: **for**  $j = 1$  to 4 **do**
  - 2:     Find beam peak angles,  $Pa_j$
  - 3:     Find beam boundary angles,  $Ba_j$
  - 4:     Find gain at beam peak,  $GPa_j$
  - 5:     Find gain at boundary angles,  $GBa_j$
  - 6:     Compute difference in gain between neighboring beams to obtain Boundary Conditions,  $Bc$
  - 7:     Using,  $Ba_j$ , segment coverage area into azimuth positions for localization leaving  $1^\circ$  gap between beams for boundary users localization.
-

### 3.9.2 Angle Of Arrival Estimation Model

Considering all the pixel points to be occupied with UDs in a FSPL environment. Applying the FSPL environment model, RSS of each UD is calculated at each beam position to obtain a matrix of RSS so that for all beam positions there are four dimensional matrix of RSS values from four main beam positions. The fifth main position is determined using the fourth RSS of the second symmetrical bi-directional beam of  $(0, 180)$  phase. The AoA of each radio device is the beam position where the highest RSS value for that radio device was measured when compared to measured value at other beam positions. Beam positions four and five were differentiated on the algorithm using the second maximum RSS value. If the second maximum RSS is position  $+I$ , then the AoA is position  $+II$  but if the second highest RSS is position  $-I$ , then the AoA is  $-II$ . For the boundary positions classification, if the difference between measured RSS of two beams sharing a boundary fall within the boundary condition for that boundary, then the user is classified as being in that boundary. In this way, each of the UD were classified into one of the nine azimuth position sectors. All UD at each pixel point was correctly classified into azimuth sector where they belong. This figure also show that a thin layer of boundary users exist within the 1m spacing between users. This is an indication that most of the users will be located within the actual sector of the coverage area but if boundary users exist, the system will be able to indicate users that occur in boundary for better decision making. It is also noticed that more boundary users exist between positions 0 and  $+I$  or 0 and  $-I$  than between positions  $+I$  and  $+II$  or  $-I$  and  $-II$ . It should be noted that the estimated AoA is not a precise estimate but a sector estimate and so accuracy is based on the beam width at each beam steered positions. Algorithm 4 is a step by step approach to developing the AoA estimation model.

### 3.9.3 Angle Of Arrival Estimation Of Sample Users

To test the AoA estimation model, twenty randomly distributed users within the network coverage area in a FSPL environment were simulated. User distribution and actual positions are shown in Figure 3.16a. At each azimuth position, RSS was measured and maximum RSS based AoA estimation model was applied to determine the AoA of each user. Figure 3.16b shows the estimated AoA of these users and the measured maximum RSS among all beams which were used for estimation. This figure shows that all users were correctly classified into their sector angle where they are located. The same process was repeated for twenty other random samples of users with correct AoA estimation achieved.

Since fading and noise is inevitable in any environment and this will cause incorrect measured RSS, normally distributed random error was introduced in the system by generate random numbers between plus and minus multiples of FSPL environment standard deviations

**Algorithm 4** Angle of arrival estimation algorithm**Input:**Boundary Conditions,  $Bc = [Bc_1, Bc_2, Bc_3, Bc_4]$ **Output:**Estimated AoA,  $\theta'$ Neighboring Position,  $NP = [NP1, NP2, NP3, NP4]$ 

- 1: **for**  $j \leftarrow 1 : 4$  **do** ▷ Algorithm 2
- 2:     Measure RSS of all users  $i : m$  ▷ Algorithm 1
- 3: A set of measured RSS at each beam position,  $RSS_j|_{j \leftarrow 1:4}$
- 4: Determine beam position with maximum RSS,  $P = \arg \max_j RSS_{\beta_i, j}$
- 5: Determine beam position with second maximum  $NP$
- 6: Determine Boundary beam RSS difference,  $\{Bd1, Bd2, Bd3, Bd4\}$
- 7: **for**  $i = 1$  to  $m$  **do**
- 8:     **if**  $P_i = 1$  OR  $2$  AND  $Bd1_i \leq Bc_2$  **then**  
 $\theta'_i = +B1$
- 9:     **else if**  $P_i = 1$  OR  $3$  AND  $Bd3_i \leq Bc_3$  **then**  
 $\theta'_i = -B1$
- 10:    **else if**  $P_i = 2$  OR  $4$  AND  $Bd2_i \leq Bc_1$  **then**  
 $\theta'_i = +B2$
- 11:    **else if**  $P_i = 3$  OR  $4$  AND  $Bd4_i \leq Bc_4$  **then**  
 $\theta'_i = -B2$
- 12:    **else if**  $P_i = 2$  **then**  
 $\theta'_i = +I$
- 13:    **else if**  $P_i = 3$  **then**  
 $\theta'_i = -I$
- 14:    **else if**  $P_i = 4$  AND  $NP_i = 2$  **then**  
 $\theta'_i = +II$
- 15:    **else if**  $P_i = 4$  AND  $NP_i = 3$  **then**  
 $\theta'_i = -II$
- 16:    **else**  
 $\theta'_i = 0$

as given in Table 3.7. This is to check the effect of these environmental factors on the measured RSS and investigate how this would affect the system accuracy. To test this, random users at some points within the network were considered. Different samples and levels of error up to 100 samples and  $\pm 20dB$  in FSPL environment were added to measured RSS and still 100% correct AoA estimation for all environments were obtained. It can therefore be concluded that environment noise in measured RSS will have insignificant effect on the AoA estimation in this system. This system is area based and not point based, therefore, the AoA estimation is based on the sector location and not on a precise angular

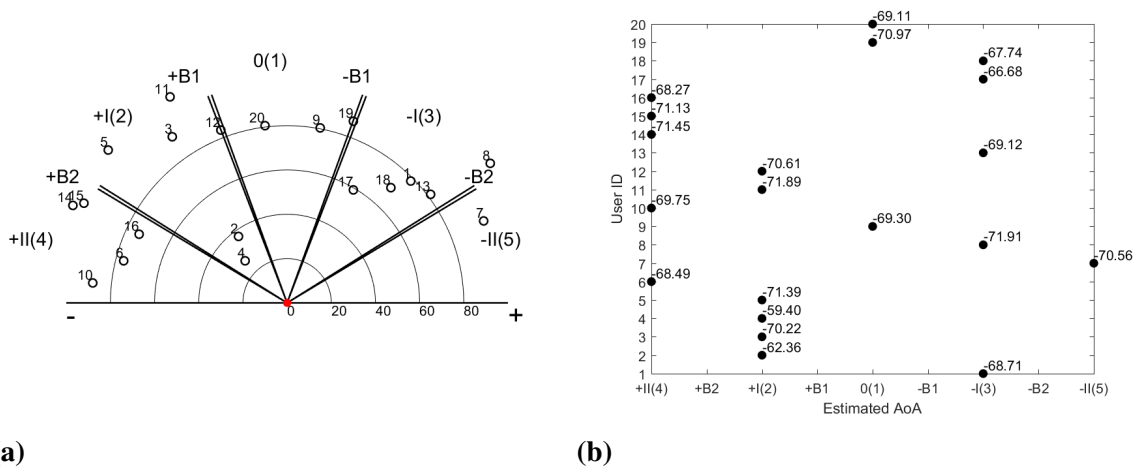


**Fig. 3.16** AoA Estimation of 20 random users (a) actual location (b) AoA classification of users

location. AoA estimation with this system is 100% accurate and robust for its purpose. Due to its cost considerations from design and simplicity of algorithm, it is cost effective as well.

### 3.10 Range Estimation

In this section, the aim is to develop a range estimation model that can be used to predict range of users at the observer point using measured RSS from UDs located at any point in the network at any of the environments. Even though the propagation models used in this research can be described by their slopes as presented in Subsection 3.8.1, a regression analysis was used to determine the relationship between RSS and distance. This gives the flexibility of standardizing the RSS of each model by centering to zero mean and scaling to unit standard deviation. This is necessary since euclidean distance measure is sensitive to magnitudes. Therefore, with standardization, all models are equally weighed creating better opportunity for model performance comparison. For each of the modeled environments, regression analysis was applied to relate RSS to distance. RSS measured from each UD at 1m distance from each other at each azimuth position peak was graphed with their distances to obtain a quadratic relationship between RSS and distance as shown in Figure 3.17.

Only RSS-range relationship for positions 0 and +I for all environments are represented in this figure because the plot for azimuth positions 0, +II and -II are identical while positions +I and -I are identical too. This means that RSS-Range classification in a steered beam array system is azimuth position dependent with identical classification on signal sum and difference azimuth positions which are different from identical off broadside left and right RSS-distance relationship. It can be seen that RSS-range model lags by certain amount in relation to distance at +I azimuth position in all environments due to reduction in gain when

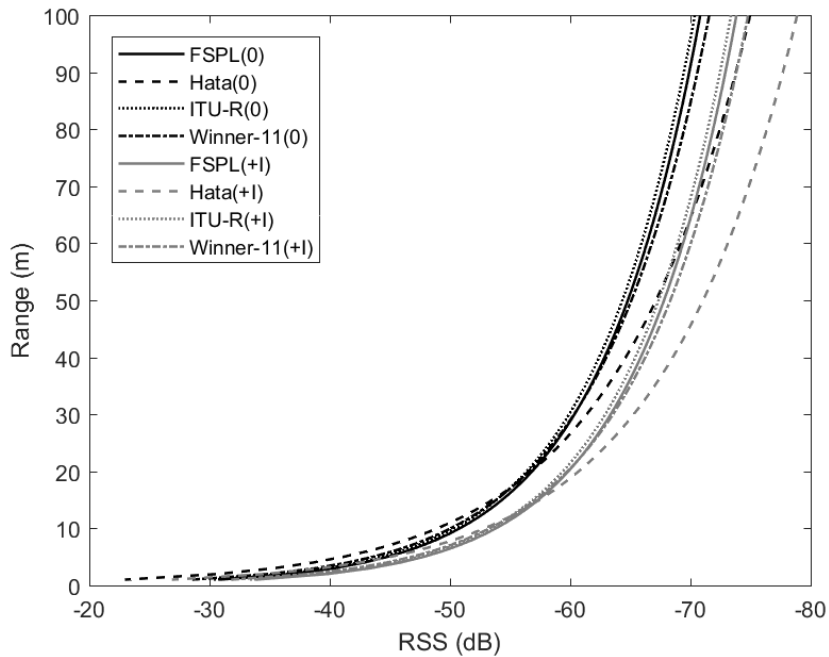


**Fig. 3.17** Range estimation models based on beam position in four environments

beam is steered. A further investigation on how this affects range estimation was carried out and discussed later. For users at beam peaks separated by 1m distance each, RSS was classified to distance for each of the environment models. As described in Algorithm 5, for any given environment, the environment is modeled using the pathloss model equation, then the radio link model is established between the observer system and the UDs. Combining the environment model and the radio link model, the RSS from each UD is resolved for each beam position giving a matrix of RSS.

Polynomial regression is a statistical regression analysis in which the relationship between independent variable, RSS and the dependent variable, distance is modeled as an  $n^{th}$  degree polynomial. To develop the range estimation model for each of the environment, a  $6^{th}$  order polynomial curve was fitted on the RSS-range relationships to obtain the coefficients that is the least square best fit for the range. A polynomial of  $6^{th}$  degree was used because it is the optimal degrees Figure 3.18 is an example of the data and the polynomial fitting range model showing the best fit for a FSPL environment. To improve the algorithm, centering and scaling transformation was applied using mean and standard deviation as shown on Table 3.8.

This means that for any  $i^{th}$  user in any given environment, instead of using measured RSS to estimate range, new measured RSS,  $R\hat{S}_i = \frac{RSS_i - \mu_{RSS}}{\sigma_{RSS}}$  is used, where  $\mu_{RSS}$  and  $\sigma_{RSS}$

---

**Algorithm 5** Environment RSS Algorithm
 

---

**Input:**

Pixel Range  $R_{pixel}$   
 Frequency,  $f$   
 Transmitter power  $P_{Tx}$   
 Transmit antenna gain  $G_{Tx}$   
 Receiving antenna gain  $G_{Rx}$   
 Array Gain for four main azimuth positions,  $G = [G_{\beta_1}, G_{\beta_2}, G_{\beta_3}, G_{\beta_4}]$

**Output:**

UD Signal strength at each beam position,  $RSS_{\beta_1}, RSS_{\beta_2}, RSS_{\beta_3}, RSS_{\beta_4}$   
 Range estimation model for each azimuth position  $RM = Rm_{\beta_1}, Rm_{\beta_2}, Rm_{\beta_3}, Rm_{\beta_4}$

**Step1: Model environment and measure RSS** ▷ see step 4 of Algorithm 1

- 1: Apply path-loss equations for given environment ▷ See 3.7
- 2: Apply Equation 2.31 to obtain the link model for all UD in a given environment,  $LM$ .

**Step2: Build range estimation model**

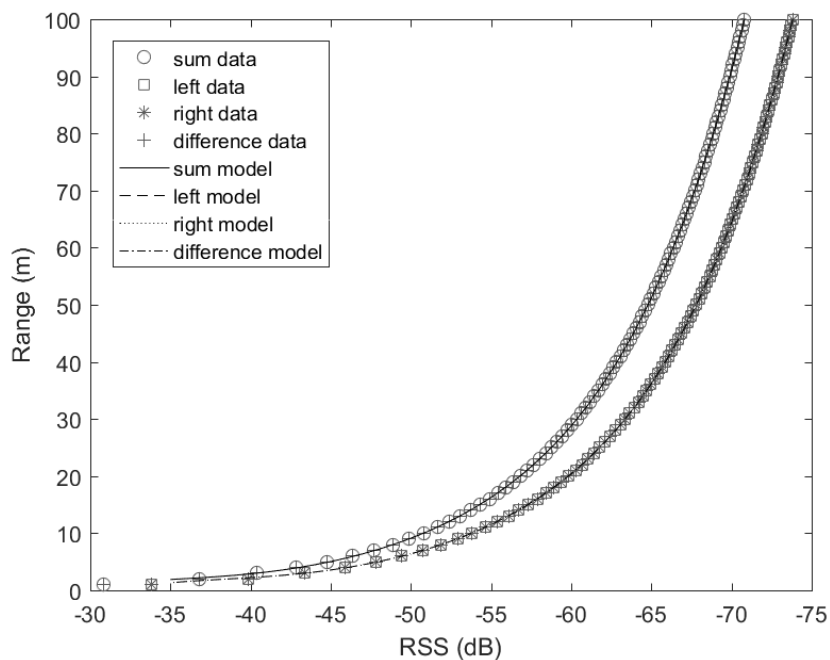
- 3: **for**  $\beta_j = 1$  to 4 **do** ▷ Phase state,  $\beta$ , which determine the beam positions
  - 4:      $RSS_{\beta} = LM + G_{\beta}$
  - 5:     **if**  $\beta = 1$  **then**
  - 6:          $Rm_{\beta} = RSS_{\beta}$  of sum azimuth
  - 7:     **else if**  $\beta = 2$  **then**
  - 8:          $Rm_{\beta} = RSS_{\beta}$  of left azimuth
  - 9:     **else if**  $\beta = 3$  **then**
  - 10:          $Rm_{\beta} = RSS_{\beta}$  of right azimuth
  - 11:     **else if**  $\beta = 4$  **then**
  - 12:          $Rm_{\beta} = RSS_{\beta}$  of difference azimuth
  - 13:     Collect all range model as a matrix,  $RM$
- 

are mean and standard deviation of  $i^{th}$  measured RSS respectively. Using these values, RSS is centered at zero and scaled to have unit standard deviation. The polynomial equations are the same for all 4 propagation environments but with different centering and scaling values. For each environment, azimuth positions 0 and +II have the same mean that is different from the mean of azimuth positions +I and -I. This means that the same range estimation model can be used to estimate the range of users in broadside and endfire positions but can not be used for users located off broadside else error in range estimation will be encountered. On the other hand, the same range model can be used for left and right off broadside users. This reduces computational complexity by 50% so that instead of solving through four equations, only two is resolved.

An Angle Adaptive Range Model (AARM) was then developed as presented on Algorithm 6. AARM estimate range of users based on the estimated AoA of those users using the

**Table 3.8 Range estimation model equations for four azimuth positions in different environments**

Azimuth positions	Range model equation	Mean (dBm)	STDev (dB)
FSPL 0	$-0.08RSS^5+0.99RSS^4-5.16RSS^3+16.63RSS^2-35.24RSS+37.95$	-65.81	8.06
+I	$-0.08RSS^5+0.99RSS^4-5.16RSS^3+16.63RSS^2-35.24RSS+37.95$	-68.83	8.06
-I	$-0.08RSS^5+0.99RSS^4-5.16RSS^3+16.63RSS^2-35.24RSS+37.95$	-68.83	8.06
+II	$-0.08RSS^5+0.99RSS^4-5.16RSS^3+16.63RSS^2-35.24RSS+37.95$	-65.81	8.06
HATA 0	$-0.08RSS^5+0.99RSS^4-5.16RSS^3+16.63RSS^2-35.24RSS+37.95$	-67.43	10.48
+I	$-0.08RSS^5+0.99RSS^4-5.16RSS^3+16.63RSS^2-35.24RSS+37.95$	-71.37	10.48
-I	$-0.08RSS^5+0.99RSS^4-5.16RSS^3+16.63RSS^2-35.24RSS+37.95$	-71.37	10.48
+II	$-0.08RSS^5+0.99RSS^4-5.16RSS^3+16.63RSS^2-35.24RSS+37.95$	-67.43	10.48
ITU 0	$-0.08RSS^5+0.99RSS^4-5.16RSS^3+16.63RSS^2-35.24RSS+37.95$	-65.36	8.06
+I	$-0.08RSS^5+0.99RSS^4-5.16RSS^3+16.63RSS^2-35.24RSS+37.95$	-68.38	8.06
-I	$-0.08RSS^5+0.99RSS^4-5.16RSS^3+16.63RSS^2-35.24RSS+37.95$	-68.38	8.06
+II	$-0.08RSS^5+0.99RSS^4-5.16RSS^3+16.63RSS^2-35.24RSS+37.95$	-65.36	8.06
WINNER 0	$-0.08RSS^5+0.99RSS^4-5.16RSS^3+16.63RSS^2-35.24RSS+37.95$	-65.93	8.67
+I	$-0.08RSS^5+0.99RSS^4-5.16RSS^3+16.63RSS^2-35.24RSS+37.95$	-69.18	8.67
-I	$-0.08RSS^5+0.99RSS^4-5.16RSS^3+16.63RSS^2-35.24RSS+37.95$	-69.18	8.67
+II	$-0.08RSS^5+0.99RSS^4-5.16RSS^3+16.63RSS^2-35.24RSS+37.95$	-65.93	8.67

**Fig. 3.18 FSPL range estimation model showing RSS-Range data and the 6<sup>th</sup> order polynomial curve fitting as an optimum fit for the data**

correct RSS-range model for their azimuth positions. Comparing the environments, standard deviation is the same for FSPL and ITU but with small difference in mean. This is to say that the two environments are centered in slightly different places but RSS data spread around the center is the same. This shows that FSPL and ITU environments have very similar characteristics when compared to HATA and WINNER.

---

**Algorithm 6** Angle Adaptive Range Estimation Model (AARM)
 

---

**Input:**Estimated AoA,  $\theta'$ ;Range estimation model for each azimuth position  $RM = \{Rm_{\beta_1}, Rm_{\beta_2}, Rm_{\beta_3}, Rm_{\beta_4}\}$ Measured RSS from all beam positions,  $RSS = RSS_1, RSS_2, RSS_3, RSS_4$ **Output:**Users Estimated range,  $R$ 

```

1: for  $i = 1$  to  $m$  do                                ▷  $m$  is number of users
2:   if  $\theta'_i = 1$  OR 102 OR 103 then
3:      $RSS_i = RSS_{1i}$                                 ▷ use measured RSS at azimuth position 0
4:     estimate  $R_i$  using range model,  $Rm_1$ 
5:   else if  $\theta'_i = 2$  then
6:      $RSS_i = RSS_{2i}$                                 ▷ use measured RSS at azimuth position +I
7:     estimate  $R_i$  using range model,  $Rm_2$ 
8:   else if  $\theta'_i = 3$  then
9:      $RSS_i = RSS_{3i}$                                 ▷ use measured RSS at azimuth position -I
10:    estimate  $R_i$  using range model,  $Rm_3$ 
11:   else if  $\theta'_i = 4$  OR 204 OR 305 OR 5 then
12:      $RSS_i = RSS_{4i}$                                 ▷ use measured RSS at azimuth position +II
13:     estimate  $R_i$  using range model,  $Rm_4$ 
14:   else
15:      $R_i = 0$ 

```

---

### 3.10.1 Range Estimation Of Users In Known Environment

To test the range estimation model, the twenty users of Figure 3.16a whose AoA were estimated above were considered as users scattered within the network coverage whose range is to be estimated. Users RSS were measured in all four environments from all azimuth positions, their AoA were estimated based on position with highest RSS for each environment (Algorithm 4). Using these RSS for instance as shown in Figure 3.16b for FSPL environment, range estimation model for each environment was applied to estimate all user range using the RSS that classified them into a particular AoA where they belong. Figure 3.19 shows the estimated range in the four known environments with their actual range shown as well. From this range estimation plot, it was identified that users 6, 10, 14, 15 and 16 located in azimuth position +II has their range correctly estimated with error of  $\pm 1^\circ$  or no error at all. The same thing apply to positions -II and 0 where user ID numbers 7 and 20 are located. User ID number 9 is also located in azimuth 0 but has an error in range estimate of 4m. This is due to it's deviation from azimuth center, the more deviated users are from azimuth center, the more error in range estimation. All users located on azimuth positions +I and -I have

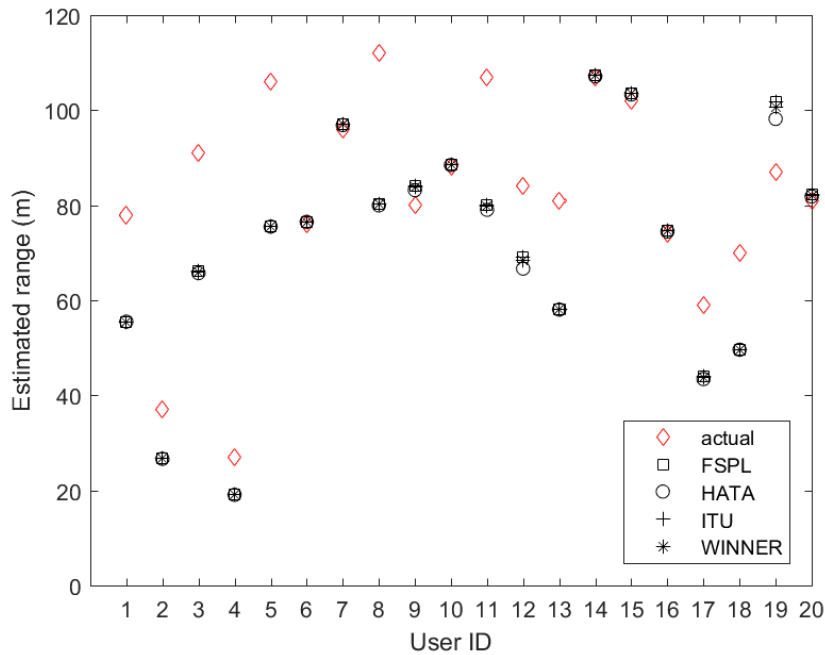


**Fig. 3.19** Range estimation of users in four different known ideal environments showing greater range error with users 1, 2, 3, 4, 5, 8, 12, 13, 17, 18 located in azimuth positions +I and -I but lesser error with other users because they were located in other azimuth positions

their range estimated with high error bounds. Twenty more random users were simulated and from result obtained, it can be confirmed that range estimation is azimuth position dependent with positions +I and -I having most angular deviation error followed by position 0. More accurate range estimate is gotten from azimuth position +II. It can also be noticed that users ID numbers 12 and 19 also have high range estimation error because they are very close to the boundary. They are not completely located at the boundary because the difference in gain (dB) between azimuth positions that share the boundary is not up to the boundary condition threshold. This is an indication that more error may be encountered for users located at the boundary and the error is referred to as ‘boundary user error’ to be investigated later.

### 3.11 Errors in Range Estimation

It has been identified that even for a perfect and well modeled environment where only pathloss is the only loss experienced, under-estimation occur for users located at azimuth position +I and -I peaks. This is an error due to the beam position where they are located. We therefore tag this error as ‘error due to beam position’ to be investigated later. Secondly we considered users systematically arranged at the edge ( $1^\circ$  to boundary) of azimuth position 0 as well as +I for each environment, assuming perfect and correctly modeled environment.

Figure 3.20 is a plot of the estimated range versus the actual range. Apart from the error

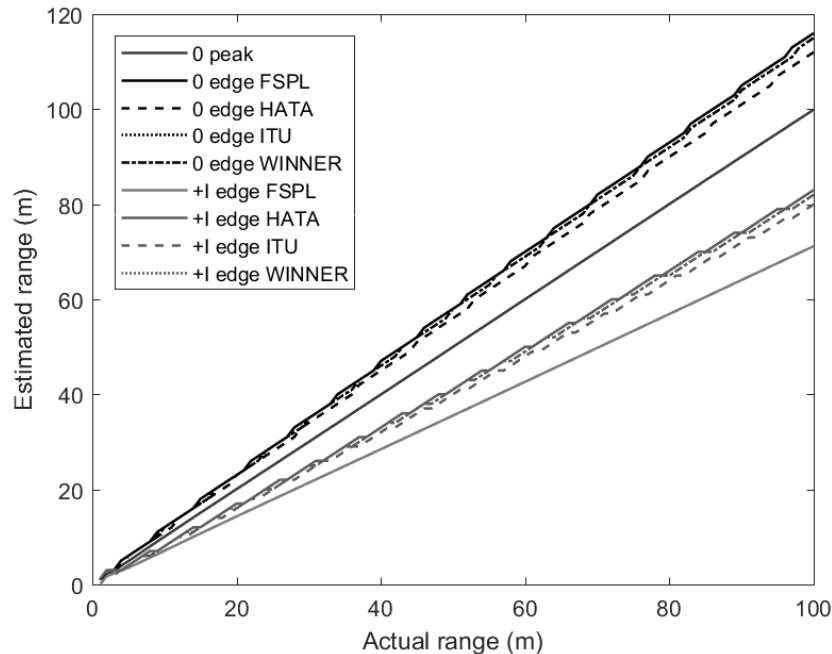


**Fig. 3.20** Range estimation in all known environments for both broadside and off broadside users showing over-estimation error as users are deviated from peak

due to azimuth position, there is error in estimated range of users at azimuth position edges. As seen from Figure 3.20, this error is in the form of over-estimation. This means that over-estimation is encountered as users are deviated from the peak. considering the five azimuth localization positions for the 100 meter range, the probability of users occurring exactly at the azimuth peak is only approximately 2.8% and the remaining 97.2%, users occur at angles deviated from the peak where an error in estimate is expected. Subsequently, this error will be called ‘error due to angular deviation’.

### 3.11.1 Effect of Beam Position on Range Estimation

Having identified that RSS-Range classification is azimuth position dependent, the aim therefore is to carry out an investigation on how this discrepancies may cause error in range estimation and find a possible solution to mitigate against the error for more accurate results. Considering users at beam peaks for the four main beam positions, RSS was measured, range was estimated using models of Table 3.8 for each azimuth peak position user. Result of Figure 3.21 shows that correct range estimation up to a maximum coverage range of 100m is only obtained for users at azimuth positions 0 and +II peaks but not for users at azimuth positions +I and -I peaks. At azimuth positions +I and -I, only a maximum range of approximately

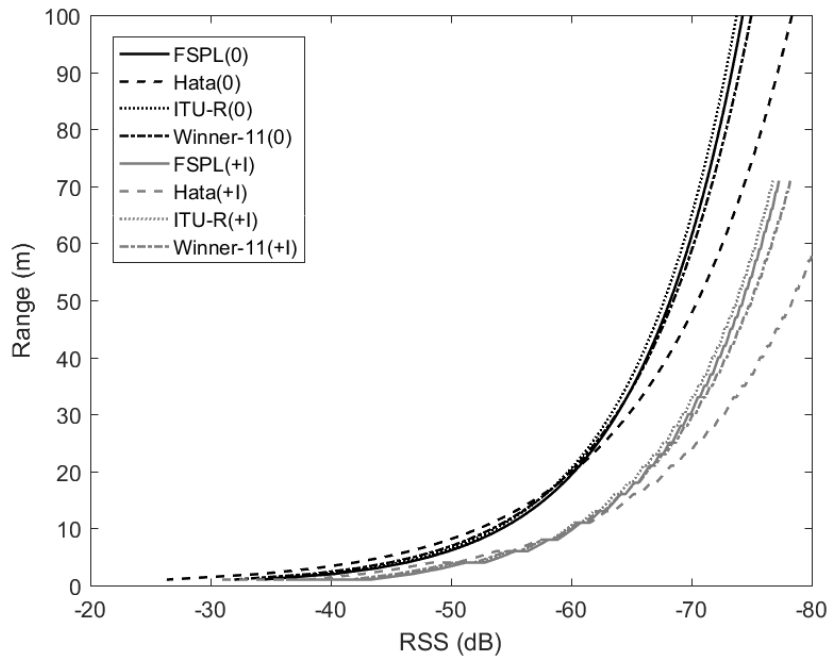


**Fig. 3.21** *Estimated range of azimuth peak users for four different environments showing correct estimation for broadside and difference users but under-estimation for left and right of broadside users*

71m is obtainable for the 100m nominal range. This shows an under-estimation for users at left and right of broadside but not for users at signal sum and difference positions. We can conclude that accuracy of range estimation with this model will be azimuth position dependent. Users located at beams 0, +II and -II azimuth positions will have their range estimated with less error but users located at beams +I and -I positions will encounter high error even if the user is exactly at beam peaks.

### 3.11.2 Effect of User Azimuth Direction on Range Estimation

To investigate the effect of edge user position on range estimation, users at azimuth position edges (1 degree to the boundary) in each azimuth position were considered. For positions 0 and +II, the range estimate of users arranged on the left and others arranged on the right is same but for azimuth positions +I and -I, estimates are equal for both positions but left and right edges of +I or -I position users are different. This show that azimuth positions 0 and +II are symmetrical but azimuth positions +I and -I are not. Figure 3.22 shows a plot of the estimated range for azimuth position 0 edge users (continuous dark line), position +I right (faint dashed line) and left edge users (faint dotted line) and position +II edge users (dark dash and dot line) in FSPL environment. From this figure it can be seen that error value

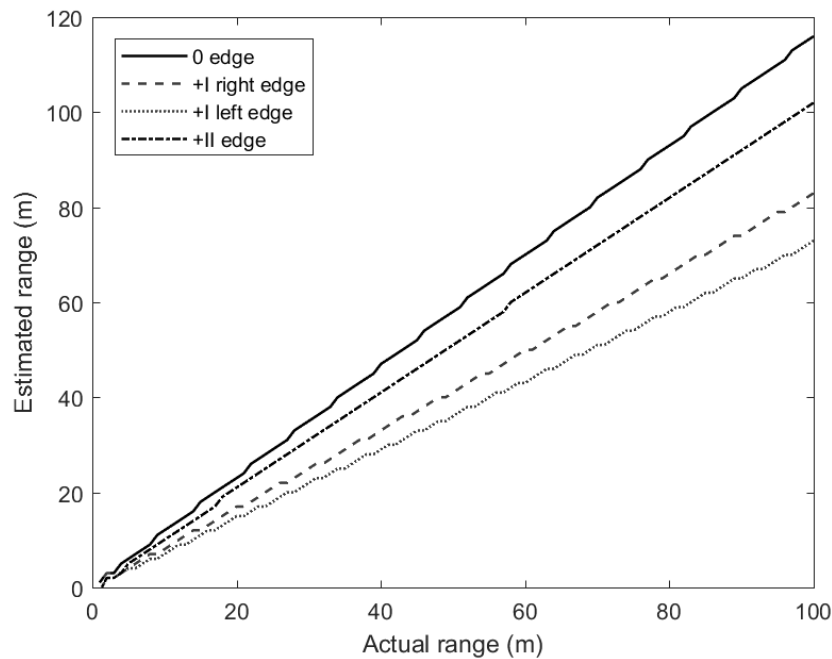


**Fig. 3.22** Range estimation of FSPL beam edge users showing that there is difference in range estimation for users at +I position left and right edges

is dependent on the azimuth location of the user. Azimuth position 0 gives more error spread than position +II. This means that more error due to angular deviation will be encountered if users are located in position 0 area than in position +II area. Range estimates at positions +I and -I are expected to be lower than positions 0 and +II but here it has also been noticed that the estimate is different when users are on left (dotted faint line) and right (dashed faint line) edges of positions +I and -I as shown on Figure 3.22.

### 3.11.3 Effect of Unknown Environment on Range Estimation

The simulation so far has assumed that the environment of RSS measurement was known and so correct environment range model was used for range estimation. Considering a situation where the environment is unknown and so we can not identify the correct range model to be used for range estimation. To investigate the effect of unknown environment on range estimation, users were systematically arranged on the center of azimuth position 0 (1:1:100)m in FSPL, HATA, ITU-R and WINNER-11 environments as illustrated with red cross on top part of Figure 3.23. The four environment range models were used to estimate range of users located in each of the environments. Figure 3.23 shows the range estimation results from each model in each of the environment scenarios. From Figure 3.23, it can be seen that only the range model of it's own environment was able to estimate user range from



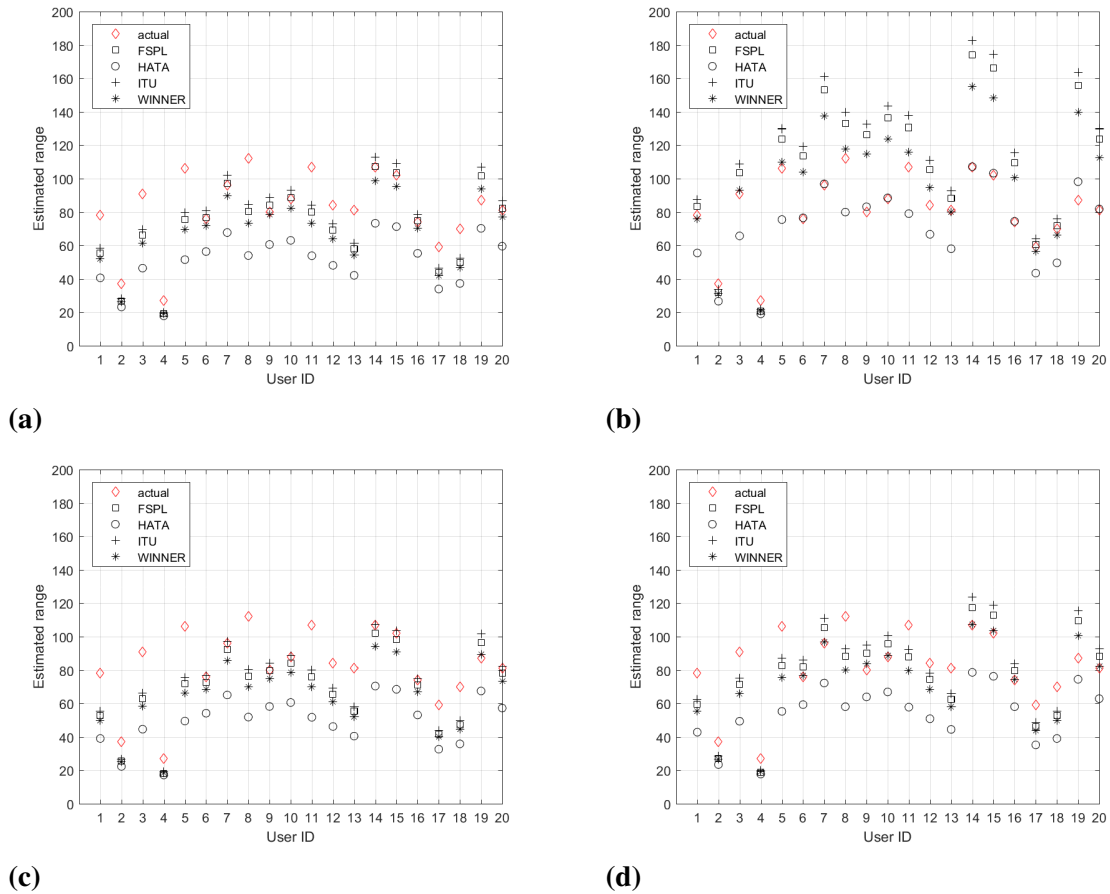


**Fig. 3.24** Range estimation of randomly distributed users in unknown ideal (a) FSPL (b) HATA (c) ITU-R (d) WINNER-11 environments showing that randomly distributed users encounter different kinds of errors based user azimuth location but best estimate is achieved if environment is known

From this figure, it can be seen that for users not affected by already identified errors like users 6,10,14,15 and 16, the best estimate is gotten using the model for that environment. The mean absolute error (MAE) in range estimation obtained in each environment and by each environment model for the twenty sample users are summarized in Table 3.9. From this

**Table 3.9** Mean absolute error in range estimation of users for all environments using all range models

	FSPL	HATA	ITU	WINNER
FSPL	12.62m	30.85m	13.12m	15.83m
HATA	29.57m	12.59m	35.02m	19.89m
ITU	14.75m	32.86m	12.62m	18.54m
WINNER	13.52m	27.83m	14.06m	12.62m

result, a MAE of 12.62m is encountered in FSPL, HATA and WINNER environments using their own range models but between 27m and 30m using HATA model in these environments. It can therefore be concluded that incorrect environment model gives rise to higher error values. Four major system errors that will be inherent on the system if not taken care of are therefore identified. First is the error due to beam position, second is error due to angular deviation, third is boundary user error and fourth is error due to unknown environment. The goal then is to find a way to eradicate or reduce these errors to a bearable minimum in the system.

## 3.12 Range Estimation Error Prediction

In this section, the four identified system errors; error due to beam position, error due to angular deviation, boundary user error and error due to unknown environment were modeled to find a possible solution to eradicate or reduce them.

### 3.12.1 Error Due To Beam Position

Error due to beam position is the unique error encountered by users at azimuth positions +I and -I due to their position making them under-estimate range as shown with users 1, 2, 3, 4, 5, 11, 13, 17 and 18 in Figure 3.19. This is a fundamental error because from the range model of Figure 3.21, the RSS-Range relationship is incorrect at azimuth positions +I and -I as compared to 0 and +II. This can be approached by applying amplitude variation for the different beam steering weighting. This approach will need hardware implementation on the feed network which will increase complexity. Another option would be to compensate for the differences on the algorithm which is simpler and easier needing no hardware implementation. Algorithm based was applied.

### 3.12.2 Beam Position Error Model (BPEM)

The aim at this point is to develop a mathematical model for predicting the required error compensation factor to compensate for beam position error in the system. To do this, users were systematically arranged in azimuth position +I centre in all environments as shown on top left corner of Figure 3.25a, their RSS were calculated and both AoA and range were estimated as already discussed. Beam Position Error Values (BPEV) were calculated which are residuals of the estimated range from the actual range. Environment is assumed to be known. The BPEV is plotted in Figure 3.25a which looks more like a straight line graph. Therefore, based on least square error approach and using polyfit function in matlab, a polynomial of first order was fitted on the data to obtain coefficients  $b_1 = 0.41$  and  $b_2 = 0.03$  which represent the slope and intercept of the BPEV respectively. Equations 3.11, 3.11, 3.11 and 3.11 are the BPEM equation for FSPL, HATA, ITU and WINNER environments

respectively. These are the BPEMs for future beam position error prediction.

$$BPEM_{FSPL} = 0.41R_i + 0.03 \quad (3.11)$$

$$BPEM_{HATA} = 0.41R_i + 0.01 \quad (3.12)$$

$$BPEM_{ITU} = 0.41R_i + 0.03 \quad (3.13)$$

$$BPEM_{WINNER} = 0.41R_i + 0.02 \quad (3.14)$$

where  $R_i$  is the estimated range of  $i^{th}$  user. For any user whose AoA is +I or -I, BPEM is used to predict a compensation value that is added to the estimated distance to compensate for under-estimation due to its azimuth position so that the new estimated range of user  $i$  in say FSPL environment becomes:

$$R'_{BPEM_i} = R_i + BPEV'_i \quad (3.15)$$

Where  $R_i$  and  $R'_{BPEM_i}$  are the estimated range of  $i^{th}$  user before and after BPEM respectively.  $BPEV'_i$  is the predicted beam position error value for  $i^{th}$  user. To test this model, BPEM was applied for the users arranged on azimuth position +I centre (Figure 3.25a top left) in FSPL environment to obtain result of Figure 3.25b. This result gives a mean absolute range

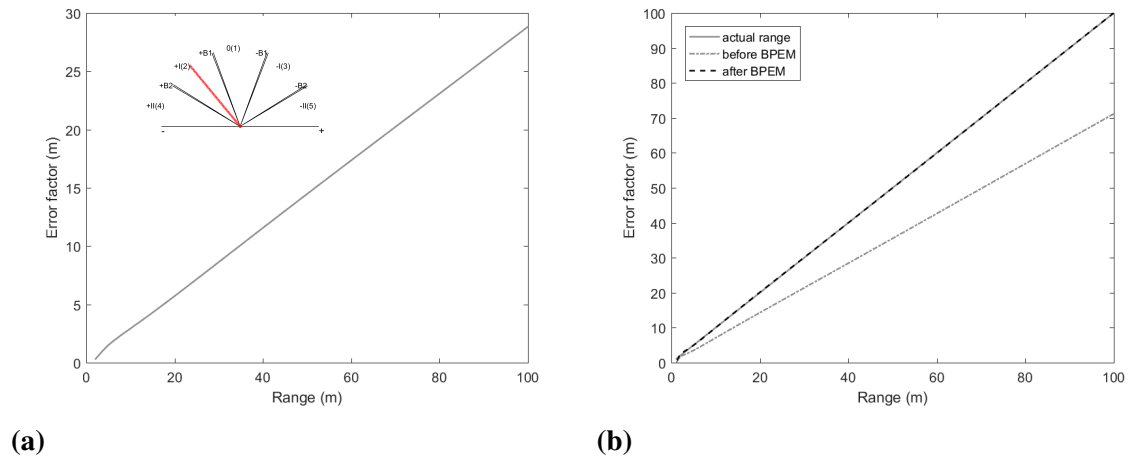


**Fig. 3.25 Improved range estimate with BPEM (a) BPEV for development of BPEM Equation (b) estimated range in FSPL environment for users in azimuth position +I centre before and after BPEM**

estimation error of approximately 14.6m and 0.06m before and after BPEM respectively. This means a percentage error reduction (PER) of 99.6%. It can therefore be concluded that in ideal case, by adding the compensation value generated by BPEM to estimated range of

azimuth position +I or -I centre users, very accurate range estimation is achieved. A step by step approach to developing and implementing the BPEM is given in Algorithm 7.

---

**Algorithm 7** BPEM Algorithm
 

---

**Input:**

Estimated range of users,  $R$ ;

**Output:**

polynomial coefficients ( $b_1, b_2$ )

Estimated range of users after BPEM,  $R'_{BPEM}$ ;

1: For any given environment:

**Step1: Compute the BPEV**

2: Generate users at +I azimuth position centre

3: Apply Algorithm 6 to estimate user range,  $R_{BPEV}$

4:  $BPEV \leftarrow R_{actual} - R_{BPEV}$

**Step2: Fit a polynomial to data and determine the BPEM**

5: Compute the coefficients,  $b_1$  and  $b_2$  that best fits data BPEV based on least square error

**Step3: Apply BPEM to estimated range of users**

6: **for**  $i \leftarrow 1 : m$  **do**

7:     **if**  $\theta'_i = 2$  OR  $3$  **then**

8:          $R'_i = R_i + (b_1R + b_2)$

▷ New estimated user range after BPEM

9:     **else**

10:          $R'_i = R_i$

---

### 3.12.3 Error Due To Angular Deviation

Error due to angular deviation refers to error encountered by users that are not located at azimuth position centers. This error is unavoidable in this system because with only two antenna elements, a wide beam is expected. This error would naturally be reduced with pencil beam [222] which means more antenna elements, more cost and complexity which is against the design criteria in this research. Moreover, considering the design application, the system should be able to cope with a manageable value of this error. Therefore, an investigation on this error targeting the possibility of reducing it to a bearable minimum was carried out. From Figure 3.22, it has been shown that azimuth positions +I and -I are unsymmetrical while 0 and +II are symmetrical. In this error investigation, four azimuth position edge users were therefore considered and these include; azimuth positions +I, 0, -I and -II (same as +II).

#### Angular Deviation Error Model (ADEM)

The target here is to carry out an investigation on how accuracy of user range estimation is affected as users are located away from the azimuth position center. The expectation is to develop a mathematical model that can be used to reduce this error to a possible

bearable minimum. It should be noted that angular deviation error investigation and ADEM development is based on estimated range after BPEM has been applied. Considering the worst case edge user scenario where users are located  $1^\circ$  to the boundary of these azimuth positions. Users were systematically arranged in azimuth positions +I, 0, -I and -II edges separated by 1m from each other as shown with red dots on Figure 3.26a. These sample of users cover both edges of the unsymmetrical +I and -I azimuth positions as well as Positions 0 and +II edges. Range of users were estimated and estimates were compared with the actual range. The difference was then halved to obtain the Angular Deviation Error value (ADEV) for all four azimuth edges considered and for all four environments. Figure 3.26a shows the ADEV for these users in FSPL environment. This is better described as a linear graph than a curve, therefore a first order polynomial was fitted on the data to develop a set of ADEM equations with coefficients  $b_1$  and  $b_2$  for each of the azimuth edge positions and for each environment as presented in Table 3.10.

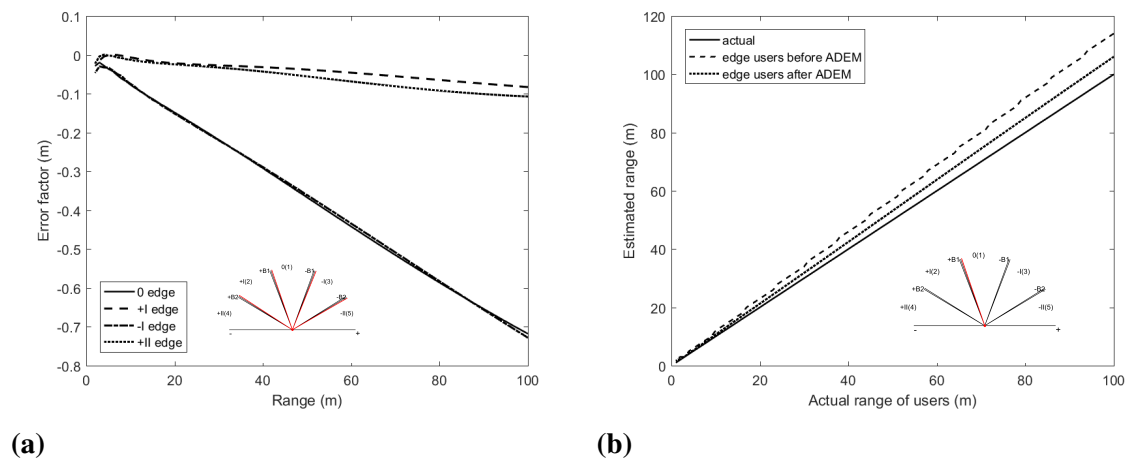


**Fig. 3.26** Angular deviation error model (ADEM) (a) angular deviation error model (ADEM) for FSPL environment based on half the residual (b) range estimation error reduced by half for +I azimuth position edge users

**Table 3.10** ADEM equations for four main azimuth positions in different environments

Azimuth Positions	FSPL	HATA	ITU	WINNER
$ADEM_{+I}$	$-10.1 \times 10^{-3}R + 24.5 \times 10^{-3}$	$-7.75 \times 10^{-3}R + 18.4 \times 10^{-3}$	$-10.1 \times 10^{-3}R + 24.5 \times 10^{-3}$	$-9.39 \times 10^{-3}R + 22.6 \times 10^{-3}$
$ADEM_0$	$-80.8 \times 10^{-3}R - 51.4 \times 10^{-3}$	$-61.2 \times 10^{-3}R - 36.5 \times 10^{-3}$	$-80.8 \times 10^{-3}R - 51.5 \times 10^{-3}$	$-74.8 \times 10^{-3}R - 46.8 \times 10^{-3}$
$ADEM_{-I}$	$-81.0 \times 10^{-3}R - 32.3 \times 10^{-3}$	$-61.3 \times 10^{-3}R - 16.7 \times 10^{-3}$	$-81.0 \times 10^{-3}R - 31.7 \times 10^{-3}$	$-75.0 \times 10^{-3}R - 26.9 \times 10^{-3}$
$ADEM_{+II}$	$-13.2 \times 10^{-3}R + 26.0 \times 10^{-3}$	$-10.0 \times 10^{-3}R + 12.3 \times 10^{-3}$	$-13.2 \times 10^{-3}R + 25.4 \times 10^{-3}$	$-12.2 \times 10^{-3}R + 21.2 \times 10^{-3}$

ADEM equations are therefore applied for future prediction of ADEV for any estimated user range in any of the four environments based on the estimated AoA of that user. The new

estimated user range is then given by:

$$R'_{ADEM_i} = R'_{BPPEM_i} + ADEV'_i \quad (3.16)$$

Where  $R'_{ADEM_i}$  is the new estimated range of  $i^{th}$  user after ADEM has been applied,  $R_{BPPEM_i}$  is the estimated range after BPPEM has been applied and  $ADEV'_i$  is the predicted ADEV for  $i^{th}$  user.

To test the ADEM, users arranged at +I azimuth edge positions in all environments were used. Results before/after ADEM gives a MAE of 7.4m/3.17m, 5.6m/2.5m, 7.4m/3.17m and 6.85m/2.97m in FSPL, HATA, ITU and WINNER respectively giving a PER of 57.2, 55.5, 57.2 and 56.7 respectively. It can therefore be concluded that by adding the ADEM compensation value to estimated range, the estimated range error is reduced by at least 50% for edge users. A step by step algorithm to developing the ADEM is shown in Algorithm 8.

#### 3.12.4 Improved Angular Deviation Error Model (IADEM)

The ADEM investigation so far has been based only on azimuth position edge users which is  $1^\circ$  to the boundary. In this case 50% error reduction in range estimation is achieved using an ADEV divisor of 2 i.e. half the residual. It is expected that as users move towards the azimuth position center, the PER will start decreasing and at azimuth center position, a 50% error increase would be the case. For this reason, an optimum divisor that would achieve less MAE based on users covering a whole azimuth position (center and edge inclusive) be considered. Systematic users were generated at each  $1^\circ$  angle and for every 1m distance apart, covering edge to edge of 0 azimuth position as shown on red in Figure 3.27. Range was estimated with assumption that environment of RSS measurement was known. ADEM was applied for divisor values of 1 in a space of 1 to 20. At each divisor level, the MAE in range estimation was calculated. The divisor level that returned the minimum MAE was considered as the divisor that would provide the optimum solution for angular deviation error reduction in this system. Result of Figure 3.27, shows that the optimum solution is obtained with a divisor of 4 as indicated with a filled circle.

IADEM was compared with ADEM using users covering the azimuth position 0 as shown in Figure 3.27 for FSPL environment. Their range estimation result give a MAE of 2.53m before ADEM (i.e. after BPPEM) but a MAE of 2.26m and 1.85m after ADEM and IADEM respectively. From this result, it can be seen that a PER of 10.81% and 27.13% are achieved with ADEM and IADEM respectively, giving 18% more reduction in range estimation error With IADEM when compare to ADEM. Instead of half the Angular Deviation Error Value

---

**Algorithm 8** ADEM Algorithm
 

---

**Input:**

Estimated range after BPEM,  $R'_{BPEM}$ ;  
 Estimated AoA,  $\theta'$ ;

**Output:**

Estimated range after ADEM,  $R'_{ADEM}$ ;

**Step1: Develop ADEM equation**

- 1: Define beam edge angles for azimuth positions +I, 0, -I and -II
- 2: For any given environment:
- 3: **for**  $j \leftarrow 1 : 4$  **do** ▷ azimuth user positions
- 4:     Generate users at  $j^{th}$  azimuth positions in interval of 1m
- 5:     Measure RSS of users ▷ Algorithm 1
- 6:     Estimate AoA,  $\theta'$  and neighboring Position,  $NP$  of users ▷ Algorithm 4
- 7:     Estimate range of users ▷ Algorithm 6
- 8:     Apply BPEM to estimated range,  $R'_{BPEM}$  ▷ Algorithm 7
- 9:     Calculate,  $ADEV_j = (R - R'_{ADEM_j})/2$
- 10:    Fit a polynomial of best fit to ADEV data to obtain  $b_{1j}, b_{2j}$

**Step2: Apply ADEM to estimated range after BPEM**

- 11: **for**  $i \leftarrow 1 : m$  **do** ▷ m is number of users
  - 12:    **if**  $(\theta'_i \leftarrow +I$  OR  $-I)$  AND  $(NP_i \leftarrow +II$  OR  $-II)$  **then**
  - 13:        $R'_{ADEM_i} \leftarrow R'_{BPEM_i} + b_{1_{ADEV'_+I}} \times R'_{BPEM_i} + b_{2_{ADEV'_+I}}$  ▷ Predict ADEV using  
 $ADEM_{+I}$
  - 14:    **else if**  $\theta'_i \leftarrow 0$  AND  $(NP_i = +I$  OR  $-I)$  **then**
  - 15:        $R'_{ADEM_i} \leftarrow R'_{BPEM_i} + b_{1_{ADEV'_0}} \times R'_{BPEM_i} + b_{2_{ADEV'_0}}$  ▷ Predict ADEV using  $ADEM_0$
  - 16:    **else if**  $(\theta'_i \leftarrow +I$  OR  $-I)$  AND  $NP_i = 0$  **then**
  - 17:        $R'_{ADEM_i} \leftarrow R'_{BPEM_i} + b_{1_{ADEV'_{-I}}} \times R'_{BPEM_i} + b_{2_{ADEV'_{-I}}}$  ▷ Predict ADEV using  
 $ADEM_{-I}$
  - 18:    **else if**  $(\theta'_i \leftarrow +II$  OR  $-II)$  AND  $(NP_i \leftarrow +I$  OR  $-I)$  **then**
  - 19:        $R'_{ADEM_i} = R'_{BPEM_i} + b_{1_{ADEV'_{-II}}} \times R'_{BPEM_i} + b_{2_{ADEV'_{-II}}}$  ▷ Predict ADEV using  
 $ADEM_{-II}$
  - 20:    **else**  $R'_{ADEM_i} = R'_{BPEM_i}$
- 

(ADEV), a quarter the ADEV was used to develop an improved Angular Deviation Error Model (IADEM) of Table 3.11.

### 3.12.5 Range Estimation Of Random Sample Users With BPEM and ADEM

So far, systematic users were used to investigate, develop and test the identified errors. Practically, users are not deployed systematically in a wireless network environment, therefore

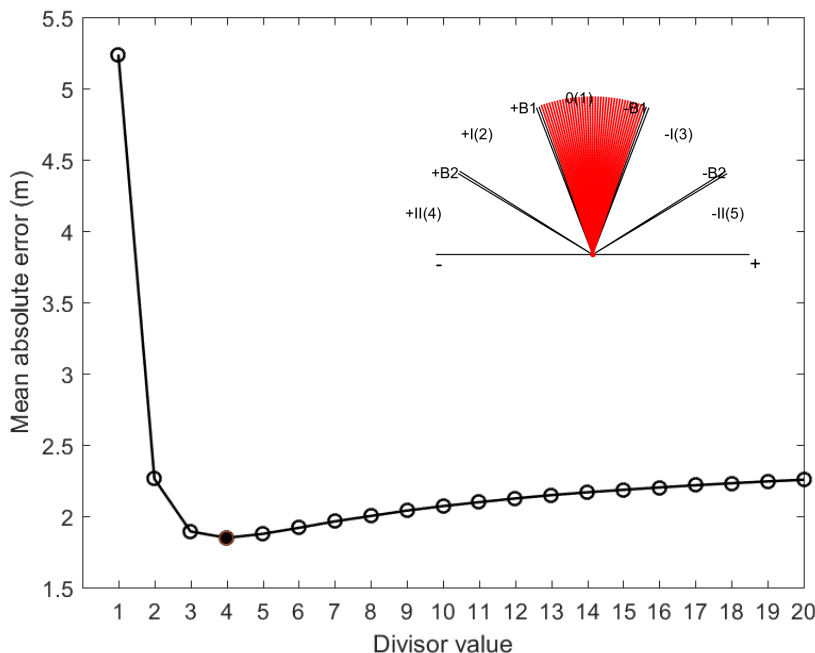


**Fig. 3.27** Dividing factor used in developing ADEM to achieve optimum error reduction in range estimation

**Table 3.11** IADEM equations for four main azimuth positions in different environments

Azimuth Positions	FSPL	HATA	ITU	WINNER
$ADEM_{+I}$	$-4.22 \times 10^{-3}R + 12.1 \times 10^{-3}$	$-3.24 \times 10^{-3}R + 8.88 \times 10^{-3}$	$-4.22 \times 10^{-3}R + 12.1 \times 10^{-3}$	$-3.92 \times 10^{-3}R + 11.1 \times 10^{-3}$
$ADEM_0$	$-36.1 \times 10^{-3}R - 24.6 \times 10^{-3}$	$-27.4 \times 10^{-3}R - 17.7 \times 10^{-3}$	$-36.1 \times 10^{-3}R - 24.7 \times 10^{-3}$	$-33.5 \times 10^{-3}R - 22.5 \times 10^{-3}$
$ADEM_{-I}$	$-36.1 \times 10^{-3}R - 18.6 \times 10^{-3}$	$-27.4 \times 10^{-3}R - 10.9 \times 10^{-3}$	$-36.1 \times 10^{-3}R - 18.3 \times 10^{-3}$	$-33.5 \times 10^{-3}R - 16.0 \times 10^{-3}$
$ADEM_{+II}$	$-5.87 \times 10^{-3}R + 16.2 \times 10^{-3}$	$-4.46 \times 10^{-3}R + 9.42 \times 10^{-3}$	$-5.86 \times 10^{-3}R + 15.9 \times 10^{-3}$	$-5.44 \times 10^{-3}R + 13.9 \times 10^{-3}$

random users were also used to test these error models. To appreciate the effect and be able to compare with result obtained when these errors were identified, the same twenty random users of Figure 3.16a in FSPL environment was used. Figures 3.28a and 3.28b are show the estimated range of distributed random users before and after ADEM.

From result of Figure 3.28a, it can be seen that range of users in azimuth positions +I and -I (user ID numbers 1, 2, 3, 4, 5, 11, 13, 17 and 18) were estimated with minimal error. MAE before and after BPEM for this sample is 12.6m and 2.36m respectively giving a PER of 81%. Error due to angular deviation is still noticeable with users 9 and 12. Figure 3.28b is the range estimation plot after applying the angular deviation error model. Users 9 and 12 errors were reduced from an over-estimation of approximately 3.8m to 0.9m and 12.1m to 8.9m. respectively. MAE after ADEM for this sample is approximately 1.66m giving a PER of approximately 30% between BPEM and ADEM application.

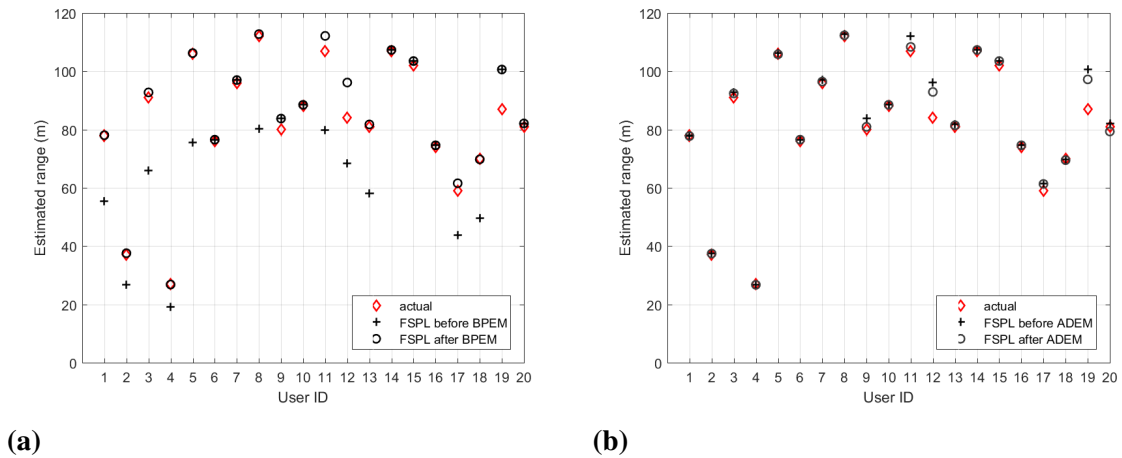


**Fig. 3.28** Range estimation of randomly distributed users (a) before (after BPEM) (b) after ADEM showing better range estimation accuracy for users located at azimuth positions  $+I$  and  $-I$  and users deviated from the azimuth center

### 3.12.6 Boundary User Error Model (BUEM)

Boundary user error are errors peculiar to the users at the boundary. This error occur because there is no beam switched to the boundary rather they are dependent on two adjacent beams. Users at the boundary were not captured by the ADEM because they are beyond the beam edge. Since there is possibility of users occurring at the boundary, errors in range estimation of users at the boundary was modeled.

The aim is to carry out an investigation on how accuracy of range estimation with this system is affected by azimuth position boundary users. The target is to develop mathematical BUEM equations for future prediction and compensation of range error due to users located at the boundary for more accurate user range estimation. To develop the BUEM, systematic users separated by 1m distance from each other was generated at boundary center positions for the four boundaries  $+B2$ ,  $+B1$ ,  $-B1$ ,  $-B2$  as shown with red dots in Figure 3.29a. Range of these users were estimated using adaptive angle range estimation model with BPEM and ADEM applied. Difference between estimated range and actual range were calculated for each user and halved to obtain the boundary user error value (BUEV) for all four environments and for all four azimuth boundary positions. Figure 3.29a shows the Boundary User Error Model (BUEM) for all four environments for users arranged at boundary  $+B1$ . Fitting a polynomial into BUEV, coefficients of the polynomial are obtained to form the BUEM equations shown in Table 3.12 which are used for future prediction of the BUEV' for any user whose AoA is estimated to be at the boundary.

**Table 3.12** *BUEM equations for four main azimuth positions in different environments*

Boundary Positions	FSPL	HATA	ITU	WINNER
+B2	$-11.0 \times 10^{-3}R + 24.6 \times 10^{-3}$	$-8.41 \times 10^{-3}R + 18.7 \times 10^{-3}$	$-11.0 \times 10^{-3}R + 24.6 \times 10^{-3}$	$-10.2 \times 10^{-3}R + 22.7 \times 10^{-3}$
+B1	$-85.3 \times 10^{-3}R - 52.8 \times 10^{-3}$	$-64.5 \times 10^{-3}R - 37.4 \times 10^{-3}$	$-85.3 \times 10^{-3}R - 52.9 \times 10^{-3}$	$-78.9 \times 10^{-3}R - 48.0 \times 10^{-3}$
-B1	$-85.3 \times 10^{-3}R - 52.8 \times 10^{-3}$	$-64.5 \times 10^{-3}R - 37.4 \times 10^{-3}$	$-85.3 \times 10^{-3}R - 52.9 \times 10^{-3}$	$-78.9 \times 10^{-3}R - 48.0 \times 10^{-3}$
-B2	$-14.6 \times 10^{-3}R + 90.2 \times 10^{-3}$	$-11.2 \times 10^{-3}R + 65.9 \times 10^{-3}$	$-14.6 \times 10^{-3}R + 90.1 \times 10^{-3}$	$-13.6 \times 10^{-3}R + 82.6 \times 10^{-3}$

The predicted BUEV' for any boundary user is then added to the estimated range as given in Equation 3.17 to compensate for error due to their being positioned at the boundary.

$$R'BUEM_i = R'ADEM_i + BUEV'_i \quad (3.17)$$

BUEM was tested for systematic users arranged in all four boundary in all environments, obtained results gave a MAE of 8.72 (3.62), 6.59 (2.87) 8.72 (3.62) and 8.07 (3.40) before (after) BUEM which means a PER of 58.53%, 56.45% 58.53% and 57.90 in FSPL, HATA, ITU and WINNER environments respectively. A plot of the estimated range of users arranged in +B1 boundary in FSPL environment before and after BUEM is shown in Figure 3.29a. Algorithm 9 is a step by step approach to developing and implementing the BUEM.

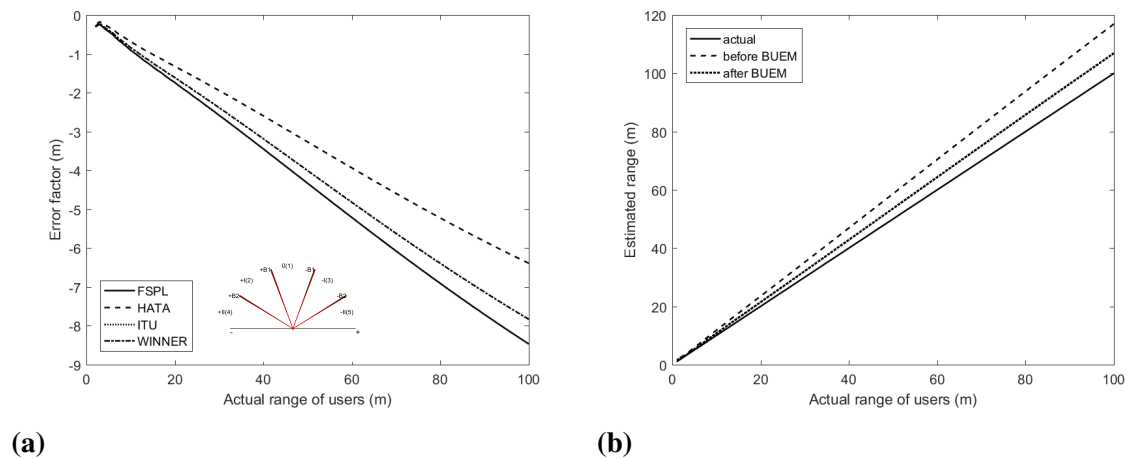


**Fig. 3.29** *Boundary user error model (BUEM) (a) calculated BUEV used to develop the BUEM in all four environments (b) range estimation error of +B1 boundary users reduced by half*

### 3.12.7 Performance Analysis of System Error Models

The performance of simulated error models, BPEM, IADEM, and BUEM were tested for both systematic and random users. For the former, more samples of users covering the entire network coverage area (boundaries inclusive) at  $1^\circ$  angle and 1m distance from each other in FSPL environment were considered. Using the percentage error in the system before

---

**Algorithm 9** BUEM Algorithm
 

---

**Input:**Estimated range after ADEM,  $R'_{ADEM}$ Estimated AoA,  $\theta'$ ;**Output:**Estimated range after BUEM,  $R'_{BUEM}$ **Step1: Develop ADEM equation**

- 1: Define boundary angles for azimuth positions +I, 0, -I and -II
- 2: For any given environment:
- 3: **for**  $j \leftarrow 1 : 4$  **do** ▷ azimuth user positions
- 4:   Generate users at  $j^{th}$  azimuth positions in interval of 1m
- 5:   Measure RSS of users ▷ Algorithm 1
- 6:   Estimate AoA,  $\theta'$  ▷ Algorithm 4
- 7:   Estimate range of users ▷ Algorithm 6
- 8:   Apply BPEM to estimated range,  $R'_{BPEM}$  ▷ Algorithm 7
- 9:   Calculate,  $BUEV_j = (R - R'_{BPEM_j})/2$
- 10:   Fit a polynomial of best fit to BUEV data to obtain  $b_{1j}, b_{2j}$

**Step2: Apply BUEM to estimated range after BPEM and ADEM**

- 11: **for**  $i \leftarrow 1 : m$  **do** ▷ m is number of users
  - 12:   **if**  $(\theta'_i \leftarrow +B2)$  **then**
  - 13:      $R'_{BUEM_i} \leftarrow R'_{ADEM_i} + b_{1_{BUEV'+B2}} \times R'_{ADEM} + b_{2_{ADEV'+B2}}$  ▷ Predict ADEV using  
 $BUEM_{+B2}$
  - 14:   **else if**  $(\theta'_i \leftarrow +B1)$  **then**
  - 15:      $R'_{BUEM_i} \leftarrow R'_{ADEM_i} + b_{1_{BUEV'+B1}} \times R'_{ADEM} + b_{2_{ADEV'+B1}}$  ▷ Predict ADEV using  
 $BUEM_{+B1}$
  - 16:   **else if**  $(\theta'_i \leftarrow -B1)$  **then**
  - 17:      $R'_{BUEM_i} \leftarrow R'_{ADEM_i} + b_{1_{BUEV'-B1}} \times R'_{ADEM} + b_{2_{ADEV'-B1}}$  ▷ Predict ADEV using  
 $BUEM_{-B1}$
  - 18:   **else if**  $(\theta'_i \leftarrow -B2)$  **then**
  - 19:      $R'_{BUEM_i} \leftarrow R'_{ADEM_i} + b_{1_{BUEV'-B2}} \times R'_{ADEM} + b_{2_{ADEV'-B2}}$  ▷ Predict ADEV using  
 $BUEM_{-B2}$
  - 20:   **else**  $(R'_{BUEM_i} = R'_{ADEM_i})$
- 

any of the error models were applied as the reference, resulting MAE after applying each model was calculated as given in Table 3.13. This result shows that BPEM reduces the error by approximately 78.8% which is a good improvement. On the other hand, applying IADEM achieves a PER of 84.3% which is about 26.3% over what is achieved with just BPEM. By implementing BUEM, range estimation error reduction for boundary users were also implemented achieving a PER of 26.5% over BPEM. PER between ADEM and BUEM

**Table 3.13 Performance evaluation of BPEM, IADEM and BUEM using systematic users**

Error models	Before (MAE (m))	After (MAE (m))	% Error Reduction (%)
BPEM	6.43	1.367	78.75
IADEM	6.43	1.007	84.35
BUEM	6.43	1.005	84.37

is only about 0.2% but this is understandable since BUEM affects only boundary users and out of the entire sample of 180 angles by 100 users, boundary users are only 4 angles by 100 users which is just about 2.3% of the entire sample. Summarily, these three range estimation error models will improve the estimated range accuracy in this system by 84.37% which is a significant positive effect on the system.

To carry out error model performance test for random users, the twenty random users being used in this thesis were considered. Result of Figure 3.30 shows a MAE of 12.61m and 2.36m for before and after BPEM. A MAE of 1.66m was achieved after IADEM as well as after BUEM. This is the same because there was no boundary user among the sample users. In total, 86.9% error in range estimation reduction was achieved by using these error models in this system for range estimation of these random sample users. For one hundred samples of 20 and also 100 other random users, an average of 87.0% and 87.2% PER were achieved. In summary, it can be concluded that these error models have significant positive effect on the performance of this system.

### 3.12.8 Environment Adaptive Range Model (EARM)

It has been established that best range and localization estimation is obtained if the environment of RSS measurement is known. In two phase localization system, first phase is used to know the environments by a process of fingerprinting which is time and cost intensive. This system avoids this but carries out an investigation on range estimation in four different environments with the intention of developing a mathematical EARM model that can be used to determine the environment of RSS measurement among all four environments. If the correct environment is identified, the system can then adopt the estimated range by that environment model as the most accurate range estimate for users in that network. To develop the Environment Adaptive Range Model (EARM), users systematically arranged at azimuth position +I center were considered. RSS was evaluated in each of the four environments and the range was estimated in each case. For all measured RSS in each environment and in each azimuth position, all environment range models of Table 3.8 were used to estimate user range. Figure 3.31 shows a plot of the actual user range against the estimated range of users in each case. In this plot, environment is differentiated by color and models by line

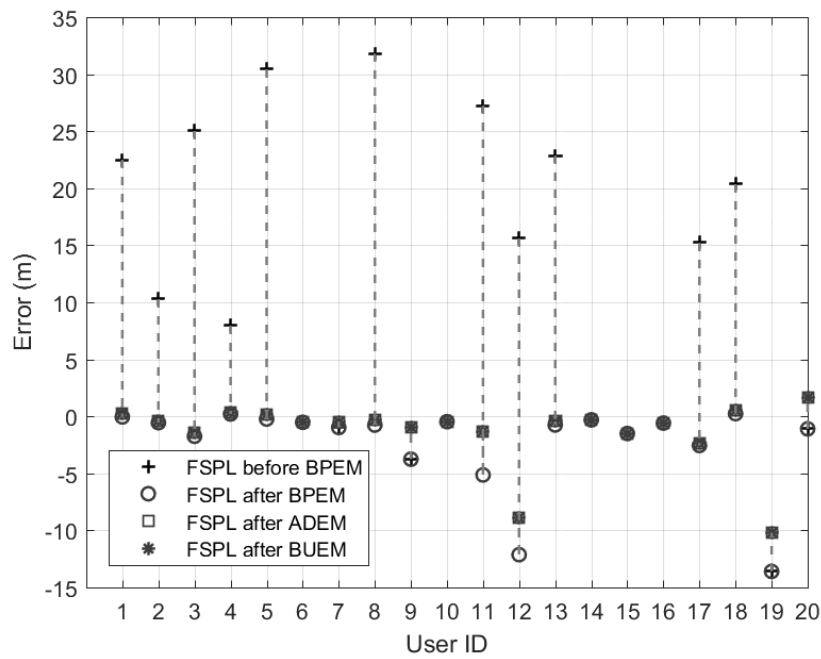


**Fig. 3.30** Performance evaluation of BPEM, IADEM and BUEM using random sample users

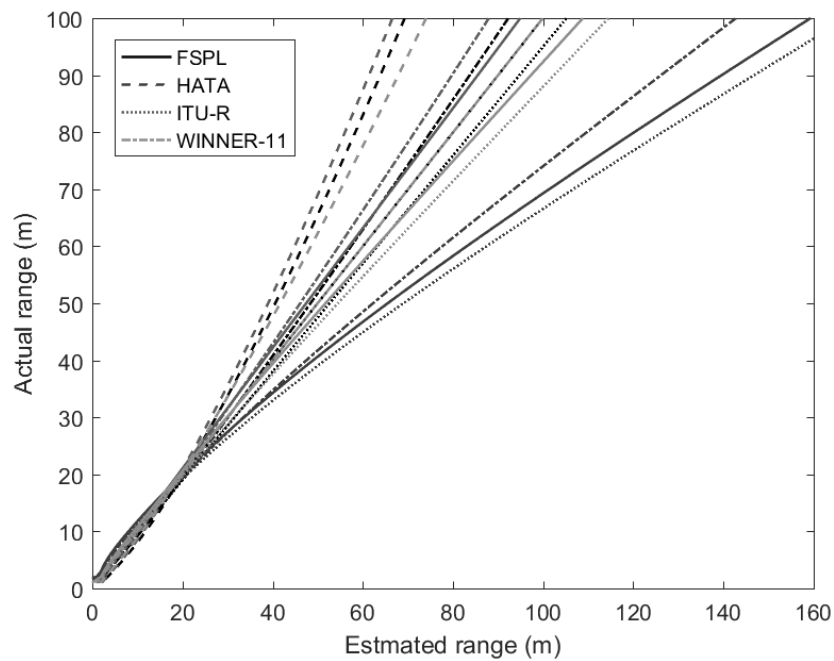


**Fig. 3.31** Range prediction using estimated range in four different environments with four range models in each environment for EARM development

style. This Figure shows that each model estimates range differently in each environment. It can also be noticed that in each environment, only the model of that environment return the correct user range estimates from 1m to 100m.

Polynomial of second order was identified to fit this data with least mean absolute error. Therefore 2<sup>nd</sup> order polynomial was fitted on this plot data to derive different equations given in Table 3.14 which describes how range is estimated in different environments using different range models. From Table 3.14, it can be seen that the equations are different for

**Table 3.14 Environment adaptive range estimation models**

Models	FSPL	Mean	Std
FSPL	$0.00R'^2 + 29.01R' + 50.50$	50.50	29.01
HATA	$2.47R'^2 + 29.44R' + 48.06$	39.48	18.91
ITU	$0.01R'^2 + 29.01R' + 50.49$	53.18	30.54
WINNER	$0.72R'^2 + 29.05R' + 49.79$	48.28	26.40
HATA			
FSPL	$-2.53R'^2 + 29.434R + 53.00$	70.58	48.20
HATA	$0.00R'^2 + 29.01R + 50.50$	50.50	29.01
ITU	$-2.52R'^2 + 29.43R + 53.00$	74.29	50.65
WINNER	$-1.86R'^2 + 29.24R + 52.34$	65.69	42.77
ITU			
FSPL	$0.00R'^2 + 29.01R + 50.50$	47.95	27.55
HATA	$2.47R'^2 + 29.44R + 48.06$	37.93	18.17
ITU	$0.00R'^2 + 29.01R + 50.50$	50.50	29.01
WINNER	$0.71R'^2 + 29.05R + 49.80$	46.01	25.16
WINNER			
FSPL	$-0.72R'^2 + 29.05R + 51.21$	53.07	32.01
HATA	$1.82R'^2 + 29.24R + 48.70$	40.87	20.60
ITU	$-0.71R'^2 + 29.04R + 51.20$	55.88	33.69
WINNER	$0.00R'^2 + 29.01R + 50.50$	50.50	29.01

each range model in each environment but the same for models in their own environment. For instance, FSPL range model used in FSPL environment is same with HATA model used in HATA environment and they are the same for other environments. This equation therefore, describes the range estimation equation for the correct environment of measurement which will subsequently referred to as the EARM. For all measured RSS in any given environment, range is estimated using all four environment range models. EARM was then applied in each case to predict range for the correct environment. By evaluating the error between estimated range and predicted range for all users in the environment, range model with the least average error was returned as the environment of RSS measurement and the estimated range of all

users by the predicted environment model was adopted as the best range estimate. Algorithm 10 is a step by step approach to developing the EARM.

---

**Algorithm 10** EARM Algorithm

---

**Input:**

Estimated range after BUEM,  $R'_{BUEM}$

**Output:**

Estimated range after EARM,  $R'_{EARM}$

**Step1: Develop EARM equation**

- 1: For any given environment:
- 2: **for**  $R_m \leftarrow 1 : 4$  **do** ▷ environment range model
- 3:     Generate users at +I azimuth positions center
- 4:     Measure RSS of users ▷ Algorithm 1
- 5:     Estimate AoA,  $\theta'$  ▷ Algorithm 4
- 6:     Estimate range ▷ Algorithm 6
- 7:     Fit a polynomial of best fit to BUEV data to obtain  $b_1, b_2, b_3$

**Step2: Apply EARM to identify environment of RSS measurement**

- 8:     **for**  $i \leftarrow 1 : m$  **do**
  - 9:         Evaluate,  $EARM_i = b_1 \times R_{BUEM_i}^2 + b_2 \times R'_{BUEM_i} + b_3$
  - 10:  $\forall (i_1 : i_m); R'_{EARM} = \arg \min_{R_m} |R'_{BUEM} - EARM|$
- 

EARM was tested using systematic users at azimuth position +I center and result of Table 3.15 shows that for measured RSS in all four environments, correct environment of RSS measurement was identified in each case by applying EARM. EARM was also tested with random sample users but only FSPL environment was identified as ITU while others were correctly identified. More accurate results are achieved if the environments were clearly different. If the environments are similar, there is not much error in range estimate because any of the chosen environments will produce similar results for the estimated range.

**Table 3.15** Mean absolute error after EARM for four different environments

	FSPL (m)	HATA (m)	ITU (m)	WINNER (m)
FSPL	0.03	33.49	5.23	5.54
HATA	32.64	0.03	37.64	25.62
ITU	5.23	38.76	0.03	10.16
WINNER	5.49	26.12	10.10	0.03

### 3.12.9 Noise Model

Practically, there is no perfect environment, all environments are prone to noise, attenuation and interference. Any environment is also prone to change in characteristics due to

change in vegetation or construction of new building etc. The effect of these environmental changes on the system performance was investigated. Normally noise in information theory is modeled as additive white Gaussian noise (AWGN) which is a basic noise model used to mimic the effect of many random processes that occur in nature. Any noise experienced in the system or in the environment would cause error in measured RSS.

A close investigation on how much of range estimation error will be encountered for different levels of error in simulated RSS was carried out. For deterministic errors of  $-1\sigma$ ,  $0.5\sigma$  and  $1\sigma$  on measured RSS in FSPL environment, the error in estimated range is as shown in Figure 3.32a. If noise adds to simulated RSS, over-estimation occurs but if noise subtracts from simulated RSS, then under-estimation occurs. As expected, error spread increases with  $\pm$ error value in added RSS and also with distance. In real life error is random as shown in Figure 3.32b and not deterministic. The level of noise that will occur in any environment at any given time is not predictable so the interest lies on determining how well the system can cope with some levels of this noise.

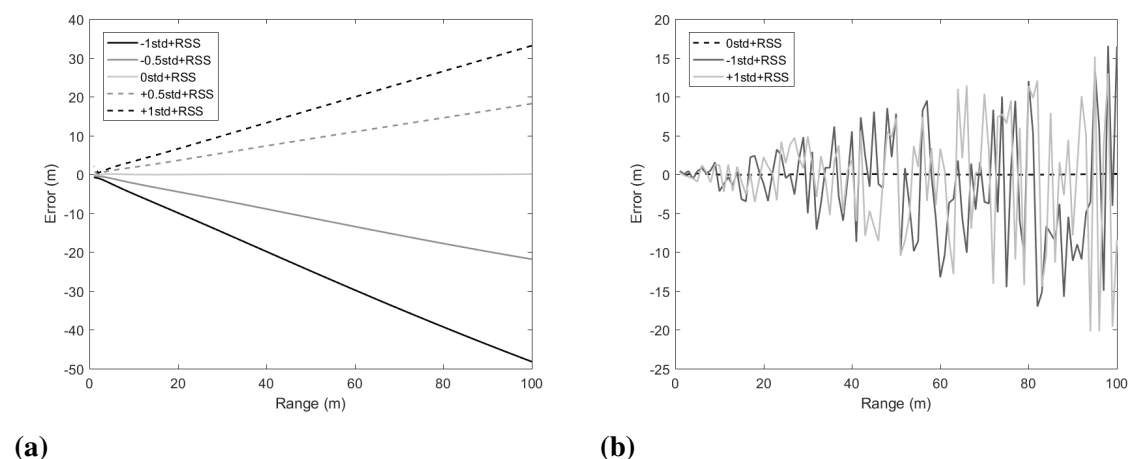


**Fig. 3.32** Boundary user error model using +B1 boundary users (a) error spread with distance for  $\pm 0.5$  error in measured RSS (b) +B1 expected error for multiples of random error in measured RSS

Occurrence of over-estimation or under-estimation can not be predicted in practical sense, hence, there is need to apply statistical tools like mean, median or mode to get a single value that better represents the expected value. Twenty different random noise were added to the measured RSS of the sample users in the four main azimuth positions as shown in Figure 3.33. Mean, median and mode were calculated for each user and plotted as well. By calculating the mean error, it was found out that mean gives a result closer to the measured RSS before

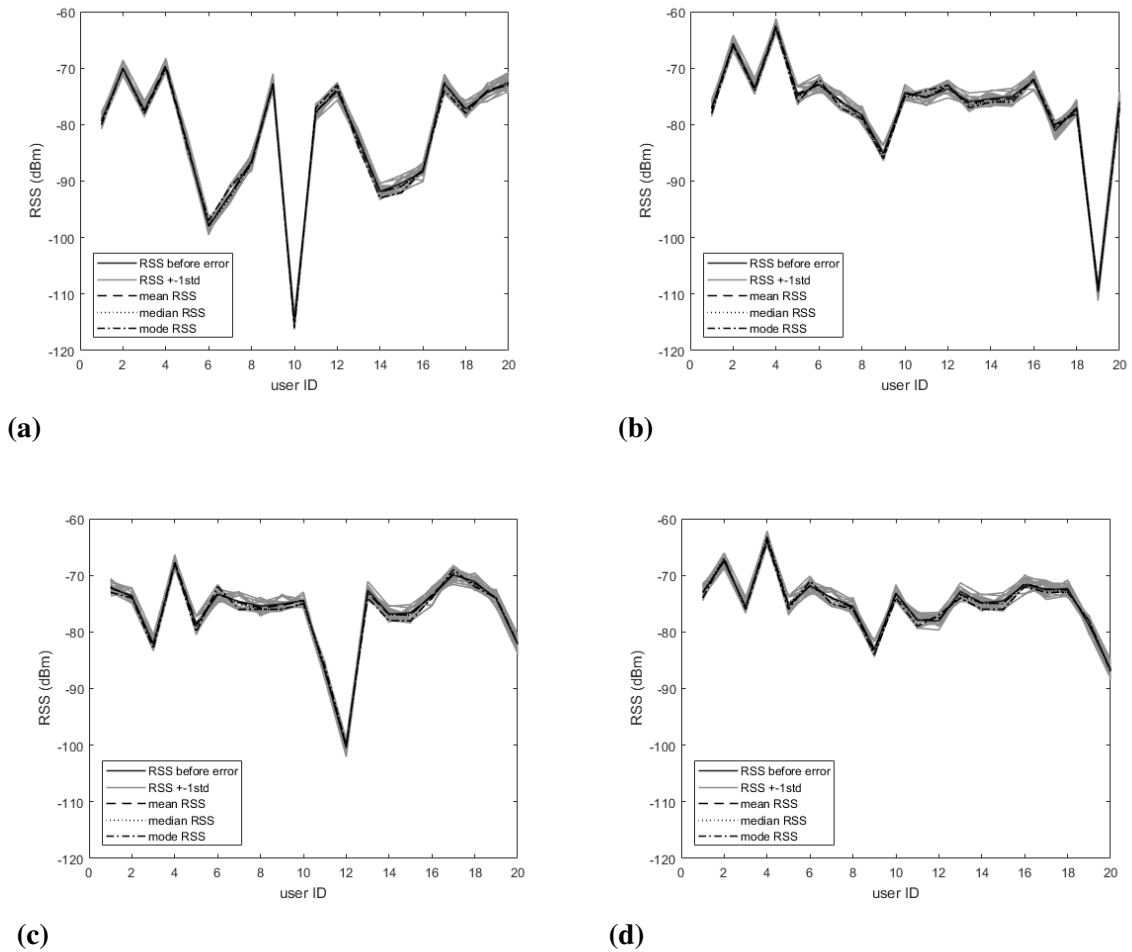


**Fig. 3.33** Measured RSS of twenty sample users at four main azimuth positions (a) 0 (b) +I (c) -I (d) +II with mean, median and mode to determine the best statistical tool for more accurate result

adding error than median and mode as shown in Table 3.16. By taking many measurements and using the mean value, effect of noise on the measured result will be reduced.

**Table 3.16** Statistical Evaluation of Measured RSS with Random Noise

	Mean (m)	Median (m)	Mode (m)
RSS at 0	0.20	0.33	0.73
RSS at +I	0.21	0.33	0.71
RSS at -I	0.20	0.34	0.82
RSS at +II	0.22	0.37	0.77

### 3.13 System Application in 2-tier HetNet

In this section, the system is simulated for the purpose of its design application which is to identify optimum positions for small cell deployment based on user cluster. The aim is to resolve user AoA and range to locate users into different classes of the network location positions. By counting the number of users in each class, user cluster was resolved and locations for small cell deployment identified. Considering a micro-pico HetNet where picocells are required to be deployed within an existing macrocell. Some of the cellular network parameters as discussed in [183, 223] and summarized in Table 3.17 were adopted. The network coverage area was simulated for a nominal range of 500m but still with the

**Table 3.17 LTE-A Parameters For Simulation**

Simulation Parameter	values
Macro cell ISD	500 m
Max Macro Tx Power	46dBm
Max Pico Tx Power	30dBm
Macro antenna gain	14dBi
Minimum distance between pico and macrocells	75m
Minimum distance between picos	40m
Minimum distance between macro and users device	25m
Minimum distance between pico and users device	10m
Number of user devices per macrocell	30
Number of user devices per picocell	7

worst case scenario of dipole elements for both transmitter and receiver and a transmitter power of 0dBm. Considering 50 users scattered within the network coverage area as shown in Figure 3.34 whose locations are to be identified and used for evaluating optimum small cell deployment positions.

To identify optimum positions for small cell deployment, the system measures RSS from user devices in different azimuth positions. Using the received data, AoA as well as range of each user with all error models applied for more accurate result is obtained. Users are then classified into angle and range classes of the network coverage area. By counting the number of users in each angle and range class, user clusters are determined as shown in Figure 3.35b for the deployed fifty sample users. In this figure, the system identifies positions for small cell deployment as those locations with circled values with an assumption that the network operators have decided that small cells are deployed at locations with seven or more users given in Table 3.17. The system also displays the coordinates of these locations as well as the population of users in those locations as shown on the table of Figure 3.35b. In this way,

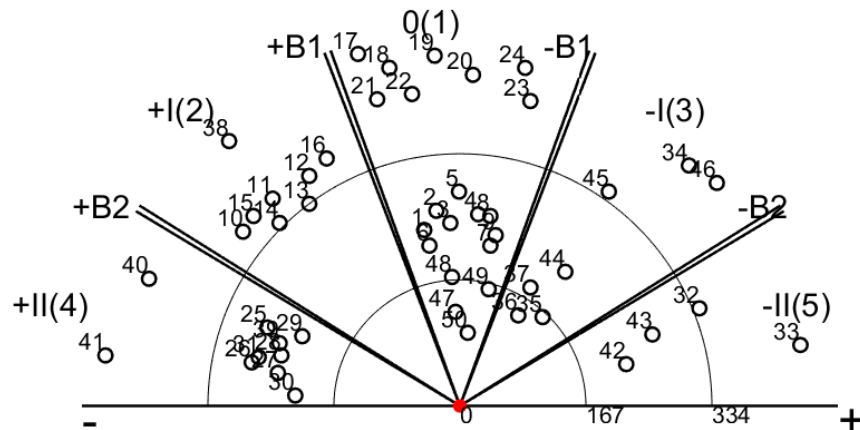


**Fig. 3.34** Fifty distributed users in a macro-pico HetNet for user cluster localization and small cell deployment location identification

the operators are not only able to know the optimal position for small cell deployment but also they are able to decide what type of small cell to be deployed in those locations based on the expected capacity requirement predicted by user counts.

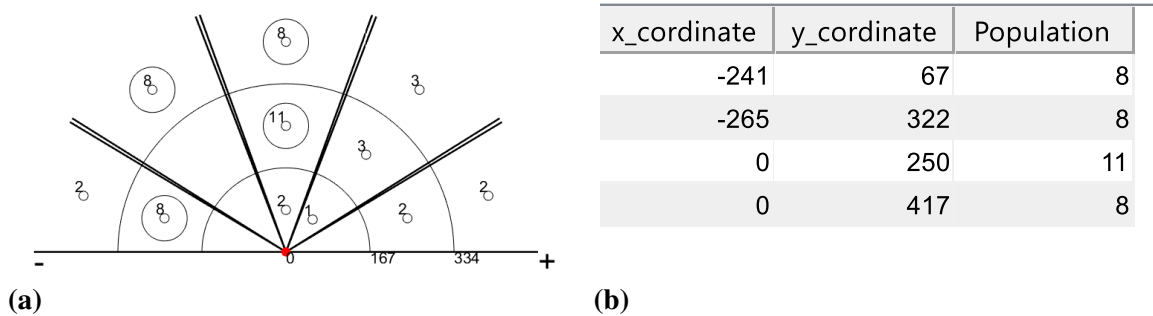


**Fig. 3.35** User cluster localization (a) optimum location for small cell deployment (b) coordinates of small cell deployment positions with opportunity for cell type deployment decision

Assuming random error in measured RSS up to  $\pm 1\sigma$  in FSPL environment has occurred, simulation was carried out to check what the effect of this error would be on user cluster localization and small cell deployment position identification. Figures 3.36a and 3.36b are the results obtained from the noisy environment and have shown that for random error within  $\pm 1\sigma$ , the system is able to identify three out of the four small cell deployment positions previously identified in a non-noisy environment.

### 3.14 Effect Of Non Line Of Sight On Range Estimation

Non-Line-of-sight (NLOS) effect is a serious issue in RSS based localization because the signal path is blocked causing reflection, diffraction and scattering. NLOS propagation model is normally worst in indoor radio propagation. Considering a situation where the user

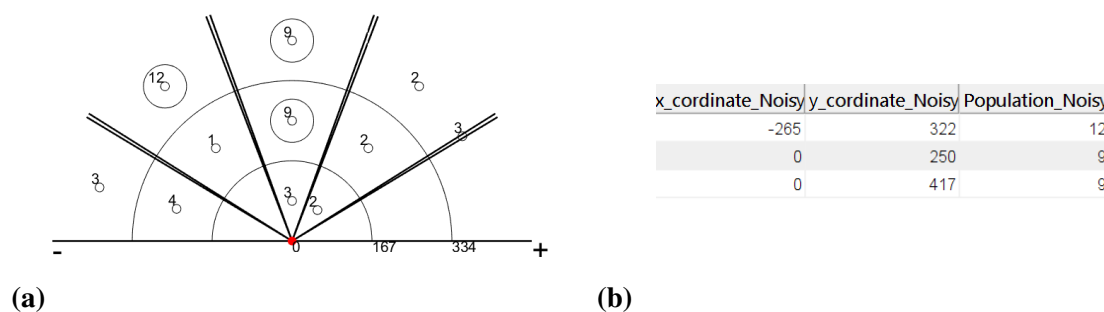


**Fig. 3.36** User cluster localization in a noisy environment (a) optimum location for Small cell deployment in a noisy environment (b) coordinates of positions for Small cell deployment in a noisy environment

is located in a building and the system is outdoor so that the signal has to pass through the walls of the building. In this simulation, it is assumed that only one wall is obstructing the indoor user from the outdoor system. Non line of sight ITU-R [220] and WINNER-II (C1) [221] empirical pathloss models of Equations 3.18 and 3.19 were considered to check the effect of NLOS in this system. Winner-II C1 is for sub-urban macro-cell and assumes one or two walls into the building.

$$ITU_{NLOS} = -28 + 14n + 20 \log(F_c [MHz]) + 40 \log(d[m]) \quad (3.18)$$

$$WINNER_{NLOS} = (44.9 - 6.55 \log(h_{BS})) \log(d[m]) + 23 \log(F_c [GHz]) + 31.46 + 5.83 \log(h_{BS}) \quad (3.19)$$

where,  $n$  is number of walls,  $h_{BS}$  is base station height ITU and WINNER line of sight were used as a reference to check the effect of NLOS. Table 3.18 is the range estimation model for the ITU and WINNER NLOS. Comparing with the ITU and WINNER LOS range estimation

**Table 3.18** Range Estimation Model Equations For Four azimuth Positions in Different Environments

Azimuth positions	Range model equation	Mean (dBm)	STDev (dB)
ITU (NLOS) +I	$-0.08RSS^5 + 0.99RSS^4 - 5.16RSS^3 + 16.63RSS^2 - 35.24RSS + 37.95$	-112.69	16.12
0	$-0.08RSS^5 + 0.99RSS^4 - 5.16RSS^3 + 16.63RSS^2 - 35.24RSS + 37.95$	-106.67	16.12
-I	$-0.08RSS^5 + 0.99RSS^4 - 5.16RSS^3 + 16.63RSS^2 - 35.24RSS + 37.95$	-112.69	16.12
+II	$-0.08RSS^5 + 0.99RSS^4 - 5.16RSS^3 + 16.63RSS^2 - 35.24RSS + 37.95$	-106.67	16.12
WINNER (NLOS) +I	$-0.08RSS^5 + 0.99RSS^4 - 5.16RSS^3 + 16.63RSS^2 - 35.24RSS + 37.95$	-84.03	14.41
0	$-0.08RSS^5 + 0.99RSS^4 - 5.16RSS^3 + 16.63RSS^2 - 35.24RSS + 37.95$	-78.65	14.41
-I	$-0.08RSS^5 + 0.99RSS^4 - 5.16RSS^3 + 16.63RSS^2 - 35.24RSS + 37.95$	-84.03	14.41
+II	$-0.08RSS^5 + 0.99RSS^4 - 5.16RSS^3 + 16.63RSS^2 - 35.24RSS + 37.95$	-78.65	14.41

models of Table 3.8, it can be seen that the equations are the same but NLOS has lower mean and higher standard deviation. Figure 3.37a is a plot of the RSS-distance relationship for

both LOS and NLOS for the two environment models. From this figure, it can be seen that if measurement is taken in a NLOS environment but range estimation is performed using LOS model as it is designed for this system, over-estimation will occur with large bound of error. For instance, assuming a measured RSS in a WINNER NLOS environment, the estimated range using the WINNER LOS range model gives an over estimation of 900m at an actual range of 100m as shown in Figure 3.37b. The estimated range for measured RSS in ITU NLOS environment at 100m is approximately  $9.59 \times 10^3$ . To mitigate against these large error bounds, the difference between estimated range using LOS and NLOS range models were calculated for the two environment cases to obtain the NLOS model values. By fitting a least square plot on the NLOS model value in each case, mathematical NLOS mitigation equations are obtain as given by Equations 3.20 and 3.21 for ITU and WINNER respectively.

$$NLOS_{MitITU} = 0.99\hat{R}_i - 5.80 \quad (3.20)$$

$$NLOS_{MitWINNER} = 0.90\hat{R}_i - 11.24 \quad (3.21)$$

where  $\hat{R}$  is estimated range using the LOS range estimation model.

For any estimated range using RSS measured from NLOS environment, the equation is used to predict the NLOS mitigation value which is subtracted from the estimated range to compensate for the effect of NLOS and obtain a more accurate range estimate. Figure 3.37b shows the estimated range of 0 azimuth position center users before and after NLOS error mitigation. This result has shown a MAE of  $4.50 \times 10^3$ m and 0.61m before and after NLOS mitigation in ITU environment. In Winner environment, a MAE of 329.17m and 2.59m are obtained before and after NLOS mitigation respectively. This gives a PER of 99.9% and 99.2% in ITU and WINNER environments respectively. In conclusion, for any measured RSS in a NLOS environment, the NLOS mitigation equations can successfully be used to drastically reduce the effect of NLOS error to obtain a more accurate range estimate.

### 3.15 Summary of Simulation Study

The aim of this chapter was to carry out a simulation of the designed observer system presented in chapter 3. This is to determine how the system would work in real sense and ensure that system has the capacity to perform the purpose of it's design before proceeding to implementation. Simulation of an observer system which is a localization system that uses RSS to estimate AOA, range and classify users into clusters to identify optimum positions for small cell deployment was carried out. A model of network environment was simulated in MATLAB, users were modeled as pixel of points within the coverage area. With known

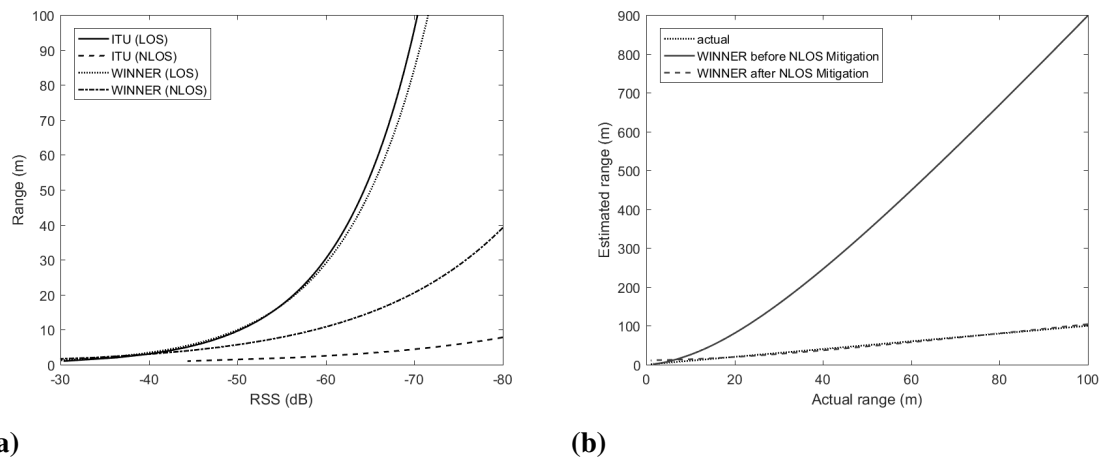


**Fig. 3.37** *Effect of NLOS on range estimation (a) line of sight and Non line of sight ITU and WINNER channel models (b) estimated range before and after NLOS mitigation in WINNER environment*

coordinates of users relative to the observer system coordinate which was (0,0), user angle and distance were calculated. Using these known parameters, AoA and range models were developed for future estimation of user position. To simulate the observer system, two omnidirectional antenna elements were modeled in an array to generate a broadside directional beam which was steered two steps left and right to create positions for AoA estimation. User AoA was determined by beam position that measured highest RSS. Simulation results have shown that even to as large as  $\pm 20$ dB random error in measured RSS, AoA can still be correctly estimated. User range was determined using regression analysis to develop a model that relates RSS to range in four different environments. By applying the correct range estimation model, user range is predicted using measured RSS. Three different system range estimation errors were identified and BPEM, ADEM and BUEM models were developed to reduce the errors as the case may be. It was also identified that correct range estimation is only obtainable if the environment of measurement is known, therefore EARM was also developed to help the system identify the correct range model to ensure accurate estimate. Result have shown that by applying these error models, 83.9% error reduction is achieved. System was simulated to identify optimum positions for small cell deployment in a perfect as well as in a noisy environment. Result have shown that positions for small cell deployment can be identified but in practical environment where random noise exist, not all the small cell deployment positions are identified. By taking several measurements and averaging measured RSS, correct number of positions for small cell deployment was identified. NLOS effect was also modeled and a mathematical model for NLOS compensation was developed

for ITU and WINNER environment. Result have shown that error in estimation is reduced by 99.9% and 99.2% in ITU and WINNER environments respectively. By design and algorithm simulation, system has shown low cost and complexity and have also shown high accuracy for it's purpose. These simulation results have shown the novelty of achieving a localization system with the capability of finding the AoA, range and user clusters with only two antennas avoiding the multi antenna elements of a standard adaptive array system. On the other hand, three different error models have been developed for more accurate results in a switched beam localization systems. Yet another novelty is that the simulation results have shown that this system is applicable in an entirely new area of identifying locations for small cell deployment in a 2-tier HetNet. Subsequent chapters presents the practical implementation and testing of the simulated system.



# Chapter 4

## System Implementation

### 4.1 Introduction

In this chapter, a prototype implementation of the proposed, designed and simulated observer system is presented. The implementation process is aimed at building the prototype system to be used for experiment where the performance and applicability of the system will be tested. First a decision on the network for implementation was taken followed by the system implementation using the chosen network.

A schematic structure of the observer system to be implemented is shown in Figure 4.1. The two antennas as designed are shown, separated by 61mm which is  $\lambda/2$  for 2.45GHz frequency. Each antenna is connected through a phase shifter for phase weighting to a combiner for output summing. S1 and S2 are switches that are controlled to select a particular transmission line for phase shifter 1 (PS1) whereas S3 and S4 are the switches for phase shifter 2 (PS2). ESP 8266 Thing digitally controls the switches via control points A and B as labeled to select the required transmission line length, placing the antenna on a particular phase state. By selecting A and B for both antennas 1 and 2, the desired phase of each antenna is activated steering the beam to required azimuth direction where the ESP 8266 Thing measures RSS acquired using a personal laptop for filtering, analysis and localization. The stages for implementation is presented in three main parts, the array system, phase weighting, and the adaptive algorithm implementations.

### 4.2 Implementing Network

As previously explained in literature review, many types of wireless networks exist. Out of all the existing wireless networks, the observer system have potential application in cellular, WiFi and ZigBee (M2M and IoT). The work presented in this thesis is designed for implementation in a 2-tier HetNet where the macro-BS stands as an overloaded umbrella big

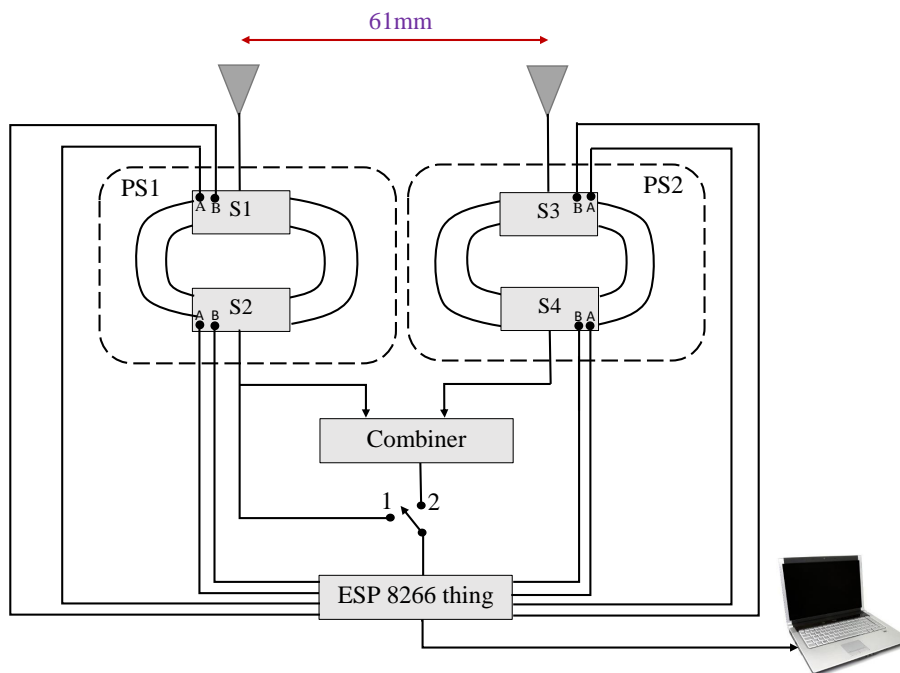


**Fig. 4.1** *Structural illustration of the observer system*

cell of 500m coverage radius with > 50 voice and data users (Assuming a 3-sector WCDMA with 5MHz carrier/sector) in one-half of the BTS coverage. There is need to find positions to deploy smaller cell within the existing big cell so as to offload traffic from the big cell. From our design, the required data is RSS. A WiFi network can be used to mimic the big cell and with other WiFi APs as users, communication can be achieved between the umbrella WiFi and the WiFi APs so their RSS can be measured and used to determine their locations. For this prototype implementation, WiFi network was chosen because no license is required and there are low cost WiFi modules available in market. Wi-Fi uses the Industrial, Scientific, and Medical (ISM) spectrum which is unlicensed. This makes the radio spectrum accessible to users without the need for regulations and restrictions that are applicable in other wireless networks like cellular. Bearing in mind that this spectrum is also shared by many other users and as a result may introduce interference to the system, a filtering process to eliminate unwanted Wi-Fi network picked up by the observer system was incorporated in the system algorithm (Section 4.7.3). Implementation using Wi-Fi network gives us a full control of the application and testing compared to a cellular network which would require permission to test system.

Two main Wi-Fi bands that can be used for the implementation are the 2.4 to 2.5GHz band or the 5.725 to 5.875GHz bands. The former is very popular and it is used by 802.11b,

g, and n. The later is used by 802.11a and n but being at a higher frequency, shorter coverage range is achieved and equipment costs are higher but with less interference. With 2.4GHz band more options for choosing components is assured and interference can be traded off for cost and coverage range, more so as interference can be taken care of in the algorithm using a filtering process which would select only the required users in the network based on their programmed identity. A Wi-Fi network of 2.4 to 2.5GHz band is therefore chosen for experimental implementation and testing of the prototype observer system.

### 4.3 Array System Implementation

Since RSS is a composite output of environment and array gain, the higher the antenna gain, the stronger the received signal and the wider the coverage. Apart from considering an antenna that resonates at the desired frequency of operation, a high gain antenna was also desired. As simulated, the desire is two vertically polarized omni-directional antennas as array elements.

#### 4.3.1 System Array Elements

Array system was implemented using two piece of antennas manufactured by RFTechnics Limited [224], with part number RFT-OMV-09-24. Each antenna is of 9dBi minimum gain, vertically polarized, collinear antenna having an omni-directional azimuth pattern operating in the 2.4GHz ISM band. The antenna is designed to be applied as access Point/Base Station for 802.11 b/g. Other features of the antenna that are of interest to this application include; suitability for both indoor and outdoor application, excellent performance across frequency band, no beam tilting is required which makes implementation easier and it has a nominal impedance of 50 ohms which gives assurance for impedance matching.

Input reflection coefficient ( $S_{11}$ ) test of the two antennas were carried out to certify that there is good impedance matching that would guaranty transmission of most of the radio wave. Test was carried out using Agilent Technologies E5071B Vector Network Analyzer (VNA). Figure 4.2 shows the result obtained. From this result,  $S_{11}$  values at the antenna operating frequency band of 2.4 to 2.5GHZ are below  $-15\text{dB}$  which is less than the typical  $S_{11}$  value of  $-10\text{dB}$ . With the assumption that antennas are low loss, this means that negligible power will be reflected and so most of the power received by the array are delivered to the combiner.

#### 4.3.2 Antenna Array Testing

Antenna array radiation was tested in the GBSAR anechoic chamber located at C22, Portobello building. This is a  $6 \times 4\text{m}$  partially anechoic chamber that was designed for synthetic aperture radar (SAR) measurements. The 2-element antenna array was placed

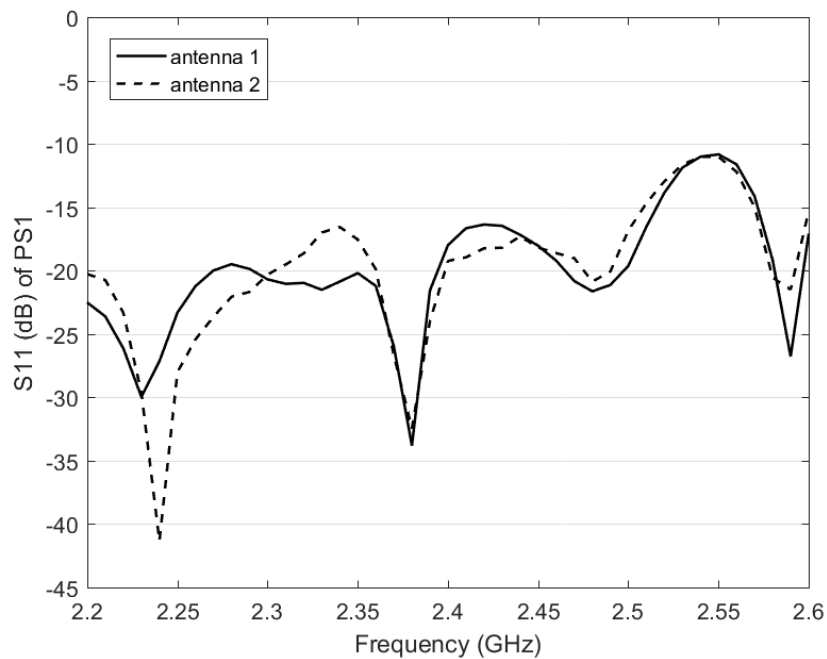


**Fig. 4.2** *Input reflection coefficient ( $S_{11}$ ) test of the antennas used for the observer system implementation*

on top of a turntable at a height of 1.1m at the center of the chamber (Figure 4.3b left). A 1 - 18GHz, transmitter horn antenna with 6.3dBi gain at 2.45GHz [225] was placed at one diagonal of the chamber at approximately the same height as the array (Figure 4.3b right), 3.4m from the array facing the anechoic part of the chamber. The horn antenna was connected to port 1 of the network analyzer and transmit power set to 0dBm (-30dB) from the computer control system. The array was vertically polarized and each of the antennas in the array system were connected to a combiner via a phase shifter with Antenna 1 connected to PS 1 and antenna 2 to PS2, making antenna 1 the reference antenna. Combined output of the two antennas was then connected to port 2 of the network analyzer.

The General Purpose Interface Bus (GPIB) port of the network analyzer was connected to a computer system from where the chamber was controlled and output data was collected and saved. The phase shifters were controlled using ESP8266 thing module programmed in arduino IDE. Program shown in Appendix A for first measurement. Four measurements were performed for the required phase states of Table 4.4. Measurement started at the bearing as shown in Figure 4.4, counting from  $-180^\circ$  to  $180^\circ$  at a step of  $1^\circ$  taking 361 samples of data for frequency ranges 2.2 to 2.7GHz. In each measurement, the array is rotated clockwise by the turntable at a speed of  $10^\circ s^{-1}$  and acceleration of  $250^\circ s^{-2}$  to take its bearing. After each

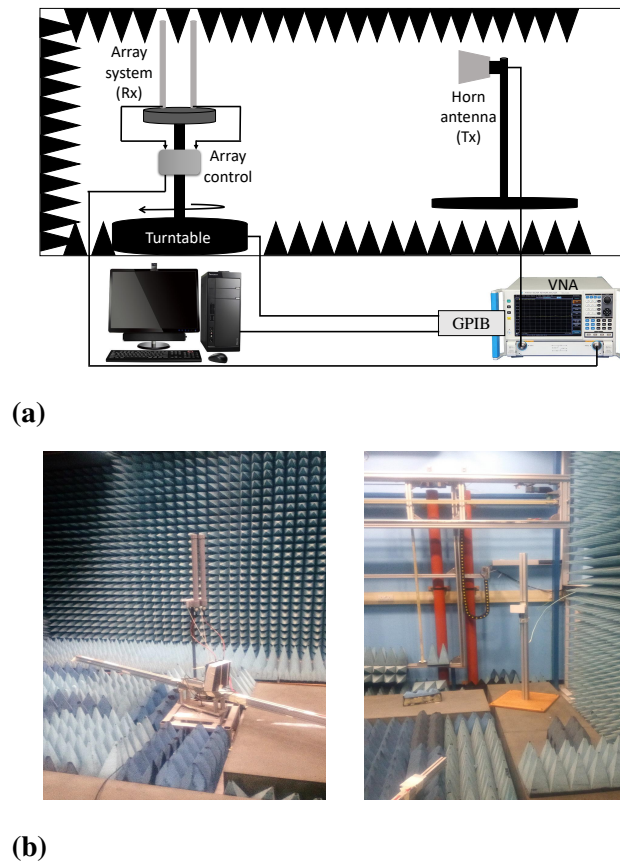


**Fig. 4.3** Array measurement in GBSAR anechoic chamber (a) schematic setup (b) experimental setup inside the chamber

measurement, the next control pin (A and B) states of the phase shifters as presented in Table 4.1 were uploaded to the micro-controller for the next measurements. For all measurements, system was powered using a fully charged 5V USB power bank.

### 4.3.3 Antenna Array Result and Analysis

Measured radiation pattern at a frequency of 2.45GHz for the four states are shown in Figure 4.5. From this figure, it can be seen that at same phase, a broadside beam was formed though with some phase offset error and beam steering was achieved at other selected phase combinations to place main beam at desired directions. These results have also shown deep nulls for the same phase at array axis positions where the fourth phase combination have shown peak. The broadside beam has shown a peak position at  $-17^\circ$  instead of  $0^\circ$ . This is an indication that there is a phase offset error of  $17^\circ$  in the measurement.

The result of Figure 4.5 have shown a wide beam width at each beam positions as expected of a two element array. The technique applied for AoA estimation in this research is based on the beam position with maximum RSS compared to the other beam positions.

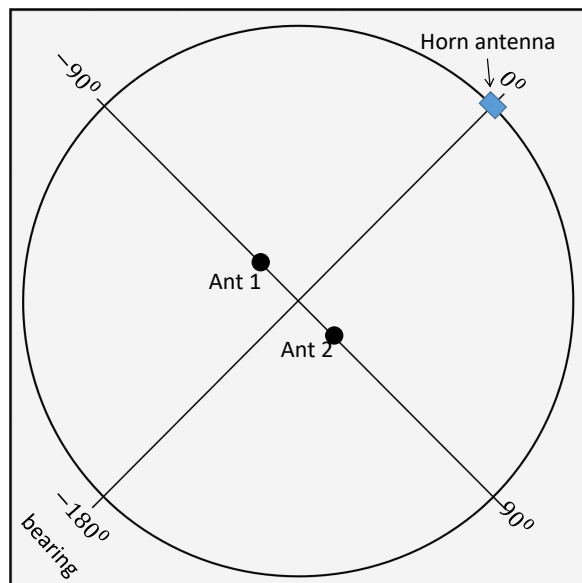


**Fig. 4.4** Array measurement in GBSAR anechoic chamber

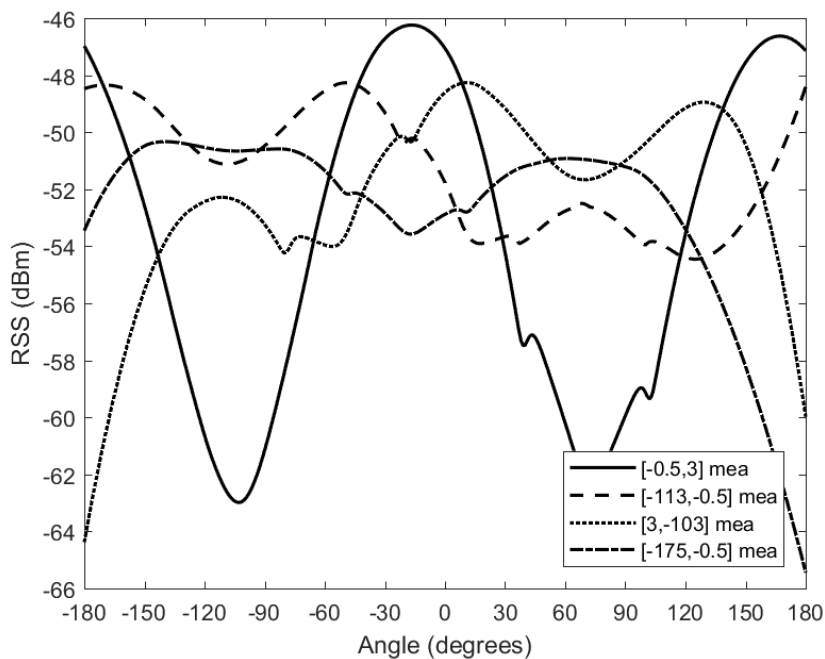


**Fig. 4.5** Measured RSS from the horn antenna transmitter by the array system receiver at all phase states

This technique is not directly dependent on the beam width but on the relative uniqueness of the beam based on determining the beam corresponding to the maximum RSS. This means

that this technique can only be applicable if at each angle only one beam position returns a maximum. In the cases where this hypothesis/axiom does not hold true, we can determine that the user is located on a beam boundary. Figure 4.6 is a plot of the radial angle verses the beam positions with maximum RSS. This result have shown that maximum RSS is achieved

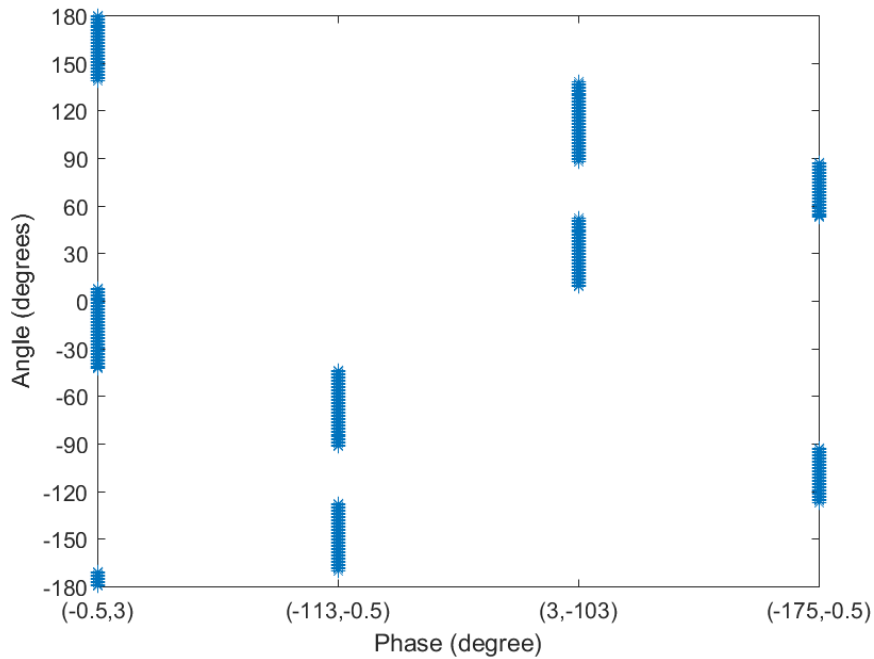


**Fig. 4.6** *Angles of highest RSS for each antenna phase combinations showing unique beam maximum radiation at all angles*

with phase combinations  $[-0.5, 3]$  at  $(-180 \text{ to } -171)^\circ$ ,  $(-43 \text{ to } 8)^\circ$  and  $(139 \text{ to } 180)^\circ$ . In this case, only two peaks was expected at broadside but due to the identified phase offset, three peaks has occurred. The cause of this offset is investigated later in the following section. Phase combinations  $[-113, -0.5]$  show maximum RSS at  $(-170 \text{ to } -128)^\circ$  and  $(-92 \text{ to } -44)^\circ$  while phase combinations  $[3, -103]$  show maximum RSS at  $(9 \text{ to } 52)^\circ$  and  $(88 \text{ to } 138)^\circ$ . At phase combinations  $[-175, -0.5]$  which is the endfire position, maximum RSS was obtained at  $(-127 \text{ to } -93)^\circ$  and  $(53 \text{ to } 87)^\circ$ . These results have shown that apart from a  $1^\circ$  boundary gap between beams, no overlap in maximum measured RSS between beams is expected.

#### 4.3.4 Antenna Array Measurement Error Investigation

The offset error identified in the array radiation pattern measurement was further investigated to find out if the error was from the phase shifters in the system or from the measuring chamber. The phase shifters were bypassed and the antennas were connected straight to the

combiner with identical low loss RF cables of 0.45m length. The radiation patterns were measured with antenna 1 as reference in the same chamber using the same setting. Cable were swapped between antennas 1 and 2 making antenna 2 the reference and measurement was repeated. This was to change the combined output of the array by  $180^\circ$ . Figure 4.7 is the result of this test measurement which also show the offset error in the same negative direction for both measurements. It was expected that if the error was not from the chamber features, the second measurement would have shown an offset error towards the positive direction as also shown on the result figure. This confirms that the offset error is not inherent in the designed system rather it is due to the design features of the chamber. To compensate for this error, all measured radiation pattern for all phases are shifted  $17^\circ$  to the right. To this effect, the phase offset error is not expected to affect field measurements.

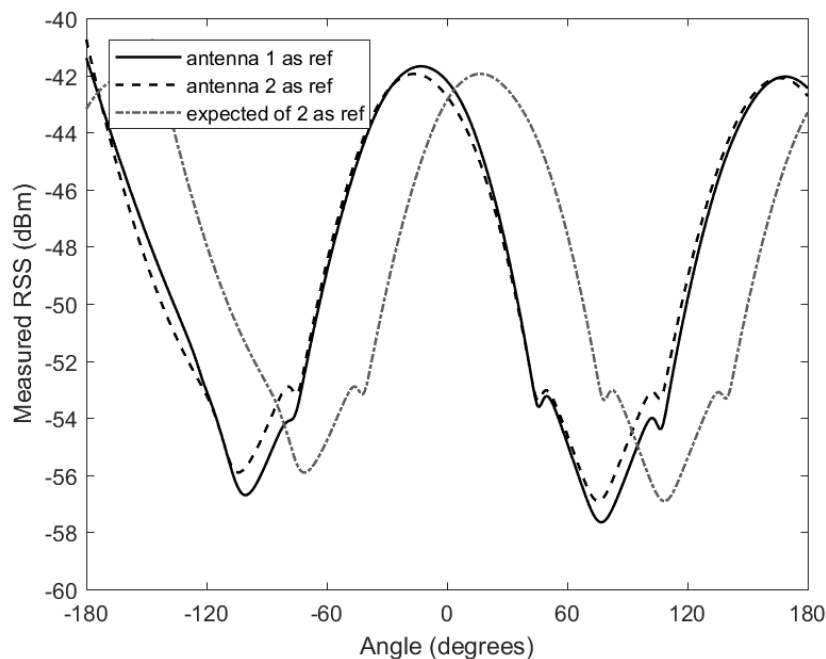


**Fig. 4.7** Phase offset error investigation showing that error is as a result of chamber features and not the array system under test

### 4.3.5 Antenna Array Radiation Pattern Of Interest

Following the turntable movement and array placement of Figure 4.4, the area of interest to this research is from the array axis towards the location of the horn antenna back to the other side of the array axis ( $-90^\circ$  to  $0^\circ$  to  $90^\circ$ ). Considering this array movement of interest and compensating for the  $17^\circ$  phase offset error due to chamber features, the measured radiation pattern was re-drawn and compared with simulation in free space. The

simulation parameters include; transmitter power of  $-30\text{dB}$  ie  $0\text{dBm}$ , gain of  $6.3\text{dB}$  and distance of  $3\text{m}$ . The receiver antenna gain is  $9\text{dB}$ . Both simulation and measured radiation pattern from all beam positions are shown in Figure 4.8. Differences in measured RSS at peak

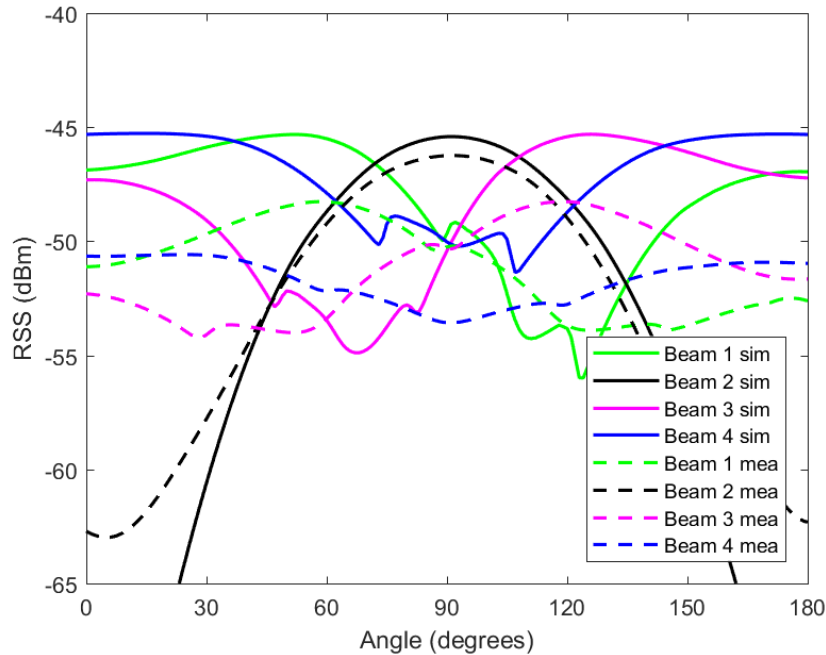


**Fig. 4.8** *Measured and simulated array radiation patterns at each beam steered positions*

positions between simulation and experiment for beams 1, 2, 3 and 4 are  $0.83$ ,  $2.95$ ,  $2.95$  and  $5.31\text{dB}$  respectively. This result have shown a close relationship between experimental radiation pattern measured in anechoic chamber and simulation result.

## 4.4 Phase Shifter implementation

As decided in chapter 3, a switched line phase shifter is used as it is simple to design and its phase shift is approximately a linear function of frequency. The phase shift is only dependent on the length of transmission lines and it is very stable over time and temperature. SP4T switches were chosen for the design because fewer switches will be required which means less insertion losses. RF energy does not pass through unused sections of transmission line system.

### 4.4.1 SLPS Implementation with Coaxial Cables

A simple and easy to implement phase shifter was designed using two HMC241ALP3E switches manufactured by Analog devices and introduced in Section 3.5. The HMC241ALP3E switch incorporates a 2:4 line decoder that provides logic control from two logic input lines

to select one of the four radio frequency (RF) lines as implemented on Table 4.1. The transmission line was provided using different calculated lengths of coaxial cables. A semi-ridged coaxial cable was considered for this application because it can make a curve bend avoiding sharp bends that could change the line characteristic impedance, may also create a short cut thereby shortening the line length and so the phase. A coaxial cable manufactured by Belden was used to implement this design. This is a 50 Ohm Microwave coaxial Cable, semi-ridged, RG-405/U type, silver-plated copper-covered steel conductor with Teflon insulation. According to the datasheet of [226] nominal velocity of RF propagation through this cable is 69.5% of the speed of light.

From Equation 2.9, change in line length required to achieve the desired phase step of  $60^\circ$  is given by  $\Delta L = (\Delta\phi \times \lambda_n) / 2\pi$ , where  $\Delta L$  is difference in line length between a delay line and the reference line,  $\Delta\phi$  is required phase step and  $\lambda_n$  is RF velocity as it propagates through this cable with nominal velocity of cable considered.  $\Delta L$  was therefore calculated to be 14.1mm.

Considering the minimum possible length that can be used to connect from the closest terminal of first evaluation board to the corresponding terminal of the second, the following cable lengths (86, 100, 114 and 128)mm were chosen for the design. SMA connectors were fitted at the ends of the cables and connected to the evaluation boards as shown on the schematic design and implemented on the switched line phase shifter of Figure 4.9.

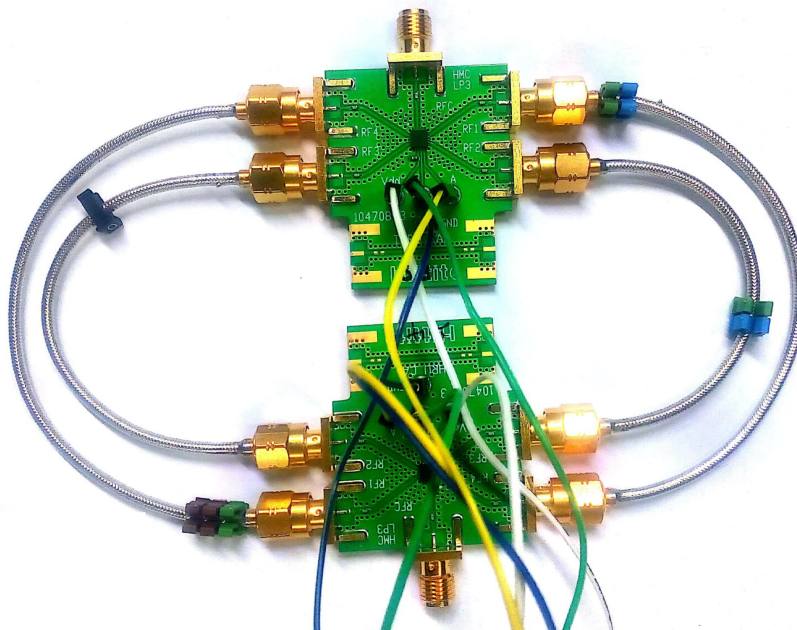


**Fig. 4.9** *Implemented switched line phase shifter using two HMC241ALP3E SP4T switches*

Considering the switch truth table on the data sheet of [216], a control truth table for our design was worked out as shown in Table 4.1 where  $S1_A$ ,  $S1_B$ ,  $S2_A$  and  $S2_B$  are control A of switch 1, control B of switch 1, control A of switch 2 and control B of switch 2 respectively.

**Table 4.1 Control Truth Table Of SLPS design**

A	B	Signal path state	$S1_A$	$S1_B$	$S2_A$	$S2_B$	Active lines
0	0	RF1	1	0	0	1	L1
1	0	RF2	0	1	1	0	L2
0	1	RF3	0	0	1	1	L3
1	1	RF4	1	1	0	0	L4

## 4.5 Phase shifter Testing

Flat phase shift over frequency can on its own be used to judge a phase shifter in a phased array application because it ensures that the pointing angle does not change even when there is a shift in frequency. The implemented phase shifters with coaxial cables in Chapter 5 were tested using HEWLETT PACKARD 8720D 50MHz - 20GHz Vector Network Analyzer (VNA) at a center frequency of 2.45GHz and frequency span of 2GHz. The VNA carries out a relative phase measurement between the phase of the signal going into the phase shifter to the phase of its response signal which can be either reflected or transmitted. In all our test, we assume that accurate calibration has been performed and so the difference in phase between the two signals (phase shift) is a result of the electrical characteristics of the phase shifter under test.

The two phase shifters were measured with primary focus on frequency range of 2.4GHz to 2.5GHz with particular interest on the operating frequency of 2.45GHz. Phase measurement of port 2 from port 1 (S21) was carried out. Phase shifter control for testing was achieved using ESP8266 module programmed in arduino following control states of Table 4.1 for each line test. Control code is shown in Appendix A.

### 4.5.1 Phase Measurement

Phase shifter was calibrated on L1 of phase shifter 1 (PS1), all other delay lines (L2, L3 and L4) were tested. Still with calibration on PS1 L1, the second phase shifter 2 (PS2) was also tested to obtain the result of Figure 4.10a. From this figure, the line phase at 2.45GHz for PS1 (L1, L2, L3, L4) and PS2 (L1, L2, L3, L4) are  $(-0.5^\circ, -53^\circ, -103^\circ, -164^\circ)$  and  $(3^\circ, -61^\circ, -113^\circ, -175^\circ)$  respectively. In the same way, phase shifter 2, line 1 (PS2L1) was calibrated as the reference phase and all other lines of both phase shifters were tested. Result of Figure 4.10b gives a line phase of  $(-1^\circ, -53^\circ, -104^\circ, -165^\circ)$  and  $(0^\circ, -64^\circ, -116^\circ, -178^\circ)$  for PS1 and PS2 (L1, L2, L3 and L4) respectively. These results are summarized in

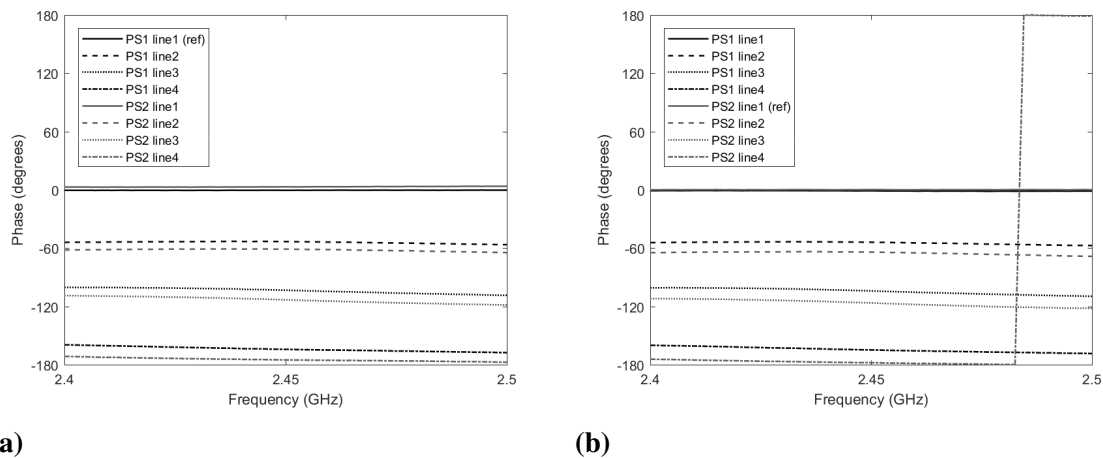


**Fig. 4.10** Phase Switching between PS1 and PS2 with (a) PS1 line 1 as reference (b) PS2 line 1 as reference showing phase switching at  $-179^\circ$

Table 4.2.

#### 4.5.2 Phase Measurement Result Analysis

Results of measured phase shift of the transmission line lengths are summarized in Table 4.2. The phase difference between the reference line length and the delay line lengths are also shown. Looking at the calculated phase errors of measured values when compared with the simulated phase differences, PS2 as a reference gives values closer to the simulated phase values than when PS1 is reference.

**Table 4.2** Measured Phase Result of PS1 and PS2

Required Phase ( $^\circ$ )	PS1 line phase ( $^\circ$ )	PS2 line phase ( $^\circ$ )	$\phi_1 - \phi_{1L1ref}$ ( $^\circ$ )	Phase Error (PS1L1 <sub>ref</sub> )( $^\circ$ )	$\phi_2 - \phi_{2L2ref}$ ( $^\circ$ )	Phase Error (PS2L1 <sub>ref</sub> )( $^\circ$ )
0	-0.5	3	0 (ref)	0	0 (ref)	0
60	-53	-61	-52.5	-7.5	-64	4
120	-103	-113	-102.5	-17.5	-116	-4
180	-164	-175	-163.5	-16.5	-178	-2

Our major interest with these phase shifters is achieving a steady phase over the 100MHz frequency band. Result of Table 4.3 was derived from the relative phase states of Figures 4.10a and 4.10b. It shows the minimum, maximum and the difference in phase measurement for PS1 line 1 as reference as well as for PS2 line 1 as reference over the frequency band 2.4 and 2.5GHz. This result have shown that using PS1 as the reference phase shifter, PS1 and PS2 lines L1, L2, L3 and L4 will have a phase deviation of  $0.31^\circ$ ,  $3.40^\circ$ ,  $8.23^\circ$ ,  $8.14^\circ$  and  $1.01^\circ$ ,  $3.89^\circ$ ,  $9.70^\circ$ ,  $5.96^\circ$  respectively giving a phase deviation mean of  $5.08^\circ$ . On the

other hand if PS2 is used as the reference phase shifter, PS1 and PS2 lines L1, L2, L3 and L4 will have a phase deviation of  $0.82^\circ$ ,  $4.02^\circ$ ,  $8.89^\circ$ ,  $8.66^\circ$ ,  $0.29^\circ$ ,  $4.89^\circ$ ,  $10.26^\circ$  and  $180^\circ$  respectively giving a phase deviation mean of  $27.23^\circ$ . For a steady phase over frequency band, our desire is to achieve a difference of zero between the maximum and minimum phases measured in each transmission line across all frequencies within the frequency band. It is therefore clear that even though PS2 showed phase values closer to simulation, a more steady phase between both antennas over the required frequency band is better achieved by using PS1 as the reference phase shifter. This resolution is obvious in Figure 4.10b where PS2 is used as reference, at 2.48GHz frequency, the phase switched from  $-179$  to  $+179$ . This is because the VNA does not display phase difference that is more than  $\pm 180^\circ$ . This is so because measurement is made at discrete frequencies, and the data point at  $+180^\circ$  and  $-180^\circ$  may not be measured for the selected sweep. At the closest discrete value before the  $180^\circ$  value, the phase shift raps round through  $180^\circ$  phase difference. PS1 was therefore used as the reference phase shifter in the array testing because a more stable result is obtained with PS1 as reference phase shifter.

**Table 4.3 Phase Plot Over Frequency Span of 2.4 to 2.5GHz**

PS1 L1 ref	PS1 L1	PS1 L2	PS1 L3	PS1 L4	PS2 L1	PS2 L2	PS12 L3	PS2 L4
Min ( $^\circ$ )	-0.60	-56.45	-108.67	-167.70	2.76	-64.72	-118.64	-177.51
Max ( $^\circ$ )	-0.29	-53.05	-100.44	-159.55	3.77	-60.83	-108.95	-171.55
Diff ( $^\circ$ )	0.31	3.40	8.23	8.14	1.01	3.89	9.70	5.96
PS2 L1 ref								
Min ( $^\circ$ )	-1.55	-57.51	-109.68	-168.70	-0.11	-68.59	-122.09	-179.90
Max ( $^\circ$ )	-0.73	-53.48	-100.79	-160.03	0.18	-63.70	-111.83	179.99
Diff ( $^\circ$ )	0.82	4.02	8.89	8.66	0.29	4.89	10.26	180

### 4.5.3 Return Loss Result and Analysis

Return loss of the phase shifter was also tested to check how well the phase shifter will match to a 50 ohm impedance of the antenna. A typical  $S_{11}$  value is  $-10$  or less [227] but result Figure 4.11 have shown  $S_{11}$  values below  $-11$ dB for a wider frequency band of 1.5 to 3.5GHz and below  $-15$ dB at required band of 2.4 to 2.5GHz for all transmission lines.

## 4.6 Summing Array Output Implementation

An RF power combiner combines or sums different signals into a single output without making any form of transformation or change to the input signals. When reversed, a power combiner becomes a power divider splitting a single RF input signal into two equal parts. A power combiner/divider is a passive element requiring no power to operate but it adds insertion loss as a divider (half power goes down each leg) for a two input port combiner

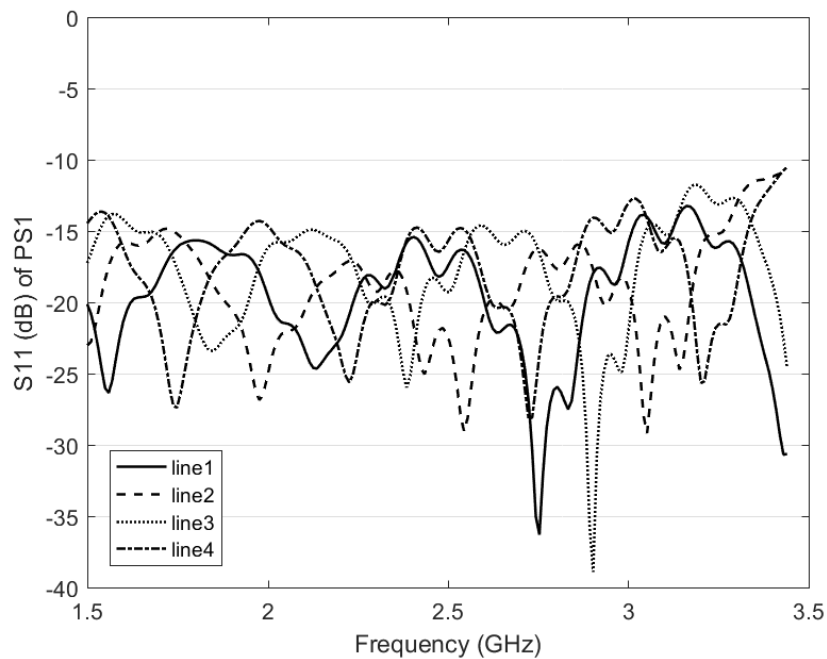


**Fig. 4.11** Phase shift  $S_{11}$  measurement of PSI

and multiple more losses for higher number of ports. Using only two antenna system as compared to multiple elements in a phased array, loss is also reduced at this level.

From the system block diagram of Figure 3.2, the signals from the two antennas needed to be summed and this was achieved using a two-way Fairview Microwave power divider/splitter (a.k.a combiner) with SMA connectors, part number MP8424-2. The power divider was rated for a minimum frequency of 2 GHz and a maximum frequency of 4 GHz according to the on-line datasheet [228] which makes it suitable for our application. It has a 50 Ohm impedance and a maximum input power of 30 Watts. To ensure good impedance matching and that no wave is reflected back,  $S_{11}$  measurement was carried out on the combiner using Agilent Technologies E5071B vector network analyzer (VNA). There are three ports in this combiner, the two input ports where antennas 1 and 2 are connected and the combiner output referred to as ports 1, 2 and 3 respectively. Figure 4.12 is the  $S_{11}$  measurement result of the combiner for frequency bands of 1.6 to 3.6GHz. From this figure, input reflection coefficients ( $\Gamma_{in}$ ) for  $S_{31}$  and  $S_{32}$  is  $< -12$  which means that most of the power coming in into ports 1 and 2 are delivered to port 3. ( $\Gamma_{in}$ ) for  $S_{13}$  and  $S_{23}$  is approximately  $> -6$  which is above the typical  $S_{11}$  value showing that most of the power delivered to port 3 is not reflected back to ports 1 or 2. Based on these results, it is believed most of the power from the antenna array will be received at the combiner output for more reliable localization.

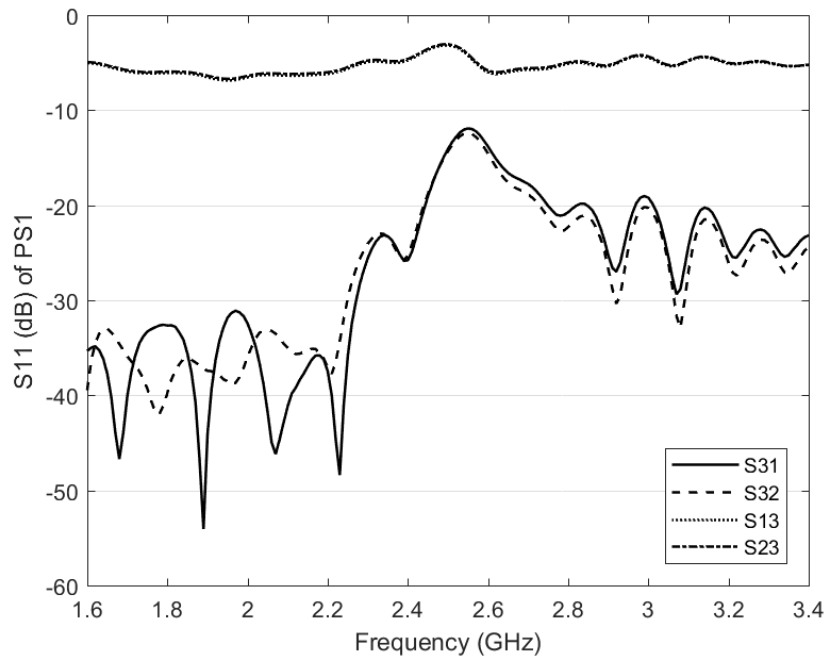


**Fig. 4.12** *Input reflection coefficient measurement ( $S_{11}$ ) of the 2 Way SMA power combiner to ensure proper impedance matching and good radio wave radiation*

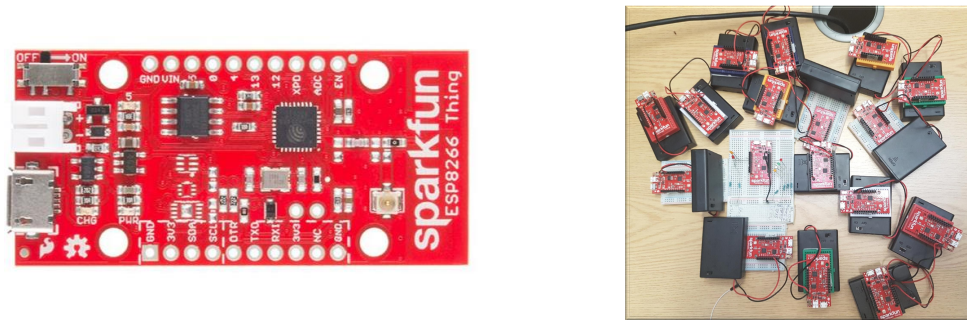
## 4.7 Small Cell Localization Algorithm Implementation

The adaptive algorithm block performs four main tasks; controls the phase weighting of antennas 1 and 2, measures RSS from users in the network and processes data to resolve AoA, range and user cluster localization. Finally, using the processed data, it determines optimum position for small cell deployment. This section presents implementation of these tasks in two broad heading; hardware and software implementations.

### 4.7.1 Hardware Implementation

Among some popular programmable boards like arduino uno, raspberry pie and an ESP8266thing [168, 229, 230], an ESP8266 Thing was chosen for the algorithm implementation because of its cost effectiveness. Esp8266thing, popularly called the 'Thing' is cheap, has built-in WiFi and provision for an external antenna via the u.FL connector. It is development friendly due to its broken out pins and includes three opportunities for powering (LiPo, USB and battery). Easy to use for connecting things to the cloud. Most importantly, there is an ESP8266 board add-on which makes it possible for it to be programmed using the popular Arduino IDE. Unlike the arduino-uno that has fourteen General Purpose Input/Output (GPIO) pins, ESP8266 thing board has eleven I/O pins but that is sufficient for this project as only eight are required to control the phase shifters.

SparkFun's ESP8266 new development board of Figure 4.13a was used for the hardware implementation of both the users as well as the system adaptive algorithm. The users were powered using three 1.5 volts batteries connected in series to achieve a 4.5 volt DC supply. The system was powered using the laptop. By interfacing a 3.3V Sparkfun FTDI basic with the Thing, C++ programs written in arduino IDE were uploaded to the Thing.



(a)

(b)

**Fig. 4.13** *Hardware implementation of network users (a) ESP8266 Thing used for adaptive algorithm implementation (b) programmed micro-controller as users*

### Phase Shifter Control

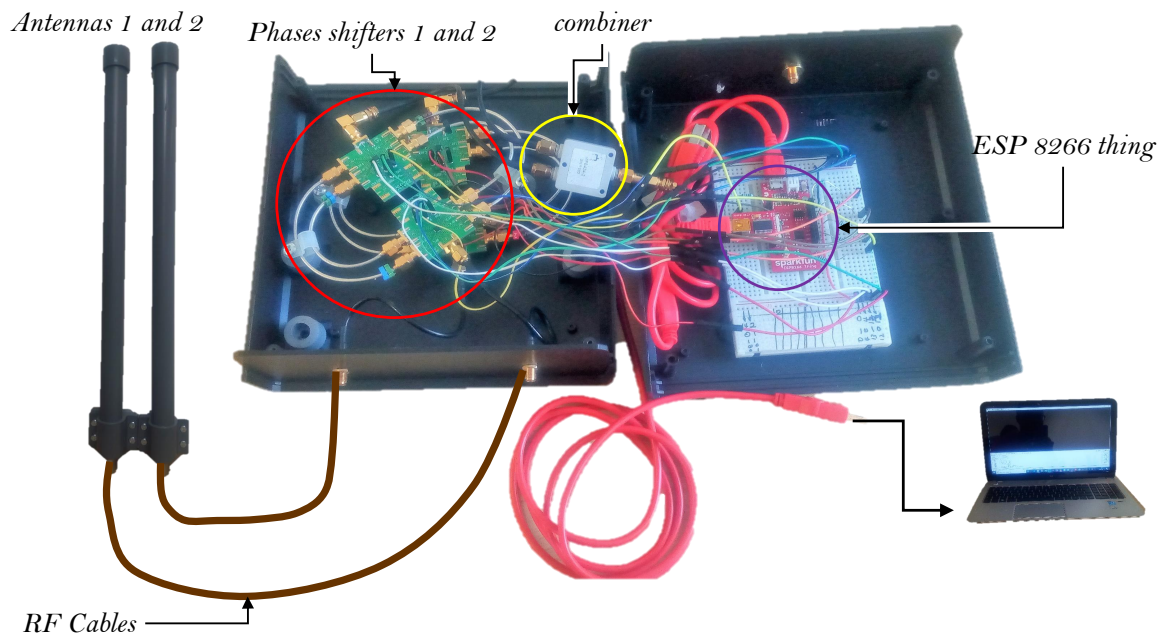
Considering the SLPS truth table of Table 4.1 and also the required phase states of the two antennas, a system control truth table was developed as shown in Table 4.4. Following the pin descriptions on [231] and avoiding GPIO pins 6 to 11 that are used to connect the flash memory chip and GPIO15, GPIO0 and GPIO2 that are used during boot loader, GPIO pins 4, 5, 12, 13, 14 and 16 were used to control phase shifters 1 and 2.  $S3_B$  and  $S4_B$  are permanently connected to ground and VCC respectively since they remained at the same voltage level for all switching states.

According to the HMC241ALP3E switch datasheet of [216], the voltage and current required for an active low are  $0 - 0.8V$  at  $0.2\mu A$  and  $1 - 5V$  at  $40\mu A$  for an active high. To ensure safe operation of the switches, 20K ohms resistors were used to drop some voltage out of the measured input voltage of 3.27V to allow 2.5V into the switch and a current limited to a maximum of  $40\mu A$ .

A picture of the implemented observer system hardware as structured in Figure 4.1 is shown in Figure 4.14. The phase shifters are circled in red, combiners in yellow and Esp 8266 Thing in purple. The brown lines represents the brown RG 142 RF cables used to connect the phase shifters to the antennas. Antennas 1 and 2 are shown as labeled. The red cable with USB end connects the output from ESP 8266 Thing to a personal laptop as obviously shown.

**Table 4.4 System Control Truth Table**

Phase state		Phase shifter1				Phase shifter2			
Ant 1	Ant 2	4 $S1_A$	5 $S1_B$	12 $S2_A$	13 $S2_B$	14(SCL) $S3_A$	GND $S3_B$	16 $S4_A$	Vcc $S4_B$
0	0	1	0	0	1	1	0	0	1
120	0	0	0	1	1	1	0	0	1
0	120	1	0	0	1	0	0	1	1
180	0	1	1	0	0	1	0	0	1

**Fig. 4.14 Implemented hardware of the observer system showing both internal and external circuitries**

### 4.7.2 Software Implementation of Network

The ESP8266 was programmed on arduino IDE using C++ programming language. It can be configured in three WiFi modes namely; as a WiFi station (device), WiFi Access Point (AP), or both (WiFi station/AP). In station mode, it can connect to a WiFi network but cannot host a WiFi network. When programmed in AP mode, the thing can form its own WiFi network that other WiFi enabled devices can be connected to. In both modes, the ESP8266 can simultaneously work as a device of its own network (AP) that other devices can connect to and at other time connect to other networks.

### Software Implementation Of Users

Seventeen users were used in this project and each of them was programmed as WiFi access point (AP) with different SSID for identification. Users were programmed as APs so that they can host their own WiFi and BS can connect to them. First the ESP8266WiFi.h library was included on the code to provide all the functionalities needed to set the access point. Then the network name (SSID) and password were specified. Next, setup function was started by opening a serial connection, to output some messages to serial monitor mainly for debugging. By calling the softAP function, both the SSID and password variables already defined are passed as input. These steps to programming the 'thing' as a network user (WiFi AP) are summarised in Algorithm 11.

---

#### Algorithm 11 Users programmed as APs

---

- 1: Define network ID (SSID and password)
  - 2: Define network static IP (local, gateway and subnet)
  - 3: Begin serial port
  - 4: Configure access point (WiFi.softAPConfig(local IP, gateway, subnet))
  - 5: Set up a soft access point to establish a Wi-Fi network (WiFi.softAP(ssid, password))
- 

### Software Implementation Of Observer System

The system which is the base station was configured as station mode to be able to connect to the users and measure their RSS. As in programming users, the ESP8266WiFi.h library was included on the code to provide all required functionalities. A 0.1 second timer was set to provide some delays between processes. Pins 4, 5, 12, 13, 14, 16 as well as scanning time interval were declared. Pre-defined pin states of Table 4.4 were defined as an array. On the setup, serial communication was initialized to enable display of RSS via serial port. System was set to station mode and disconnected from all WiFi networks to allow connection to required networks. Additionally all pins were initialized as an output pin. As a loop, the system connects to one antenna as an omni-directional antenna, scans the network to find users, if no user is found, the system re-scans the network until users are found. If users are found, the system declares the number of users found and captures measured RSS (dBm) of each user with their corresponding SSID. This process repeats for a total of ten scans. This is used as a reference to know users on the network that are to be located.

Next, the system starts the first iteration by activating the first row of the pin states to place the two elements at phases  $[0^\circ, 0^\circ]$ . The system then carries out ten scans of the network and measure RSS in each case. The same process is carried out for all four iterations to obtain five data set of ten subsets each. Each subset is a set of all users found in the network with their measured RSS. The main sets are these subsets for ten scans obtained from reference,

$[0^\circ, 0^\circ]$ ,  $[120^\circ, 0^\circ]$ ,  $[0^\circ, 120^\circ]$ ,  $[180^\circ, 0^\circ]$  array phase scans. After a complete scan, the system delays for 20 seconds during which data is exported for analysis. Algorithm 12 is the system software implementation algorithm.

---

**Algorithm 12** System Data Acquisition Algorithm

---

**Step1: Starting up**

- 1: start system and set timer
- 2: Set scanning interval
- 3: Define pin arrays for phase shifter control
- 4: Define pin array states

**Step2: System and network Setup**

- 5: Initialize serial communication
- 6: Set WiFi mode to station
- 7: Disconnect from any connected network
- 8: Initialize each pin as output

**Step3: Find users in the network**

- 9: Connect to one omni-directional antenna
- 10: Scan network, if no network is found, wait and re-scan until network is found
- 11: Count number of networks found and display
- 12: Measured RSS of all found networks and print with their individual SSID
- 13: Repeat scanning and RSS capture for ten scans

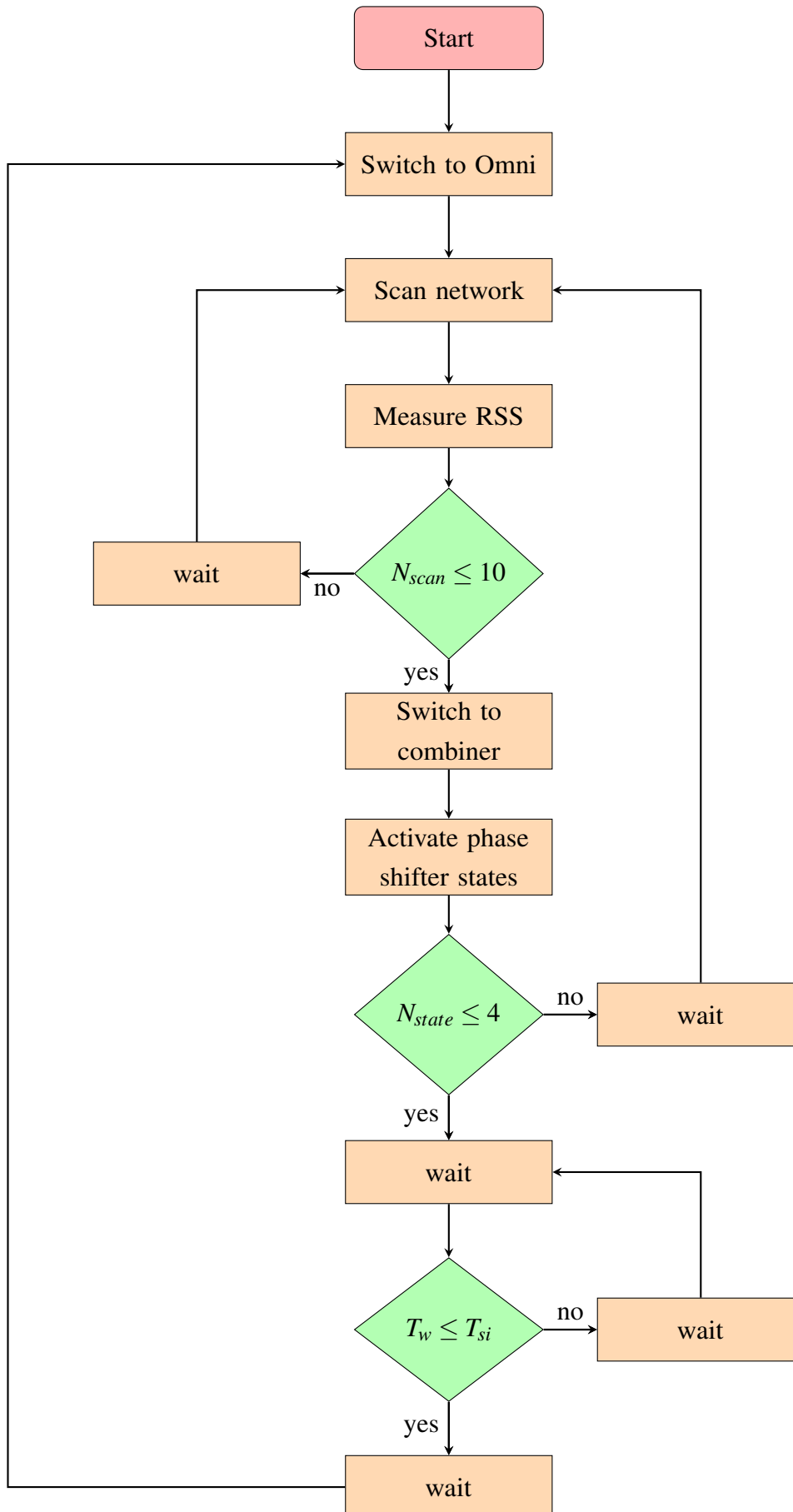
**Step4: Collect data for localization**

- 14: Switch system to antenna array
  - 15: Activate first row of pin states array
  - 16: Scan network
  - 17: Measured RSS of all found networks and print with their individual SSID
  - 18: Repeat scanning and RSS capture for ten scans
  - 19: Update pin state and repeat scanning and RSS measurement for all pin array states.
  - 20: Wait for a period of scanning interval and repeat process
- 

**System Implementation Flowchart**

The system flowchart is shown in Flowchart 4.7.2. At the start of the process, system declares six hardware pins and set them as output. It also set the scanning intervals and the timer. It then begin serial communication and set WiFi to station mode. After initialization, the single-pole-double-throw (SPDT) switch is then switched to position ‘1’ as indicated in Figure 4.1 to enable only antenna 1 to be in operation for omni-directional effect. Network is scanned to identify users in the network. Ten scan is performed to ensure all users are captured. This is the ‘reference’ stage of the operation where users in the network are captured. The system then switches to the combiner output to activate the array system. Hardware pin states are activated for the iteration counts and if the iteration count is within

the four selected phase states, the system goes back to perform ten scans of the network. At each scan, RSS is measured. After the four iterations (phase states) are performed, data is exported to run as a life script in MATLAB where data filtering and processing are performed. The system delays for a scan interval period of twenty seconds (20sec) and then starts the process all over again. The network operator is able to monitor cluster localization and possible positions for small cell deployment at about every thirty seconds (30sec) which is adjustable to suit operator desire by altering the scan delay time on the algorithm.



### 4.7.3 Data filtering and analysis

Since our experiment was based on WiFi network, the system measures RSS from our users as well as all other WiFi networks in the same frequency band within the vicinity. There is therefore a need to filter the data and extract the required users that we have deployed for localization analysis. A script written in MATLAB was used for data filtering as presented in Algorithm 13. Measured data containing both wanted and unwanted users are imported to MATLAB, then the data is segmented into five main sets of measured data which include the reference, beam positions 1, 2, 3 and 4 (four iterations). The system further segments each main set into ten subsets containing data from each scan. Users that are not bearing the required network name which starts with 'Dorathy' are then deleted from the data string. Wanted users are extracted from all ten reference scans using union to identify users in the network. Beam position measured data are then sorted in accordance with the reference scan data. Mean of the ten scans is then calculated for each user to obtain measured RSS for each users at each beam position.

---

#### Algorithm 13 WiFi Data Filtering

---

**Input:**

number of scan

**Output:**

user ID

user measured RSS

- 1: Import and open measured data
  - 2: Separate each data of main set (ref and the four iterations)
  - 3: Separate each data of subsets (each scan)
  - 4: Identify unwanted network and delete
  - 5: Sort users according to users recorded by reference set
  - 6: Replace any missing data element with mode of the ten scans for that users
  - 7: Find the mean value for each user and for each phase
- 

### 4.7.4 User localization and small cell deployment Implementation

Localization of users and finding position for small cell deployment was implemented using MATLAB script running on personal laptop. The implementation algorithm first calls up the filtration function to produce the measured RSS (filtered data) from the main beam positions as given in Equation 4.1. These measured data are with some variation from expected value due to system and environment errors.

$$RSS_{\beta} = [RSS_{\beta_1} \ RSS_{\beta_2} \ RSS_{\beta_3} \ RSS_{\beta_4}]^T \quad (4.1)$$

The system first applies the AoA estimation model explained in Chapter 4, Section 3.9, subsection 3.9.2 to estimate user sector angles. Using  $RSS_{\beta}$  as input, the system determines which of the beam RSS have measured the highest RSS among all other beam positions for each user. The beam with highest RSS is returned as the AoA of that user. It then applies the Angle Adaptive Range Model (AARM) of Subsection 3.10 to estimate range of users based on their estimated AoA using all four models. The system calculates RSS-distance relationship using data at the beam peaks for the specified nominal range to develop range estimation model for each beam position. Depending on the estimated AoA of each user, the correct range estimation model is applied to estimate user range.

To improve the accuracy of estimated range, the system applies the developed error models of Section 3.12. First it applies the Beam Position Error Model (BPEM) of Subsection 3.12.1 to reduce error in estimation due to the beam position users appear. Secondly, the system applies Angular Deviation Error Model (ADEM) of Subsection 3.12.3 to reduce error due to users not appearing at the beam peak and then the Boundary User Error Model (BUEM) of Subsection 3.12.6 is applied to reduce error of users at the boundary. After all error models are applied, the output is a more accurate estimated range of the four environment models. The system then applies Environment Adaptive Range Model (EARM) to identify the closest environment that best describe the measured data. Estimated range of model returned by EARM is taken as the most accurate range estimate of users in the network. Using the accurate estimated range and the estimated AoA, users are classified into the created users AoA/range sections. Due to few users used in this experiment, it is assumed that requirement for small cell deployment is minimum of two users within the experimental coverage space of 50m radius. The system then counts the number of users in each section and returns sections with users greater than two as positions requiring small cell deployment. Localization and small cell implementation is presented in Algorithm 14.

## 4.8 Conclusion

This chapter has presented the implementation of both the system and the deployment network used for experiment in the next chapter. First the array system was implemented. A high gain collinear antenna was modeled in CST microwave and then simulated as an array of two elements to obtain the radiation pattern of the array. Obtained result of Figure 3.5 has shown beam peaks at expected beam positions but with different values of maximum gain at the peak of each beam positions. This confirms that RSS-distance classification should be beam position dependent and justifies the development of Angle Adaptive range model (AARM) and Beam Position Error Model (BPEM) described in chapter 3 and implemented in the system algorithm in this chapter. Secondly, Switched line phase shifter was also

implemented using switches and coaxial cables and then the state of art implementation on a pcb version was deigned and presented in this chapter. The phase shifter control and RSS measurement was implemented using low cost ESP8266 board. Finally data filtering, localization and small cell deployment position identification were all implemented using MATLAB script running on a personal computer.

---

**Algorithm 14** System Localization Algorithm
 

---

**Input:**

Measured RSS  $RSS_{\beta}$   
 Calculated range  
 BPEM  
 ADEM  
 BUEM

**Output:**

Estimated user AoA  
 Estimated user range  
 Small cell deployment positions

- 1: Estimate AoA of users using AoA Estimation model   ▷ Chapter 4, Subsection 3.9.2
  - 2: **for**  $Rm = 1$  to number of environments **do**   ▷ range models are FSPL, HATA, ITU, WINNER-11
  - 3:   **for**  $users = 1$  to number of users **do**
  - 4:     Estimate range of users using angle adaptive range model (AARM),  $R_{AARM}$
  - 5:     Apply BPEM to estimated range,  $R_{BPEM}$
  - 6:     Apply ADEM to  $R_{BPEM}$  to obtain  $R_{ADEM}$
  - 7:     Apply BUEM to  $R_{ADEM}$  to obtain  $R_{BUEM}$
  - 8:      $UR = R_{BUEM}$  ▷ estimated range of users is the range after BUEM for all models
  - 9: Apply EARM to determine model with best range model
  - 10:  $UR = R(Rm)_{EARM}$    ▷ accurate estimated range of users is the range estimated by the predicted environment model
  - 11: Allocate users into created azimuth and range positions based on estimated AoA and Range
  - 12: Count number of users in each position section
  - 13: If section user count  $\geq$  small cell requirement, circle position for small cell deployment
  - 14: Print coordinates of small cell deployment positions
-

# Chapter 5

## Experimental Validation

### 5.1 Introduction

This chapter presents the experimental validations of the observer system for the optimization of 2-tier HetNets. Practical testing of the system both outdoor and indoor are presented. Experimental results were analyzed.

### 5.2 Methodology

The algorithm in this system are based on AoA and range estimation which are both dependent of mean RSS data. AoA uses the beam positions and the RSS received at each position to determine which beam the user is located. From the antenna array measurement shown of Figure 4.5, it was shown experimentally that at selected phases, beam-forming and beam-steering can be achieved with each beam uniquely having a maximum at some angular range compared to other beam positions. For AoA estimation testing, RSS of all users found in the network are measured from all azimuth positions. By applying the AoA estimation algorithm on the measured data, AoA of each user is determined. Using the same RSS data, range of users are determined by applying all four range estimation models with all error models for more accurate result. The environment adaptive model is then applied to predict environment of measurement. Range estimated by the predicted environment is adopted as the most accurate estimation. AoA and range estimation is combined by the algorithm to localize users and determine user cluster and optimum small cell deployment positions.

The method applied in this system algorithm is entirely dependent on (1) the ability of system to measure different values of RSS from each azimuth positions for AoA estimation algorithm to work. (2) That measured RSS decreases exponentially with distance for range estimation algorithm to produce reliable result. (3) That different scans at the same distance are closely related to avoid outliers that would cause large deviation on the mean value causing

inaccurate range estimation. A preliminary test is first carried out to statistically certify that reliable data can be obtained in real environment for the system validation. Correlation and P-Value tests with adoption of the scientific statistically significant threshold of 0.5 (50%) and 0.05 respectively were applied. The P-value evaluates how well a sample data supports the argument that a null hypothesis is true. Hypothesis tests are used to test the validity of a claim that is made about a population, the claim on trial is the null hypothesis while the alternative hypothesis is the one to believe if the null is untrue. P-value in hypothesis test is used to weigh the strength of the sample data in relation to the entire population. A P-value of  $\leq 0.05$  suggests that the sample provides enough evidence to reject the null hypothesis for the entire population. A P-value of 0.05 means that there is only 5% probability that the null hypothesis is true. Following the preliminary measurement and analysis is a real data acquisition and algorithm testing for system validation.

### 5.2.1 Outdoor Experimental Setup

Outdoor experiment was performed in the open field space at Ponderosa park in Sheffield. This is a rectangular space with dimension of approximately  $100 \times 50\text{m}$  surrounded by thick forest at three sides and tall buildings some distance away at one side. The ground consists of short grasses and with no obvious obstacle. With these features, this park was considered as an open space and suitable to be used as a test environment for the simulated line of sight operation. Outdoor experiment was performed three times on different days. First a preliminary test was performed for statistical analysis of the relationship between RSS and distance. Second was a trial outdoor experiment to test the algorithm and then third was the final test to confirm system and algorithm performance. A picture of the final test scenario is shown in Figure 5.1.

A reference position was taken at half the length of longer side (50m) and edge of the shorter side (0m). This position was considered as the reference, (0,0) coordinate position. Observer system was located at this position as circled with yellow marker and shown in Figure 5.1. This creates a rectangular coverage area with 50m space, left, right and in front of the observer system. The array elements were mounted on a tripod stand at a height of 0.9m. Phase shifters, combiners and other components were all coupled in a black plastic box of  $198 \times 188 \times 70\text{mm}$  dimension and was mounted by the side of the tripod stand. System was powered using a fully charged personal laptop which also do the data capturing using RealTerm serial monitor as well as processing and localization in Matlab. Seventeen users were used in this experiment and were placed within the rectangular coverage area some of which were captured by the camera and circles in red markers as shown in Figure 5.1.



**Fig. 5.1** *Outdoor experimental setup showing some of the distributed users on red and deployed observer system on yellow*

### 5.2.2 Indoor Experimental Setup

Indoor experiment was performed in C34 Portobello center in the University of Sheffield with eight users deployed as shown in Figure 5.2. The observer system was located at 'BS' position as indicated on the deployment setup. Users on red dots are numbered according to the last two digits of their SSID. The setup also shows the new assigned ID which ensures user privacy is maintained. In this case, the new IDs are based on the ascending order of the SSID so that 'DorathyWiFiNode10' and 'DorathyWiFiNode40' corresponds to new IDs of '1' and '8' respectively as shown on the superimposed modeled actual user positions.

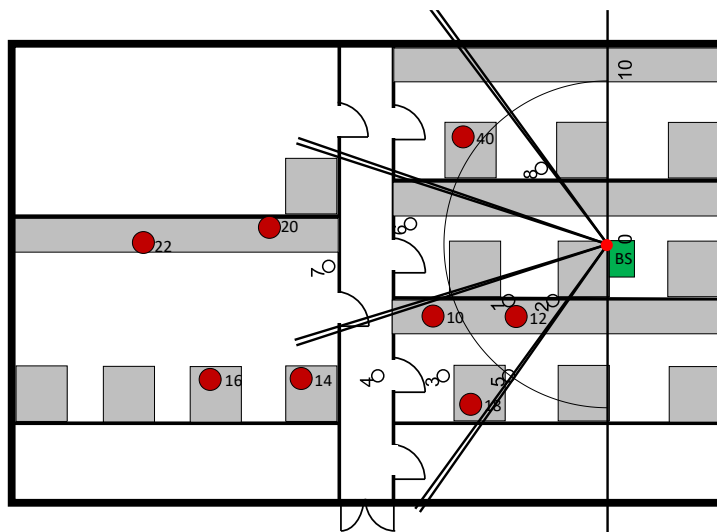


**Fig. 5.2** *Indoor experimental setup*

### 5.3 Outdoor Round-Trip RSS Measurement

The first preliminary test was the round-trip measurement. This is to confirm the existing theory which states that RSS decreases exponentially with distance. This is necessary because the range estimation model is based on this theory. To check if this is true for this system, One of the 9dB omni-directional antenna from RFTechnics Limited was connected to ESP8266 through the external antenna U.F.L connector provided on the board. The ESP8266 was programmed to scan WiFi network and measure RSS. One of the users already programmed as AP with user ID 'DorathyWiFiNode40' mounted on a tripod stand was held to walk 1m from the observer point position in an open field to about 100m distance away from the system and then back to the system. The measured RSS (dBm) as well as a fitting curve showing the expected RSS is shown in Figure 5.3. This result shows that as the user moved away from observer point, measured RSS decreases but increases as the user walked back toward the observer position. This is a preliminary test and it has confirmed the existing theory that there is an exponential relationship between RSS and distance. The measured data have shown scattered points with variations when compared with the expected data. This due to multipath and variation in height as user is being moved to and fro.

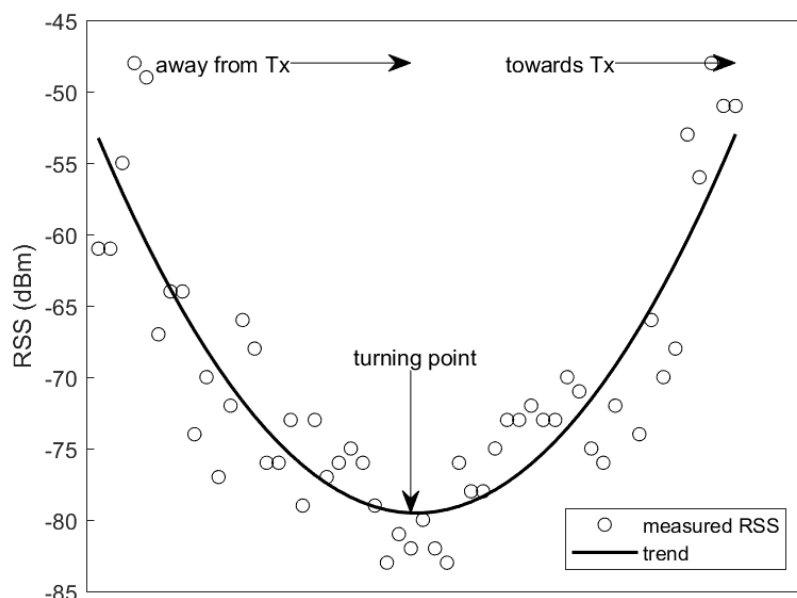


**Fig. 5.3** *On-the-fly to and fro movement from 1 to 100m to check RSS-distance relationship*

## 5.4 Outdoor RSS-Distance Relationship Test

This second preliminary test is aimed at testing the relationship between RSS and distance using multiple scan. This is to certify that there is close relationship between measured RSS at each distance and compare the experimental range estimation model with simulation model. The experiment to obtain data for this test was performed using a single 9dB omni-directional antenna connected to ESP8266 thing. The ESP8266 was programmed to perform ten WiFi scans at every scan period. User 'DorathyWiFiNode40' was used as the network user in this experiment. Measurement was performed at every 1m distance from the observer point up to 100m distance. At each distance, ten RSS measured data from each scan was obtained. All measured data are shown in Figure 5.4. These data were used for statistical analysis to test RSS-distance hypothesis. From this result, it can be observed that deep nulls are obtained at

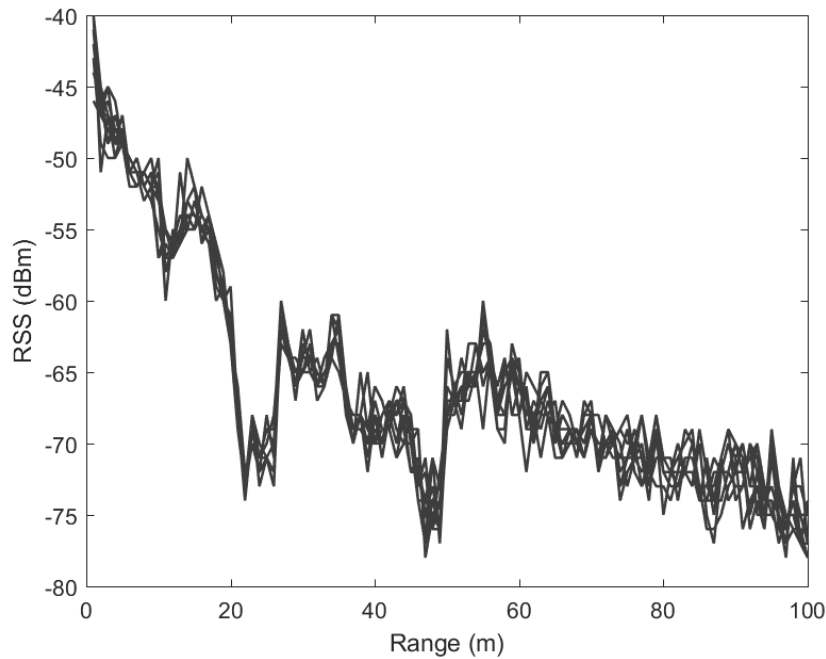


**Fig. 5.4** Ten measured RSS using omni-directional antenna to test RSS-distance hypothesis

distances 11m, 22m and 47m from BS. This draws attention to the two-ray reflection model given by Equation (5.1) with first null position given by Equation (5.2).

$$P_r = \frac{P_t G_t G_r}{(4\pi R/\lambda)^2} \times 4 \sin^2 \left( \frac{2\pi h_t h_r}{\lambda R} \right) \quad (5.1)$$

$$R = \frac{2h_t h_r}{\lambda} \quad (5.2)$$

where  $P_t$  and  $P_r$  are transmitter and receiver power,  $G_t$  and  $G_r$  are transmitter and receiver gain,  $h_t$  and  $h_r$  are transmitting and receiving antenna heights respectively,  $R$  is range,  $\lambda$  is wavelength of radio wave and range where the null appear is given by Equation (5.2).

With  $h_t = h_r = 0.9\text{m}$  and for a frequency of 2.45GHz as implemented in this experiment, the location of first signal null is calculated to be approximately 13m which is close to the experimental first null position of 11m. The experimental result may have been influenced by factors like transmitting and receiving antennas being on the same height or not being high enough which are not ideal for a 2-ray model. Other nulls after the first one increases in distance by the same amount so that analytically, the second and third nulls should appear at a distance of 26m and 39m respectively. The experimental result has also shown the increase in subsequent null distances by the first null distance value. This means that the environment of measurement most likely exhibits a two-ray reflection model to be investigated further in future work since this model was not part of the simulated algorithm models in this research. The idea then is that even though the environment of measurement is unknown, the system should be able to classify the environment to the closest one among the four environment models used in this study.

#### 5.4.1 Outdoor Measured RSS Distribution

In statistics, two methods for working out the correlation between two variables are Pearson or Spearman's approach. The Pearson correlation coefficient is the most widely used. It measures the strength of the linear relationship between normally distributed variables. When the variables are not normally distributed or the relationship between the variables is not linear, Spearman rank correlation method is used. A normal distribution is expected because for multiple measured RSS at each distance, majority of the measured values should lie close to the mean value. To check if the measured data is normally distributed, a histogram of the all measured RSS is plotted as shown in Figure 5.5. This result have shown a normally distributed data set that is positively skewed. Based on this, for all statistical correlation analysis, Pearson correlation coefficient is used.

#### 5.4.2 Effect Of Noise on Measured RSS

In RSS based localization, noise can be defined as the standard deviation of measured RSS at same distance in the same environment. Even with the same device, different RSS is measured at same distance due to ambient noise [232]. To investigate what the effect of noise would be on this system, measured RSS data at each distance for ten different network scans were plotted as an error bar of sample standard deviations from the mean. Figure 5.6a shows the result for each 5m interval of range. This result have confirmed that even with the same device at the same distance in the same environment, different scans will result to varying

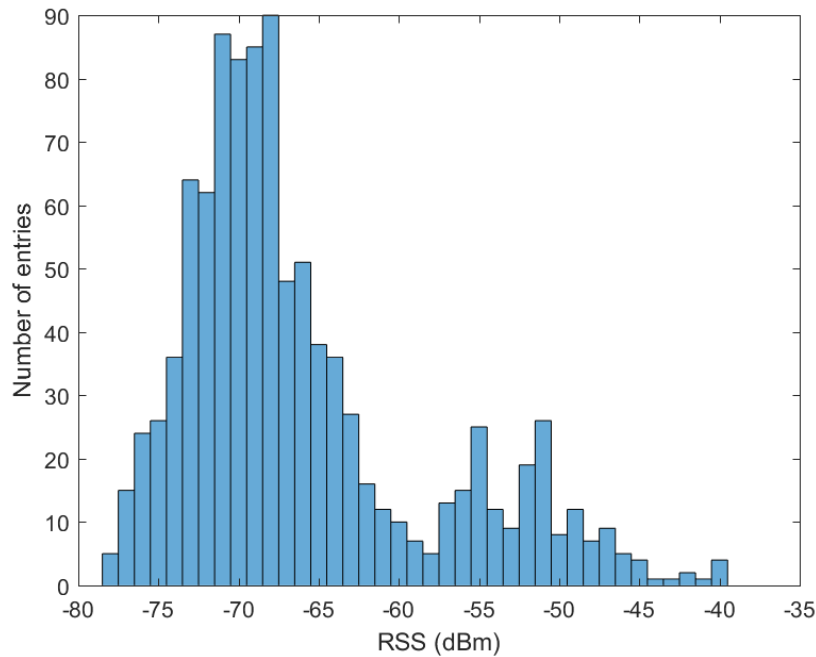


**Fig. 5.5** Histogram plot of average measured RSS to check the distribution of measured RSS data

RSS values due to ambient noise. Figure 5.6b shows the amount of deviation encountered due to this noise. Result have shown that the standard deviation due to noise expected in this

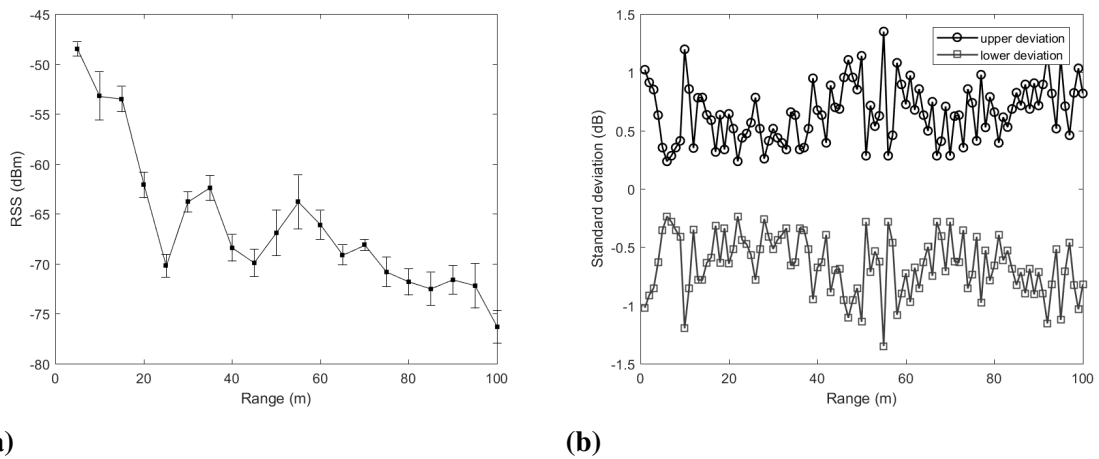


**Fig. 5.6** Deviation of measured RSS at each distance for ten scans (a) deviation from mean RSS (b) amount of deviation

particular environment is within  $\pm 1.3$ dB. This standard deviation is with same radio device but can vary with different devices. Noise obtained from different environments will also be different due to characteristics of the propagation in that environment. Signal attenuation

also varies with time, geographical position and radio frequency in the form of fading which can be due to multipath, weather like rain and obstacles having shadowing effect on the propagating signal.

### 5.4.3 Attenuation Rate (Ar)

The rate at which received signal strength decreases with distance is referred to as attenuation rate. This is given as  $RSS \propto \frac{1}{d^\alpha}$ . In most places in literature the attenuation rate is approximated using the pathloss exponent [233] giving a theoretical value of 2 in free space environment. Practically attenuation rate is higher [232]. The attenuation rate was calculated using both simulated data for the four environment models and the experimental measured field data by finding the semi-log plot of RSS relationship with distance. The slope of which was calculated to obtain attenuation rate of approximately 20dB/decade in both FSPL and ITU, 26dB/decade in HATA, 22dB/decade in WINNER and 17dB/decade in experiment. for the open space environment. Attenuation rate follows the power law which states that the relative change in one quantity results in a proportional relative change in another. This means that in this environment with this system, for every doubled distance, RSS drops by these amount in the specified environments.

### 5.4.4 Difference In Measured RSS Per Distance Test

A strong certainty that there is an inverse relationship between RSS and distance have been obtained. This means that as distance increases RSS decreases. There is also need to ascertain that there is significant difference between RSS measured at different distances. We therefore come up with a hypothesis which states that *if there is significant difference between RSS at different distances, then different RSS values can be related to unique distance values for range estimation model*. The null and alternate hypothesis are thus stated;

- H<sub>0</sub>: There is statistically no significant difference between measured RSS at each distance for all scans
- H<sub>A</sub>: There is statistically significant difference between measured RSS at each distance for all scans

From this hypothesis, we believe that there is a significant difference between RSS values at each distance for all scan periods. A statistical correlation and P-value test was performed to find the correlation of all data from all scan with distance. The result obtained is  $Pv = 3.71 \times 10^{-23}$  and  $Corr = -0.793$  which rejects the null hypothesis and accepts that there is significant difference in measured RSS between distances.

### 5.4.5 Measured RSS At Same Distance But Different Scans

It is expected that multiple scans at the same distance should have closely related RSS values. We can then state a hypothesis that *If the same or closely related values of RSS are measured at the same distance at different scan periods, there will be stability in measured data and error in range estimation will be reduces.* The null and alternate hypothesis are thus stated;

- H0: There is statistically significant difference between scan period
- HA: There is statistically no significant difference between each scan periods

A correlation test was carried out on all data obtained from all the ten scans for all distances. The correlation coefficients showing how each data set for each scan relates to another data set for other scans are shown in Table 5.1.

**Table 5.1 Correlation between different scans for the same distance range**

	Scan 1	Scan 2	Scan 3	Scan 4	Scan 5	Scan 6	Scan 7	Scan 8	Scan 9	Scan 10
Scan 1	1.00	0.97	0.97	0.97	0.97	0.96	0.97	0.96	0.95	0.94
Scan 2	0.97	1.00	0.95	0.97	0.96	0.96	0.96	0.95	0.95	0.94
Scan 3	0.97	0.95	1.00	0.97	0.97	0.96	0.97	0.97	0.96	0.95
Scan 4	0.97	0.97	0.97	1.00	0.97	0.97	0.97	0.97	0.97	0.96
Scan 5	0.97	0.96	0.97	0.97	1.00	0.97	0.98	0.98	0.98	0.97
Scan 6	0.96	0.96	0.96	0.97	0.97	1.00	0.98	0.98	0.98	0.98
Scan 7	0.97	0.96	0.97	0.97	0.98	0.98	1.00	0.98	0.99	0.98
Scan 8	0.96	0.95	0.97	0.97	0.98	0.98	0.98	1.00	0.99	0.99
Scan 9	0.95	0.95	0.96	0.97	0.98	0.98	0.99	0.99	1.00	1.00
Scan 10	0.94	0.94	0.95	0.96	0.97	0.98	0.98	0.99	1.00	1.00

From Table 5.1, it can be seen that all but two scan data sets passed the 0.95 (95%) scientific level required of a normal distribution. Only scan 2 and 10 and also scan 1 and 2 have values of 0.94 which is 0.01 below the required threshold. Since 96% of the data have shown that data obtained at multiple scans are positively correlated, there is high certainty that the data collected during multiple scan will be stable for accurate localization.

### 5.4.6 Experimental Range Estimation Model

Experimental RSS-distance classification was plotted and compared with simulation. Simulation was performed using the following parameters; transmitter (ESP8266 thing) power of 0.4455W, Tx gain of 2.14dBi and Rx gain of 9dBi which are the experimental parameters. Simulation was for all four environments and mean measured RSS for ten scans in each distance were used in this comparison. Figure 5.7a shows the plotted RSS against distance for all environments. This result have shown that lower RSS value than

expected is measured in physical environment when compared to simulation. This indicates that in physical environment, over-estimation is most likely to occur than under-estimation. Figure 5.7b is the attenuation rates in all four simulated environments and in experimental environment. This result has shown that the rate at which RSS decreases with distance in FSPL, HATA, ITU, WINNER and experimental environments are 20dB/decade, 26dB/decade, 20dB/decade, 22dB/decade and 17dB/decade respectively. The higher the attenuation rate, the faster the curve plot levels off causing lower resolution in distance. Experimental result has shown too good attenuation rate even compared with free space model which is not expected. This suggests that maybe signal ducting may have occurred or the propagation was within the interference zone. These are possible due to the inadequate transmitting and receiving antenna heights. Future work would include further investigation with higher antenna heights atleast at one end of the transmission link. An experimental attenuation of 17dB/decade is a good indication of high resolution in distance meaning that good RSS-distance classification and accurate localization are possible.

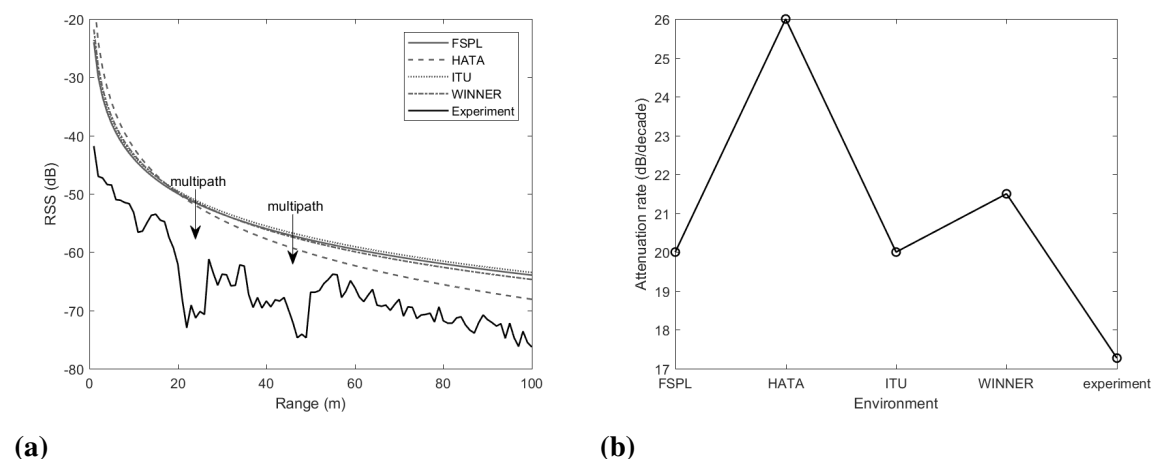


**Fig. 5.7 Comparison of simulated and experimental (a) RSS (dBm) in relation to distance (b) attenuation rate**

## 5.5 Outdoor Network Trial Experiment

The aim of this section is to run a trial experiment to test both the system and the algorithm. The expectation is that when the deployed system is switched on, it should scan the network to identify users in the network, then run ten scans and in each case, measure RSS of all identified users. System was able to scan the network, identify users in the network and measure their RSS at each scan. Figure 5.8a shows a model of the experimental environment with deployed users in their actual positions. Mean of the experimental measured RSS of

these users from four main azimuth positions were obtained and plotted as shown in Figure 5.8b. From the measured data of Figure 5.8b, it was discovered that the system is not able to

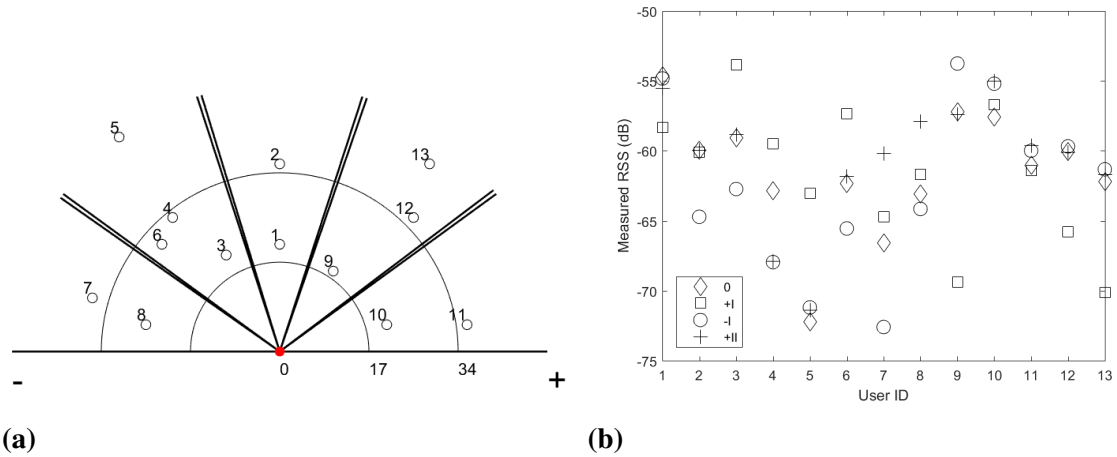


**Fig. 5.8** User deployment for trial experiment showing (a) actual user position before localization (b) measured RSS from user devices at all azimuth positions

identify all users at every scan and also only thirteen users out of seventeen were identified. There were some challenges of heavy breeze and occasional light showers of rain during the experiment which may have affected the measurement but since multiple scans were taken at each beam direction, out of the ten measurements, all users were found in at least seven places. The system used the mode of all measured data for each user at each beam position to fill up for unmeasured data before calculating the mean. This ensures that equal data set is used for fair analysis.

### Measured RSS Result Analysis

From result of Figure 5.8b, it can be seen that for each user, highest RSS has been measured in only one azimuth position compared to other positions. For instance, position 0 measured highest RSS for use 1 and 2 while position +I measured highest value for users 3, 4, 5 and 6. The same with other azimuth positions like -I and +II which have obviously measured highest RSS for user 9 and 7 respectively compared to others. From this measurement, it is expected that the system's AoA algorithm which is based on maximum RSS will be able to correctly resolve AoA estimation of users. Also, for users 7, 8, 10, 11 that position +II has measured highest RSS, it is expected that the system is able to identify users at azimuth position -II based on the neighboring position as applied on the model.

### 5.5.1 AoA Estimation

The aim at this stage of the experiment is for the system to use the measured RSS to resolve AoA of each user by applying the AoA estimation model. Since from the measured

data, it has been seen that for each user, different RSS have been measured at different azimuth positions and one of the positions has recorded highest RSS compared to others, it is expected that the system is able to locate the angular position of each user. Using the measured RSS, the system resolves the AoA of each user by applying the AoA estimation model. Result is shown in Figure 5.9a with the highest measured RSS of each user printed.

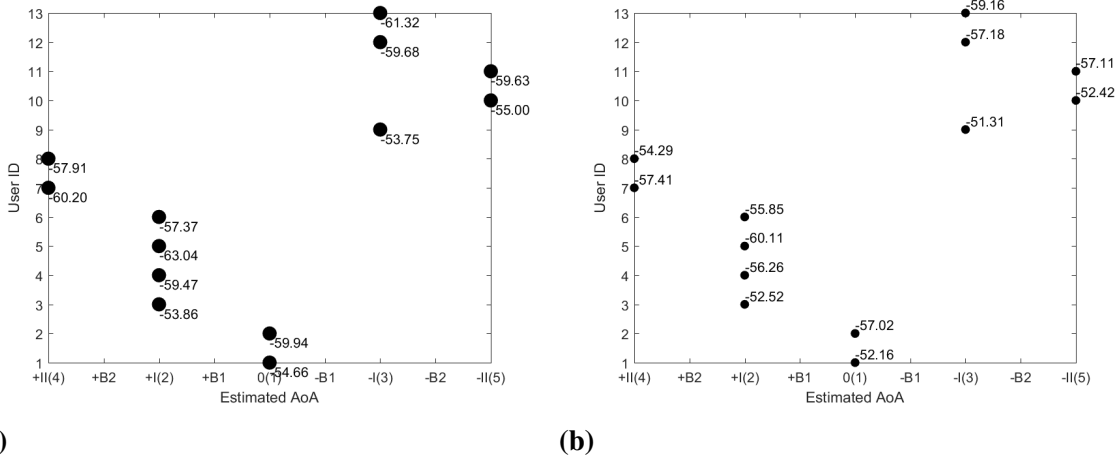


**Fig. 5.9** AoA estimation results (a) experiment (b) simulation showing accurate AoA estimation for both simulation and experiment

### AoA Estimation Result Analysis

Comparing estimated AoA with actual user azimuth positions of Figure 5.8a, It can be seen that users 1 and 2 located at beam 1 were correctly classified as being in position 0 which is broadside while users 3 to 6, and 9,12,13 were located at  $+I$  (beam 2) and  $-I$  (beam 3) which are right and left of broadside respectively. Users 7, 8 and 10, 11 were also correctly located at azimuth positions  $+II$  and  $-II$  respectively. These results have shown that the AoA estimation model is accurate for its purpose and the neighboring beam approach used to create azimuth  $-II$  position from  $+II$  data saving hardware implementation complexity and switching time is working well. Simulated AoA estimation result is also shown in Figures 5.9b. Comparing simulation and experimental AoA estimation results, both have shown 100% accuracy for the used sample, confirming the efficiency of this system for the purpose of AoA estimation.

### 5.5.2 Range Estimation and Environment Prediction

The aim at this stage is for the system to resolve user range using the same measured RSS that was used for AoA estimation. It is expected that the system is able to apply the four range models representing four different environment scenarios with all developed error models to resolve the range of each user. Out of all estimated range by the models, it is

expected that the system is able to predict the most likely environment of measurement which should give the best range estimate.

The system applies the range estimation models (FSPL, HATA, ITU, WINNER) to estimate the range of users using the measured RSS. All estimated range were then applied to the environment prediction model, to predicted the environment of measurement. Results have shown prediction values (mean absolute error of relative prediction from all models in each environment) of 33.41, 42.72, 31.86 and 33.97m for FSPL, HATA, ITU and WINNER respectively. This shows that ITU is the most likely environment of measurement. It can also be seen from this result that FSPL, ITU and WINNER which were identified as closely related models have shown close values while HATA which was a bit different from others has shown visibly different value. This result have shown that even though all applied models were for open space, the system is able to identify the environment of measurement which produces the best accurate range estimate. Result will be more obvious with highly different environment models like LOS combined with NLOS.

Since it has been identified that noise error in measured RSS between 0 and  $\pm 1.3\sigma$ dB may occur and that predominantly less measured RSS than expected is most likely, a compensation factor of  $1.3\sigma/2$ dB was added to measured RSS in each environment for noise compensation. The new values of RSS are then used to estimate range of users. Result of Figure 5.10 shows actual, ITU simulated and experimental estimated range of users using all environment models. Mean absolute error in range estimation between actual and experiment are 2.51m, 3.56m, 2.19m and 2.54m for FSPL, HATA, ITU and WINNER respectively. Comparing simulation and experiment, MAE in range estimation between experiment and simulation in ITU environment is 1.36m. This means that the mean deviation of experiment from simulation is approximately 1m and 2m from actual range.

To see the effect of the developed range estimation models on this system, range estimation before and after applying each model were implemented. Results show that MAE with only AARM (Before BPEM) was 12.41m but after BPEM it was 2.23m giving a PER of 82.03%. After BPEM and ADEM, the MAE became 2.19m i.e 1.74% further error reduction after BPEM. Error reduction remained the same after BUEM was applied because there was no user located at the boundary. Summarily, a total of 82.34% reduction in range estimation error is achieved.

### **Experimental Range Estimation Result Analysis**

From Figure 5.10, it can be seen that range estimation is achievable with this system with manageable error level. Apart from HATA which has a model that is well deviated from others, all other models are on the average, about 2.5m close to actual range. Deviation of

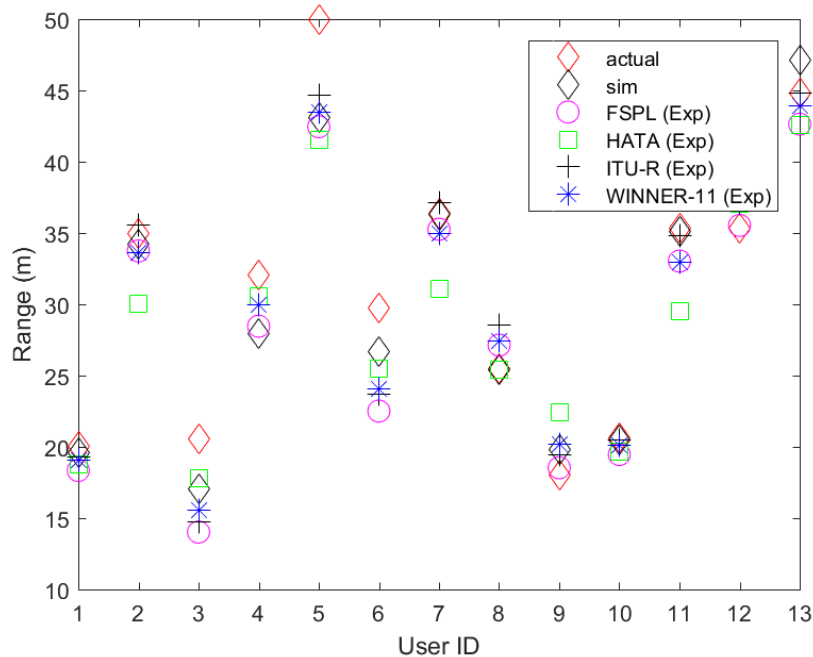


**Fig. 5.10** Experimental range estimation showing actual, simulated and experimental estimate

experiment from simulation in predicted environment is just approximately 1m which means that system is applicable and would works as modeled in simulation with a mean difference of  $\leq 1.5\text{m}$  of range estimation in most of the environments.

From the result obtained before noise compensation, apart from users 3, over estimation was predominant so that by adding the noise compensation factor, user range estimation error was reduced bringing estimate much closer to simulation. Noise in the environment may have caused under-estimation of users number 3 so that by adding the noise compensation value, more estimation error is introduced. Since noise is a random process there is no way to know which user have been positively or negatively affected, therefore judgment based on mean absolute error is adopted. Results have also shown that with the error models applied, error in range estimation is reduced by 82.34%.

### 5.5.3 User Cluster Localization And Small Cell Deployment

The aim at this part of the experiment is to see if the system is able to locate user clusters and identify locations for small cell deployment based on a set threshold. Our expectations in this research is that the system is able to locate users into clusters within each section of the coverage area where users exist and then circle locations that are qualified for small cell deployment. It is also expected that the system displays the coordinated of the small cell deployment positions relative to the observer system.

Since only few (seventeen) users were used in this experiment, it was assumed that locations with up to two users are qualified for small cell deployment. Due to the small experimental area, coverage area was shared into three range sectors. Combining the estimated AoA and range, users are classified into clusters by counting the number of users in each azimuth-range sectors of the coverage area. Figures 5.11a and 5.11b are results of experimental and simulated user clusters respectively. The system also displayed the small cell deployment coordinates relative to observer system.

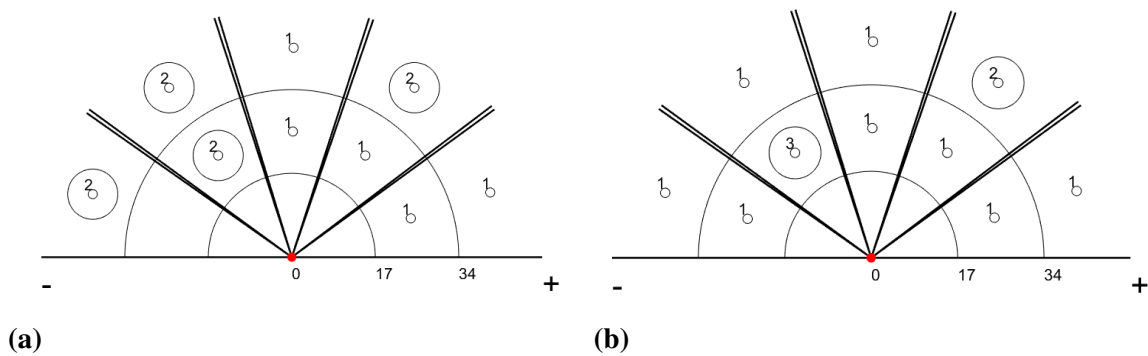


**Fig. 5.11** *User cluster localization and optimum small cell deployment position identification using (a) experimental (b) simulation data*

### User Cluster and Small Cell Deployment Result Analysis

From results of Figures 5.11a and 5.11b, simulation has identified two small cell deployment locations whereas experiment identified the same two locations plus another extra two location making a total of four small cell deployment locations. This is due to over estimation of two of the users as a result of noise in measurement. This error may have been caused by bad weather condition during this experiment. Also with few users and few threshold for small cell as used here, this is expected but with higher number of users required for small cell deployment, this discrepancies will be reduced. The possibility of user cluster and small cell deployment position identification is promising with the results obtained in this experiment.

## 5.6 Outdoor Final Experiment

The aim of this second experiment is to verify results of the trial experiment taking precautions for the short falls of the first trial. Good weather was confirmed before proceeding for this experiment so the environment of measurement was calm with gentle breeze. System was deployed as described in Section 5.2.1 and photo shown in Figure 5.1. A model of the deployment and actual users locations are shown in Figure 5.12a. RSS was measured as expected and mean measured RSS result shown in Figure 5.12b. From this result, it

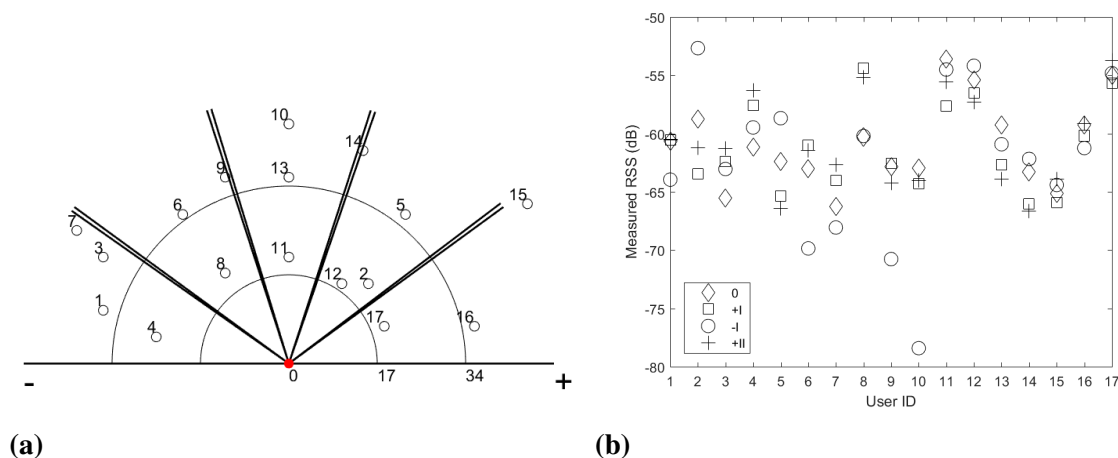


**Fig. 5.12** User deployment for final experiment showing (a) actual user position before localization (b) measured RSS from user devices at all azimuth positions

can be seen that all seventeen users were identified and it is obvious that for each user, only one azimuth position has recorded highest RSS compare to other azimuth positions. This confirms the trial experimental result which has shown that users can be classified into azimuth positions using highest measured RSS. This measured RSS were then used to estimate both AoA and Range as presented next.

### 5.6.1 AoA Estimation

Using mean measured RSS for each user at all azimuth positions, the system applies the AoA estimation model to estimate user azimuth positions. Figures 5.13a and 5.13b are the estimated AoA of users using experimental and simulated data respectively with the highest measured RSS of each user printed beside it. Comparing experimental and simulated results, every users were located in the same azimuth position for both experiment and simulation. Comparing with actual user location of Figure 5.12a, both simulated and experiment results have shown 100% accuracy in range estimation for the distributed users.

### 5.6.2 Range Estimation and Environment Prediction

The system applies all four range estimation models using the measured RSS as input data in each case to estimate user range with all error model and noise compensation. All estimated range were then used to predict environment of measurement. Result of Figure 5.14 shows the experimental estimated range with actual and simulated range for each user. By applying the environment adaptive range model, the system returned FSPL as the environment of RSS measurement. Both trial and final experiment were performed in the same environment but ITU and FSPL were predicted respectively. The trial result may

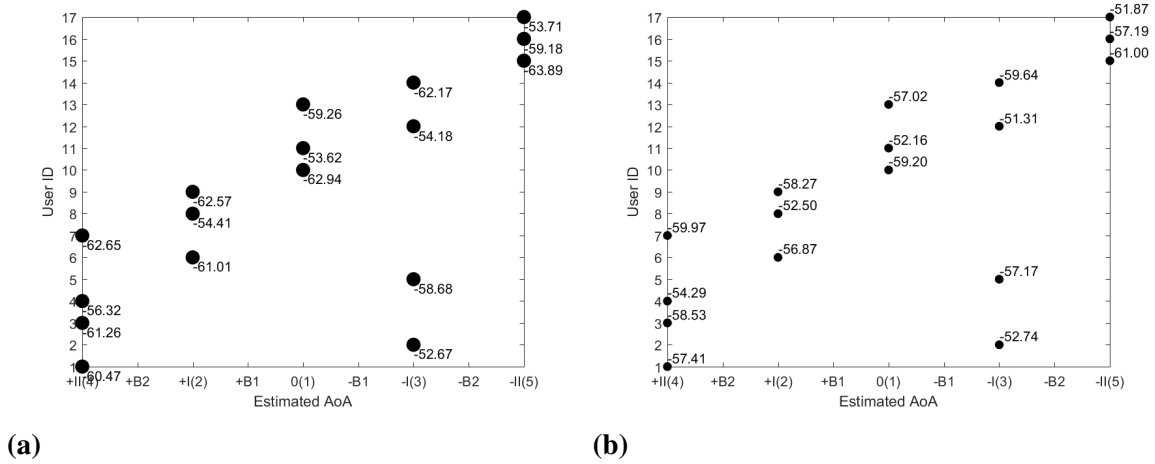


**Fig. 5.13 AoA Estimation Results (a) experiment (b) simulation showing accurate AoA estimation for both simulation and experiment**

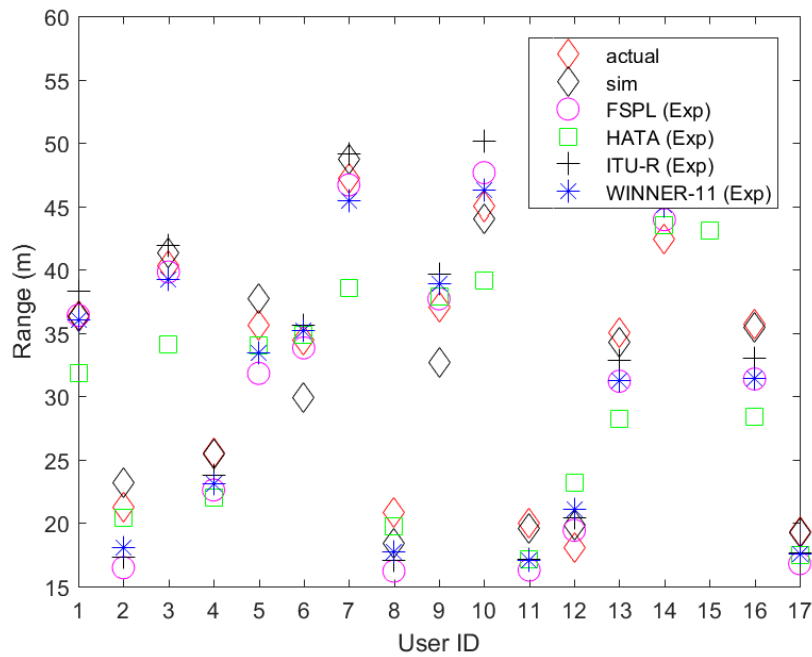


**Fig. 5.14 Estimated range of users using all four range models with experimental measured RSS as input**

have been affected by weather condition as already discussed but in any case, the EARM is not expected to be 100% correct since a practical environment is hardly predictable at all times. However, both experiments have predicted two closest environments which shows that EARM is acceptably accurate.

### Experimental Validation of Error Models

To experimentally validate the developed range estimation error models which include BPEM, ADEM and BUEM. User range were estimated using angle adaptive range model (AARM), that is before beam position error model (BPEM) was applied. Then range were re-estimated after BPEM, angular deviation error model (ADEM) and also after boundary user error model (BUEM). Unfortunately, no user was located at the boundary in this sample, therefore ADEM and BUEM are expected to produce the same result. Figure 5.15 is the plot of mean absolute error in range estimation before and after each range estimation error model was applied.

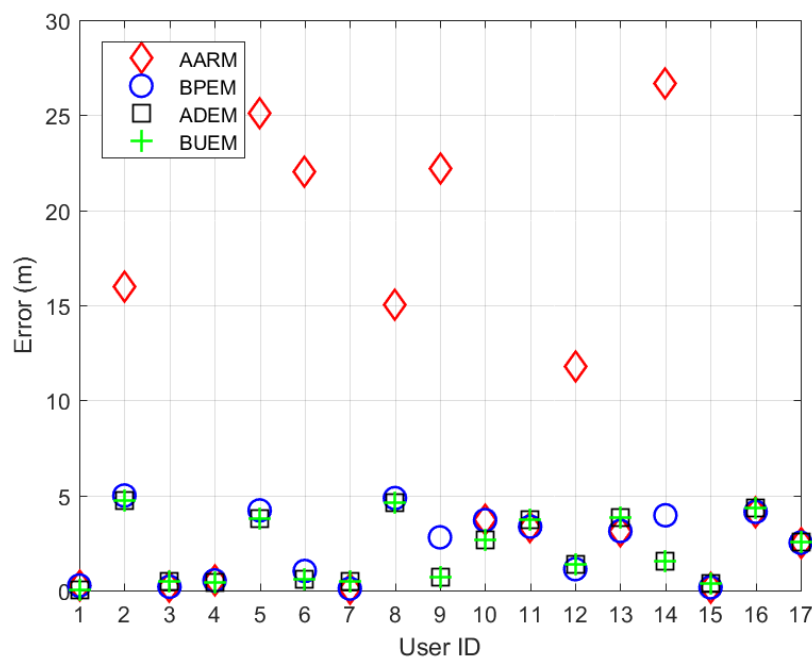


**Fig. 5.15** *Experimental validation of developed error models showing mean absolute error in range estimation after AARM, BPEM, ADEM and BUEM*

### Range Estimation and Error Model Result Analysis

Range estimation result of Figure 5.14 has shown a close relationship between actual and simulated results. Experimental estimate has pre-dominantly shown over-estimation which may be due to other losses in the environment. As already identified in simulation, error is less for users in azimuth positions +II and -II (User IDs 1, 3, 4, 7, 15, 16 and 17) than in other azimuth positions. Visually, there is very close relationship between actual, simulated and experimental results. From Figure 5.15, effect of BPEM was obviously shown with users 2, 5, 6, 9, 12 and 14 located at azimuth positions +I and -I with error in estimated

range reduced from 15.96m to 4.99m in user 2, 25.08m to 4.21m in user 5, 22.02m to 1.02m in user 6, 22.19m to 2.79m in user 9, 11.76m to 1.11m in user 12 and 26.66m to 3.95m in user 14. Effect of ADEM is obvious with users deviated from the azimuth position centers like users 9 and 14 with error in range estimation reduces from 2.79m to 0.69m and from 3.95m to 1.56m respectively. The MAE in range estimation after AARM, BPEM, ADEM and BUEM are approximately 9.22m, 2.41m, 2.13m and 2.13m respectively. As expected, this result has shown the same value for ADEM and BUEM. This gives a percentage error reduction (PER) of 73.88% before and after BPEM and 11.68% before and after ADEM with BPEM already applied. Summarily, with all error models applied in this system, error in range estimation is experimentally confirmed to be reduced by approximately 76.93%.

### 5.6.3 User Cluster Localization And Small Cell Deployment

The system algorithm is then applied to estimate user clusters and small cell deployment positions. As in the trial experiment, network area is shared into three equal range locations because of small experimental nominal range. A small cell deployment threshold of 2 is also assumed due to few number of users used in this experiment. Figures 5.16a and 5.16b show the located user clusters with positions for small cell deployment indicated by circling and the coordinates of the deployment positions relative to the BS respectively. Matching the user

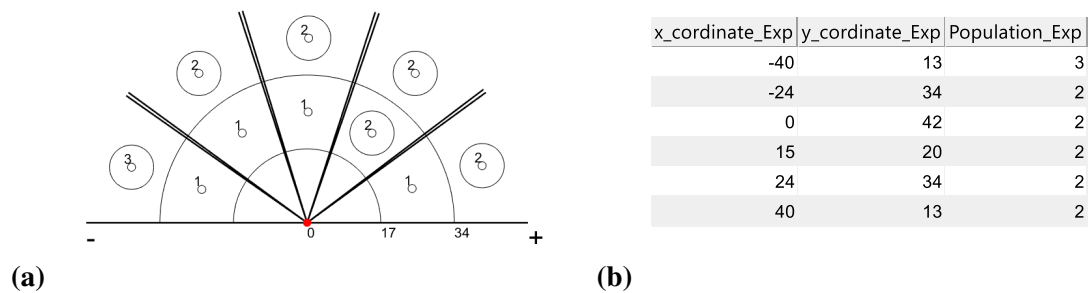


**Fig. 5.16** Experimental small cell deployment strategy showing (a) user cluster localization (b) small cell deployment position coordinates relative to BS

cluster localization result with the actual user location of Figure 5.12a, it is certain that users have been correctly located into their relevant clusters. The system has also able to correctly identify positions for small cell deployment. This experiment unlike the trial experiment has shown 100% accuracy for the deployed users. It should be noted that this may not be the case for a larger coverage area and for all samples but it shows that high accuracy is most likely to be achieved.

## 5.7 Indoor Wireless Local Area Network Application

The system was also tested for indoor application assuming it is part of a WLAN router. The aim is for the system to identify location for a femocell deployment within the existing network. Due to the small deployment space, 20m coverage length, shared into two range sectors was considered. A model of the deployment setup is shown in Figure 5.17a and already described in Section 5.2.2. The system measures RSS of distributed indoor users from all four azimuth positions, results shown in Figure 5.17b.

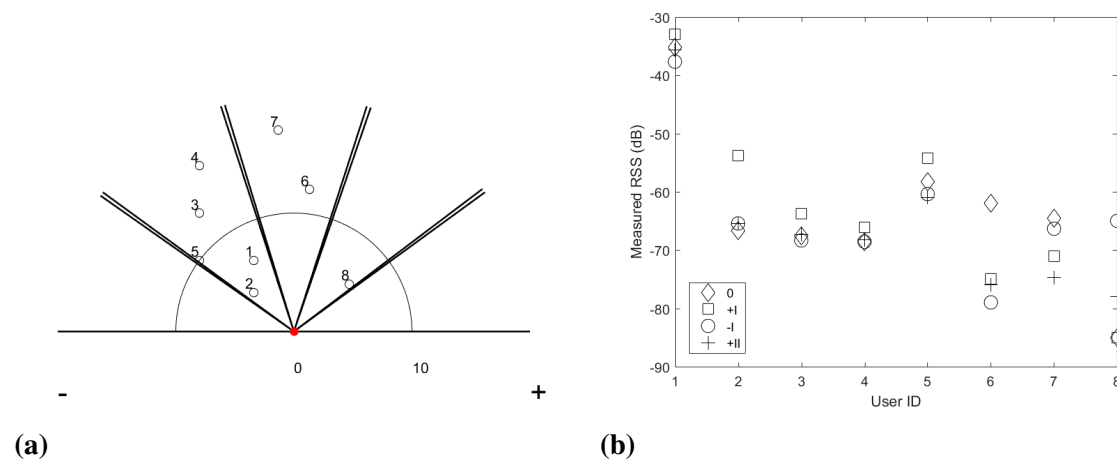


**Fig. 5.17** User deployment for Indoor experiment showing (a) actual user position before localization (b) measured RSS from user devices at all azimuth positions

### 5.7.1 Indoor Experimental AoA Estimation

Using the measured RSS, the AoA estimation algorithm is applied to estimate AoA of users. Figures 5.18a and 5.18b are the experimental and simulated AoA estimation respectively. From these results, it can be observed that all users AoA were correctly determined by both simulation and experiment. It can therefore be concluded that the AoA estimation using this system also produces an accurate result in indoor environment.

### 5.7.2 Indoor Experimental Range Estimation

The system then uses the maximum measured RSS as determined by AoA estimation algorithm and printed in Figure 5.18a to estimate range of users. Figure 5.19 is the estimated range using all four range estimation models. This result has shown over-estimation for all users due to NLOS effect as simulated in Section 3.14. The MAE in range estimation using FSPL, HATA, ITU and WINNER are 27.49m, 24.25m, 29.36m and 27.47 respectively. With this large error, it is extremely difficult to correctly identify locations for small cell deployment.

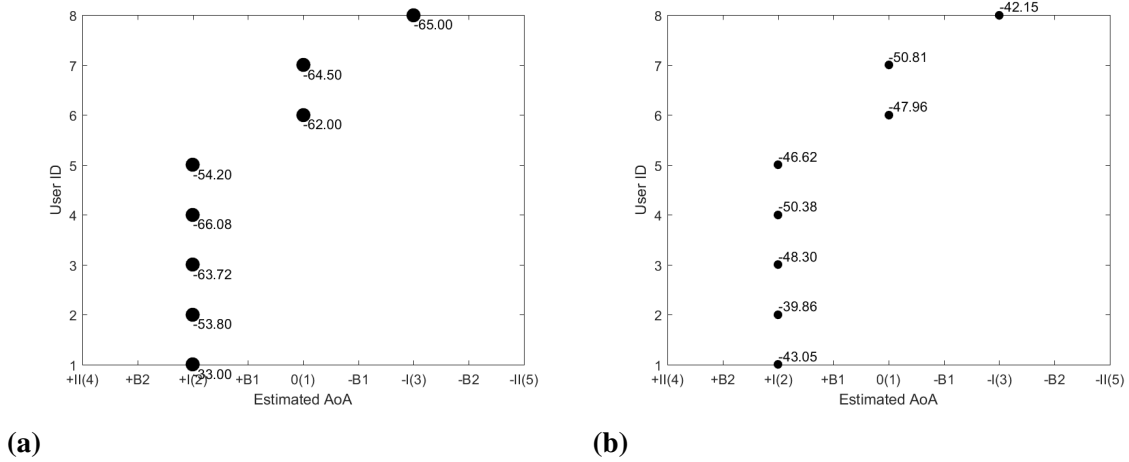


**Fig. 5.18 AoA Estimation Results (a) Experiment (b) Simulation showing accurate AoA estimation for both simulation and experiment in indoor environment**

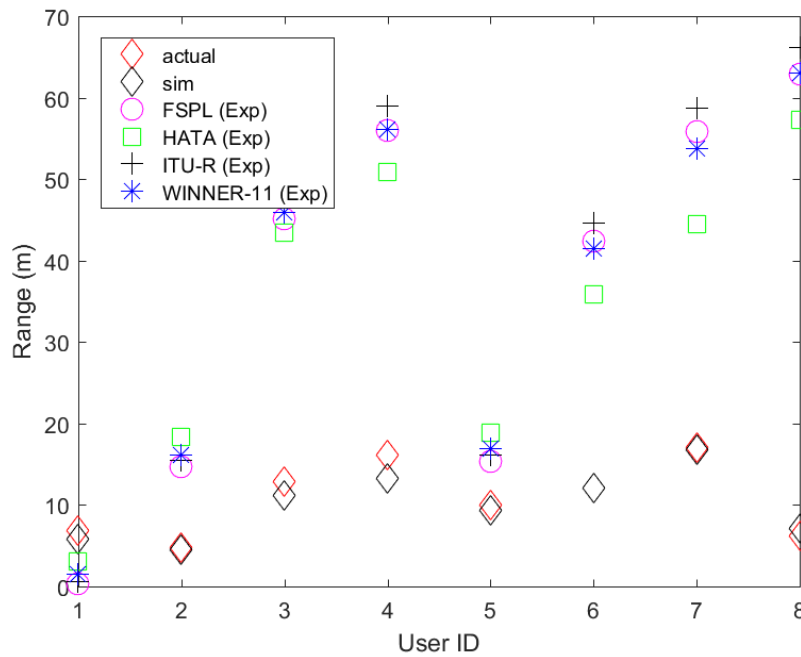


**Fig. 5.19 Actual, simulated and experimental range estimated in indoor environment using all four range estimation models before NLOS mitigation**

### 5.7.3 Indoor Experimental Range Estimation with NLOS Mitigation

To obtain a more accurate range estimate, the two developed ITU and WINNER based NLOS mitigation models of Equations 3.20 and 3.21 were applied to the estimated range by all range models. Figures 5.20a and 5.20b show the new estimated range of users with ITU

and WINNER based NLOS mitigation applied respectively. These results give a MAE of

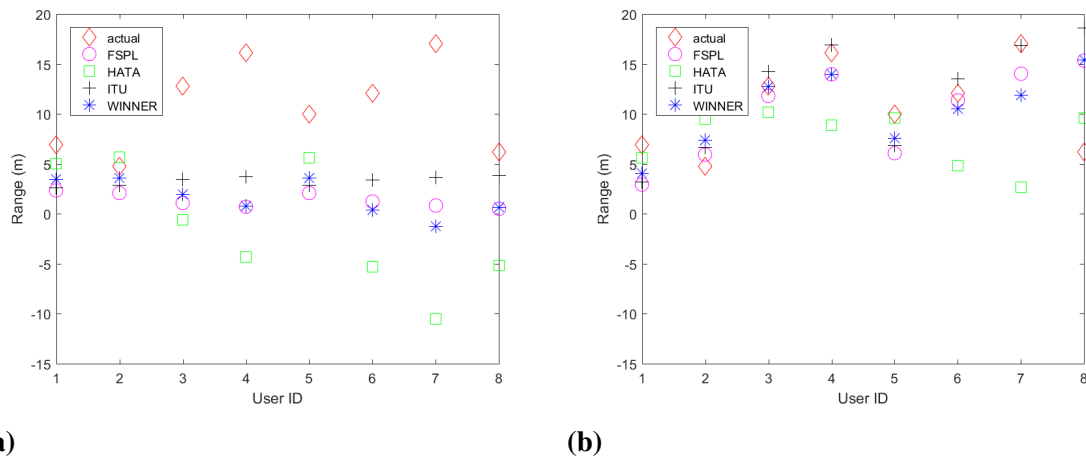


**Fig. 5.20** Indoor Experimental range estimation with all four range estimation models after NLOS mitigation using (a) ITU (b) WINNER based NLOS mitigation models

9.37m, 12.17m, 7.44m and 9.11m and a PER of 65.92%, 49.81%, 74.64% and 66.85% for FSPL, HATA, ITU and WINNER respectively using ITU based NLOS mitigation Model. With WINNER based NLOS mitigation Model, a MAE of 3.14m, 5.18m, 3.14m and 3.28m and a PER of 88.56%, 78.63%, 89.31%, 88.07% for FSPL, HATA, ITU and WINNER respectively is obtained. These results have shown that WINNER based NLOS error mitigation model performs better than ITU based NLOS error mitigation for all range models with an average percentage system error reduction of 64.31% and 86.14% for ITU and WINNER based NLOS error mitigation models respectively.

#### 5.7.4 Indoor User Cluster Localization and Small Cell Deployment

Next is for the system to determine user cluster locations and optimum positions for small cell deployment. Figures 5.21a and 5.21b show the user cluster localizations with optimum small cell deployment positions circled as identified by the system before and after NLOS error mitigation respectively. Before NLOS error mitigation was applied, the system identified two positions for small cell deployment with user clusters of 2 and 4 which when compared with the actual user positions of 5.17a, it is incorrect. After NLOS error mitigation, user cluster and small cell deployment were correctly identified. It is therefore obvious that over-estimation occur due to NLOS effect but it is effectively taken care of using the developed WINNER based NLOS error mitigation model for more accurate range estimation.

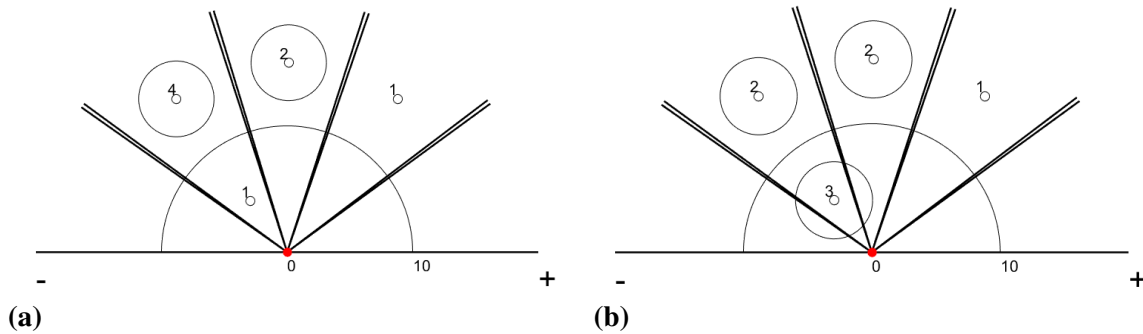


**Fig. 5.21** Indoor cluster localization and small cell deployment positions (a) before (b) after NLOS error mitigation

### WLAN Application Result Analysis

Result obtained from indoor deployment has shown that with NLOS error mitigation, the system was able to identify user clusters and locations for small cell deployment. This means that if system is deployed in busy places like airports, locations of user cluster can promptly be identified for femtocell deployment to offload traffic from existing one and ensure balanced load and good QoS in the network at all times. The NLOS error mitigation models were applied on the open space based system to locate users indoors. This means that the system can be used for both indoor and outdoor without having to re-design the entire system algorithm.

## 5.8 Conclusions

Experimental validation of the designed and simulated observer system that would help wireless network operators identify locations for small cell deployment has been presented. The system blocks designed, simulated and implemented in chapters 3, 4 and 5 respectively was experimentally validated in this chapter. Outdoor experiments were carried out twice in an open space of Ponderosa park in Sheffield with a network of WiFi APs as users. RSS of deployed users were measured in each case by the system and using the acquired data, user AoA, range and cluster were located. 100% accurate AoA estimation of users were achieved in both experiments. Environment of RSS measurement was predicted to be ITU in first experiment and user range were estimated with 1.36m mean deviation from simulation in the predicted environment and 2.19m mean deviation from actual user range. By applying the developed error models, error in range estimation was reduced by 82.34%. In second experiment, environment was predicted as FSPL and range estimation were estimated with deviation from simulation and actual range of 2.83m and 2.13m respectively. Improvement in range estimation of 76.93% was achieved by all error models. The same environment

has been predicted as ITU as well as FSPL by both environments because both environment models are very closely related. System identified correct positions for small cell deployment as simulated but with two extra positions in first experiment due to over-estimation caused by poor environment condition during measurement. With more users in the network and higher threshold of number of users required for small cell deployment, this discrepancy with simulation will be reduced or eradicated. The second experiment have correctly identified all positions for small cell deployment. Secondly, system was tested for indoor application and have shown that user cluster can also be correctly identified by applying the developed NLOS error mitigation model. WINNER based NLOS error mitigation model was shown to perform better than ITU based with a mean PER of 86.14% and 64.31% respectively. This means that in busy places like airports, system can be used to promptly identify user cluster and positions for more AP deployment without having to redesign the system algorithm for indoors. Deploying pico or microcell in located users cluster positions outdoor or femto in indoor, the macrocell is offloaded from it's traffic overload, balanced load is assured on the network and good QoS and customer satisfaction is achieved. In general, system has shown very close relationship with simulation results which means that system works as simulated in Chapter 4 with minimal error that does not disrupt its proposed and simulation achieved performances.

# Chapter 6

## Conclusions and Future Work

### 6.1 Conclusions

This thesis presents research into small cell deployment in 2-tier heterogeneous networks as a solution to meeting future capacity demands. Small cell deployment in areas of high user concentration is a strategy that offloads traffic from the existing network, ensures high QoS to users and a balanced load in the network. Operators ability to promptly identify high user concentration locations allows for quick decision making on small cell deployment. This research work presents a novel strategy for small cell deployment within areas of high user concentration. The concept is for mobile operators to have an observer based system incorporated in a mobile cellular network base transceiver station (BTS) to periodically monitor the cell coverage area and identify regions of high concentration of mobile users for small cell deployment in 2-tier heterogeneous networks. The aim is for the location algorithm to have a level of accuracy which is within the reasonable constraints of the urban built environment i.e  $\pm 5 - 15\text{m}$ . The main novelty of this research lies on these three areas;

- ***The application:*** Prior to this research, there was no existing system that helps network operators identify optimum locations for prompt small cell deployment in 2-tier HetNet.
- ***The System:*** Prior to this research, there was no practical centralized localization system with only two antenna elements that resolve AoA, range and user cluster using only measured RSS.
- ***The System Algorithm:*** Prior to this research, there was no hybrid AoA/RSS localization algorithm with only one BS and implemented only in one phase.

The design, simulation and implementation of a prototype observer system for optimum small cell position identification have been presented. In the design, only two antenna elements were used in an array to ensure reduced cost and complexity as against multiple

antennas normally used in a standard antenna array system. This is to ensure that the system does not add unreasonable cost and complexity to the already expensive BTS infrastructure. To ensure simplicity and adaptability of the system, a phase only beam-forming and beam-steering was used to generate a beam and steer the beam to other locations dividing the entire network coverage into azimuth sectors. By further sharing the coverage area into range sectors, different azimuth-range sections for user cluster localization was created. AoA estimation model was developed based on azimuth position from where maximum RSS was measured and range estimation model which is angle adaptive was developed based on statistical regression analysis (AARM). The system algorithms were based on a simple, anonymous RSS data for both AoA and range estimation.

In the course of simulation of the system, five new mathematical models, AARM, BPEM, ADEM, BUEM and EARM were developed. Angle adaptive range model (AARM) is a model that estimates user range based on the estimated AoA of that user. Beam position error model (BPEM) is a model that predicts the error in range estimation that is peculiar to users located left and right of broadside. Angular deviation error model (ADEM) is a model that predicts the error due to users not located at the azimuth center. Boundary user error model (BUEM) is an error model that predicts error peculiar to users located at the boundary. Environment adaptive range model (EARM) is a model that predicts the environment of RSS measurement for best range estimation model identification. These error models are shown to have reduced the system range estimation error by up to 84%. The effect of non line of sight was also investigated and compensated for in the system. Simulation result with different samples of users gave good results that led to the system being implemented.

Both outdoor and indoor experimental validation of the system performance was carried out using a WiFi based system. AoA estimation model produced 100% accuracy in two experiments. Range estimation error was shown to be 12.41m and 9.22m in first and second experiments respectively — this is approximately the width of a 3-lane motorway. With error models applied, the estimated range error in both experiments were reduced to 2.19m and 2.13m respectively — this is approximately the width of a footpath. A percentage error reduction of 82% and 77% were achieved by applying the error models for the first and second experiments respectively giving a PER of 80% on average of the two experiments with seventeen users. Results have shown that system is able to correctly identify user clusters and positions for small cell deployment with minimal error. A prototype system has been designed and tested to validate the efficiency of the localization algorithm within real environment. The system utilized 17 wireless nodes operating within the 2.4GHz ISM frequency band. Experimental results were shown to be very close to simulation and with this

network operators will be able to identify user clusters and optimum positions to deploy small cells. By knowing the population of users in each cluster as the system displays, operators will be able to decide the most suitable type of small cell to deploy at a given small cell location. The system was also tested for indoor application and extension to human tracking and a promising results have been achieved.

By deploying femto-, pico- or microcells at the user cluster locations as identified by this system, balanced load, high QoS and substantial traffic offload will be achieved in the network. The operators are also able to promptly know when an unexpected hotspot has occurred and be able to deploy a mobile BTS as already proposed in research literature.

## 6.2 Research Contribution To Science, Engineering and Technology

The research work presented in this thesis offers a novel approach to prompt small cell deployment in a 2-tier HetNet. This involved a design and implementation of an observer system as proposed from the beginning. At the path of achieving the objective of this research, the following bits of contributions to this area of Communication Engineering have also been achieved.

- ***A simple But Accurate Two Element Adaptive Array AoA Estimation Model:*** Generally, in an adaptive beam smart antenna systems, numerous antenna elements are combined in an array to generate a directional beam that is used to receive signals and with suitable algorithm, to resolve AoA of those signals. Due to the multiple antennas and required feed network involved, an array system is considered to be expensive, complex and cumbersome. This research shows that it is not in all applications that numerous antenna elements are required in a smart antenna system. Achieving AoA estimation with just two elements in this research has shown that depending on the application involved, minimum number of antenna elements to form an array can be applied and still achieve a good result for its purpose.
- ***A Real Time RSS Based Range Estimation Model:*** Range-based localization that uses RSS as a matrix is normally characterized by fingerprinting which involves on-line and off-line phases. An intensive work of coverage area mapping of RSS to distance is involved during the off-line phase requiring both man power and enormous cost of money and time. On the other hand, this results in site specific application. During the on-line phase, the computation complexity of searching the database for best matching RSS-distance data is also enormous. This research has presented an

RSS based range estimation model that bypasses the off-line phase entirely, applying a simple regression model to calculate range using real time measured RSS.

- ***BPEM for More Accurate Range Estimation In Steered Beam Localization Systems:*** Fingerprinting approach is popular in RSS-based range estimation because it's complexity and cost is most times traded off for accuracy. A range estimation model built using statistical analysis is usually characterized with errors running in hundreds of meters. This research has identified that in a steered beam array system, RSS-distance classification is not the same in all beam positions. When range model is built with the assumption that they are the same, a huge amount of error occurs. In order to reduce error in range estimation, a mathematical model to compensate for the differences in beam positions on the range estimation was developed.
- ***ADEM For Improved Accuracy In A Wide Beam-width Localization System:*** The fewer the number of antenna elements used in an array for localization system, the wider the beam width of the produced beam. With only two elements, a wide broadside beam was produced. Using RSS measured at beam peak to characterize distance results in estimation error of users deviated from the beam peak. This research identified that great amount of error that makes the total mean error of the system high is from users deviated from the peak in such systems. This research therefore developed a mathematical model that reduces the effect of this error.
- ***BUEM For Improved Localization Accuracy Of Users Located At The Boundary:*** This research has identified that between 1m spacing of users in a steered beam system, boundary users exist. For this reason, users at the boundary were considered in AoA estimation and can be located as being in the boundary. Since no beam has a peak at the boundary and these boundaries are beyond each neighboring beams, their error in range estimation is beyond the normal error due to angular deviation. This research has also introduced and developed an error model to reduced error in range estimation of boundary users.
- ***Environment Adaptive Algorithm For Improved Accuracy In RSS Based Localization Systems:*** This research has identified that the best range estimate is obtained using the correct model for any environment. It was also identified that unbearable error occurs if propagation environment is not well characterized (wrong model). To ensure that best estimate is achieved, this research has used four different environments to develop an environment adaptive algorithm that identifies which environment best describes the measured data. The Range estimated using the model of the predicted

environment gives the best range estimate. In this way range estimation error is further reduced.

- ***NLOS error mitigation models:*** This research has developed two NLOS error mitigation models based on ITU and WINNER range estimation models. This can be applied in any indoor localization system to mitigate against error caused by NLOS. It was identified that WINNER based model performs better than ITU based model with simulation PER results of 99.9% and 99.2% and experimental results of 86.14% and 64.31% respectively.
- ***A Hybrid Localization Algorithm with NLOS Error Mitigation:*** Hybrid localization algorithm is the state of art in this area. AoA/RSS approach is existing but applies two phases [234] with raised complexity and cost or uses triangulation [235] requiring at least three BSs to locate one user. This research presents a centralized hybrid RSS/AoA localization algorithm that requires only one phase (real time) and one BS to locate all users in the network. LOS environment were considered in developing the algorithm but it was extended to NLOS application by developing a mathematical model to compensate for the NLOS effect for two of the environments most popularly used for indoor applications (ITU and WINNER).
- ***A novel strategy For Small Cell Deployment In A 2-tier HetNet with user concentration identification:*** Small cell deployment strategies that existed were either 'blind' in which case small cells are randomly or cell edge deployed or that they are based on long term data traffic collection which results in latency in decision making for small cell deployment. Recent research proposed mobile small cell deployment in high user concentration but leaves the operators with ability to identify HUC locations. Possible solution would be with GPS since all modern phones are GPS capable but unfortunately users are already questioning their privacy with GPS. This research has provided a simple prototype design that will help mobile operators to promptly identify HUC positions for small cell deployment with anonymous data reassuring customers of their privacy. With this system, the already proposed mobile small cell deployment strategy can smoothly be implemented to solve the problem of unexpected hotspots.

### 6.3 Future Work

This research has focused so much on the algorithm and has demonstrated the applicability and performance of the system with a prototype design. During the course of reviewing literature and designing the prototype system, many ideas of what an improved version would look like was conceived and presented as future work in this section.

- **Compact design:** Size was not part of the design criteria from the beginning of this research but since the system has a potential for indoor application, there is need to consider size in the improved version of the system. A conceived idea is having the antenna and the phase shifters all as a PCB design so that every member of the system is a portable content of the black box, avoiding the use of standing out antennas.
- **Cellular Network Design and Testing:** The idea presented in this work was mainly for cellular network application. Due to the license requirement and protocols involved in getting permission to test the system and owing to the fact that this is the first and a prototype design which still needs improvement and redesigning, a WiFi network was used to demonstrate the idea. future work will include implementation for cellular networks like GSM or 4G with more available users for further testing of the system.
- **Reconfigurable System:** Designed phase Shifters and antennas used in this project are for a specified network frequency application. Reconfigurable phase shifters [236] and antennas [237] that can operate at different frequencies for multiple applications have been presented in literature. In other to make the system more universal, future work would consider the design of a reconfigurable phase shifters and antennas for a more universal system design.
- **Mobile Application:** To follow the trend of smart world, future work should also incorporate a mobile app that the operator can use to monitor the system output on the go. This may include a pop-up alert system to alert an operator when the cluster exceeds a certain threshold and would require immediate action.

# References

- [1] Mobile now accounts for nearly 70% of digital media time [comScore]. URL <https://marketingland.com/mobile-now-accounts-nearly-70-digital-media-time-comscore-210094>.
- [2] Number of 4G mobile subscribers worldwide 2010-2020 | Forecast. URL <https://www.statista.com/statistics/226101/global-4g-mobile-subscriber-forecast/>.
- [3] Cisco. Cisco Visual Networking Index: Global Mobile Data Traffic Forecast Update, 2016–2021 White Paper - Cisco, 2017. URL <https://www.cisco.com/c/en/us/solutions/collateral/service-provider/visual-networking-index-vni/mobile-white-paper-c11-520862.html#AnalyzingtheExpandingRole>.
- [4] Seiamak Vahid, Rahim Tafazolli, and Marcin Filo. Small Cells for 5G Mobile Networks. In *Fundamentals of 5G Mobile Networks*, pages 63–104. John Wiley & Sons, Ltd, Chichester, UK, may 2015. ISBN 9781118867464. doi: 10.1002/9781118867464.ch3. URL <http://doi.wiley.com/10.1002/9781118867464.ch3>.
- [5] Shelly Salim, Christian Oey, and Sangman Moh. Are Heterogeneous Cellular Networks Superior to Homogeneous Ones? *Lecture Notes in Computer Science*, pages 751361–68, 2012. URL <https://hal.inria.fr/hal-01551342>.
- [6] A Ghosh, N Mangalvedhe, R Ratasuk, B Mondal, M Cudak, E Visotsky, T A Thomas, J G Andrews, P Xia, H S Jo, H S Dhillon, and T D Novlan. Heterogeneous cellular networks: From theory to practice. *Communications Magazine, IEEE*, 50(6):54–64, 2012. doi: 10.1109/MCOM.2012.6211486.
- [7] Chung Shue Chen, Van Minh Nguyen, and Laurent Thomas. On Small Cell Network Deployment: A Comparative Study of Random and Grid Topologies. In *2012 IEEE Vehicular Technology Conference (VTC Fall)*, pages 1–5. IEEE, sep 2012. ISBN 978-1-4673-1881-5. doi: 10.1109/VTCFall.2012.6398953. URL <http://ieeexplore.ieee.org/document/6398953/>.
- [8] Muhammad Zeeshan Shakir, Khalid A. Qaraqe, Hina Tabassum, Mohamed-Slim Alouini, Erchin Serpedin, and Muhammad Ali Imran. Green heterogeneous small-cell networks: toward reducing the CO2 emissions of mobile communications industry using uplink power adaptation. *IEEE Communications Magazine*, 51(6):52–61, jun 2013. ISSN 0163-6804. doi: 10.1109/MCOM.2013.6525595. URL <http://ieeexplore.ieee.org/document/6525595/>.

- [9] Luis Carlos Goncalves, Pedro Sebastiao, Nuno Souto, and Americo Correia. Addressing cell edge performance by extending ANDSF and Inter-RAT UE steering. In *2014 11th International Symposium on Wireless Communications Systems (ISWCS)*, pages 465–469. IEEE, aug 2014. ISBN 978-1-4799-5863-4. doi: 10.1109/ISWCS.2014.6933398. URL <http://ieeexplore.ieee.org/document/6933398/>.
- [10] Ana Nika, Asad Ismail, Ben Y. Zhao, Sabrina Gaito, Gian Paolo Rossi, and Haitao Zheng. Understanding data hotspots in cellular networks. In *10th International Conference on Heterogeneous Networking for Quality, Reliability, Security and Robustness*, pages 70–76. IEEE, aug 2014. ISBN 978-1-6319-0025-9. doi: 10.1109/QSHINE.2014.6928662. URL <http://ieeexplore.ieee.org/document/6928662/>.
- [11] Aymen Jaziri, Ridha Nasri, and Tijani Chahed. Performance Analysis of Small Cells’ Deployment under Imperfect Traffic Hotspot Localization. In *2015 IEEE Global Communications Conference (GLOBECOM)*, pages 1–6. IEEE, dec 2015. ISBN 978-1-4799-5952-5. doi: 10.1109/GLOCOM.2015.7417356. URL <http://ieeexplore.ieee.org/document/7417356/>.
- [12] Han-Shin Jo, Young Jin Sang, Ping Xia, and Jeffrey G. Andrews. Heterogeneous Cellular Networks with Flexible Cell Association: A Comprehensive Downlink SINR Analysis. *IEEE Transactions on Wireless Communications*, 11(10):3484–3495, oct 2012. ISSN 1536-1276. doi: 10.1109/TWC.2012.081612.111361. URL <http://ieeexplore.ieee.org/document/6287527/>.
- [13] Yejun He, Man Chen, Baohong Ge, and Mohsen Guizani. On WiFi Offloading in Heterogeneous Networks: Various Incentives and Trade-off Strategies. *IEEE Communications Surveys & Tutorials*, pages 1–1, 2016. ISSN 1553-877X. doi: 10.1109/COMST.2016.2558191. URL <http://ieeexplore.ieee.org/document/7458774/>.
- [14] Nan E, Xiaoli Chu, and Jie Zhang. Mobile Small-Cell Deployment Strategy for Hot Spot in Existing Heterogeneous Networks. In *2015 IEEE Globecom Workshops (GC Wkshps)*, pages 1–6. IEEE, dec 2015. ISBN 978-1-4673-9526-7. doi: 10.1109/GLOCOMW.2015.7414060. URL <http://ieeexplore.ieee.org/document/7414060/>.
- [15] Reza Monir Vaghefi and R. Michael Buehrer. Asynchronous time-of-arrival-based source localization. In *2013 IEEE International Conference on Acoustics, Speech and Signal Processing*, pages 4086–4090. IEEE, may 2013. ISBN 978-1-4799-0356-6. doi: 10.1109/ICASSP.2013.6638427. URL <http://ieeexplore.ieee.org/document/6638427/>.
- [16] Alireza Ghelichi, Kumar Yelamarthi, and Ahmed Abdelgawad. Target localization in Wireless Sensor Network based on Time Difference of Arrival. In *2013 IEEE 56th International Midwest Symposium on Circuits and Systems (MWSCAS)*, pages 940–943. IEEE, aug 2013. ISBN 978-1-4799-0066-4. doi: 10.1109/MWSCAS.2013.6674805. URL <http://ieeexplore.ieee.org/document/6674805/>.
- [17] Siddharth Prakash Rao, Ian Oliver, Silke Holtmanns, and Tuomas Aura. We know where you are! In *2016 8th International Conference on Cyber Conflict (CyCon)*, pages 277–293. IEEE, may 2016. ISBN 978-9-9499-5449-0. doi: 10.1109/CYCON.2016.7529440. URL <http://ieeexplore.ieee.org/document/7529440/>.

- 
- [18] Thrivikrama, Vikas Ganjigunte Ashok, and A Srinivas. A novel two-stage self correcting GPS-free localization algorithm for GSM mobiles. In *2011 Fifth IEEE International Conference on Advanced Telecommunication Systems and Networks (ANTS)*, pages 1–6. IEEE, dec 2011. ISBN 978-1-4673-0094-0. doi: 10.1109/ANTS.2011.6163634. URL <http://ieeexplore.ieee.org/document/6163634/>.
- [19] Prima Kristalina, Aries Pratiarso, Tessy Badriyah, and Erik Dwi Putro. A wireless sensor networks localization using geometric triangulation scheme for object tracking in urban search and rescue application. In *2016 2nd International Conference on Science in Information Technology (ICSITech)*, pages 254–259. IEEE, oct 2016. ISBN 978-1-5090-1721-8. doi: 10.1109/ICSITech.2016.7852643. URL <http://ieeexplore.ieee.org/document/7852643/>.
- [20] Mahmoud H. Qutqut, Hatem Abou-zeid, Hossam S. Hassanein, A. M. Rashwan, and Fadi M. Al-Turjman. Dynamic small cell placement strategies for LTE Heterogeneous Networks. In *2014 IEEE Symposium on Computers and Communications (ISCC)*, pages 1–6. IEEE, jun 2014. ISBN 978-1-4799-4277-0. doi: 10.1109/ISCC.2014.6912536. URL <http://ieeexplore.ieee.org/document/6912536/>.
- [21] Techniques for increasing the capacity of wireless broadband networks: UK, 2012-2030 Annexes A1 -A6 Produced by Real Wireless on behalf of Ofcom. URL [www.realwireless.biz](http://www.realwireless.biz).
- [22] Yeonhee Pak, Kyungsik Min, and Sooyong Choi. Performance evaluation of various small-cell deployment scenarios in small-cell networks. In *The 18th IEEE International Symposium on Consumer Electronics (ISCE 2014)*, pages 1–2. IEEE, jun 2014. ISBN 978-1-4799-4592-4. doi: 10.1109/ISCE.2014.6884453. URL <http://ieeexplore.ieee.org/lpdocs/epic03/wrapper.htm?arnumber=6884453>.
- [23] John Hoadley and Payam Maveddat. Enabling small cell deployment with HetNet. *IEEE Wireless Communications*, 19(2):4–5, apr 2012. ISSN 1536-1284. doi: 10.1109/MWC.2012.6189405. URL <http://ieeexplore.ieee.org/document/6189405/>.
- [24] M.F. Iskander and Zhengqing Yun. Propagation prediction models for wireless communication systems. *IEEE Transactions on Microwave Theory and Techniques*, 50(3):662–673, mar 2002. ISSN 00189480. doi: 10.1109/22.989951. URL <http://ieeexplore.ieee.org/document/989951/>.
- [25] S R Surya and G Adiline Magrica. A survey on wireless networks attacks. In *2017 2nd International Conference on Computing and Communications Technologies (ICCCT)*, pages 240–247. IEEE, feb 2017. ISBN 978-1-5090-6221-8. doi: 10.1109/ICCCT2.2017.7972278. URL <http://ieeexplore.ieee.org/document/7972278/>.
- [26] Understanding Small-Cell Wireless Backhaul. URL <http://www.electronicdesign.com/communications/understanding-small-cell-wireless-backhaul>.
- [27] H.N.B. Meriem and S. Tabbane. Simulations of frequency hopping schemes with power control in a GSM network. In *VTC2000-Spring. 2000 IEEE 51st Vehicular Technology Conference Proceedings (Cat. No.00CH37026)*, volume 3, pages 2380–2383. IEEE, 2000. ISBN 0-7803-5718-3. doi: 10.1109/VETECS.2000.851698. URL <http://ieeexplore.ieee.org/document/851698/>.

- [28] Lajos Hanzo, Mohammed El-Hajjar, and Osamah Alamri. Near-Capacity Wireless Transceivers and Cooperative Communications in the MIMO Era: Evolution of Standards, Waveform Design, and Future Perspectives. *Proceedings of the IEEE*, 99(8): 1343–1385, aug 2011. ISSN 0018-9219. doi: 10.1109/JPROC.2011.2148150. URL <http://ieeexplore.ieee.org/document/5893900/>.
- [29] Xueyi Liang, Hailin Liu, and Qiang Wang. 4G Heterogeneous Networks Base Station Planning Using Evolutionary Multi-objective Algorithm. In *2015 11th International Conference on Computational Intelligence and Security (CIS)*, pages 248–252. IEEE, dec 2015. ISBN 978-1-4673-8660-9. doi: 10.1109/CIS.2015.68. URL <http://ieeexplore.ieee.org/document/7396298/>.
- [30] Takehiro Nakamura, Satoshi Nagata, Anass Benjebbour, Yoshihisa Kishiyama, Tang Hai, Shen Xiaodong, Yang Ning, and Li Nan. Trends in small cell enhancements in LTE advanced. *IEEE Communications Magazine*, 51(2):98–105, feb 2013. ISSN 0163-6804. doi: 10.1109/MCOM.2013.6461192. URL <http://ieeexplore.ieee.org/document/6461192/>.
- [31] Hung-Yun Hsieh, Shih-En Wei, and Cheng-Pang Chien. Optimizing Small Cell Deployment in Arbitrary Wireless Networks with Minimum Service Rate Constraints. *IEEE Transactions on Mobile Computing*, 13(8):1801–1815, aug 2014. ISSN 1536-1233. doi: 10.1109/TMC.2013.135. URL <http://ieeexplore.ieee.org/document/6636292/>.
- [32] Aliye Ozge Kaya and Doru Calin. On the Wireless Channel Characteristics of Outdoor-to-Indoor LTE Small Cells. *IEEE Transactions on Wireless Communications*, 15(8): 5453–5466, aug 2016. ISSN 1536-1276. doi: 10.1109/TWC.2016.2558559. URL <http://ieeexplore.ieee.org/document/7468566/>.
- [33] David Lopez-Perez, Ming Ding, Holger Claussen, and Amir H. Jafari. Towards 1 Gbps/UE in Cellular Systems: Understanding Ultra-Dense Small Cell Deployments. *IEEE Communications Surveys & Tutorials*, 17(4):2078–2101, 2015. ISSN 1553-877X. doi: 10.1109/COMST.2015.2439636. URL <http://ieeexplore.ieee.org/document/7126919/>.
- [34] W.K. Lai and G.C. Coghill. Channel assignment for a homogeneous cellular network with genetic algorithms. In *Proceedings of ANZIS '94 - Australian New Zealand Intelligent Information Systems Conference*, pages 263–267. IEEE. ISBN 0-7803-2404-8. doi: 10.1109/ANZIS.1994.396970. URL <http://ieeexplore.ieee.org/document/396970/>.
- [35] Yingjie You, Kenneth L. Ford, Jonathan M. Rigelsford, and Timothy O'Farrell. Analysis of the use of beam reconfigurable antennas in a homogeneous cellular network deployment. In *2014 Loughborough Antennas and Propagation Conference (LAPC)*, pages 169–172. IEEE, nov 2014. ISBN 978-1-4799-3662-5. doi: 10.1109/LAPC.2014.6996348. URL <http://ieeexplore.ieee.org/document/6996348/>.
- [36] Ralf Bendlin, Vikram Chandrasekhar, Runhua Chen, Anthony Ekpenyong, and Eko Onggosanusi. From homogeneous to heterogeneous networks: A 3GPP Long Term Evolution rel. 8/9 case study. In *2011 45th Annual Conference on Information Sciences and Systems*, pages 1–5. IEEE, mar 2011. ISBN 978-1-4244-9846-8. doi: 10.1109/CISS.2011.5766247. URL <http://ieeexplore.ieee.org/document/5766247/>.

- 
- [37] Weisi Guo, Siyi Wang, Xiaoli Chu, Jie Zhang, Jiming Chen, and Hui Song. Automated small-cell deployment for heterogeneous cellular networks. *IEEE Communications Magazine*, 51(5):46–53, may 2013. ISSN 0163-6804. doi: 10.1109/MCOM.2013.6515046. URL <http://ieeexplore.ieee.org/document/6515046/>.
- [38] Qi Zeng, Hayan Nasser, and Gabriele Gradoni. A Secure Waveform Format for Interference Mitigation in Heterogeneous Uplink Networks. *IEEE Access*, 6:41688–41696, 2018. ISSN 2169-3536. doi: 10.1109/ACCESS.2018.2858840. URL <https://ieeexplore.ieee.org/document/8418367/>.
- [39] Trung VU Kien and Sungoh Kwon. Cooperative Interference Mitigation Algorithm in Heterogeneous Networks \*. (11), 2015. doi: 10.1587/transcom.E98.B.2238. URL <http://jultika.oulu.fi/files/nbnfi-fe201802153430.pdf>.
- [40] B. Pasquereau and Y. Le Helloco. Predicting cellular network performances with cell-level monte-carlo simulations. In *VTC-2005-Fall. 2005 IEEE 62nd Vehicular Technology Conference, 2005.*, volume 1, pages 387–391. IEEE. ISBN 0-7803-9152-7. doi: 10.1109/VETECF.2005.1557938. URL <http://ieeexplore.ieee.org/document/1557938/>.
- [41] Hesham ElSawy, Ahmed Sultan-Salem, Mohamed-Slim Alouini, and Moe Z. Win. Modeling and Analysis of Cellular Networks Using Stochastic Geometry: A Tutorial. *IEEE Communications Surveys & Tutorials*, 19(1):167–203, 2017. ISSN 1553-877X. doi: 10.1109/COMST.2016.2624939. URL <http://ieeexplore.ieee.org/document/7733098/>.
- [42] Weisi Guo and T. O’Farrell. Relay Deployment in Cellular Networks: Planning and Optimization. *IEEE Journal on Selected Areas in Communications*, 31(8):1597–1606, aug 2013. ISSN 0733-8716. doi: 10.1109/JSAC.2013.130821. URL <http://ieeexplore.ieee.org/document/6330085/>.
- [43] Weisi Guo and Siyi Wang. Interference-Aware Self-Deploying Femto-Cell. *IEEE Wireless Communications Letters*, 1(6):609–612, dec 2012. ISSN 2162-2337. doi: 10.1109/WCL.2012.091312.120576. URL <http://ieeexplore.ieee.org/document/6308771/>.
- [44] Hakim Ghazzai, Elias Yaacoub, Mohamed-Slim Alouini, Zaher Dawy, and Adnan Abu-Dayya. Optimized LTE Cell Planning With Varying Spatial and Temporal User Densities. *IEEE Transactions on Vehicular Technology*, 65(3):1575–1589, mar 2016. ISSN 0018-9545. doi: 10.1109/TVT.2015.2411579. URL <http://ieeexplore.ieee.org/document/7056465/>.
- [45] Yen-Wen Chen and Wang-Hsin Lu. Small cells placement scheme in metropolitan area environment. In *2016 18th Asia-Pacific Network Operations and Management Symposium (APNOMS)*, pages 1–6. IEEE, oct 2016. ISBN 978-4-88552-304-5. doi: 10.1109/APNOMS.2016.7737193. URL <http://ieeexplore.ieee.org/document/7737193/>.
- [46] Hamit Taylan Yuce, Edward Mutafungwa, and Jyri Hamalainen. A Planning and Optimization Framework for Hybrid Ultra-Dense Network Topologies. In *2018 22nd Conference of Open Innovations Association (FRUCT)*, pages 280–289. IEEE, may 2018. ISBN 978-952-68653-4-8. doi: 10.23919/FRUCT.2018.8468304. URL <https://ieeexplore.ieee.org/document/8468304/>.

- [47] Chouchang Yang and Huai-rong Shao. WiFi-based indoor positioning. *IEEE Communications Magazine*, 53(3):150–157, mar 2015. ISSN 0163-6804. doi: 10.1109/MCOM.2015.7060497. URL <http://ieeexplore.ieee.org/document/7060497/>.
- [48] Nasim Alikhani, Shima Amiranloo, Vahideh Moghtadaiee, and Seyed Ali Ghorashi. Fast fingerprinting based indoor localization by Wi-Fi signals. In *2017 7th International Conference on Computer and Knowledge Engineering (ICCKE)*, pages 241–246. IEEE, oct 2017. ISBN 978-1-5386-0804-3. doi: 10.1109/ICCKE.2017.8167884. URL <http://ieeexplore.ieee.org/document/8167884/>.
- [49] Ahmed H. Salamah, Mohamed Tamazin, Maha A. Sharkas, and Mohamed Khedr. An enhanced WiFi indoor localization system based on machine learning. In *2016 International Conference on Indoor Positioning and Indoor Navigation (IPIN)*, pages 1–8. IEEE, oct 2016. ISBN 978-1-5090-2425-4. doi: 10.1109/IPIN.2016.7743586. URL <http://ieeexplore.ieee.org/document/7743586/>.
- [50] Weixing Xue, Weining Qiu, Xianghong Hua, and Kegen Yu. Improved Wi-Fi RSSI Measurement for Indoor Localization. *IEEE Sensors Journal*, 17(7):2224–2230, apr 2017. ISSN 1530-437X. doi: 10.1109/JSEN.2017.2660522. URL <http://ieeexplore.ieee.org/document/7835628/>.
- [51] Chen-Shu Wang and Li-Fang Kao. The Optimal Deployment of Wi-Fi Wireless Access Points Using the Genetic Algorithm. In *2012 Sixth International Conference on Genetic and Evolutionary Computing*, pages 542–545. IEEE, aug 2012. ISBN 978-1-4673-2138-9. doi: 10.1109/ICGEC.2012.142. URL <http://ieeexplore.ieee.org/document/6456841/>.
- [52] Intel. Different Wi-Fi Protocols and Data Rates. URL <https://www.intel.co.uk/content/www/uk/en/support/articles/000005725/network-and-i-o/wireless-networking.html>.
- [53] Perminder Dhawan, Amit Mukhopadhyay, and Carlos Urrutia-Valdes. Macro and small cell/Wi-Fi networks: An analysis of deployment options as the solution for the mobile data explosion. *Bell Labs Technical Journal*, 18(1):59–79, jun 2013. ISSN 1538-7305. doi: 10.1002/bltj.21593. URL <http://ieeexplore.ieee.org/lpdocs/epic03/wrapper.htm?arnumber=6771073>.
- [54] Ferran Adelantado, Xavier Vilajosana, Pere Tuset-Peiro, Borja Martinez, Joan Melia-Segui, and Thomas Watteyne. Understanding the Limits of LoRaWAN. *IEEE Communications Magazine*, 55(9):34–40, 2017. ISSN 0163-6804. doi: 10.1109/MCOM.2017.1600613. URL <http://ieeexplore.ieee.org/document/8030482/>.
- [55] Ibrar Yaqoob, Ejaz Ahmed, Ibrahim Abaker Targio Hashem, Abdelmuttlib Ibrahim Abdalla Ahmed, Abdullah Gani, Muhammad Imran, and Mohsen Guizani. Internet of Things Architecture: Recent Advances, Taxonomy, Requirements, and Open Challenges. *IEEE Wireless Communications*, 24(3):10–16, jun 2017. ISSN 1536-1284. doi: 10.1109/MWC.2017.1600421. URL <http://ieeexplore.ieee.org/document/7955906/>.
- [56] P. McDermott-Wells. What is Bluetooth? *IEEE Potentials*, 23(5):33–35, jan 2005. ISSN 0278-6648. doi: 10.1109/MP.2005.1368913. URL <http://ieeexplore.ieee.org/document/1368913/>.

- 
- [57] Mohammed Abdulaziz Ikram, Mohammad Dahman Alshehri, and Farookh Khadeer Hussain. Architecture of an IoT-based system for football supervision (IoT Football). In *2015 IEEE 2nd World Forum on Internet of Things (WF-IoT)*, pages 69–74. IEEE, dec 2015. ISBN 978-1-5090-0366-2. doi: 10.1109/WF-IoT.2015.7389029. URL <http://ieeexplore.ieee.org/document/7389029/>.
- [58] Abrar Alkhamisi, Mohamed Saleem Haja Nazmudeen, and Seyed M. Buhari. A cross-layer framework for sensor data aggregation for IoT applications in smart cities. In *2016 IEEE International Smart Cities Conference (ISC2)*, pages 1–6, Alkhamisi2016, sep 2016. IEEE. ISBN 978-1-5090-1846-8. doi: 10.1109/ISC2.2016.7580853. URL <http://ieeexplore.ieee.org/document/7580853/>.
- [59] Hiroshi Tokito, Masahiro Sasabe, and Hirotaka Nakano. Improvement of the capacity of wireless networks by optimizing communication distance. In *2007 9th IFIP International Conference on Mobile Wireless Communications Networks*, pages 11–15. IEEE, sep 2007. ISBN 978-1-4244-1719-3. doi: 10.1109/ICMWCN.2007.4668171. URL <http://ieeexplore.ieee.org/document/4668171/>.
- [60] Junfeng Xiao, Rose Hu, Yi Qian, Lei Gong, and Bo Wang. Expanding LTE network spectrum with cognitive radios: From concept to implementation. *IEEE Wireless Communications*, 20(2):12–19, apr 2013. ISSN 1536-1284. doi: 10.1109/MWC.2013.6507389. URL <http://ieeexplore.ieee.org/document/6507389/>.
- [61] Paraskevi Petropoulou, Emmanouel T. Michailidis, Athanasios D. Panagopoulos, and Athanasios G. Kanatas. Radio Propagation Channel Measurements for Multi-Antenna Satellite Communication Systems: A Survey. *IEEE Antennas and Propagation Magazine*, 56(6):102–122, dec 2014. ISSN 1045-9243. doi: 10.1109/MAP.2014.7011023. URL <http://ieeexplore.ieee.org/document/7011023/>.
- [62] Lianfeng Zou, Shulabh Gupta, and Christophe Caloz. Dispersion code modulation for enhanced spectral efficiency in wireless communications. In *2016 IEEE International Symposium on Antennas and Propagation (APSURSI)*, pages 1851–1852. IEEE, jun 2016. ISBN 978-1-5090-2886-3. doi: 10.1109/APS.2016.7696632. URL <http://ieeexplore.ieee.org/document/7696632/>.
- [63] Vu Nguyen Ha, Long Bao Le, and Ngoc-Dung Dao. Coordinated Multipoint Transmission Design for Cloud-RANs With Limited Fronthaul Capacity Constraints. *IEEE Transactions on Vehicular Technology*, 65(9):7432–7447, sep 2016. ISSN 0018-9545. doi: 10.1109/TVT.2015.2485668. URL <http://ieeexplore.ieee.org/document/7287780/>.
- [64] Mohammed Abduljawad M. Al-Shibly, Mohamed Hadi Habaebi, and Jalel Chebil. Carrier aggregation in Long Term Evolution-Advanced. In *2012 IEEE Control and System Graduate Research Colloquium*, pages 154–159. IEEE, jul 2012. ISBN 978-1-4673-2036-8. doi: 10.1109/ICSGRC.2012.6287153. URL <http://ieeexplore.ieee.org/document/6287153/>.
- [65] Xavier Gelabert, Peter Legg, and Christer Qvarfordt. Small Cell densification requirements in high capacity future cellular networks. In *2013 IEEE International Conference on Communications Workshops (ICC)*, pages 1112–1116. IEEE, jun 2013. ISBN 978-1-4673-5753-1. doi: 10.1109/ICCW.2013.6649403. URL <http://ieeexplore.ieee.org/document/6649403/>.

- [66] Xiaohu Ge, Song Tu, Guoqiang Mao, Cheng-Xiang Wang, and Tao Han. 5G Ultra-Dense Cellular Networks. *IEEE Wireless Communications*, 23(1):72–79, feb 2016. ISSN 1536-1284. doi: 10.1109/MWC.2016.7422408. URL <http://ieeexplore.ieee.org/document/7422408/>.
- [67] Abdelrahman Arbi and Timothy O’Farrell. Energy efficiency in 5G access networks: Small cell densification and high order sectorisation. In *2015 IEEE International Conference on Communication Workshop (ICCW)*, pages 2806–2811. IEEE, jun 2015. ISBN 978-1-4673-6305-1. doi: 10.1109/ICCW.2015.7247604. URL <http://ieeexplore.ieee.org/document/7247604/>.
- [68] Bashar Romanous, Naim Bitar, Ali Imran, and Hazem Refai. Network densification: Challenges and opportunities in enabling 5G. In *2015 IEEE 20th International Workshop on Computer Aided Modelling and Design of Communication Links and Networks (CAMAD)*, pages 129–134. IEEE, sep 2015. ISBN 978-1-4673-8186-4. doi: 10.1109/CAMAD.2015.7390494. URL <http://ieeexplore.ieee.org/document/7390494/>.
- [69] A.H. Zahran, Ben Liang, and A. Saleh. Mobility Modeling and Performance Evaluation of Heterogeneous Wireless Networks. *IEEE Transactions on Mobile Computing*, 7(8):1041–1056, aug 2008. ISSN 1536-1233. doi: 10.1109/TMC.2007.70776. URL <http://ieeexplore.ieee.org/document/4378382/>.
- [70] Min-Sung Kim, Hui Won Je, and Fouad A. Tobagi. Cross-Tier Interference Mitigation for Two-Tier OFDMA Femtocell Networks with Limited Macrocell Information. In *2010 IEEE Global Telecommunications Conference GLOBECOM 2010*, pages 1–5. IEEE, dec 2010. ISBN 978-1-4244-5636-9. doi: 10.1109/GLOCOM.2010.5683791. URL <http://ieeexplore.ieee.org/document/5683791/>.
- [71] Yuqi Liu, Xianrong Wan, Hui Tang, Jianxin Yi, Yiyao Cheng, and Xun Zhang. Digital television based passive bistatic radar system for drone detection. In *2017 IEEE Radar Conference (RadarConf)*, pages 1493–1497. IEEE, may 2017. ISBN 978-1-4673-8823-8. doi: 10.1109/RADAR.2017.7944443. URL <http://ieeexplore.ieee.org/document/7944443/>.
- [72] Van Minh Nguyen and Marios Kountouris. Performance Limits of Network Densification. *IEEE Journal on Selected Areas in Communications*, 35(6):1294–1308, jun 2017. ISSN 0733-8716. doi: 10.1109/JSAC.2017.2687638. URL <http://ieeexplore.ieee.org/document/7886368/>.
- [73] Nikola Petrovic and Dusan Savkovic. LTE performance in a hybrid indoor DAS (Active vs. Passive). In *2015 23rd Telecommunications Forum Telfor (TELFOR)*, pages 141–144. IEEE, nov 2015. ISBN 978-1-5090-0055-5. doi: 10.1109/TELFOR.2015.7377434. URL <http://ieeexplore.ieee.org/document/7377434/>.
- [74] Gongchao Su, Lemin Li, Xiaohui Lin, and Hui Wang. On the optimal small cell deployment for energy-efficient heterogeneous cellular networks. In *2014 Sixth International Conference on Ubiquitous and Future Networks (ICUFN)*, pages 172–175. IEEE, jul 2014. ISBN 978-1-4799-3494-2. doi: 10.1109/ICUFN.2014.6876775. URL <http://ieeexplore.ieee.org/lpdocs/epic03/wrapper.htm?arnumber=6876775>.

- 
- [75] Yosub Park, Jihaeng Heo, Hyunsoo Kim, Hano Wang, Sooyong Choi, Takki Yu, and Daesik Hong. Effective Small Cell Deployment with Interference and Traffic Consideration. In *2014 IEEE 80th Vehicular Technology Conference (VTC2014-Fall)*, pages 1–5. IEEE, sep 2014. ISBN 978-1-4799-4449-1. doi: 10.1109/VTCFall.2014.6965951. URL <http://ieeexplore.ieee.org/lpdocs/epic03/wrapper.htm?arnumber=6965951>.
- [76] Israfil Bahceci. On femto-cell deployment strategies for randomly distributed hotspots in cellular networks. In *2014 IEEE Wireless Communications and Networking Conference (WCNC)*, pages 2330–2335. IEEE, apr 2014. ISBN 978-1-4799-3083-8. doi: 10.1109/WCNC.2014.6952713. URL <http://ieeexplore.ieee.org/document/6952713/>.
- [77] Sara Landstrom, Hideshi Murai, and Arne Simonsson. Deployment Aspects of LTE Pico Nodes. In *2011 IEEE International Conference on Communications Workshops (ICC)*, pages 1–5. IEEE, jun 2011. ISBN 978-1-61284-954-6. doi: 10.1109/iccw.2011.5963602. URL <http://ieeexplore.ieee.org/document/5963602/>.
- [78] Version Control Item Description Source Real Wireless Client Ofcom Report title Techniques for increasing the capacity of wireless broadband networks: UK, 2012-2030 Sub title Produced by Real Wireless on behalf of Ofcom Issue date. 2012. URL <http://static.ofcom.org.uk/static/uhf/real-wireless-report.pdf>.
- [79] D.L. Sengupta and T.K. Sarkar. Maxwell, Hertz, the Maxwellians and the early history of electromagnetic waves. In *IEEE Antennas and Propagation Society International Symposium. 2001 Digest. Held in conjunction with: USNC/URSI National Radio Science Meeting (Cat. No.01CH37229)*, volume 1, pages 14–17. IEEE. ISBN 0-7803-7070-8. doi: 10.1109/APS.2001.958782. URL <http://ieeexplore.ieee.org/document/958782/>.
- [80] D.J. Cichon. The Heinrich Hertz wireless experiments at Karlsruhe in the view of modern communication. In *International Conference on 100 Years of Radio*, volume 1995, pages 1–6. IEE, 1995. ISBN 0 85296 649 0. doi: 10.1049/cp:19950782. URL <http://digital-library.theiet.org/content/conferences/10.1049/cp{ }19950782>.
- [81] Hugh Griffiths. Early history of bistatic radar. In *European Radar Conference (EuRAD), 2016 13th*, 2016. ISBN 9782874870453. URL <https://ieeexplore.ieee.org/document/7811695>.
- [82] Hongwei Liu, Huikai Zang, Shenghua Zhou, and Yunhe Cao. Monostatic radar range–Doppler sidelobe suppression using nearly orthogonal waveforms. *IET Radar, Sonar & Navigation*, 10(9):1650–1659, dec 2016. ISSN 1751-8784. doi: 10.1049/iet-rsn.2015.0636. URL <http://digital-library.theiet.org/content/journals/10.1049/iet-rsn.2015.0636>.
- [83] Jeong Woo Choi and Sung Ho Cho. 3D positioning algorithm based on multiple quasi-monostatic IR-UWB radar sensors. In *2017 IEEE Radar Conference (RadarConf)*, pages 1531–1535. IEEE, may 2017. ISBN 978-1-4673-8823-8. doi: 10.1109/RADAR.2017.7944450. URL <http://ieeexplore.ieee.org/document/7944450/>.
- [84] Changzhi Li, Zhengyu Peng, Tien-Yu Huang, Tenglong Fan, Fu-Kang Wang, Tzyy-Sheng Horng, Jose-Maria Munoz-Ferreras, Roberto Gomez-Garcia, Lixin Ran, and

- Jenshan Lin. A Review on Recent Progress of Portable Short-Range Noncontact Microwave Radar Systems. *IEEE Transactions on Microwave Theory and Techniques*, 65(5):1692–1706, may 2017. ISSN 0018-9480. doi: 10.1109/TMTT.2017.2650911. URL <http://ieeexplore.ieee.org/document/7836309/>.
- [85] David Middleton. Statistical theory of signal detection. *Transactions of the IRE Professional Group on Information Theory*, 3(3):26–51, mar 1954. ISSN 2168-2690. doi: 10.1109/IREPGIT.1954.6373398. URL <http://ieeexplore.ieee.org/document/6373398/>.
- [86] E. J. Kelly and R. P. Wishner. Matched-Filter Theory for High-Velocity, Accelerating Targets. *IEEE Transactions on Military Electronics*, 9(1):56–69, 1965. ISSN 0536-1559. doi: 10.1109/TME.1965.4323176. URL <http://ieeexplore.ieee.org/document/4323176/>.
- [87] Dylan Eustice, Charles Baylis, and Robert J. Marks. Woodward’s ambiguity function: From foundations to applications. In *2015 Texas Symposium on Wireless and Microwave Circuits and Systems (WMCs)*, pages 1–17. IEEE, apr 2015. ISBN 978-1-4673-8069-0. doi: 10.1109/WMCaS.2015.7233208. URL <http://ieeexplore.ieee.org/document/7233208/>.
- [88] Long Pang, Feng-bo Mao, Yi-zhuang Xie, and He Chen. A high performance digital signal processor for monopulse tracking radar. In *2016 IEEE 13th International Conference on Signal Processing (ICSP)*, pages 1485–1488. IEEE, nov 2016. ISBN 978-1-5090-1344-9. doi: 10.1109/ICSP.2016.7878073. URL <http://ieeexplore.ieee.org/document/7878073/>.
- [89] Sandra Nowok, Simon Kueppers, Harun Cetinkaya, Martin Schroeder, and Reinhold Herschel. Millimeter wave radar for high resolution 3D near field imaging for robotics and security scans. In *2017 18th International Radar Symposium (IRS)*, pages 1–10. IEEE, jun 2017. ISBN 978-3-7369-9343-3. doi: 10.23919/IRS.2017.8008132. URL <http://ieeexplore.ieee.org/document/8008132/>.
- [90] PCWorld. A brief history of GPS | PCWorld. URL <https://www.pcworld.com/article/2000276/a-brief-history-of-gps.html>.
- [91] S. N. Parmar, S. Nainan, K. Bakade, and D. Sen. An efficient mobile GPS navigator, tracker and altimeter system for location based services. In *2013 International Conference on Advances in Technology and Engineering (ICATE)*, pages 1–4. IEEE, jan 2013. ISBN 978-1-4673-5619-0. doi: 10.1109/ICAdTE.2013.6524760. URL <http://ieeexplore.ieee.org/document/6524760/>.
- [92] Deepak Punetha and Vartika Mehta. Protection of the child/ elderly/ disabled/ pet by smart and intelligent GSM and GPS based automatic tracking and alert system. In *2014 International Conference on Advances in Computing, Communications and Informatics (ICACCI)*, pages 2349–2354. IEEE, sep 2014. ISBN 978-1-4799-3080-7. doi: 10.1109/ICACCI.2014.6968490. URL <http://ieeexplore.ieee.org/lpdocs/epic03/wrapper.htm?arnumber=6968490>.
- [93] H.A. Karimi and J.T. Lockhart. GPS-based tracking systems for taxi cab fleet operations. In *Proceedings of VNIS '93 - Vehicle Navigation and Information Systems*

- 
- Conference*, pages 679–682. IEEE. ISBN 0-7803-1235-X. doi: 10.1109/VNIS.1993.585719. URL <http://ieeexplore.ieee.org/document/585719/>.
- [94] Pattarakamon Rangsee, Paweena Suebsombat, and Phakphoom Boonyanant. Simplified low-cost GPS-based tracking system for soccer practice. In *2013 13th International Symposium on Communications and Information Technologies (ISCIT)*, pages 724–728. IEEE, sep 2013. ISBN 978-1-4673-5580-3. doi: 10.1109/ISCIT.2013.6645948. URL <http://ieeexplore.ieee.org/document/6645948/>.
- [95] Bharath Patil, Radhika Patil, and Andre Pittet. Energy saving techniques for GPS based tracking applications. In *2011 Integrated Communications, Navigation, and Surveillance Conference Proceedings*, pages J8–1–J8–10. IEEE, may 2011. ISBN 978-1-4577-0593-9. doi: 10.1109/ICNSURV.2011.5935335. URL <http://ieeexplore.ieee.org/document/5935335/>.
- [96] C. Hackman, S. M. Byram, V. J. Slabinski, and J. C. Tracey. USNO GPS/GLONASS PNT products: Overview, and GPS&#x002B;GLONASS vs GLONASS only PPP accuracy. In *2014 IEEE/ION Position, Location and Navigation Symposium - PLANS 2014*, pages 793–803. IEEE, may 2014. ISBN 978-1-4799-3320-4. doi: 10.1109/PLANS.2014.6851444. URL <http://ieeexplore.ieee.org/document/6851444/>.
- [97] J.M. Zagami, S.A. Parl, J.J. Bussgang, and K.D. Melillo. Providing universal location services using a wireless E911 location network. *IEEE Communications Magazine*, 36 (4):66–71, apr 1998. ISSN 01636804. doi: 10.1109/35.667415. URL <http://ieeexplore.ieee.org/document/667415/>.
- [98] Sun Ok Park, Mi-Young Huh, Wook Hyun, Jae Cheon Han, and Shin Gak Kang. SIP based VoIP System for E911 Service. In *COIN-NGNCON 2006 - The Joint International Conference on Optical Internet and Next Generation Network*, pages 97–99. IEEE, jul 2006. ISBN 978-89-955301-4-6. doi: 10.1109/COINNGNCON.2006.4454576. URL <http://ieeexplore.ieee.org/document/4454576/>.
- [99] Nico Deblauwe and Peter Ruppel. Combining GPS and GSM Cell-ID positioning for Proactive Location-based Services. In *2007 Fourth Annual International Conference on Mobile and Ubiquitous Systems: Networking & Services (MobiQuitous)*, pages 1–7. IEEE, 2007. ISBN 978-1-4244-1024-8. doi: 10.1109/MOBIQ.2007.4450985. URL <http://ieeexplore.ieee.org/document/4450985/>.
- [100] M. Boussedjra, J. Mouzna, P. Bangera, and M.M. Manohara Pai. Map-Based Location Service for VANET. In *2009 International Conference on Ultra Modern Telecommunications & Workshops*, pages 1–6. IEEE, oct 2009. ISBN 978-1-4244-3942-3. doi: 10.1109/ICUMT.2009.5345470. URL <http://ieeexplore.ieee.org/document/5345470/>.
- [101] D M Ashok, M. M. Manohara Pai, and Joseph Mouzna. Efficient map based location service for VANETs. In *2011 11th International Conference on ITS Telecommunications*, pages 387–392. IEEE, aug 2011. ISBN 978-1-61284-668-2. doi: 10.1109/ITST.2011.6060087. URL <http://ieeexplore.ieee.org/document/6060087/>.
- [102] J. Hightower, B. Brumitt, and G. Borriello. The location stack: a layered model for location in ubiquitous computing. In *Proceedings Fourth IEEE Workshop on Mobile Computing Systems and Applications*, pages 22–28. IEEE Comput. Soc, 2002. ISBN

- 0-7695-1647-5. doi: 10.1109/MCSA.2002.1017482. URL <http://ieeexplore.ieee.org/document/1017482/>.
- [103] Hemat Kumar Maheshwari. *Optimizing Range Aware Localization in Wireless Sensor Networks ( WSNs )*. PhD thesis, 2011.
- [104] Z Tao, P Bonnifait, V Fremont, and J Ibanez-Guzman. Mapping and localization using GPS, lane markings and proprioceptive sensors. In *Intelligent Robots and Systems (IROS), 2013 IEEE/RSJ International Conference on*, pages 406–412, 2013. ISBN 2153-0858. doi: 10.1109/IROS.2013.6696383.
- [105] V R Jain, R Bagree, A Kumar, and P Ranjan. wildCENSE: GPS based animal tracking system. In *Intelligent Sensors, Sensor Networks and Information Processing, 2008. ISSNIP 2008. International Conference on*, pages 617–622, 2008. doi: 10.1109/ISSNIP.2008.4762058.
- [106] C Heywood, C Connor, D Browning, M C Smith, and B Wang. GPS tracking of intermodal transportation: System integration with delivery order system. In *Systems and Information Engineering Design Symposium, 2009. SIEDS '09.*, pages 191–196, 2009. doi: 10.1109/SIEDS.2009.5166179.
- [107] P Adesso, L Bruno, and R Restaino. Adaptive localization techniques in WiFi environments. In *Wireless Pervasive Computing (ISWPC), 2010 5th IEEE International Symposium on*, pages 289–294, 2010. doi: 10.1109/ISWPC.2010.5483731.
- [108] Cheng Bo, Du Rong, Yang Bo, Yu Wenbin, Chen Cailian, and Guan Xinping. An Accurate GPS-Based Localization in Wireless Sensor Networks: A GM-WLS Method. In *Parallel Processing Workshops (ICPPW), 2011 40th International Conference on*, pages 33–41, 2011. ISBN 1530-2016. doi: 10.1109/ICPPW.2011.32.
- [109] Ssu Kuo-Feng, Ou Chia-Ho, and H C Jiau. Localization with mobile anchor points in wireless sensor networks. *Vehicular Technology, IEEE Transactions on*, 54(3): 1187–1197, 2005. doi: 10.1109/TVT.2005.844642.
- [110] Ruifeng Chen, Zhangdui Zhong, and Minming Ni. Cluster Based Iterative GPS-Free Localization for Wireless Sensor Networks. In *2011 IEEE 73rd Vehicular Technology Conference (VTC Spring)*, pages 1–5. IEEE, may 2011. ISBN 978-1-4244-8332-7. doi: 10.1109/VETECS.2011.5956536. URL <http://ieeexplore.ieee.org/document/5956536/>.
- [111] Zhang Dengyi, Liu Feng, Wang Lei, and Xing Yuanxiu. DV-Hop localization algorithms based on centroid in wireless sensor networks. In *Consumer Electronics, Communications and Networks (CECNet), 2012 2nd International Conference on*, pages 3216–3219, 2012. doi: 10.1109/CECNet.2012.6201891.
- [112] Yingjie Zhang, Kai Wang, Shenfang Yuan, Hao Yang, Zongxiang Chen, and LuSheng Ge. Research of WSN Node localization algorithm based on Weighted DV-HOP. In *Control and Decision Conference (CCDC), 2012 24th Chinese*, pages 3826–3829, 2012. doi: 10.1109/CCDC.2012.6244614.

- 
- [113] Li Shanliang, Huang Liusheng, Wu Junmin, Xu Hongli, and Wang Jichun. NBLs: Neighbor-information-based localization system for wireless sensor networks. In *Communication Systems Software and Middleware and Workshops, 2008. COMSWARE 2008. 3rd International Conference on*, pages 91–94, 2008. doi: 10.1109/COMSWA.2008.4554385.
- [114] K Kaemarungsi. Efficient design of indoor positioning systems based on location fingerprinting. In *Wireless Networks, Communications and Mobile Computing, 2005 International Conference on*, volume 1, pages 181–186 vol.1, 2005. doi: 10.1109/WIRLES.2005.1549406.
- [115] Jiang Jinfang, Han Guangjie, Xu Huihui, Shu Lei, and M Guizani. LMAT: Localization with a Mobile Anchor Node Based on Trilateration in Wireless Sensor Networks. In *Global Telecommunications Conference (GLOBECOM 2011), 2011 IEEE*, pages 1–6, 2011. ISBN 1930-529X. doi: 10.1109/GLOCOM.2011.6133668.
- [116] Jianguo Wang, Zhongsheng Wang, Ling Zhang, Fei Shi, and Guohua Song. A New Anchor-Based Localization Algorithm for Wireless Sensor Network. In *Distributed Computing and Applications to Business, Engineering and Science (DCABES), 2011 Tenth International Symposium on*, pages 239–243, 2011. doi: 10.1109/DCABES.2011.5.
- [117] K Kucuk, A Kavak, H Yigit, and C Ozdemir. A novel localization technique for wireless sensor networks using adaptive antenna arrays. In *Radio and Wireless Symposium, 2008 IEEE*, pages 483–486, 2008. doi: 10.1109/RWS.2008.4463534.
- [118] G Karthiga, C Preethi, and R D H Devi. Localization in wireless sensor network based on mobile anchor and chord selection. In *Communication and Network Technologies (ICCNT), 2014 International Conference on*, pages 124–128, 2014. doi: 10.1109/CNT.2014.7062738.
- [119] D Arbula. Distributed algorithm for anchor-free network localization using angle of arrival. In *Industrial Electronics, 2008. ISIE 2008. IEEE International Symposium on*, pages 792–797, 2008. doi: 10.1109/ISIE.2008.4677294.
- [120] Tao Du, Shouning Qu, Qingbei Guo, and Lianjiang Zhu. A simple efficient anchor-free node localization algorithm for wireless sensor networks. *International Journal of Distributed Sensor Networks*, 13(4):155014771770578, apr 2017. ISSN 1550-1477. doi: 10.1177/1550147717705784. URL <http://journals.sagepub.com/doi/10.1177/1550147717705784>.
- [121] K.Y.K. Leung, T.D. Barfoot, and H. Liu. Decentralized Localization of Sparsely-Communicating Robot Networks: A Centralized-Equivalent Approach. *IEEE Transactions on Robotics*, 26(1):62–77, feb 2010. ISSN 1552-3098. doi: 10.1109/TRO.2009.2035741. URL <http://ieeexplore.ieee.org/document/5371975/>.
- [122] E Elnahrawy, Li Xiaoyan, and R P Martin. The limits of localization using signal strength: a comparative study. In *Sensor and Ad Hoc Communications and Networks, 2004. IEEE SECON 2004. 2004 First Annual IEEE Communications Society Conference on*, pages 406–414, 2004. doi: 10.1109/SAHCN.2004.1381942.

- [123] Steven Kinio and James K. Mills. Localized Electroporation With Dielectrophoretic Field Flow Fractionation: Toward Removal of Circulating Tumour Cells From Human Blood. *IEEE Transactions on NanoBioscience*, 16(8):802–809, dec 2017. ISSN 1536-1241. doi: 10.1109/TNB.2017.2764380. URL <http://ieeexplore.ieee.org/document/8070960/>.
- [124] Duan Hongyu, Jiang Hong, and Wei Yingchun. CFAR-Based TOA Estimation and Node Localization Method for UWB Wireless Sensor Networks in Weibull Noise and Dense Multipath. In *Computational Intelligence & Communication Technology (CICT), 2015 IEEE International Conference on*, pages 308–311, 2015. doi: 10.1109/CICT.2015.164.
- [125] Le Trung-Kien and N Ono. Reference-distance estimation approach for TDOA-based source and sensor localization. In *Acoustics, Speech and Signal Processing (ICASSP), 2015 IEEE International Conference on*, pages 2549–2553, 2015. doi: 10.1109/ICASSP.2015.7178431.
- [126] M I Jais, P Ehkan, R B Ahmad, I Ismail, T Sabapathy, and M Jusoh. Review of angle of arrival (AOA) estimations through received signal strength indication (RSSI) for wireless sensors network (WSN). In *Computer, Communications, and Control Technology (I4CT), 2015 International Conference on*, pages 354–359, 2015. doi: 10.1109/I4CT.2015.7219597.
- [127] B S Mohammed and N H Noori. An alternative approach for angle of arrival estimation. In *Antennas and Propagation (EuCAP), 2014 8th European Conference on*, pages 2200–2204, 2014. doi: 10.1109/EuCAP.2014.6902247.
- [128] E Nakamori, D Tsukuda, M Fujimoto, Y Oda, T Wada, H Okada, and K Mutsuura. A new indoor position estimation method of RFID tags for continuous moving navigation systems. In *Indoor Positioning and Indoor Navigation (IPIN), 2012 International Conference on*, pages 1–8, 2012. doi: 10.1109/IPIN.2012.6418858.
- [129] N Patwari, A O Hero, M Perkins, N S Correal, and R J O’Dea. Relative location estimation in wireless sensor networks. *Signal Processing, IEEE Transactions on*, 51(8):2137–2148, 2003. doi: 10.1109/TSP.2003.814469.
- [130] Tom Van Haute, Bart Verbeke, Eli De Poorter, and Ingrid Moerman. Optimizing Time-of-Arrival Localization Solutions for Challenging Industrial Environments. *IEEE Transactions on Industrial Informatics*, 13(3):1430–1439, jun 2017. ISSN 1551-3203. doi: 10.1109/TII.2016.2550531. URL <http://ieeexplore.ieee.org/document/7447766/>.
- [131] Florian Meyer, Alessandra Tesei, and Moe Z. Win. Localization of multiple sources using time-difference of arrival measurements. In *2017 IEEE International Conference on Acoustics, Speech and Signal Processing (ICASSP)*, pages 3151–3155. IEEE, mar 2017. ISBN 978-1-5090-4117-6. doi: 10.1109/ICASSP.2017.7952737. URL <http://ieeexplore.ieee.org/document/7952737/>.
- [132] Angelo Coluccia and Alessio Fascista. On the Hybrid TOA/RSS Range Estimation in Wireless Sensor Networks. *IEEE Transactions on Wireless Communications*, 17(1):361–371, jan 2018. ISSN 1536-1276. doi: 10.1109/TWC.2017.2766628. URL <http://ieeexplore.ieee.org/document/8091100/>.

- 
- [133] Wen Yutian, Tian Xiaohua, Wang Xinbing, and Lu Songwu. Fundamental limits of RSS fingerprinting based indoor localization. In *Computer Communications (INFOCOM), 2015 IEEE Conference on*, pages 2479–2487, 2015. doi: 10.1109/INFOCOM.2015.7218637.
- [134] Yu Feng, Jiang Minghua, Liang Jing, Qin Xiao, Hu Ming, Peng Tao, and Hu Xinrong. Expansion RSS-based Indoor Localization Using 5G WiFi Signal. In *Computational Intelligence and Communication Networks (CICN), 2014 International Conference on*, pages 510–514, 2014. doi: 10.1109/CICN.2014.117.
- [135] T Stoyanova, F Kerasiotis, K Efstathiou, and G Papadopoulos. Modeling of the RSS Uncertainty for RSS-Based Outdoor Localization and Tracking Applications in Wireless Sensor Networks. In *Sensor Technologies and Applications (SENSORCOMM), 2010 Fourth International Conference on*, pages 45–50, 2010. doi: 10.1109/SENSORCOMM.2010.14.
- [136] T Stoyanova, F Kerasiotis, C Antonopoulos, and G Papadopoulos. RSS-based localization for wireless sensor networks in practice. In *Communication Systems, Networks & Digital Signal Processing (CSNDSP), 2014 9th International Symposium on*, pages 134–139, 2014. doi: 10.1109/CSNDSP.2014.6923812.
- [137] Israat Tanzeena Haque and Chadi Assi. Profiling-Based Indoor Localization Schemes. *IEEE Systems Journal*, 9(1):76–85, mar 2015. ISSN 1932-8184. doi: 10.1109/JSYST.2013.2281257. URL <http://ieeexplore.ieee.org/document/6609072/>.
- [138] Negar Etemadyrad and Jill K. Nelson. A sequential detection approach to indoor positioning using RSS-based fingerprinting. In *2016 IEEE Global Conference on Signal and Information Processing (GlobalSIP)*, pages 1127–1131. IEEE, dec 2016. ISBN 978-1-5090-4545-7. doi: 10.1109/GlobalSIP.2016.7906017. URL <http://ieeexplore.ieee.org/document/7906017/>.
- [139] Chainarong Kittiyanyunya and Monai Krairiksh. Dual-band conical-scanning Yagi-Uda antenna. In *2017 IEEE International Symposium on Antennas and Propagation & USNC/URSI National Radio Science Meeting*, pages 1979–1980. IEEE, jul 2017. ISBN 978-1-5386-3284-0. doi: 10.1109/APUSNCURSINRSM.2017.8073032. URL <http://ieeexplore.ieee.org/document/8073032/>.
- [140] D.S. Prinsloo, P. Meyer, R. Maaskant, and M.V. Ivashina. Quad-mode antenna for wide-scan sparse arrays. In *2015 IEEE International Symposium on Antennas and Propagation & USNC/URSI National Radio Science Meeting*, pages 1516–1517. IEEE, jul 2015. ISBN 978-1-4799-7815-1. doi: 10.1109/APS.2015.7305147. URL <http://ieeexplore.ieee.org/document/7305147/>.
- [141] B. Pavan Kumar, Chandrakanta Kumar, V. Senthil Kumar, and V. V. Srinivasan. Optimal Radiation Pattern of the Element for a Spherical Phased Array with Hemispherical Scan Capability. *IEEE Antennas and Wireless Propagation Letters*, pages 1–1, 2017. ISSN 1536-1225. doi: 10.1109/LAWP.2017.2745541. URL <http://ieeexplore.ieee.org/document/8017423/>.

- [142] Kamil Yavuz Kapusuz, Yakup Sen, Metehan Bulut, Ilter Karadede, and Ugur Oguz. Low-profile scalable phased array antenna at Ku-band for mobile satellite communications. In *2016 IEEE International Symposium on Phased Array Systems and Technology (PAST)*, pages 1–4. IEEE, oct 2016. ISBN 978-1-5090-1447-7. doi: 10.1109/ARRAY.2016.7832648. URL <http://ieeexplore.ieee.org/document/7832648/>.
- [143] Mohammad Nikfalazar, Mohsen Sazegar, Arshad Mehmood, Alex Wiens, Andreas Friederich, Holger Maune, Joachim R. Binder, and Rolf Jakoby. Two-Dimensional Beam-Steering Phased-Array Antenna With Compact Tunable Phase Shifter Based on BST Thick Films. *IEEE Antennas and Wireless Propagation Letters*, 16:585–588, 2017. ISSN 1536-1225. doi: 10.1109/LAWP.2016.2591078. URL <http://ieeexplore.ieee.org/document/7511716/>.
- [144] What is the difference between a conventional Radar and the SAR? URL <https://www.quora.com/What-is-the-difference-between-a-conventional-Radar-and-the-SAR>.
- [145] M Malajner, Z Cucej, and D Gleich. Angle of arrival estimation using a single omnidirectional rotatable antenna. In *Wireless Information Technology and Systems (ICWITS), 2012 IEEE International Conference on*, pages 1–4, 2012. doi: 10.1109/ICWITS.2012.6417683.
- [146] A Hakkarainen, J Werner, N Gulati, D Patron, D Pfeil, H Paaso, A Mammela, K Dandekar, and M Valkama. Reconfigurable antenna based doa estimation and localization in cognitive radios: Low complexity algorithms and practical measurements. In *Cognitive Radio Oriented Wireless Networks and Communications (CROWNCOM), 2014 9th International Conference on*, pages 454–459, 2014. doi: 10.4108/icst.crowncom.2014.255730.
- [147] S Sivasundarapandian. Performance analysis of multi-band multiple beamforming butler matrix for smart antenna systems. In *Robotics, Automation, Control and Embedded Systems (RACE), 2015 International Conference on*, pages 1–5, 2015. doi: 10.1109/RACE.2015.7097291.
- [148] Hua Meng-Chang, Hsu Cheng-Han, Liao Wen-Jiao, Yao Chia-Chi, Yeh Ting-Hung, and Liu Hsin-Chin. Direction-of-arrival estimator using array switching on software defined radio platform. In *Antennas and Propagation (APSURSI), 2011 IEEE International Symposium on*, pages 2821–2824, 2011. ISBN 1522-3965. doi: 10.1109/APS.2011.5997113.
- [149] Marko Malajner, Dušan Gleich, and Peter Planinšič. Angle of Arrival estimation algorithms using Received Signal Strength Indicator. *Journal of Microelectronics, Electronic Components and Materials*, 45(4):237–248, 2015. URL <file:///C:/Users/user/Downloads/Angle{ }URN-NBN-SI-DOC-O4FYKB1C.pdf>.
- [150] Stanislav Ogurtsov and Slawomir Koziel. Sidelobe reduction in linear antenna arrays with corporate-feeds of non-uniform power distribution. In *2017 11th European Conference on Antennas and Propagation (EuCAP)*, pages 3259–3263. IEEE, mar 2017. ISBN 978-8-8907-0187-0. doi: 10.23919/EuCAP.2017.7928131. URL <http://ieeexplore.ieee.org/document/7928131/>.

- 
- [151] A. Morini, M. Farina, T. Rozzi, and G. Venanzoni. An Effective Strategy for the Optimization of the Phase Distribution of Large Arrays Based on a Full-Wave Model. In *2006 IEEE Antennas and Propagation Society International Symposium*, pages 4205–4208. IEEE, 2006. ISBN 1-4244-0123-2. doi: 10.1109/APS.2006.1711557. URL <http://ieeexplore.ieee.org/document/1711557/>.
- [152] Hayat Errifi, Abdennaceur Baghdad, Abdelmajid Badri, and Aicha Sahel. Electronically reconfigurable beam steering array antenna using switched line phase shifter. In *2017 International Conference on Wireless Networks and Mobile Communications (WINCOM)*, pages 1–6. IEEE, nov 2017. ISBN 978-1-5386-2123-3. doi: 10.1109/WINCOM.2017.8238147. URL <http://ieeexplore.ieee.org/document/8238147/>.
- [153] Chih-Sheng Yang, Ting-Yi Chung, Cheng-Ying Kuo, Jyh-Chyuan Jan, and Ching-Shiang Hwang. Constructing a Permanent Magnet Phase Shifter. *IEEE Transactions on Applied Superconductivity*, 28(3):1–5, apr 2018. ISSN 1051-8223. doi: 10.1109/TASC.2017.2777849. URL <http://ieeexplore.ieee.org/document/8120022/>.
- [154] K. Sakakibara, H. Sano, N. Kikuma, and H. Hirayama. Mechanically-controlled phase shifter of left-handed waveguide for beam-scanning slot array antennas. In *2010 International Conference on Electromagnetics in Advanced Applications*, pages 657–660. IEEE, sep 2010. ISBN 978-1-4244-7366-3. doi: 10.1109/ICEAA.2010.5651448. URL <http://ieeexplore.ieee.org/document/5651448/>.
- [155] Seungho Jeong, Boram An, Phirun Kim, Yongchae Jeong, and Jongsik Lim. A design of phase shifter with constant insertion loss. In *2016 Progress in Electromagnetic Research Symposium (PIERS)*, pages 3221–3221. IEEE, aug 2016. ISBN 978-1-5090-6093-1. doi: 10.1109/PIERS.2016.7735266. URL <http://ieeexplore.ieee.org/document/7735266/>.
- [156] Chong Jin, Etienne Okada, Marc Faucher, Damien Ducatteau, Mohammed Zaknoue, and Dimitris Pavlidis. A GaN Schottky Diode-based analog phase shifter MMIC. In *2014 9th European Microwave Integrated Circuit Conference*, pages 96–99. IEEE, oct 2014. ISBN 978-2-8748-7036-1. doi: 10.1109/EuMIC.2014.6997800. URL <http://ieeexplore.ieee.org/document/6997800/>.
- [157] Arati Arun Bhonkar and Udaysinh Sutar. Overview of Microstrip Line Phase Shifter. *International Journal of Advanced Research in Computer and Communication Engineering*, 5(5), 2016. ISSN 2278-1021. doi: 10.17148/IJARCCE.2016.55121. URL <https://www.ijarcce.com/upload/2016/may-16/IJARCCE121.pdf>.
- [158] Kishan Sharma, Ananjan Basu, and Shibank. Koul. High power 6-bit digital phase shifter for airborne IFF application. In *2016 Asia-Pacific Microwave Conference (APMC)*, pages 1–4. IEEE, dec 2016. ISBN 978-1-5090-1592-4. doi: 10.1109/APMC.2016.7931371. URL <http://ieeexplore.ieee.org/document/7931371/>.
- [159] J.-J. Hung, L. Dussopt, and G.M. Rebeiz. Distributed 2- and 3-Bit W-Band MEMS Phase Shifters on Glass Substrates. *IEEE Transactions on Microwave Theory and Techniques*, 52(2):600–606, feb 2004. ISSN 0018-9480. doi: 10.1109/TMTT.2003.821941. URL <http://ieeexplore.ieee.org/document/1266886/>.

- [160] Yulin Huang, Jingfu Bao, Xinyi Li, Yiling Wang, and Yijia Du. A 4-bit switched-line phase shifter based on MEMS switches. In *10th IEEE International Conference on Nano/Micro Engineered and Molecular Systems*, pages 405–408. IEEE, apr 2015. ISBN 978-1-4673-6695-3. doi: 10.1109/NEMS.2015.7147454. URL <http://ieeexplore.ieee.org/lpdocs/epic03/wrapper.htm?arnumber=7147454>.
- [161] Shila Shamsadini, Souren Shamsinejad, Pedram Mousavi, and Kambiz Moez. Improved 60GHz loaded-line phase shifter using tunable inductor. In *2016 IEEE International Symposium on Antennas and Propagation (APSURSI)*, pages 1141–1142. IEEE, jun 2016. ISBN 978-1-5090-2886-3. doi: 10.1109/APS.2016.7696278. URL <http://ieeexplore.ieee.org/document/7696278/>.
- [162] M. X. Xiao, S. W. Cheung, and T. I. Yuk. A wideband 360° analog phase shifter design. In *2009 Canadian Conference on Electrical and Computer Engineering*, pages 524–527. IEEE, may 2009. ISBN 978-1-4244-3509-8. doi: 10.1109/CCECE.2009.5090186. URL <http://ieeexplore.ieee.org/document/5090186/>.
- [163] Nagaveni D. Doddamani, Harishchandra, and Anil V. Nandi. Design of SPDT Switch, 6 Bit Digital Attenuator, 6 Bit Digital Phase Shifter for L-Band T/R Module using 0.7  $\mu\text{M}$  GaAs MMIC Technology. In *2007 International Conference on Signal Processing, Communications and Networking*, pages 302–307. IEEE, feb 2007. ISBN 1-4244-0996-9. doi: 10.1109/ICSCN.2007.350752. URL <http://ieeexplore.ieee.org/document/4156634/>.
- [164] G.L. Tan, R.E. Mihailovich, J.B. Hacker, J.F. DeNatale, and G.M. Rebeiz. A very-low-loss 2-bit X-band RF MEMS phase shifter. In *2002 IEEE MTT-S International Microwave Symposium Digest (Cat. No.02CH37278)*, pages 333–335. IEEE. ISBN 0-7803-7239-5. doi: 10.1109/MWSYM.2002.1011624. URL <http://ieeexplore.ieee.org/document/1011624/>.
- [165] A. Pages-Zamora, J. Vidal, and D.H. Brooks. Closed-form solution for positioning based on angle of arrival measurements. In *The 13th IEEE International Symposium on Personal, Indoor and Mobile Radio Communications*, volume 4, pages 1522–1526. IEEE. ISBN 0-7803-7589-0. doi: 10.1109/PIMRC.2002.1045433. URL <http://ieeexplore.ieee.org/document/1045433/>.
- [166] Amir Hossein Akhavan Salmasi, Evgueni Doukhitch, and Muhammed Salamah. A Hybrid TOA/AOA Hardware-Oriented Algorithm for Mobile Positioning. In *2011 International Conference on Broadband and Wireless Computing, Communication and Applications*, pages 40–44. IEEE, oct 2011. ISBN 978-1-4577-1455-9. doi: 10.1109/BWCCA.2011.47. URL <http://ieeexplore.ieee.org/document/6103013/>.
- [167] Ali Noroozi and Mohammad Ali Sebt. Algebraic solution for three-dimensional TDOA/AOA localisation in multiple-input–multiple-output passive radar. *IET Radar, Sonar & Navigation*, 12(1):21–29, jan 2018. ISSN 1751-8784. doi: 10.1049/iet-rsn.2017.0117. URL <http://digital-library.theiet.org/content/journals/10.1049/iet-rsn.2017.0117>.
- [168] Ishita Gupta, Varsha Patil, Chaitali Kadam, and Shreya Dumbre. Face detection and recognition using Raspberry Pi. In *2016 IEEE International WIE Conference*

- 
- on *Electrical and Computer Engineering (WIECON-ECE)*, pages 83–86. IEEE, dec 2016. ISBN 978-1-5090-3745-2. doi: 10.1109/WIECON-ECE.2016.8009092. URL <http://ieeexplore.ieee.org/document/8009092/>.
- [169] Andy Vesa and Arpad Iozsa. Direction - of - Arrival estimation for uniform sensor arrays. In *2010 9th International Symposium on Electronics and Telecommunications*, pages 249–252. IEEE, nov 2010. ISBN 978-1-4244-8457-7. doi: 10.1109/ISETC.2010.5679326. URL <http://ieeexplore.ieee.org/document/5679326/>.
- [170] Renzheng Cao, Binyue Liu, Feifei Gao, and Xiaofei Zhang. A Low-Complex One-Snapshot DOA Estimation Algorithm with Massive ULA. *IEEE Communications Letters*, 21(5):1071–1074, may 2017. ISSN 1089-7798. doi: 10.1109/LCOMM.2017.2652442. URL <http://ieeexplore.ieee.org/document/7815358/>.
- [171] Shibin Ge and Changyu Sun. The DOA of wideband signals estimation by using ESPRIT based on K-means. In *Instrumentation and Measurement, Sensor Network and Automation (IMSNA), 2013 2nd International Symposium on*, pages 856–859, 2013. doi: 10.1109/IMSNA.2013.6743412.
- [172] A Azarbar, O Mehdinejad, and M Kazerooni. Improvement of 2-D DOA estimation with tapered Matrix Pencil algorithm. In *Microwaves, Radar and Remote Sensing Symposium (MRRS), 2011*, pages 291–293, 2011. doi: 10.1109/MRRS.2011.6053657.
- [173] M Y Siyal, J Ahmed, U Mujahid, and Taufeeq. Spectral estimation algorithm for smart antenna system with modified ULA. In *Information, Communications and Signal Processing (ICICS) 2013 9th International Conference on*, pages 1–4, 2013. doi: 10.1109/ICICS.2013.6782845.
- [174] Mubashir Alam and Khalid Jamil. Maximum likelihood (ML) based localization algorithm for multi-static passive radar using range-only measurements. In *2015 IEEE Radar Conference*, pages 180–184. IEEE, oct 2015. ISBN 978-1-4673-9655-4. doi: 10.1109/RadarConf.2015.7411876. URL <http://ieeexplore.ieee.org/document/7411876/>.
- [175] A Satish and R Kashyap. Architecture models for maximum likelihood direction of arrival estimation. In *Systems, Man and Cybernetics, 1992., IEEE International Conference on*, pages 1218–1223 vol.2, 1992. doi: 10.1109/ICSMC.1992.271621.
- [176] Shin Jong-Woo, Lee Young-Jun, and Kim Hyoung-Nam. Reduced-Complexity Maximum Likelihood Direction-of-Arrival Estimation Based on Spatial Aliasing. *Signal Processing, IEEE Transactions on*, 62(24):6568–6581, 2014. doi: 10.1109/TSP.2014.2367454.
- [177] Y.T. Chan, H.Y.C. Hang, and P.-C. Ching. Exact and Approximate Maximum Likelihood Localization Algorithms. *IEEE Transactions on Vehicular Technology*, 55(1):10–16, jan 2006. ISSN 0018-9545. doi: 10.1109/TVT.2005.861162. URL <http://ieeexplore.ieee.org/document/1583909/>.
- [178] Mohamed Zhaounia, Mohamed Adnan Landolsi, and Ridha Bouallegue. Hybrid TOA/AOA Approximate Maximum Likelihood Mobile Localization. *Journal of Electrical and Computer Engineering*, 2010:1–5, dec 2010. ISSN 2090-0147. doi: 10.1155/2010/942657. URL <http://www.hindawi.com/journals/jece/2010/942657/>.

- [179] Refat A. Al-Nimnim, Ali H. Muqaibel, and Mohamed A. Landolsi. Improved weighting algorithm for NLOS radiolocation. In *2009 IEEE 9th Malaysia International Conference on Communications (MICC)*, pages 730–735. IEEE, dec 2009. ISBN 978-1-4244-5531-7. doi: 10.1109/MICC.2009.5431399. URL <http://ieeexplore.ieee.org/document/5431399/>.
- [180] Jagadeesha S N. TIME OF ARRIVAL BASED LOCALIZATION IN WIRELESS SENSOR NETWORKS: A LINEAR APPROACH. *An International Journal (SIPIJ)*, 4(4), 2013. doi: 10.5121/sipij.2013.4402. URL <http://airconline.com/sipij/V4N4/4413sipij02.pdf>.
- [181] P Kasebzadeh, C Fritsche, E Ozkan, F Gunnarsson, and F Gustafsson. Joint antenna and propagation model parameter estimation using RSS measurements. In *Information Fusion (Fusion), 2015 18th International Conference on*, pages 98–103, 2015.
- [182] T F Etbeit. Advances in semi-empirical terrestrial wave propagation modeling for macrocellular environments. In *Antennas and Propagation Society International Symposium, 2003. IEEE*, volume 4, pages 907–910 vol.4, 2003. doi: 10.1109/APS.2003.1220419.
- [183] Amitabha Ghosh, Nitin Mangalvedhe, Rapeepat Ratasuk, Bishwarup Mondal, Mark Cudak, Eugene Visotsky, Timothy Thomas, Jeffrey Andrews, Ping Xia, Han Jo, Harpreet Dhillon, and Thomas Novlan. Heterogeneous cellular networks: From theory to practice. *IEEE Communications Magazine*, 50(6):54–64, jun 2012. ISSN 0163-6804. doi: 10.1109/MCOM.2012.6211486. URL <http://ieeexplore.ieee.org/document/6211486/>.
- [184] Abdulaziz Alsayyari, Ivica Kostanic, and Carlos E Otero. An empirical path loss model for Wireless Sensor Network deployment in a concrete surface environment. In *Wireless and Microwave Technology Conference (WAMICON), 2015 IEEE 16th Annual*, pages 1–6, 2015. doi: 10.1109/WAMICON.2015.7120311.
- [185] A AlSayyari, I Kostanic, and C E Otero. An empirical path loss model for Wireless Sensor Network deployment in an artificial turf environment. In *Networking, Sensing and Control (ICNSC), 2014 IEEE 11th International Conference on*, pages 637–642, 2014. doi: 10.1109/ICNSC.2014.6819700.
- [186] H U Yildiz, S Kurt, and B Tavli. The Impact of Near-Ground Path Loss Modeling on Wireless Sensor Network Lifetime. In *Military Communications Conference (MILCOM), 2014 IEEE*, pages 1114–1119, 2014. doi: 10.1109/MILCOM.2014.188.
- [187] V S Abhayawardhana, I J Wassell, D Crosby, M P Sellars, and M G Brown. Comparison of empirical propagation path loss models for fixed wireless access systems. In *Vehicular Technology Conference, 2005. VTC 2005-Spring, 2005 IEEE 61st*, volume 1, pages 73–77 Vol. 1, 2005. ISBN 1550-2252. doi: 10.1109/VETECS.2005.1543252.
- [188] F Letourneux, S Guivarch, and Y Lostanlen. Propagation models for Heterogeneous Networks. In *Antennas and Propagation (EuCAP), 2013 7th European Conference on*, pages 3993–3997, 2013.

- 
- [189] Hetal P. Mistry and Nital H. Mistry. RSSI Based Localization Scheme in Wireless Sensor Networks: A Survey. In *2015 Fifth International Conference on Advanced Computing & Communication Technologies*, pages 647–652. IEEE, feb 2015. ISBN 978-1-4799-8488-6. doi: 10.1109/ACCT.2015.105. URL <http://ieeexplore.ieee.org/document/7079160/>.
- [190] Chen Xu, D Schonfeld, and A A Khokhar. Localization and Trajectory Estimation of Mobile Objects Using Minimum Samples. *Vehicular Technology, IEEE Transactions on*, 58(8):4439–4446, 2009. doi: 10.1109/TVT.2009.2020065.
- [191] Xiaohua Tian, Ruofei Shen, Duowen Liu, Yutian Wen, and Xinbing Wang. Performance Analysis of RSS Fingerprinting Based Indoor Localization. *IEEE Transactions on Mobile Computing*, 16(10):2847–2861, oct 2017. ISSN 1536-1233. doi: 10.1109/TMC.2016.2645221. URL <http://ieeexplore.ieee.org/document/7797481/>.
- [192] T J Black, P N Pathirana, and S Nahavandi. Position estimation and tracking of an autonomous mobile sensor using received signal strength. In *Intelligent Sensors, Sensor Networks and Information Processing, 2008. ISSNIP 2008. International Conference on*, pages 19–24, 2008. doi: 10.1109/ISSNIP.2008.4761956.
- [193] Xiaoyan Li. Ratio-based zero-profiling indoor localization. In *2009 IEEE 6th International Conference on Mobile Adhoc and Sensor Systems*, pages 40–49. IEEE, oct 2009. ISBN 978-1-4244-5114-2. doi: 10.1109/MOBHOC.2009.5336964. URL <http://ieeexplore.ieee.org/document/5336964/>.
- [194] Jukka Talvitie, Markku Renfors, and Elena Simona Lohan. Distance-Based Interpolation and Extrapolation Methods for RSS-Based Localization With Indoor Wireless Signals. *IEEE Transactions on Vehicular Technology*, 64(4):1340–1353, apr 2015. ISSN 0018-9545. doi: 10.1109/TVT.2015.2397598. URL <http://ieeexplore.ieee.org/document/7024940/>.
- [195] Belaabed Abdelghani and Gao Qiang. Hybrid RSS-based fingerprinting positioning method with segmentation and KNN in cellular network. In *2017 3rd IEEE International Conference on Control Science and Systems Engineering (ICCSSE)*, pages 465–469. IEEE, aug 2017. ISBN 978-1-5386-0483-0. doi: 10.1109/CCSSE.2017.8088042. URL <http://ieeexplore.ieee.org/document/8088042/>.
- [196] P Bahl and V N Padmanabhan. RADAR: an in-building RF-based user location and tracking system. In *INFOCOM 2000. Nineteenth Annual Joint Conference of the IEEE Computer and Communications Societies. Proceedings. IEEE*, volume 2, pages 775–784 vol.2, 2000. ISBN 0743-166X. doi: 10.1109/INFCOM.2000.832252.
- [197] Moustafa Youssef and Ashok Agrawala. The Horus WLAN location determination system. In *Proceedings of the 3rd international conference on Mobile systems, applications, and services - MobiSys '05*, page 205, New York, New York, USA, 2005. ACM Press. ISBN 1931971315. doi: 10.1145/1067170.1067193. URL <http://portal.acm.org/citation.cfm?doid=1067170.1067193>.
- [198] S. Venkatraman, J. Caffery, and H.-R. You. Location using LOS range estimation in NLOS environments. In *Vehicular Technology Conference. IEEE 55th Vehicular Technology Conference. VTC Spring 2002 (Cat. No.02CH37367)*, volume 2, pages

- 856–860. IEEE. ISBN 0-7803-7484-3. doi: 10.1109/VTC.2002.1002609. URL <http://ieeexplore.ieee.org/document/1002609/>.
- [199] N. Khajehnouri and A.H. Sayed. A non-line-of-sight equalization scheme for wireless cellular location. In *2003 IEEE International Conference on Acoustics, Speech, and Signal Processing, 2003. Proceedings. (ICASSP '03)*, volume 1, pages VI-549–52. IEEE. ISBN 0-7803-7663-3. doi: 10.1109/ICASSP.2003.1201740. URL <http://ieeexplore.ieee.org/document/1201740/>.
- [200] Pi-Chun Chen. A non-line-of-sight error mitigation algorithm in location estimation. In *WCNC. 1999 IEEE Wireless Communications and Networking Conference (Cat. No.99TH8466)*, pages 316–320. IEEE. ISBN 0-7803-5668-3. doi: 10.1109/WCNC.1999.797838. URL <http://ieeexplore.ieee.org/document/797838/>.
- [201] S. Al-Jazzar, M. Ghogho, and D. McLernon. A Joint TOA/AOA Constrained Minimization Method for Locating Wireless Devices in Non-Line-of-Sight Environment. *IEEE Transactions on Vehicular Technology*, 58(1):468–472, jan 2009. ISSN 0018-9545. doi: 10.1109/TVT.2008.923670. URL <http://ieeexplore.ieee.org/document/4490152/>.
- [202] Suppachai Monta, Sathaporn Promwong, and Vongkeo Kingsakda. Evaluation of ultra wideband indoor localization with trilateration and min-max techniques. In *2016 13th International Conference on Electrical Engineering/Electronics, Computer, Telecommunications and Information Technology (ECTI-CON)*, pages 1–4. IEEE, jun 2016. ISBN 978-1-4673-9749-0. doi: 10.1109/ECTICon.2016.7561496. URL <http://ieeexplore.ieee.org/document/7561496/>.
- [203] John Lowell. Military applications of localization, tracking, and targeting. *IEEE Wireless Communications*, 18(2):60–65, apr 2011. ISSN 1536-1284. doi: 10.1109/MWC.2011.5751297. URL <http://ieeexplore.ieee.org/document/5751297/>.
- [204] A. Boukerche, H.A.B. Oliveira, E.F. Nakamura, and A.A.F. Loureiro. Secure localization algorithms for wireless sensor networks. *IEEE Communications Magazine*, 46(4):96–101, apr 2008. ISSN 0163-6804. doi: 10.1109/MCOM.2008.4481347. URL <http://ieeexplore.ieee.org/document/4481347/>.
- [205] Andre Filipe Goncalves Ferreira, Duarte Manuel Azevedo Fernandes, Andre Paulo Catarino, and Joao L. Monteiro. Localization and Positioning Systems for Emergency Responders: A Survey. *IEEE Communications Surveys & Tutorials*, 19(4):2836–2870, 2017. ISSN 1553-877X. doi: 10.1109/COMST.2017.2703620. URL <http://ieeexplore.ieee.org/document/7927385/>.
- [206] Mingxiao Lu, Xiaoguang Zhao, and Yikun Huang. Fast localization for emergency monitoring and rescue in disaster scenarios based on WSN. In *2016 14th International Conference on Control, Automation, Robotics and Vision (ICARCV)*, pages 1–6. IEEE, nov 2016. ISBN 978-1-5090-3549-6. doi: 10.1109/ICARCV.2016.7838790. URL <http://ieeexplore.ieee.org/document/7838790/>.
- [207] Noori BniLam, Glenn Ergeerts, Dragan Subotic, Jan Steckel, and Maarten Weyn. Adaptive probabilistic model using angle of arrival estimation for IoT indoor localization. In *2017 International Conference on Indoor Positioning and Indoor*

- Navigation (IPIN)*, pages 1–7. IEEE, sep 2017. ISBN 978-1-5090-6299-7. doi: 10.1109/IPIN.2017.8115864. URL <http://ieeexplore.ieee.org/document/8115864/>.
- [208] Swathi Ramnath, Abhishek Javali, Bhumika Narang, Pallavi Mishra, and Sudhir K. Routray. IoT based localization and tracking. In *2017 International Conference on IoT and Application (ICIOT)*, pages 1–4. IEEE, may 2017. ISBN 978-1-5386-1698-7. doi: 10.1109/ICIOTA.2017.8073629. URL <http://ieeexplore.ieee.org/document/8073629/>.
- [209] Ash. Coaxial Cable Attenuation Charts RF Elektronik <http://rfelektronik.se> info@rfelektronik.se. Technical report. URL <http://rfelektronik.se>.
- [210] RF Connector Overview Guide. Technical report. URL <https://linxtechnologies.com/wp/wp-content/uploads/connector{ }overview{ }guide.pdf>.
- [211] Campbell Scientific. APPLICATION NOTE The Link Budget and Fade Margin. Technical report, 2016. URL <https://s.campbellsci.com/documents/us/technical-papers/link-budget.pdf>.
- [212] Jun Zhang, S.W. Cheung, and Qi Zhu. Design of 180°-switched-line phase shifter with constant phase shift using CRLH TL. In *2014 IEEE Antennas and Propagation Society International Symposium (APSURSI)*, pages 344–345. IEEE, jul 2014. ISBN 978-1-4799-3540-6. doi: 10.1109/APS.2014.6904504. URL <http://ieeexplore.ieee.org/lpdocs/epic03/wrapper.htm?arnumber=6904504>.
- [213] Rudra L. Timsina, Richard A. Messner, and Jean L. Kubwimana. A compact design of switched line phase shifter for a microstrip phased array antenna. In *2017 Progress in Electromagnetics Research Symposium - Fall (PIERS - FALL)*, pages 1839–1844. IEEE, nov 2017. ISBN 978-1-5386-1211-8. doi: 10.1109/PIERS-FALL.2017.8293436. URL <http://ieeexplore.ieee.org/document/8293436/>.
- [214] Novarm Software. DipTrace SCHEMATIC AND PCB DESIGN SOFTWARE. Technical report. URL <https://diptrace.com/books/tutorial.pdf>.
- [215] Chaithanya Raj and S. Suganthi. Performance analysis of antenna with different substrate materials at 60 GHz. In *2017 International Conference on Wireless Communications, Signal Processing and Networking (WiSPNET)*, pages 2537–2539. IEEE, mar 2017. ISBN 978-1-5090-4442-9. doi: 10.1109/WiSPNET.2017.8300219. URL <http://ieeexplore.ieee.org/document/8300219/>.
- [216] Analog Devices. hmc241 (v00.0513). URL [www.hittite.comhttp://www.analog.com/media/en/technical-documentation/data-sheets/hmc241.pdf](http://www.analog.com/media/en/technical-documentation/data-sheets/hmc241.pdf).
- [217] Michaels Mollel and Michaelkisangiri. Comparison of Empirical Propagation Path Loss Models for Mobile Communication. 5(9):2222–1719, 2014. URL [www.iiste.org](http://www.iiste.org).
- [218] John Wiley. The Okumura-Hata Model. 2011. URL <http://www.wiley.com/legacy/wileychi/molisch/supp2/appendices/c07{ }Appendices.pdf>.
- [219] Propagation Model | ATDI. URL <http://www.atdi.com/tag/propagation-model/>.

- [220] Itu-R Recommendation. RECOMMENDATION ITU-R P.1238-7 - Propagation data and prediction methods for the planning of indoor radiocommunication systems and radio local area networks in the frequency range 900 MHz to 100 GHz. pages 1238–7, 2012. URL <https://www.itu.int/dms/pubrec/itu-r/rec/p/R-REC-P.1238-7-201202-S!PDF-E.pdf>.
- [221] Pekka Kyösti, Juha Meinilä, Lassi Hentilä, Xiongwen Zhao, Tommi Jämsä, Christian Schneider, Milan Narandžić, Marko Milojević, Aihua Hong, Juha Ylitalo, Veli-Matti Holappa, Mikko Alatossava, Robert Bultitude, Yvo De Jong, and Terhi Rautiainen Participant. WINNER II Channel Models. 2007.
- [222] Giulia Buttazzoni and Roberto Vescovo. Density Tapering of Linear Arrays Radiating Pencil Beams: A New Extremely Fast Gaussian Approach. *IEEE Transactions on Antennas and Propagation*, 65(12):7372–7377, dec 2017. ISSN 0018-926X. doi: 10.1109/TAP.2017.2765744. URL <http://ieeexplore.ieee.org/document/8080225/>.
- [223] Picocells The Applications Handbook A proven way to maximize Return-on-Spectrum. URL [http://www.crony.rs/files/File/II\\_dan\\_19\\_maj\\_2011/02\\_ipaccesseng/Picocellapplicationshandbook.pdf](http://www.crony.rs/files/File/II_dan_19_maj_2011/02_ipaccesseng/Picocellapplicationshandbook.pdf).
- [224] RFTechnics. 9 dB Omnidirectional Antenna. URL [http://www.rftechnics.com/data/RFT\\_OMV\\_09\\_24\\_Antenna.pdf](http://www.rftechnics.com/data/RFT_OMV_09_24_Antenna.pdf).
- [225] Catalogue Qwh-sl. 0 . 5 - 2 GHz Linearly Polarised Wideband Ridged Horn Antenna fitted with an N type Connector. Technical report, Steatite.
- [226] Insulation Insulation Material: Insulation Trade Name Insulation Material Dia. (in.) Mechanical Characteristics (Overall) Applicable Specifications and Agency Compliance (Overall). URL [http://www.farnell.com/datasheets/2335138.pdf?ga=2.152187581.561354287.1510939522-1080647459.1493736609&gac=1.245690032.1510569556.EAIaIQobChMI\\_4-Lha671wIVqRXTCh0K-QuQEAQYAyABEgKkJ\\_D\\_BwE](http://www.farnell.com/datasheets/2335138.pdf?ga=2.152187581.561354287.1510939522-1080647459.1493736609&gac=1.245690032.1510569556.EAIaIQobChMI_4-Lha671wIVqRXTCh0K-QuQEAQYAyABEgKkJ_D_BwE).
- [227] Kwang-Jin Koh and Gabriel M. Rebeiz. 0.13- $\mu$ m CMOS Phase Shifters for X-, Ku-, and K-Band Phased Arrays. *IEEE Journal of Solid-State Circuits*, 42(11): 2535–2546, nov 2007. ISSN 0018-9200. doi: 10.1109/JSSC.2007.907225. URL <http://ieeexplore.ieee.org/document/4362098/>.
- [228] 2 Way Power Divider SMA Connectors From 2 GHz to 4 GHz Rated at 30 Watts. URL <https://www.fairviewmicrowave.com/2-way-power-divider-sma-4-ghz-30-watts-mp8424-2-p.aspx>.
- [229] Julien Marot and Salah Bourennane. Raspberry Pi for image processing education. In *2017 25th European Signal Processing Conference (EUSIPCO)*, pages 2364–2366. IEEE, aug 2017. ISBN 978-0-9928626-7-1. doi: 10.23919/EUSIPCO.2017.8081633. URL <http://ieeexplore.ieee.org/document/8081633/>.
- [230] Fatma Ok, Murat Can, Hakan Ucgun, and Ugur Yuzgec. Smart mirror applications with raspberry Pi. In *2017 International Conference on Computer Science and Engineering (UBMK)*, pages 94–98. IEEE, oct 2017. ISBN 978-1-5386-0930-9. doi: 10.1109/UBMK.2017.8093566. URL <http://ieeexplore.ieee.org/document/8093566/>.

- 
- [231] ESP8266 Thing Hookup Guide - learn.sparkfun.com. URL <https://learn.sparkfun.com/tutorials/esp8266-thing-hookup-guide/hardware-overview>.
- [232] Kamin Whitehouse, Chris Karlof, and David Culler. A Practical Evaluation of Radio Signal Strength for Ranging-based Localization. *Mobile Computing and Communications Review*, 11:41–52, 2007. URL <https://www.semanticscholar.org/paper/A-practical-evaluation-of-radio-signal-strength-for-Whitehouse-Karlof/b4969f35de9552405afae64d155e4efef7c4275e>.
- [233] J. Miranda, R. Abrishambaf, T. Gomes, P. Goncalves, J. Cabral, A. Tavares, and J. Monteiro. Path loss exponent analysis in Wireless Sensor Networks: Experimental evaluation. In *2013 11th IEEE International Conference on Industrial Informatics (INDIN)*, pages 54–58. IEEE, jul 2013. ISBN 978-1-4799-0752-6. doi: 10.1109/INDIN.2013.6622857. URL <http://ieeexplore.ieee.org/document/6622857/>.
- [234] Gregory B. Prince and Thomas D.C. Little. A two phase hybrid RSS/AoA algorithm for indoor device localization using visible light. In *2012 IEEE Global Communications Conference (GLOBECOM)*, pages 3347–3352. IEEE, dec 2012. ISBN 978-1-4673-0921-9. doi: 10.1109/GLOCOM.2012.6503631. URL <http://ieeexplore.ieee.org/document/6503631/>.
- [235] Slavisa Tomic, Marko Beko, Rui Dinis, and Luís Bernardo. On target localization using combined RSS and AoA measurements. *Sensors (Switzerland)*, 18(4):1–25, 2018. ISSN 14248220. doi: 10.3390/s18041266.
- [236] Puneet Anand, Sonia Sharma, Deepak Sood, and C.C. Tripathi. Design of compact reconfigurable switched line microstrip phase shifters for phased array antenna. In *2012 1st International Conference on Emerging Technology Trends in Electronics, Communication & Networking*, pages 1–3. IEEE, dec 2012. ISBN 978-1-4673-1627-9. doi: 10.1109/ET2ECN.2012.6470078. URL <http://ieeexplore.ieee.org/document/6470078/>.
- [237] Joseph Costantine, Youssef Tawk, Silvio E. Barbin, and Christos G. Christodoulou. Reconfigurable Antennas: Design and Applications. *Proceedings of the IEEE*, 103(3):424–437, mar 2015. ISSN 0018-9219. doi: 10.1109/JPROC.2015.2396000. URL <http://ieeexplore.ieee.org/document/7086418/>.



# Appendix A

## Experimental Validation

### Phase shifter Testing

1. Initialise timer and ESP8266 pins

```
int timer = 0.1*1000;           // Set 0.1secs delay time
int ledPins[] = {4, 12, 13,16}; // S1A, S1B, S2A, S2B
int pinCount = 4;               // the number of pins
int Switchingtimer = 30*1000;  // set 30 seconds delay
```

2. Set pin states

```
const int Phase_Shifter_Control[4][4]={
{1,0,0,1}, //[ref] phase [0,0]
{0,1,1,0}, //phase [120,0]
{0,0,1,1}, //phase [0,120]
{1,1,0,0} //phase [0,180]
};
```

3. Initialise each pin as output pin

```
void setup() {
for (int thisPin = 0; thisPin < pinCount; thisPin++) {
pinMode(ledPins[thisPin], OUTPUT);
}
delay(timer); //give some time 0.1sec to be ready
}
```

#### 4. Activate each pin for each control state

```

void loop() {
  // select each phase shifter switch state
  for (int SwitchStates = 0; SwitchStates < 4; SwitchStates++) {
    // select each pin state
    for (int thisPin = 0; thisPin < pinCount; thisPin++) {
      // turn the pin on:
      digitalWrite(ledPins[thisPin], Phase_Sifter_Control[SwitchStates][thisPin]);
    }
    // Delay to save the line phase data
    delay(Switchingtimer);
  }
}

```

## Antenna Array Testing

### 1. Initialise timer and ESP8266 pins

```

int timer = 100;
int ledPins[] = {4, 5, 12, 13, 14, 16};
int pinCount = 6;

```

### 2. Set pin states

```

const int Phase_Sifter_Control[1][6]={
  //Collumns = STEPS 0-5
  {1,0,0,1,1,0}, //[ref] phase [0,0]
  //   {0,0,1,1,1,0}, //phase [120,0]
  //   {1,0,0,1,0,1}, //phase [0,120]
  //   {1,1,0,0,1,0} //phase [0,180]
};

```

### 3. Initialise each pin as output pin

```

void setup() {
  // the array elements are numbered from 0 to (pinCount - 1).

```

```
// use a for loop to initialize each pin as an output:
for (int thisPin = 0; thisPin < pinCount; thisPin++) {
  pinMode(ledPins[thisPin], OUTPUT);
}

for (int thisPin = 0; thisPin < pinCount; thisPin++) {
  // turn the pin on:
  digitalWrite(ledPins[thisPin], Phase_Sifter_Control[0][thisPin]);
}
}
```

#### 4. Activate each pin for each control state

```
void loop() {}
```

